A Review on the Production of Light Olefins from Hydrocarbons Cracking and Methanol Conversion

Chapter · February 2020

CITATIONS
44

READS
2,985

2 authors:

Ehsan Kianfar

255 PUBLICATIONS **4,284** CITATIONS

SEE PROFILE

Mahmoud Salimi

Islamic Azad University of Arak

27 PUBLICATIONS **811** CITATIONS

SEE PROFILE

Advances in CHEMISTRY RESEARCH

VOLUME 59

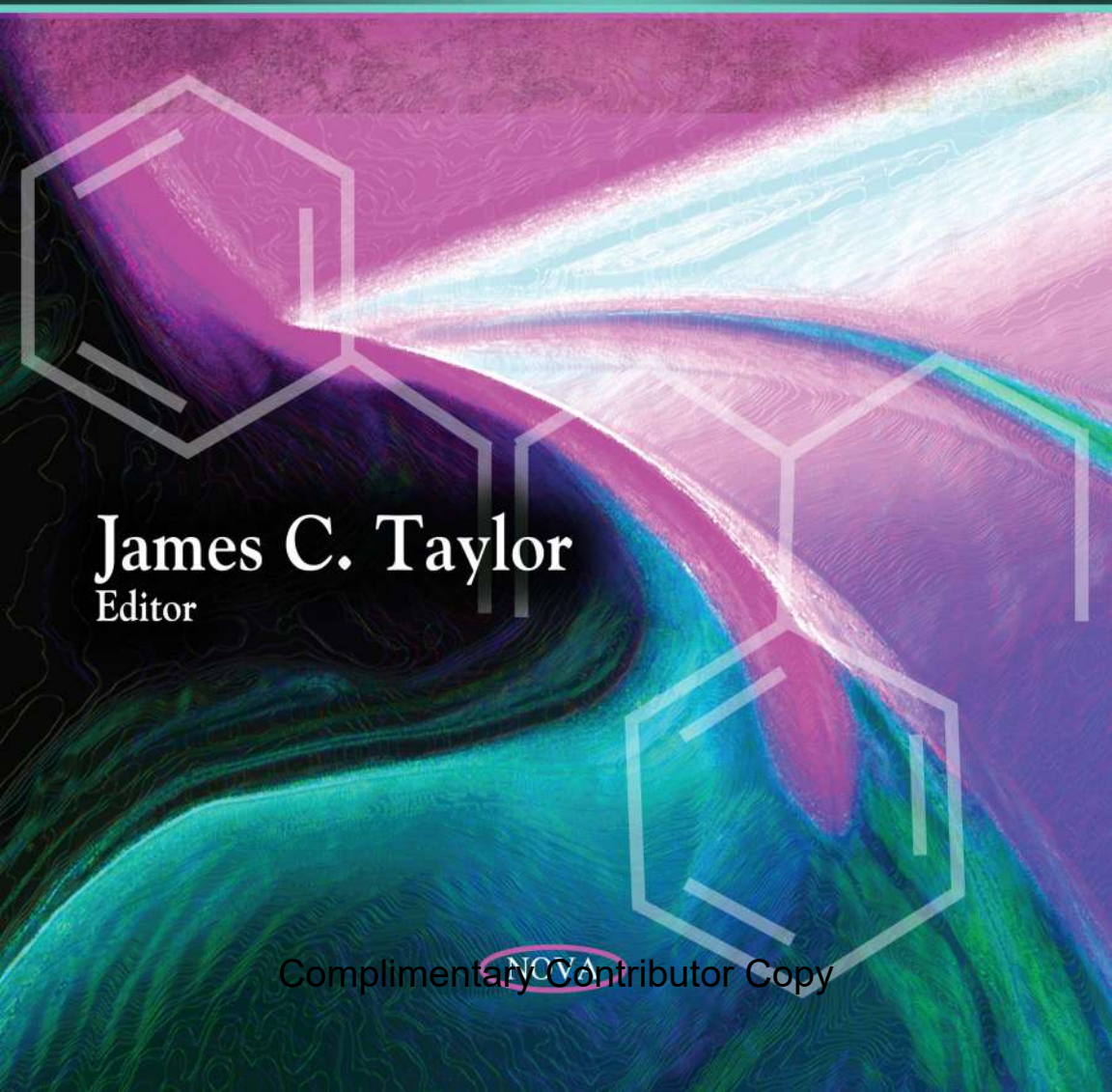

James C. Taylor
Editor

ADVANCES IN CHEMISTRY RESEARCH

VOLUME 59

ADVANCES IN CHEMISTRY RESEARCH

Additional books and e-books in this series can be found on Nova's website under the Series tab.

ADVANCES IN CHEMISTRY RESEARCH

VOLUME 59

JAMES C. TAYLOR
EDITOR

nova
science publishers
New York

NOTICE TO THE READER

Library of Congress Cataloging-in-Publication Data

ISBN: 978-1-53617-113-6
ISSN: 1940-0950

Published by Nova Science Publishers, Inc. † New York

CONTENTS

PREFACE

This compilation opens with a study on the catalytic conversion of methanol to olefins, mainly SAPO-34 and ZSM-5, as well as the synthesis, properties, applications.

A description of phenylalanine ammonia-lyase is presented in relation to structure, localization, expression, regulation, assay methods and the factors influencing phenylalanine ammonia-lyase activity, as well as its importance to the phenylpropanoid pathway for plant growth and development.

The authors critically analyze the development of molecular nanocatalysts based on organochalcogenligands and their applications in the transfer of hydrogenation.

Following this, the progress in applications of dimensional analysis and similarity theory in electrochemical kinetics and electrochemical engineering is discussed. The use of dimensionless groups in problems of current density distribution and electrochemical mass transfer is described and the similarity criteria involved are considered.

The authors focus on various solvent-minimized sample pre-treatment procedures which are inexpensive and offer minimal exposure to toxic organic solvents during sample analysis.

The concluding chapter explores bis-azides, i.e., organic compounds presenting two azido groups in their structures. Their utility in synthetic

group transformation is covered, as well as in polymer chemistry, the preparation of bioactive compounds, click chemistry, and in the synthesis of cross-linked DNA.

Chapter 1 - Methanol is a major chemical building block used to manufacture formaldehyde, MTBE, acetic acid and a wide range of other chemical products. The slowdown in MTBE demand, mainly due to the decision taken by California and later by other states in the US to eliminate its use in the gasoline, is causing some of the producers in the world to explore alternate utilization of their existing methanol plants. One such utilization is the conversion of methanol to olefins (MTO). The production of light olefins from methanol was first realized around 1977, during the development of Mobil's methanol to gasoline (MTG) process. In the MTG process, where ZSM-5 is used as a catalyst, methanol is first dehydrated to dimethyl ether (DME). The equilibrium mixture of methanol, DME and water is then converted to light olefins. Here in this research the authors study catalytic conversion of MTO, mainly SAPO-34 and ZSM-5, synthesized, properties, applications.

Chapter 2 - Phenylalanine ammonia-lyase (PAL) (E.C. 4.3.1.5) is a key and regulatory enzyme of the biosynthesis pathway of the phenylpropanoids and their derivatives. PAL catalyzes the transformation by the non-oxidative deamination of the amino acid *L*-phenylalanine in *trans*-cinnamic acid, without the requirement of cofactors; this is the first step for the biosynthesis of phenylpropanoid-derived compounds. The produced cinnamic acid is the direct precursor of several phenolic compounds, such as tannins, flavonoids, lignans, coumarins and lignins, which play an important role in plant growth and development. Studies with transgenic plants have shown that the activity of this enzyme is one of the main control points in the regulation of the phenylpropanoid route. Phenylalanine ammonia-lyase may be isolated from various sources, and its presence may be observed in a wide variety of higher plants and in some yeasts, fungi and bacteria. Immunocytochemical methods have shown that in plants, the synthesis of this enzyme can occur in the cytoplasm and chloroplasts. In many plants, a small multi-gene family encodes PAL and the expression of the *PAL* gene is regulated by several factors, such as mechanical injury, infections and plant development. The

PAL levels may fluctuate significantly at relatively short intervals in response to a wide variety of stimuli, and the concomitant increase in the phenylalanine ammonia-lyase and phenolic compounds levels has been demonstrated in plant tissues. PAL activity may be regulated by abiotic and biotic factors, such as light, wounding, temperature, UV irradiation, nutrient deficiency, herbivory, growth regulators, mechanical injuries, metal ions, insect attack, fungal and viral infections, as well as the stage of plant development and the degree of cell and tissue differentiation. In some species, elicitors induce PAL transcriptionally and enzymatically. This chapter will present a description of phenylalanine ammonia-lyase, in relation to structure, localization, expression, regulation, assay methods and the factors influencing PAL activity, as well as its importance to the phenylpropanoid pathway for plant growth and development.

Chapter 3 - Organochalcogen compounds have been used as the building blocks for the development of a variety of catalysts for several chemical transformations including transfer hydrogenation, which has been thoroughly studied during last two decades. Transfer hydrogenation, a reaction in which carbonyl compounds are reduced to the corresponding alcohols, is extremely important as it avoids the requirement and use of inflammable hydrogen gas and equipment associated to handle it. Organochalcogen ligands (with or without co-ligands) in combination with a metal salt have been used as a catalyst for this reaction. Such catalysts include both transition metal complexes as well as nano-catalysts. The catalysts, developed using organochalcogen compounds, have been reported to be less moisture- and air-sensitive. In addition, they are equally efficient as that of phosphorous based catalytic systems and, sometimes more efficient than the phosphorous counterpart. A critical analysis of the the development of molecular as well as nanocatalysts based on organochalcogen ligands and their application in the transfer hydrogenation is presented in this chapter. In addition to covering the synthesis of chalcogen ligands, their metal complexes and nanoparticles (NPs), emphasis has also been laid down on the catalytic potential and mechanisms of catalysis. It also includes the tools used for characterization as well as future scope of this area.

Chapter 4 - The progress in the application of dimensional analysis and similarity theory in electrochemical kinetics and electrochemical engineering is discussed. The use of dimensionless groups in problems of current density distribution and electrochemical mass transfer is described and the similarity criteria involved are considered. It is shown that dimensional analysis and similarity theory can be successfully used for studying the kinetics of different electrode processes, including the consideration of electrochemical charge transfer. The proper dimensionless quantities (i.e., similarity criteria) are generalized and the approximating relationships between them are analyzed. The results of numerical simulation of the kinetics of a two-stage electrochemical reaction with a partial transfer of intermediates between the electrode surface and the bulk solution are considered in the light of the concept of dimensional analysis and similarity theory. The main advantages of the application of dimensional analysis and similarity theory in pure and applied electrochemistry are summarized in this chapter.

Chapter 5 - Sample pretreatment involving extraction, pre-concentration and clean-up has become a bottleneck in the method development and sample analysis. Thus in this chapter the authors focus on various solvent-minimized sample pre-treatment procedure which are inexpensive and since a very little solvent is used in these techniques, there is minimal exposure to toxic organic solvents during sample analysis. A comparative discussion on the various advantages and limitations of each technique has also been discussed. Emphasis has been towards the selection of a method which can be used for routine analysis of drugs or environmental pollutants based on recent analytical techniques such as HPLC and GC. The effects of several variables on the method performance has been also detailed the technique of Microextraction has several advantages over traditional methods such as simple operation, miniaturization of technique and minimization of organic solvents used in sample preparation. These techniques are rapid, sensitive and virtually solvent free. Motive is towards selection of a green sample preparation techniques over traditional extraction methods in routine laboratory.

Chapter 6 - Organic azides are an important and versatile class of chemical compounds. They present industrial, academic, and biological applications. In addition, they can be obtained from a variety of synthetic methods. The present book chapter will focus specifically on bis-azides, *i.e.*, organic compounds presenting two azido ($-N_3$) groups in their structures. The utility of them is going to be covered in synthetic group transformation, polymer chemistry, in the preparation of bioactive compounds, in click chemistry, and in the synthesis of cross-linked DNA.

In: Advances in Chemistry Research ISBN: 978-1-53617-112-9
Editor: James C. Taylor

Chapter 1

A REVIEW ON THE PRODUCTION OF LIGHT OLEFINS FROM HYDROCARBONS CRACKING AND METHANOL CONVERSION

Ehsan Kianfar* *and Mahmoud Salimi*
Department of Chemical Engineering, Arak Branch,
Islamic Azad University, Arak, Iran

ABSTRACT

Methanol is a major chemical building block used to manufacture formaldehyde, MTBE, acetic acid and a wide range of other chemical products. The slowdown in MTBE demand, mainly due to the decision taken by California and later by other states in the US to eliminate its use in the gasoline, is causing some of the producers in the world to explore alternate utilization of their existing methanol plants. One such utilization is the conversion of methanol to olefins (MTO). The production of light olefins from methanol was first realized around 1977, during the development of Mobil's methanol to

* Corresponding Author's Email: e-kianfar94@iau-arak.ac.ir; ehsan_kianfar2010@yahoo.com.

gasoline (MTG) process. In the MTG process, where ZSM-5 is used as a catalyst, methanol is first dehydrated to dimethyl ether (DME). The equilibrium mixture of methanol, DME and water is then converted to light olefins. Here in this research we study catalytic conversion of MTO, mainly SAPO-34 and ZSM-5, synthesized, properties, applications.

Keywords: methanol to dimethyl ether process, fossil fuels, fixed-bed reactor, ZSM, catalyst, olefin

ABBREVIATIONS

MTG	Methanol to Gasoline
DME	Dimethyl ether
FCC	Fluid Catalytic Cracking
MTO	Methanol to olefins
HC	Hydrocarbon
NOx	Nitrogen oxides
PM	Particle matter
CO	carbon monoxides
CO_2	carbon dioxide
WHSV	Weigh hourly space velocity
GHG	Greenhouse gas
MTBE	Methyl t-butyl ether
MTA	Metric tons annually
HM	H-Mordenite
MTP	Methanol to propylene
SAPO	silica-alumina-phosphates
RGA	Refinery Gas Analyser

1. INTRODUCTION

1.1. The U.S. Methanol Market

During the 1980's and 1990's the United States was the largest methanol consuming and producing country in the world. Now that distinction goes to China with approximately 26 million tons of methanol production in 2012. But the US is making a comeback in methanol production. The methanol industry is becoming a significant player again in US natural gas consumption [1-3]. Prior to the sharp increases in natural gas prices in the late 1990's and early 2000's, the US had approximately 10 million metric tons of methanol capacity, consuming about 0.9 bcf/d of natural gas. By the end of 2005, US methanol capacity had been reduced to approximately 785 thousand tons per year, about 8 percent of its former peak. The US demand for methanol was met from imports. That's about to change. If all of the planned methanol capacity growth in the US materializes, we could see more than 16 million metric tons of new methanol capacity, which would consume an incremental volume of more than 1.4 bcf/d of natural gas. Methanol is a basic building block for many chemicals with formaldehyde, acetic acid and MTBE (for export) the three major consumers of methanol in the US. Methanol has also become a major feedstock for olefins production in China and more than 7 million metric tons per year of methanol is blended into gasoline each year in China. Small volumes are used as high performance race car fuel. It is well-known in the methanol industry that a number of new, relocated and restarts of methanol plants in the US have been announced. There are also a number of projects under evaluation that have not been announced publicly. The list might be surprising to some, but below are the projects that are underway, announced or unannounced. Capacities are nameplate and may not be the exact production capability [4-6]. The first table includes the *OCI integrated methanol and ammonia* plant which re-started last year and others that are on our highly probable list. Lyondell applied for permitting last year and current plans are to have the plant operational in early Q4 of this year. The G2X Energy plant in the Table 1 is

beginning construction immediately with completion planned for Q2, 2014 [7, 221].

Table 1. North America Methanol Expansion Forecast 2012-2016 [221]

Name	Location	Ownership	Capacity	Timing
New Projects and Re-Starts with High Probability				
OCI-Beaumont	Beaumont, TX	OCI	750	Q3 2012
Lyondell		LyondellBasell	740	Q4 2013
Former Coastel Plant	Pampa, TX	G2X Energy	65	Late 2014
Methanex	Geismar, LA	Methanex	1000	Q4 2014
Celanese	Clear Lake, TX	Celanese	1300	Q3 2015
Total			3855	
Jim Jordan & Associates, LP				

1.2. Global Marketing and Production

Methanol is a global commodity and our earnings are significantly affected by fluctuations in the price of methanol, which is directly impacted by changes in methanol supply and demand. Demand for methanol is driven primarily by levels of industrial production, energy prices and the strength of the global economy. Demand for methanol grew by 5% in 2012, leading to global demand of approximately 51 million tones, excluding demand from integrated methanol-to-olefins facilities. The increase in demand was driven by both traditional derivatives and energy-related applications in Asia, particularly in China. Industry supply additions outside of China in 2012 consisted primarily of the restart of second Motunui facility in New Zealand, which added 0.7 million tones to the site's annual operating capacity, and the restart of a 0.7 million tone facility in Beaumont, Texas [8-10, 222]. New production from supply additions inside China was consumed in that country and China continued to be a significant net importer of methanol. Overall, industry conditions were balanced in 2012 and this led to a relatively stable methanol pricing environment. Our average realized price for 2012 was $382 per tones compared with $374 per tones in 2011. The outlook for

methanol demand growth continues to be strong. The wide disparity between the price of crude oil and that of natural gas and coal has resulted in an increased use of methanol in energy-related applications, such as direct methanol blending into gasoline and DME and biodiesel production. Growth of direct methanol blending into gasoline in China has been particularly strong and we believe that future growth in this application is supported by numerous provincial and national fuel-blending standards, such as M15 or M85 (15% methanol and 85% methanol, respectively) [11-13, 222]. China is also leading the commercialization of methanol's use as a feedstock to manufacture olefins. The use of methanol to produce olefins, at current energy prices, is proving to be cost competitive relative to the traditional production of olefins from naphtha. There are now five methanol-to-olefins (MTO) plants operating in China, with the capacity to consume approximately seven million tons of methanol annually. Three of these projects were not expected to impact the merchant methanol market as they are integrated projects – coal to methanol to olefins. However, over the past two years, these plants have purchased methanol to supplement their own methanol production. The two non-integrated plants (representing over 2 million tons of methanol demand annually) are dependent on merchant methanol supply. Several other integrated and non-integrated projects are currently under construction in China and the demand for methanol as a feedstock for producing olefins is anticipated to continue to grow. While methanol demand in energy-related applications is strongest in China, there are an increasing number of countries around the world that have projects in place or are considering adopting these applications on a wider scale. Direct methanol blending into gasoline is being used in small quantities in the United Kingdom, Netherlands and Iceland, and other countries, including Australia and Israel, are conducting fuel-blending trials. DME is being produced and DME projects are under development in various countries including Japan, Taiwan, Turkey, the United States, Trinidad, India and Indonesia. We believe demand potential into energy-related applications and olefins production will continue to grow [14-17, 221]. We increased our operating capacity in 2012 and anticipate further increases over the next few years. We recently announced our commitment to add a further 0.7 million

tons of operating capacity to our New Zealand site through the restart of the Waitara Valley facility and a debottlenecking project at the Motunui site. We are relocating one of our idle Chile facilities to Geismar, Louisiana and the plant is expected to commence operations by the end of 2014. We are also considering the relocation of a second facility to the Geismar site and expect to make a decision on this project by mid-2013. Beyond our own capacity additions, there is a modest level of new capacity expected to come on stream over the next few years outside of China. There is a 0.8 million tone plant expected to restart in Channelview, Texas in 2013 and a 0.7 million tone plant expected to start up in Azerbaijan in 2013. We expect that production from new capacity in China will be consumed in that country and that higher-cost production capacity in China will need to operate in order to satisfy demand growth. Entering 2013, methanol demand has continued to be healthy, supported by a higher energy price environment. With few industry capacity additions expected over the next few years relative to expected demand growth, we believe we are well positioned with several of our own initiatives to increase operating capacity. As production from these initiatives comes on line, we believe our leadership position in the industry will be strengthened and we will have significant upside potential to cash flows and earnings. The methanol price will ultimately depend on the strength of the global economy, industry operating rates, global energy prices, new supply additions and the strength of global demand. We believe that our financial position and financial flexibility, outstanding global supply network and competitive cost position will provide a sound basis for Methanex to continue to be the leader in the methanol industry [18-20, 222].

1.3. Methanol Manufacturing in Iran

Methanol demand in Iran made up for nearly 20% of the overall demand in the Middle-East and African region in the year 2011. Like in Saudi Arabia, increases in oil prices have boosted growth in many industries in Iran. The availability of relatively cheap feedstock, combined with the healthy methanol demand from Asian countries, supported the growth of

Iran's economy during the last decade. Further capacity additions are planned in the region in the coming decade to meet the expected increase in domestic demand and the anticipated rise in export demand from Asian countries. Iran's methanol demand was mainly driven by the acetic acid sector. MTBE and DMT were the two other major methanol end-use markets. The major sector, acetic acid, is expected to witness significant growth in coming years [21-23, 222-223]. Methanol is produced naturally in the anaerobic metabolism of many varieties of bacteria, and is ubiquitous in the environment. As a result, there is a small fraction of methanol vapor in the atmosphere. Over the course of several days, atmospheric methanol is oxidized with the help of sunlight to carbon dioxide and water. Currently, Iran has achieved 10% of the world's share in methanol production and its industrial exports are available in markets of 159 countries, mainly in Iraq, China, the UAE, India and South Korea. The National Petrochemical Company, Kaveh Glass Industry Group and Public Joint Stock Company are the biggest players in the Iranian industry. Trading of Iranian petrochemical products such as polymers had ceased in Japan and South Korea, but some chemicals that are considered a necessity still had to be imported from Iran. Iran has the second-largest petrochemical output in the Middle East, next to Saudi Arabia. One important Petrochemical Complex which is a great methanol supplier in Iran is Zagros Petrochemical Co. The second unit of methanol production in the Zagros complex was put into operation, so Iran produces 12% of the whole methanol production of the world. This complex is the world biggest methanol production center. Due to enjoying sufficient natural gas source as well as prosperous international market of ethanol, the second unit was constructed by the first. Elaborating on the unit technical features for this facility is 875,000 Euros as well as 1,038 bn Rials [24-26, 222-223]. Was invested on this project. Utilizing auto-thermal reactor in reforming unit to break natural gas hydro carbora and it's changing to synthesized gas, making use of gas-cooled reactor in methanol synthesizing unit, fixing cooling towers instead of sea water, are some of the project particular and unique features. These features were applied in constructing a petrochemical unit in Assaluyeh for the first time and it proved a success. Natural gas and oxygen are the unit ingredients. Provided by South Pars

phase one and two, the required natur^#,^#al gas volume of the project is about 188,000 cm an hour. Supplied by Mobin Petrochemical Unit, the required oxygen for the project is 84,500 cm [27, 224].

2. OLEFINS GLOBAL MARKETING

Light olefins such as ethylene, propylene and butylenes are important intermediates for the petrochemical industry. Global consumption of ethylene, mainly for the production of polyethylene, is expected to increase to 114 million metric tons by 2005 from 80.5 million tons in 1998 [223-224]. Total annual market represents $300 billion marketing for Olefin components in 2011. Table 2 shows provides detailed information for each of these molecules.

Table 2. Olefins Global Production and Marketing from 2012-13 [224]

Component	Volume (MT)	Price ($/Kg)	Market (b$)	Main Applications
Ethylene	115	1.25	144	Polyethylene
Propylene	83	1.20	100	Polypropylene
Linear Butenes	37	1-2	37-74	Co-monomers in various plastics
Isobutene	15	1.7-2	25-30	Tires, Organic glass, PET, Fuels
Butadiene	10.6	1.8	19	Tires, Nylon, Coated Polymers
Isopropene	1	2	2	Tires Adhesives

2.1. Global Propylene Production and Marketing

The global propylene and derivative markets are in the midst of a major transition with repercussions for both the supply and demand side. The impact of the global shift to lighter feedstocks among steam cracker operators has set in motion developments that affect the type and location of

new investment, regional pricing levels and profitability of propylene and derivative producers. The reduction of propylene supplies from steam crackers and refineries together with the resulting higher price levels are supporting investments in on-purpose production, mainly propane-dehydrogenation and in China also coal-based processes. Higher propylene prices are also driving downstream portfolio changes as many large producers increasingly focus on higher value derivatives, particularly in North America and West Europe. Despite some consolidation, polypropylene will remain by far the largest propylene derivative well into the future [28-30, 224]. The US propylene market has seen prices rise in July and August, largely on the back of higher feedstock naphtha and propane costs. A recent spate of cracker issues has lent some tightness to supply. However, sources say buyers are starting to build their inventories before retreating to the sidelines in an effort to drive down prices. European propylene producers hold bullish price ideas for the near term, if upstream costs remain firm, and because of upcoming cracker turnarounds. Demand has been healthy in August, despite the summer holidays in Europe, because of reduced production and forthcoming plant turnarounds. Buying activity was driven by the strong performance of the upstream sectors and expectations of higher contract prices in September [31-33, 225]. In Asia, propylene prices have been supported by new downstream capacities and a series of shutdowns at crackers and propylene units. However, Chinese and Taiwanese buyers expect their import demand to weaken when new domestic capacities come on stream between August and the fourth quarter of 2013.A partial list of the propylene products and derivatives (capacity and propylene consumption data only) covered includes[225]:

- Propylene (Refinery grade; PG/CG, Total Propylene)
- Acrylic Acid
- Acrylonitrile
- Normal Butanol
- Cumene
- Epichlorohydrin
- 2-Ethylhexanol

- Isopropanol
- Oligomers
- Polypropylene
- Propylene Oxide
- FCC

2.2. Ethylene Global Marketing and Production

Major changes in the global ethylene markets are projected to take place over the next several years primarily driven by feedstock cost trends and sharply diverging consumption growth between geographic regions. China will continue to play a dominant role for both supply and demand growth as the country strives to achieve self-sufficiency at the ethylene derivative level. Investments in coal-based ethylene are in the take-off stage and will contribute about half of all announced capacity additions in China. Abundant, low cost ethane supplies from shale gas in the US are supporting a revival of investments in large integrated cracker projects, while the capacity wave in the Middle East has been abating with sharply reduced availability of new ethane supplies. Producers in the Middle East and Asia will be focusing increasingly on integrated steam cracker and refinery projects as well as higher value-added products often through diversification of product slates. In contrast, producers in Europe and developed Asian countries, such as Japan, will not only be exposed to the growing international competition, but also weak demand environment at home which may necessitate further rationalizations [34-36, 225]. The European ethylene market remains balanced, as output constraints, both planned and a few ongoing and new unplanned issues, are being offset by sizeable import volumes ex-Asia and ex-US, which have already been booked. Consumption is satisfactory, but not exceptional. There is some talk that polymer demand is weaker when compared with the non-polymer sector, although one player in the non-polymer sector suggested that its demand was also slightly less when compared with the same period last year [37-39, 225]. Ethylene

derivative players continue to struggle with the high prices, with European ethylene the highest out of all the regions, which is proving even more challenging amid the ongoing fragile economic climate, of which some downstream sectors are more resilient than others. In terms of MCP discussions for March, it is deemed too early in the month to have any precise indications, as players continue to monitor feedstock and olefin supply/demand developments. The general expectation is that producers are likely to push for an increase on the March contract price, based on higher production costs and the need to recoup losses for cracker margins, along with output constraints – both planned and unplanned. Precise targets were not yet forthcoming, although one producer suggested that the increase target would not be limited in magnitude. One buyer said it reluctantly acknowledged that a price increase would be likely if upstream costs were to remain high based on contract margin recovery [40-42, 225]. It is concerned that if the European ethylene contract price were to go up significantly over the next few months, it could further jeopardize downstream demand which remains modest. Spot margins (naphtha) slipped by €14/ton mainly due to the higher feedstock costs. Spot co-product credits rose by 3.2% following gains in all constituent chemicals. Euro-denominated spot ethylene values rose on the strengthening of the dollar, although spot prices in dollar terms were unchanged. Contract margins based on liquefied petroleum gas (LPG) softened by €35/ton due to a 2.8% gain in LPG costs. LPG prices rose by $5/ton but the effect was compounded by the stronger dollar. LPG margins retain the advantage over naphtha margins, at €43/ton [43-45, 225]. Average cracker run rates continue to be pegged around 80-85%, although a few cracker operartors said they were running closer to 90% and even above, depending on derivative portfolio and location. There is no further update on the status of the Naphtachimie cracker at the Lavera site, in France – which is a joint venture operation between INEOS and Total.

Table 3. List of recent European planned and Unplanned Ethylene Manufacturers [225]

Company	Cracker location	Timing	Planned or Unplanned
Shell	Moerdijk, the Netherlands	mid-March to end April, 6 weeks	Planned (not confirmed)
LBI	Munchmunster, Germany	mid March for around 25 days	Unplanned (not confirmed)
Versalis	Dunkirk, France	2H of February one week	Unplanned (not confirmed)
BASF	Antwerp, Belgium	26 April-24 June	Planned (not confirmed)
Total	Carling, France	April-May	Planned (not confirmed)
BPRP	Gelsenkirchen No.3, Germany	end May-early July	Planned (not confirmed)
Versalis	Priolo, Italy	August-September 6 weeks	Planned (not confirmed)
SABIC	Olefins No4, Geleen, Netherlands	15 September-20 October	Planned (not confirmed)
INEOS	Grangemouth, UK	end Q3	Planned (not confirmed)
INEOS	Cologne No 5, Germany	September-October	Planned (not confirmed)
ExxonMobil	Mossmorran, UK	Q3-2 weeks	Planned (not confimed)
Repsol	Tarragona, Spain	October-November	Planned (not confirmed)
Repsol	Sines, Portugal	December 2012 tbc	Temporarily idled

INEOS had previously said in a statement on 25 January that the unit was expected to restart in the first half of March and that repair work was well underway, following damage, which occurred on 22 December 2012. It added that once the unit would resume output, its operating rates were likely to be reduced for a period of time until the repair work is fully completed. The companies in question were not available to provide further comment at the time of writing. Repsol's cracker at Sines, in Portugal has not yet resumed output, according to the company, who declined to provide any further information. Previous reports suggested that the cracker could restart during February, according to market sources the cracker was taken down in December 2012, thought to be because of poor cracker economics, although the reason for the downtime was not officially confirmed. LyondellBasell's cracker at Muenchmuenster, in Germany is experiencing technical

problems, which is expected to lead to an unplanned outage in mid-March, which is likely to last for around 25 days, according to market sources. The company declined to comment on this in line with their policy. Maintenance is due to take place at Versalis'cracker at Dunkirk, in France next week for around 5-7days, in order to address some current technical problems [47-49, 225]. Table 3 shows List of recent European planned and Unplanned Ethylene Manufacturers.

2.3. OLEFINS Production Processes (Olefins Production Overview)

2.3.1. Steam Cracking

Steam cracking (also known as pyrolysis) of hydrocarbon feedstocks is the main source of olefins production. Virtually all ethylene and around 70% of world propylene are produced by steam cracking. 4 Hydrocarbon feedstocks most often include ethane, naphtha, and gas oil, although propane and other hydrocarbons may be used [50-51, 226]. The same process is used regardless of the feedstock employed, although capital and energy requirements will differ depending on both the feedstock and the desired product slate. While there are a number of configurations available to accomplish pyrolysis, essentially all begin with the introduction of hydrocarbon feed and steam into a tubular pyrolysis furnace. In the pyrolysis furnace the feed and steam are heated to a cracking temperature of about (800-900°C). Temperature requirements for cracking ethane will be higher than for heavier feedstocks. The distribution of the products highly depends on the feed stock used. While lower molecular weight feedstock (e.g., ethane) will give a high percentage of ethylene (see Table 4); yields of propylene will increase with higher molecular weight feedstock (e.g., naphtha). Although steam-crackers represent the most important source, propylene supply is very limited due to the low propylene yield. During the last decade, new technologies have been developed for the purpose of enhancing the propylene output of steam crackers [52-55, 226]. These technologies include Olefins Conversion Technology (OCT) by ABB

Lummus 6, Superflex Technology by Kellogg Brown & Root 7, and Propylur Technology by Lurgi. 8 OCT is based on the metathesis reaction which converts one mole of ethylene and one mole of butylenes to form two moles of propylene. When integrated with steam cracking unit, OCT is claimed to boost the propylene to ethylene ratio from 0.65 (with SC alone) up to 1.0. On the other hand, Superflex and Propylur technologies can handle wider range of hydrocarbon feeds, generally in the range of C4-C8 and can be designed to produce P/E ratios of about 0.8.

Table 4. Wt% of Products from Cracking Various Feedstocks [226]

	Ethane	**Propane**	**Naphta**	**Gas Oil**
Ethylene	76	42	31	23
Propylene	3	16	16	14
C_4	2	5	9	9
Hydrogen	9	2	2	1
Methane	6	28	17	11

2.3.2. Fluidized Catalytic Cracking (FCC)

Currently, 31.2 million tons per year or 28% of the world propylene production is being produced in the Fluid Catalytic Cracking (FCC) units. In FCC, heavy (vacuum) gas oils from refineries are cracked into lighter fractions. The most important product is gasoline with light olefins regarded as byproducts. Recently, a new catalytic cracking technology was developed, the so-called Deep Catalytic Cracking process (DCC) [56-57]. This process was developed on the basis of a normal riser-cracking process by a Chinese research institute. DCC produces light olefins from heavy feedstocks with high yields. Two distinct modes of DCC operations are reported, maximum propylene and maximum iso-olefins. The key to these processes relies on a highly selective catalysts and appropriate reaction conditions. Table 5 shows a comparison between the DCC and the conventional FCC units. A substantial increase in the light olefins yields is observed with the new DCC technology. Propane dehydrogenation

technology has gained importance in recent years due to the increase in consumption of propylene for the production of polypropylene. There are four technologies that can be licensed for propane dehydrogenation. These are CATOFIN from ABB Lummus, Oleflex from UOP, Fluidized Bed Dehydrogenation (FBD) from Snamprogetti, and Steam Active Reforming (STAR) from Phillips Petroleum.A similar technology can be applied to ethane dehydrogenation, but an economically attractive commercial reactor has not been built [58-59, 227]. The main drawback of the dehydrogenation technology is that it is equilibrium limited and hence requires high temperatures. The low conversion necessitates a large separation step to recover products and recycle large volume of unreacted paraffin. To overcome these problems, researchers are focusing in two directions: i) using membrane systems to obtain high conversion at low temperature by separating the hydrogen and shifting the process equilibrium; ii) oxidative dehydrogenation to overcome the equilibrium limitation and to operate at low temperatures [60-62, 228]. However, despite some progress made in the membrane area and in the oxidative dehydrogenation area, no commercial plants are believed to be currently operational, although pilot or demonstration plants have been built and operated.

Table 5. DCC & FCC Technologies: Yield Comparison [227-228]

Overall Yields, wt%		
	DCC	FCC
C2-	11.9	3.5
C3-C4	42.2	17.6
C5+ naphtha	26.6	54.8
Light cycle oil	6.6	10.2
Decanted oil	6.1	9.3
Coke	6.0	4.3

Loss	0.6	0.3
Total	100.0	100.0
Olefins Yields, wt%		
Ethylene	6.1	0.8
Propylene	21.0	4.9
Isobutylene	5.1	1.9
Total butylenes	14.3	8.1

2.3.3. Oxidative Coupling of Methane

A break-through in the area of methane chemistry occurred in 1982 with the publication of a paper by Keller and Bhasin [15] of Union Carbide (UC), which demonstrated that two molecules of methane could be coupled oxidatively to produce ethane and ethylene:

$$2CH_4+0.5O_2 \rightarrow C_2H_6+H_2O \quad (1)$$

$$2CH_4+O_2 \rightarrow C_2H_4+2H_2O \quad (2)$$

The initial work showed that the reaction was best carried out in a cyclic mode in which the catalyst was first oxidized and the oxidized material was then exposed to the methane, producing ethane and ethylene. Later, results obtained by Hinsen et al. [63-66, 229] have shown that a co-feed mode could be used in which both methane and oxygen was fed simultaneously to the catalyst. One year later, Lunsford and co-workers published an important paper describing the use of Li doped MgO catalysts for the reaction under co-feed conditions, demonstrating that this catalyst has high activity for converting methane to C2+ compounds in the presence of O2. 17 On the other hand, the introduction of chlorine into the reactants stream has shown to have a very positive effect on the yield of ethylene [67-70, 230]. During the last decade, a large amount of research in the MOC field has been carried out by the oil and gas companies and other large organizations. Such companies include UC, Arco, BP, Amoco, Mobil, British Gas, Standard Oil Co. and Philips Petroleum. 10 A specific example of catalyst reported by the above include a BP-type catalyst NaCl/MnOx/SiO2 prepared by the co-gel

method 19, which is reported to give a C2+ yield of 30% compared to 11.7% for the same catalyst prepared by the traditional route of impregnation. Despite the huge amount of research done on the oxidative coupling of methane, the process still suffers from some drawbacks that need to be solved before it can be commercialized [71]. These drawbacks include limited selectivity to C2 and high exothermicity of the reaction which requires special reactor design. Additionally, this is complicated by the fact that metals normally used for construction of reactors catalyze the total combustion of methane [72].

2.3.4. The Methanol to Olefins Process

Methanol is a major chemical building block used to manufacture formaldehyde, MTBE, acetic acid and a wide range of other chemical products. The slowdown in MTBE demand, mainly due to the decision taken by California and later by other states in the US to eliminate its use in the gasoline, is causing some of the producers in the world to explore alternate utilization of their existing methanol plants [73-74]. One such utilization is the conversion of methanol to olefins (MTO). The production of light olefins from methanol was first realized around 1977, during the development of Mobil's methanol to gasoline (MTG) process. In the MTG process, where ZSM-5 is used as a catalyst, methanol is first dehydrated to dimethyl ether (DME). The equilibrium mixture of methanol, DME and water is then converted to light olefins. A final reaction step leads to a mixture of higher olefins, n/*iso*-parrafins, aromatics and naphthenes [231]:

$$2CH_3OH \leftrightharpoons^{+H_2O}_{-H_2O} CH_3OCH_3 \xrightarrow{-H_2O} C_2^{=} - C_5^{=} \rightarrow \quad \text{N/iso-paraffins, aromatics, } C_6^{+} \text{ olefins} \quad (3)$$

Because they are intermediate in the MTG process, an interruption of the reaction leads to production of light olefins instead of gasoline. An appropriate process for this purpose was developed later by Mobil. Since then several attempts were made to selectively produce light olefins from methanol on zeolite catalysts, not only on medium-pore zeolites but also on

small-pore zeolites and to a lesser extent, on large-pore zeolites. Among all the investigated zeolites, ZSM-5 and SAPO-34 have received a lot of attention due to their excellent catalytic performance for the MTO reaction. Unfortunately the use of ZSM-5 zeolite results in a wide range of products, in particular aromatics and paraffins. In order to improve the selectivity to light alkenes several approaches have been proposed including operating the reactor at high space velocity and low methanol conversion and introducing some modifications on the catalyst [75-76]. The first solution introduces the need to recycle and results in a rapid catalyst deactivation. On the other hand considerable effort has been made to modify the ZSM-5 catalyst for the purpose of increasing its selectivity to light olefins. An extensive review of the literature concerning this has been given by Chang. In all cases the production of aromatics could not be avoided at high methanol conversion. The use of small pore zeolites and in particular SAPO-34 permits the selective formation of light olefins even at 100% methanol conversion. This performance has been attributed to the cage structure of SAPO-34, as compared to the channel structure in ZSM-5, and to the intermediate acidity. Currently, two MTO process technologies are available namely Mobil's MTO process and UOP/Hydro MTO process. Mobil's MTO process was demonstrated in a 100 BPD fluid bed facility in Germany. The process was originally designed for gasoline production and later extended to demonstrate the MTO process. The plant was operated at a pressure between 2.2 and 3.5 bar and a temperature of about 500°C [77-79, 232]. The catalyst used was a modified ZSM-5 zeolite type catalyst. At steady state conditions the olefin yield was more than 60%. On the other hand, UOP and Norsk Hydro have jointly developed and demonstrated an improved methanol to olefins process which has been ready for license since 1996. The process, schematically shown in Figure 1, offers a high selectivity to light olefins. 80% of the carbon in the methanol feed is converted into ethylene and propylene and 10% to butylenes giving a total light olefins yield of about 90%. By adjusting the operating conditions, ethylene to propylene product weight ratio can be changed from 1.5 to 0.75. 30 The catalyst employed is a modified silicoaluminophosphate (SAPO-34) originally discovered by Union Carbide in the 1980s. Although

thermodynamically favored, $C5^+$ hydrocarbons are produced at substantially lower level with SAPO-34 than with the ZSM-5 catalyst. Figure 1 shows UOP/Hydro MTO process.

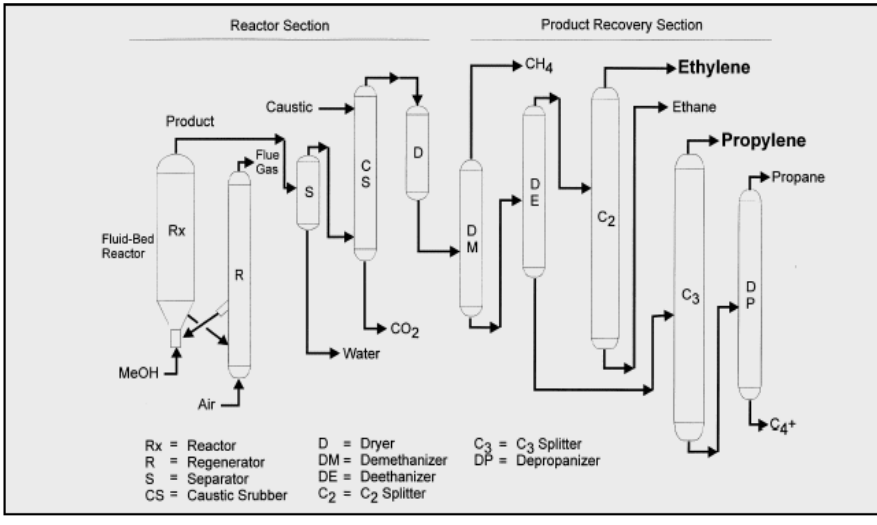

Figure 1. UOP/Hydro MTO process.

2.4. Olefin Productions: Processes Detailed Review

2.4.1. Ethylene Production Licenses

2.4.1.1. China Petrochemical Technology Co

The CBL cracking technology is a steam cracking technology developed by SINOPEC. The steam-cracking furnace for ethylene production can be designed with this technology. This technology provides processing flexibility for ethylene cracking operations and can handle feedstocks from ethane to heavy vacuum gasoil (HVGO). The CBL technology is a state-of-the art technology with low-investment cost of building new furnaces or

revamping old furnaces [80, 233]. CBL furnace is applicable to many feedstocks such as ethane, light hydrocarbons, natural gas liquids (NGLs), naphtha, light gasoline oil and HVGO. Different feedstocks can be cracked in the same furnace with varying operating condition; two feedstocks (for example, naph-tha and ethane) can also be cracked by different coils in one furnace. For heavy feedstocks in particular, the CBL technology shows special advantages—long run lengths (50 days to 70 days) and high ethylene/ propylene yields. For liquid and gas feedstocks, the characteristics of CBL technology are [233]:

- *Liquid feed:*
  - Coil configurations. Two-pass, high-selectivity coil configurations (2-1, 2/1-1, 4-1, etc.) are possible furnace designs. The first pass has a small diameter with a large specific surface area, which leads to a quick temperature increase. The second pass has a large diameter, which leads to a lower pressure drop and lower hydrocarbon partial pressure.

Appropriate coils are chosen based on different feeds and capacity requirements. The coil configura-tion of this technology combines the features of higher temperature, shorter residence time and lower hydrocarbon partial pressure and leads to the advantages of high cracking selectivity, long run length and larger capacity of a single coil.

- Transfer line exchanger (TLE). First stage or second stage options available.
- Dilution steam Injection. First stage (light feed) or second stage (heavy feed). By using this technique, coke formation from heavy oil in convection section coils can be minimized.
- Heat supply. Using a combination heat supply from hearth and sidewall allows temperature distribution of the hearth, and the heat transfer of the coil is uniform.
- High thermal efficiency. Up to 93%-94%.

- Variable frequency speed control driving motor can be adopted for induced draft fan.

- *Gas feed:*
  - For gas feed, the four-pass coil configuration (2-1-1-1) with residence time between 0.4 to 0.8 second is adopted. Linear or U type TLE is directly coupled with the outlet tube of one group of 2-1-1-1 coils. The TLE can be one stage, two stages or three stages. For ethane- cracking furnace, the running cycle is longer than 100 days. CBL technology was first commercialized in 1984, with a total of 44 units, including recently built units and revamps. To-tal processing capacity of more than 3.56 million metric tpy has been licensed.

2.4.1.2. Lummus Technology

To produce polymer-grade ethylene (99.95 vol%). Major byproducts are propylene (chemical or polymer-grade), a butadiene-rich C_7 stream, C_6 to C_8 aromatics-rich pyrolysis gasoline and high-purity hydrogen [81, 233]. Hydrocarbon feedstock is preheated and cracked in the presence of steam in tubular SRT (short residence time) pyrolysis furnaces (1). This approach features extremely high olefin yields, long runlength and mechanical integrity. The products exit the furnace at 1,500°F to 1,600°F and are rapidly quenched in the transfer line exchangers (2) that generate super high-pressure (SHP) steam. The latest generation furnace design is the SRT VII. Furnace effluent, after quench, flows to the gasoline fractionator (3) where the heavy oil fraction is removed from the gasoline and lighter fraction (liquids cracking only) [82-83, 233]. Further cooling of furnace effluents is accomplished by a direct water quench in the quench tower (4). Raw gas from the quench tower is compressed in a multistage centrifugal compressor (5) to greater than 500 psig. The compressed gas is then dried (6) and chilled. Hydrogen is recovered in the chilling train (7), which feeds the demethanizer (8). The demethanizer operates at about 100 psia, providing increased energy efficiency. The bottoms from the demethanizer go to the deethanizer (9). Acetylene in the deethanizer overhead is hydrogenated (10) or

recovered. The ethylene-ethane stream is fractionated (11) and polymer- grade ethylene is recovered. Ethane leaving the bottom of the ethylene fractionator is recycled and cracked to extinction. The deethanizer bottoms and condensate stripper bottoms from the charge compression system are depropanized (12). Methylacetylene and propadiene are hydrogenated in the depropanizer using CDHydro catalytic distillation hydrogenation technology. The depropanizer bottoms is separated into mixed C_6 and light gasoline streams (14). Polymer-grade propylene is recovered in a propylene fractionator (13).A revised flow scheme eliminates -25% of the equipment from this conventional flowsheet. It uses CDHydro hydrogenation for the selective hydrogenation of C2 through C, acetylenes and dienes in a single tower; reduces the cracked-gas discharge pressure to 250 psig; uses a single refrigeration system to replace the three separate systems; and applies metathesis to produce up to 1/3 of the propylene product catalytically rather than by thermal cracking, thereby lowering energy consumption by 15%. Energy consumptions are 3,300 kcal/kg of ethylene produced for ethane cracking and 5,000 kcal/kg of ethylene for naphtha feedstocks. Energy consumption can be as low as 4,000 kcal/kg of ethylene for naphtha feedstocks with gas turbine integration. As noted above, the new flow scheme reduces energy consumption by 14%. Approximately 40% of the world's ethylene plants use Lummus' ethylene technology. Many existing units have been significantly expanded (above 150% of nameplate) using Lummus' MCET (maximum capacity expansion technology) approach. Figure 2 shows PFD of Ethylene Production Unit under license of Lummus Technology Co [84-88, 233].

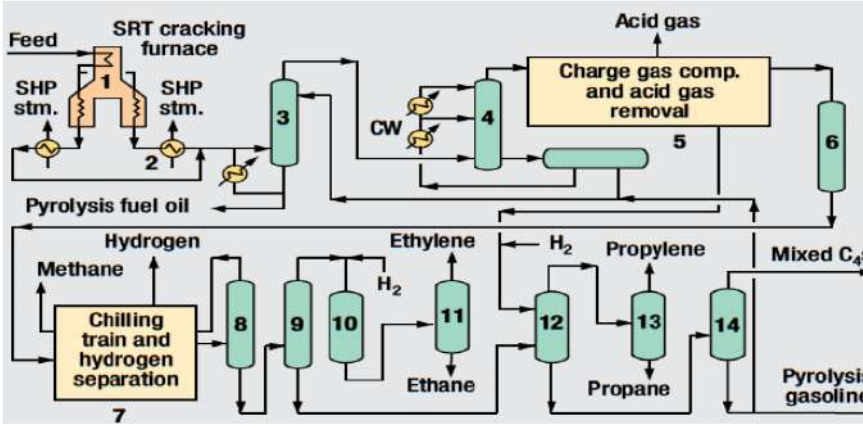

Figure 2. PFD of Ethylene Production Unit under license of Lummus Technology Co.

2.4.1.3. Linde Technology

To produce polymer-grade ethylene and propylene by thermal cracking of hydrocarbon fractions-from ethane through naphtha up to hydrocracker residue. Byproducts are a butadiene-rich C_4, stream, a C_6–C_8 gasoline stream rich in aromatics and fuel oil. Fresh feedstock and recycle streams are preheated and cracked in the presence of dilution steam in highly selective Pyro Crack furnaces (1). PyroCrack furnaces are optimized with respect to residence time, temperature and pressure profiles for the actual feedstock and the required feedstock flexibility, thus achieving the highest olefin yields. Furnace effluent is cooled in transfer line exchangers (2), generating HP steam, and by direct quenching with oil for liquid feedstocks[89-90, 233]. The cracked gas stream is cooled and purified in the primary fractionator (3) and quench water tower (5). Waste heat is recovered by a circulating oil cycle, generating dilution steam (4) and by a water cycle (5) to provide heat to reboilers and process heaters. The cracked gas from the quench tower is compressed (6) in a 4- or 5-stage compressor and dried in gas and liquid adsorbers (8). CO_2 and H_2S are removed in a caustic-wash system located before the final compressor stage. The compressed cracked gas is further cooled (9) and fed to the recovery section: front-end deethanizer (10), isothermal front-end C_2 hydrogenation (11), cold train (12), demethanizer (13) and the heat pumped low-pressure ethylene fractionatior

(14), which is integrated with the ethylene refrigeration cycle[91-93, 233]. This well-proven Linde process is highly optimized, resulting in high flexibility, easy operation, low energy consumption, low investment costs and long intervals between major turnarounds (typically five years). The C_3 from the deethanizer bottoms (10) is depropanized (15), hydrogenated (16) to remove methyl acetylene and propadiene (16) and fractionated to recover polymer grade propylene. C_4 components are separated from heavier components in the debutanizer (18) to recover a C_4 product and a C_5 stream. The C_5, together with the hydrocarbon condensates from rich gasoline product. Ethylene yields vary between 25%, 35%, 45% and 83% for gas oils, naphtha, LPG and ethane respectively. The related specific energy consumption range is 6,000/5,400/4,600 and 3,800 kcal/kg ethylene. Typical installation costs for a world-scale ISBL gas (naphtha) cracker are 800 (1,100) US$/ton installed ethylene capacity. Over 20 million tons of ethylene are produced in more than 50 plants worldwide. Many plants have been expanded in capacity up to 50% and more. Recent awards for world-scale ethylene plants include Borouge 2 and 3 (1.5 million metric ton/y each) in Abu Dhabi [94-96, 233]. Figure 3 shows PFD of Ethylene Production Unit under license of Lynde Technology Co.

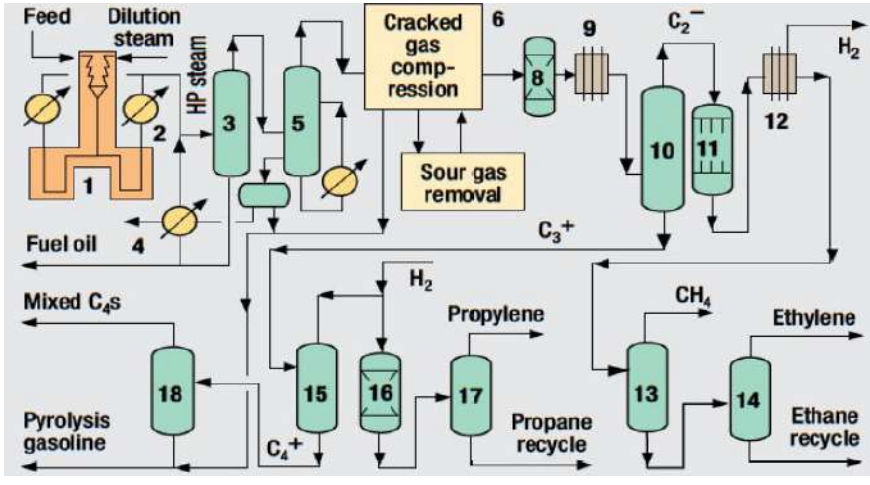

Figure 3. PFD of Ethylene Production Unit under license of Lynde Technology Co.

2.4.1.4. The Shaw Group Technology

To produce polymer-grade ethylene and propylene by thermally cracking hydrocarbon feedstocks (ethane through hydro-cracked residue). Shaw's key process technologies are[97-100, 233]:

- Ultra-selective cracking (USC) furnaces-Selective pyrolysis with proprietary quench exchanger systems
- Ripple tray and vapor flute-High capacity with fouling minimization for quench oil and quench water towers
- Advanced recovery system with heat-integrated rectifier (ARS/HRS) - Energy efficient cold fractionation.

The following description and diagram are given for liquid feedstock steam cracking. Fresh liquid feed as well as recovered ethane and propane are sent to USC furnaces (1). Contaminant removal may be installed on the fresh feed if required. A portion of the cracking heat may be supplied by gas turbine exhaust as preheated combustion air. Pyrolysis occurs at temperatures and residence time requirements specific to the feedstock and product requirements. The USC technology utilizes a number of radiant coil designs for the cracking furnaces to reduce residence time and coil pressure drop and to maximize ethylene yield. Rapid quenching preserves olefin yields and the heat of quenching is used to generate high-pressure steam. Lower temperature heat is recovered for the production of dilution steam. Pyrolysis fuel oil and gasoline by-products are recovered in the quench oil and quench water systems (2). Cracked gas (C_4 and lighter) is compressed (3), scrubbed with caustic to remove acid gases and dried prior to fractionation. C_3 and lighter components are separated from the C_4 and heavier components in the low fouling front-end dual pressure depropanizer (4). Overhead vapor of the high-pressure depropanizer is hydrogenated to remove acetylene, methyl acetylene and propadiene (5) and then routed to the HRS and demethanizer systems (6). The demethanization system includes a turbo-expander for energy efficiency and greater hydrogen recovery. Alternatively, the acetylene can be extracted as a high-purity product (8). The ARS minimizes refrigeration energy by using distributed

distillation and simultaneous heat and mass transfer in the HRS system. Two C_2 streams of varying composition are produced within the ARS/ HRS. The heavier C_2/C_3 stream is deethanized (7) and the C_2 overhead stream is fed directly to a low-pressure ethylene-ethane fractionator (9), which is integrated with the C_2 refrigeration system (9). Polymer-grade ethylene product is taken from the overhead from the ethylene-ethane fractionator.C_3s from the dual pressure depropanizer system are combined and may require further hydrogenation to remove methyl acetylene and propadiene (10). Either polymer-grade or chemical-grade propylene can be produced overhead from a propylene-propane fractionator. The propylene-propane fractionator can either be a high-pressure system that is condensed by cooling water or a low-pressure system that utilizes a heat pump (11).C_4 and heavier byproducts are further separated in a sequence of distillation steps. Ethane and propane are typically recycled to pyrolysis. Refrigeration is typically supplied by a cascade ethylene/propylene refrigeration system. Advantages of ARS technology are [101-104, 233]:

- Reduced chilling train refrigeration requirements due to chilling/ pre-fractionation in the HRS system.
- Reduced methane content in feed to the demethanizer, which reduces the demethanizer condenser duty and refrigeration loads.
- The dual feed ethylene fractionator (lower reflux ratio) reduces refrigeration loads and energy consumption.
- Reduced refrigeration demand via the use of an integrated heat pump on the ethylene-ethane fractionator.

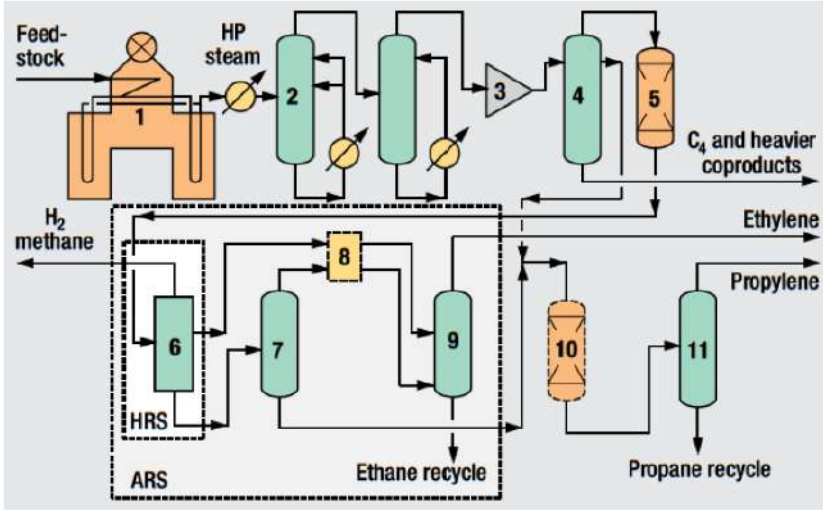

Figure 4. PFD of Ethylene Production Unit under licensed by Shaw Group Technology.

Once-through pyrolysis yields range from 57 wt% (ethane, high conversion) to 28 wt% (heavy hydrogenated gasoils) ethylene. Ultimate yields for ethylene of 85% from ethane feedstock and 32% from liquid feedstock are achieved. The ethylene plants with USC furnaces and an ARS/HRS recovery section are known for high reliability, low energy consumption, short startup time and environmental compliance. Shaw has designed and/or built 120 ethylene units. Expansion techniques based on ARS/HRS technology have increased original capacities by more than 100 percent. Shaw ethylene plants are now commonly integrated with refinery related processes such as FCC offgas recovery. Figure 4 shows PFD of Ethylene Production Unit under licensed by Shaw Group Technology.

2.4.1.5. The Technip (I) Technology

Produce polymer-grade ethylene and propylene, a butadiene-rich C_4 cut, an aromatic C_6-C_8 rich raw pyrolysis gasoline and a high-purity hydrogen by steam pyrolysis of hydrocarbons ranging from ethane to vacuum gasoils (VG0s). Progressive separation applied for concept in the fields either front-end or back-end hydrogenation is used in steam cracking. For either gaseous

(ethane/propane) or liquid (C/naphtha/gasoil) feeds, this technology is based on Technip's proprietary pyrolysis furnaces and progressive separation [105-110, 233]. This allows processing of olefins at low energy consumption with a particularly low environmental impact. The progressive separation concept is applied for either front-end hyddrogenation or back-end hydrogenation [233].

- The front-end hydrogenation corresponds to a front-end deethanizer for an ethane cracker or a front-end depropanizer for the heavier feedstocks both are placed at the third-stage discharge of the cracked-gas compressor.
- The back-end hydrogenation corresponds to a front end; the tower is placed at fifth-stage discharge.

Hydrocarbon feedstocks are preheated (also to recover heat) and then cracked by combining with steam in a tubular pyrolysis furnace at an outlet temperature ranging from 1,500°F to 1,600°F. The furnace technology can be either an SMK type (for gas cracking) or GK6 type (for liquid cracking). The GK6 type design can be oriented to a high olefins yield with very flexible propylene/ethylene ratios, or to a high BTX production. This specific approach allows long run length, excellent mechanical integrity and attractive economics. The hydrocarbon mixture at the furnace outlet is quenched rapidly in the transfer line exchangers (TLEs) or selective line exchangers (SLEs), generating high-pressure steam. In liquid crackers, cracked gas flows to a primary fractionator, after direct quench with oil, where fuel oil is separated from gasoline and lighter components, and then sent to a quench water tower for water recovery (to be used as dilution steam) and heavy gasoline production (end-point control)[111-115, 233]. In a gas cracker, cracked gas flows to a quench water tower for water recovery and removal of tars. A caustic scrubber placed at the third-stage discharge of the cracked-gas compressor removes acid gases. The compressed gas at 450 psig is dried and then chilled. For an ethane cracker, a single demethanizing stripping system operating at medium pressure is implemented; the overhead is recycled back to the cracked gas compressor. For a liquid cracker, a double

demethanizing stripping system operating at medium pressure and rebolled by cracked gas, minimizes the refrigeration required (heat integration) as well as the investment forseparating methane (top) and C_2+ cut (bottoms). A dual column concept (absorber concept: Technip's patent) is applied between the secondary demethanizer overheads, and the chilled cracked gas minimizes ethylene losses with a low-energy requirement [116-117, 233]. The high-purity hydrogen is produced in a cold box. The bottoms from the demethanizers are sent to the C_2 cut treatment for ethylene purification. The C_2 splitter is operating as a heat pump. The tower can be arranged as open heat pump integrated with the ethylene refrigerant when the front-end hydrogenation system or closed heat pump operating with the propylene refrigerant for the back-end hydrogenation scheme. The residual ethane from the C_2 splitter is recycled for further cracking. Polymer-grade propylene is separated from propane in a C_4 splitter. The residual propane is either recycled for further cracking or exported.C_4s and light gasoline are separated in a debutanizer. Gas expansion (heat recovery) and external cascade using ethylene and propylene systems supply refrigeration. The main features of Technip's patented technology are [118-120, 233]:

- Optimization of olefins yields and selection of feedstocks
- Reduced external refrigeration in the separation sections
- Auto-stable process, heat integration acts as feed forward system
- Simple process control; large usage of stripper/absorber towers (single specification) instead of distillation towers (antagonistic top and bottom specifications).

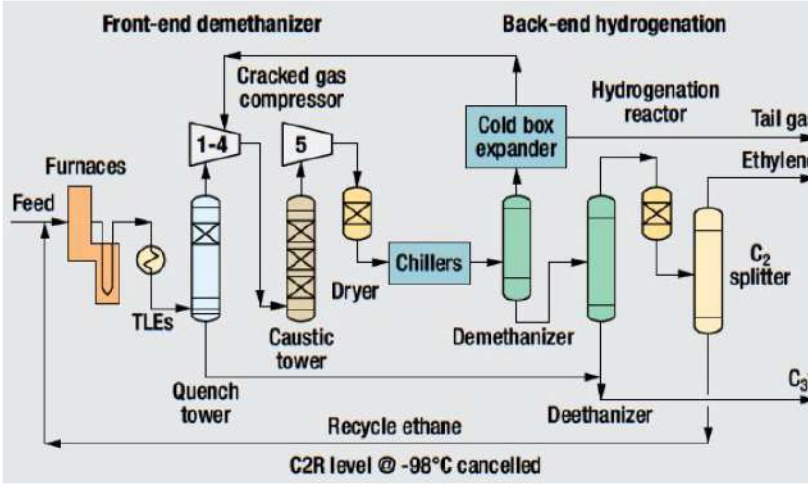

Figure 5. Progressive separation applied in Back-end hydrogenation for an ethane cracker.

Ultimate range of ethylene yields vary from 83% (ethane) to around 25% (VG0s), 35% for intermediate full-range naphtha. These correspond to the respective total olefins yields (ethylene and propylene) from 84% (ethane) to 38% (VG0s), and 49% for intermediate full-range naphtha. The specific energy consumption range is 3,100 kcal/kg ethylene (ethane) to 5,500 kcal/kg ethylene (GO) and 4,700 Kcal/Kg ethylene for an intermediate full-range naphtha. Since 2001, six grassroots ethylene plants have been awarded to Technip, out of which four have a capacity of over 1 million tpy of ethylene. In the same period, 148 furnaces using Technip's proprietary coils technology have been awarded to Technip as new furnaces or upgrading of existing facilities. More than 20 ethylene plants based on Technip's technology are in operation worldwide [121-123]. The progressive separation is also applied for plant expansions over the nominal capacity, with up to an 80% capacity increase. Figures 5-6 shows Progressive separation applied in Back-end hydrogenation for an ethane cracker and Progressive separation applied in Front-end hydrogenation for an ethane cracker.

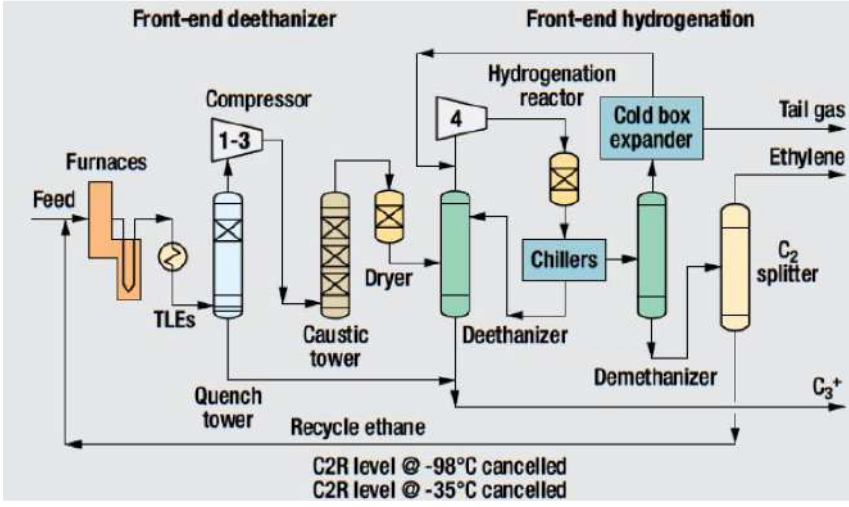

Figure 6. Progressive separation applied in Front-end hydrogenation for an ethane cracker.

2.4.1.6. The Technip (II) Technology

It is defined as Thermal cracking of a wide range of feedstocks into light olefins (mainly ethylene and propylene) and aromatics using proprietary cracking coils [124-126, 233].

Feedstocks: Ethane, propane through liquid feeds up to heavy gasoil or up to 600°C EP

Products: Cracked gas rich in Ethylene, propylene, butadiene and BTX (benzene, toluene and xylene).

Thermal cracking occurs in the presence of steam at high temperature in cracking coils located centrally in the firebox. Coil outlet temperature varies from 800°C up to 880°C depending on feed quality and cracking severity. The recent proprietary coils are GK6 and SMK coils used, respectively, for liquid and gas cracking. They feature high selectivity to ethylene, propylene, together with low coking rates (longer run length). Technip has also developed recently new patents (GK7 and Swirl Flow Tubes) to enhance both capacity and run length at lower investment cost. Cracked gases from

the furnaces coils pass through a transfer line exchanger (TLE) system, where heat is recovered to generate high-pressure steam [127-130, 233]. The primary TLEs are special S&T or linear types that ensure low to very low fouling rates and, thus, extending run lengths. Heat from the flue gases is recovered in the convection section to preheat feed and process steam, and to superheat the generated VHP. The technology is also applied to retrofit furnaces. The furnaces performances are optimized by using Technip's proprietary software SPYRO. Depending on the regulations various, options of NO abatement are incorporated. Once-through ethylene yields depend on feed characteristics and severity, and range from 58% for ethane to 36% for liquid feeds. Commercial plants: Over 550 cracking furnaces since mid-1960s have been implemented using Technip's technology. Since 2000, the SMK technology has been applied in 77 furnaces, and GK6 technology in 71 furnaces. Figure 7 shows PFD of Ethylene Production Unit under licensed by Technip Technology (II) [131-133, 233].

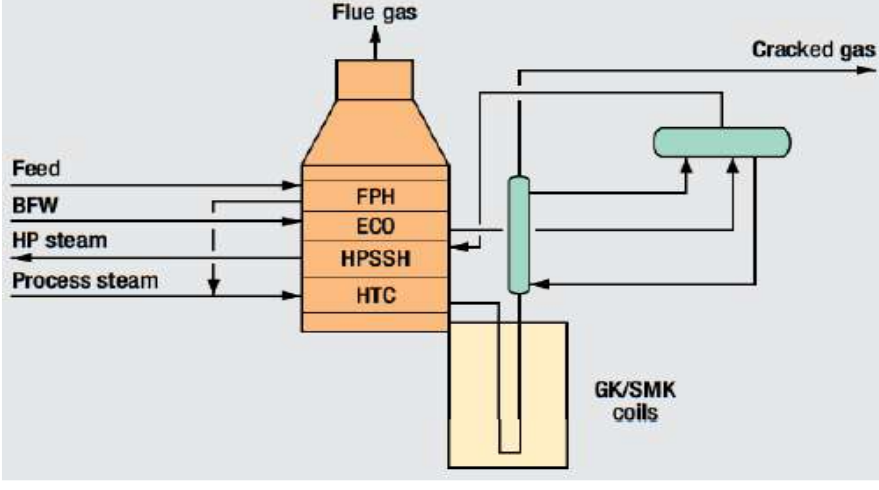

Figure 7. PFD of Ethylene Production Unit under licensed by Technip Technology (II).

2.4.1.7. The UOP LLC- Honeywell Co. Technology

The MaxEne process increases the ethylene yield from naphtha crackers by raising the concentration of normal paraffins (n-paraffins) in the naphtha-

cracker feed. The MaxEne process is the newest application of UOP's Sorbex technology. The process uses adsorptive separation to separate C5-C11 naphtha into a n-paraffins rich stream and a stream depleted of n-paraffins[134-137, 234].

Description: The separation takes place in an adsorption chamber (2) that is divided into a number of beds. Each bed contains proprietary shape-selective adsorbent. Also, each bed in the chamber is connected to a rotary valve (1). The rotary valve is used along with the shape-selective adsorbent to simulate a counter-current moving bed adsorptive separation. Four streams are distributed by the rotary valve to and from the adsorbent chamber. The streams are as follows [138-141, 233-234]:

- *Feed*: The naphtha feed contains a mixture of hydrocarbons.
- *Extract*: This stream contains n-paraffin and a liquid desorbent. Naphtha, rich in n-paraffin, is recovered by fractionation (3) and is sent to the naphtha cracker.
- *Raffinate*: This stream contains non-normal paraffin and a liquid desorbent. Naphtha, depleted in n-paraffins, is recovered by fractionation (4) and is sent to a refinery or an aromatics complex.
- *Desorbent*: This stream contains a liquid desorbent that is recycled from the fractionation section to the chamber. The rotary valve is used to periodically switch the position of the liquid feed and withdrawal points in the adsorbent chamber. The process operates in a continuous mode at low temperatures in a liquid phase [142-145, 233-235].

Ethylene yields from a naphtha cracker can be increased by over 30% using MaxEne extract as feedstock and the MaxEne raffinate can provide a 6% increase in octane-barrels from a refiner's catalytic naphtha reforming unit. Capital costs and economics depend on feed composition as well as the desired increase in ethylene and propylene production in the steam cracker. UOP's Sorbex technology is widely used in refining and petrochemical plants. The first commercial MaxEne unit is being installed in China. Figure

8 shows PFD of Ethylene Production Unit under licensed by UOP-Honeywell Co [146-150, 233-236].

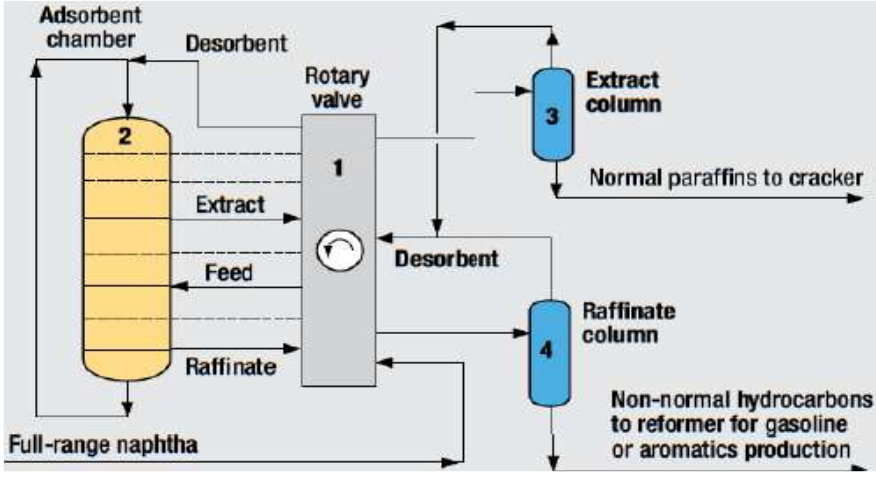

Figure 8. PFD of Ethylene Production Unit under licensed by UOP-Honeywell Co.

3. PROPYLENE PRODUCTION

3.1. Axens Technology (I)

The worldwide demand for gasoline, diesel and petrochemicals is shifting toward a greater emphasis on diesel and propylene,and flexibility to meet changing demands will be vital for refinery profitability[151-153]. Axens has developed the new FlexEne technology to expand thecapabilities of the fluid catalytic cracking (FCC) process, which is the main refinery conversion unit traditionally oriented to maximize gasoline and at times propylene. FlexEne relies on the integration of an FCC and an oligomerization unit called Polynaphtha to process light FCC olefins and to deliver good molecules back to the FCC and to provide product flexibility required by the marketplace. By adjusting the catalyst formulation and operating conditions, the FCC process is able to operate in different modes:

maxi distillate, maxi gasoline and high propylene. The combination with Polynaphtha delivers the flexibility expected by the market. In a maxi gasoline environment, the olefin-rich C_4 FCC cut is usually sent to an alkylation unit to produce alkylate and to increase the overall gasoline yield. In most recent max gasoline production schemes, alkylation has been advantageously substituted by Polynaphtha, which delivers high-quality gasoline at a much lower cost. For greater distillate production, Polynaphtha technology may be operated at higher severity to produce distillates from C_4 olefins. Additional diesel production may be supplied by operating the FCC unit in the maxi distillate mode. For greater propylene production, Axens/IFP R&D has shown that either the Polynaphtha gasoline or distillate fractions can easily crack in the FCC unit to produce Propylene. Consequently, depending uponmarket conditions, gasoline or diesel can be recycled to the FCC to produce high-value propylene and C_4 olefins. Thanks to optimized combination of FCC and oligomerization, Flex-Ene delivers the largest market product flexibility when targeting production of propylene and/or gasoline and/or distillates [154-160]. Two FlexEne units have been licensed for new R2R/Polynaphtha projects. Figure 9 shows PFD of Propylene Production Unit under licensed by Axens Co. (I).

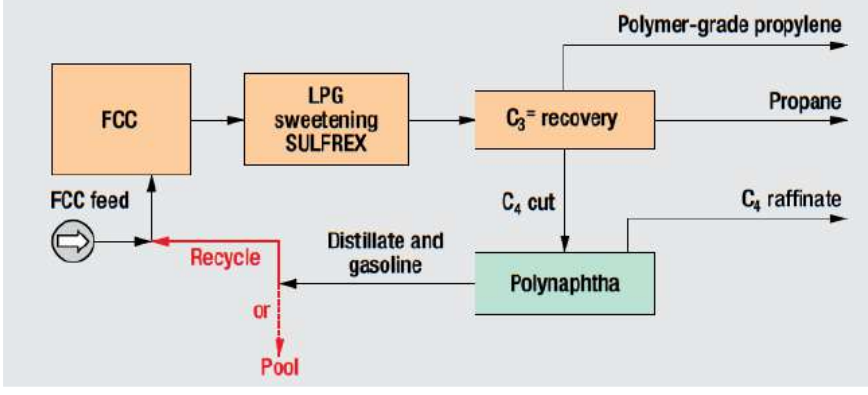

Figure 9. PFD of Propylene Production Unit under licensed by Axens Co. (I).

3.2. The Axens Technology (II)

When the process objective is maximum propylene production, specific technology features must be added to the fluid catalytic cracking (FCC)/resid FCC (RFCC) unit. The challenge is particularly greatwhen the feedstock contains residue. ZSM-5 additive is able to crack only C_7 to C_{10} olefins to LPG. Consequently, most of the C_5 and C_6 cut are not converted by ZSM-5 in the main riser. To convert this cut, it has been published by IFP and others that the optimum catalytic system is a recycle in a separate riser operating under more severe conditions-a PetroRiser. Indeed, recycling with the feed does not allow converting this light naphtha since the temperature is too low in the main riser[161-165, 237-240]. If the naphtha recycle is injected before the feed zone where the catalyst temperature is above 700°C, production of fuel gas is very high due to thermal cracking as well as detrimental side reactions specific to this thermal level. In addition, injecting light naphtha below the main feed alters the riser conditions at the point of injection of the main resid feed resulting in less than optimum performance. The conclusion of the R&D work is that recycling light naphtha to a separate riser at a temperature higher than the main riser allows cracking C_5 and C_6 olefins and also enables paraffins to produce more LPG and less C_5-70°C naphtha. An additional feedstock for propylene production is the indirect recycle of C_4 olefins. As with light naphtha, the C_4 olefins will not crack in the main riser, and a simple recycle to the PetroRiser will result in nonselective conversion of C_4 olefins. The easiest and most selective way to recycle crack the C_4 olefins into propylene is to use the benefit of a C_4 oligomerization unit (Polynaphtha) to produce longer olefins (C_8 and C_{12} olefins). These longer chain olefins will crack very selectively in the PetroRiser, thus producing more propylene as well as good quality gasoline [166-170, 237-242]. This integration is called FlexEne and presented in more details in a dedicated paragraph of the handbook. PetroRiser has been licensed in Abu Dhabi for the largest RFCC unit (127, 000 bpsd). Figure 10 shows PFD of Propylene Production Unit under licensed by Axens Co. (II).

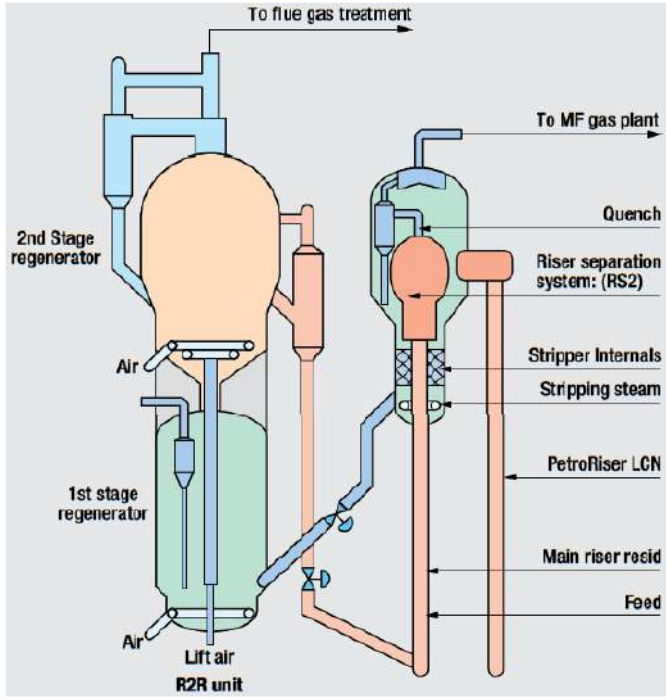

Figure 10. PFD of Propylene Production Unit under licensed by Axens Co. (II).

3.3. China Petrochemical Technology Co.

Deep-catalytic cracking (DCC) is a catalytic conversion technology that uses heavy hydrocarbon feedstocks, such as vacuum gasoil (VGO), vacuum resid (VR) or VG0 blended with deasphalted oil (DAO) to produce light olefins (ethylene, propylene and butylenes), LPG, gasoline, middle distillates, etc. The technology targets maximizing propylene production (DCC-1) and maximizing iso-olefins production (DCC-II). The DCC process overcame the limitations of conventional fluid catalytic cracking (FCC) processes [171-174]. The propylene yield of DCC is 3-5 times that of conventional FCC processes. The processing scheme of DCC is similar to that of a conventional FCC unit consisting of reaction-regeneration, fractionation and gas concentration sections. The feedstock, dispersed with steam, is fed to the system and contacted with the hot regenerated catalyst

either in a riser-plus fluidized dense-bed reactor (for DCC-I) or in a riser reactor (for DCC-II). The feed is catalytically cracked. Reactor effluent proceeds to the fractionation and gas concentration sections for stream separation and further recovery. The coke-deposited catalyst is stripped with steam and transferred to a regenerator where air is introduced and coke on the catalyst is removed by combustion. The hot regenerated catalyst is returned to the reactor at a controlled circulation rate to achieve the heat balance for the system [175-178]. The DCC has two reactor operating modes: DC C-1 (Riser-plus fluidized dense-bed reactor, maximum propylene mode) and DCC-II (Riser reactor, maximum iso-olefins mode). The DCC can process different heavy feeds VG°, DAO, coker gasoil, atmospheric residue, VR, etc. Paraffinic feedstocks are the best feeds for DCC. In DCC maximum propylene operation mode, over 20 wt% propylene yield can be obtained from paraffinic feedstocks. The naphtha and middle distillates streams from the DCC unit can be used as blending components for high-octane, commercial gasoline and fuel oil, respectively. Using a specially designed and patented zeolite catalysts, the reaction temperature in the DCC process is higher than that of conventional FCC, but much lower than that of steam cracking. Other processing benefits include [179-181]:

- Flexibility of process operation. Easy to obtain the shift of DCC operation modes by regulating the operating conditions and catalyst formulations.
- Easy separation and recovery of product streams through a similar absorption/fractionation of conventional FCC. Cryogenic separation for separating and recovering DCC product stream is not necessary.
- Contaminants found in the hydrocarbons are at trace levels in DCC lighter olefin products; thus, hydrotreating is not needed. Commercial plants: The first commercial DCC unit came onstream in 1990, and 10 DCC units have been licensed. The largest unit is 4.50 million tpy facility. It is estimated that a total of 13 units will be fully operational by the end of 2010.

3.4. The Kellogg Brown & Root LLC Technology

The application of this license is to produce propylene and ethylene from low-value, light (C_4 to C_1) hydrocarbon olefins-containing streams from ethylene plants and refineries. Suitable feeds include C_4/C_6 streams from a steam cracker, light cat-cracker C_4s and naphtha and coker gasolines. The SUPERFLEX process is a proprietary technology patented by ARCO Chemical Technology, Inc. (now LyondellBasell) and exclusively offered worldwide for license by KBR. It uses a fluidized catalytic reactor system with a proprietary catalyst to convert low-value feedstocks to predominantly propylene and ethylene products. The catalyst is very robust; thus, no feed pretreatment is required for typical contaminants such as sulfur, water, oxygenates or nitrogen [182-185]. Attractive feedstocks include C_4 and C_5 olefin-rich streams from ethylene plants, FCC naphthas or C_4s, thermally cracked naphthas from visbreakers or cokers, BTX or MTBE raffinates, C_5 olefin-rich streams removed from motor gasolines, and Fischer-Tropsch light liquids. The fluidized reactor system is similar to a refinery FCC unit and consists of a fluidized reactor/regenerator vessel, air compression, catalyst handling, flue-gas handling, and feed and effluent heat recovery. Using this reactor system with continuous catalyst regeneration allows higher operating temperatures than with competing fixed-bed reactors so that a substantial portion of the paraffins, as well as olefins, are converted. This allows for flexibility in the amounts of paraffins in the feeds to SUPERFLEX and the ability to recycle unconverted feed to extinction. Because this is a catalytic process, the CO2 footprint per ton of product is lower than conventional steam cracking. The cooled reactor effluent can be processed for the ultimate production of polymer-grade olefins. Several design options are available, including fully dedicated recovery facilities; recovery in a nearby, existing ethylene plant recovery section to minimize capital investment; or processing in a partial recovery unit to recover recycle streams and concentrate olefin-rich streams for further processing in nearby plants. Depending on the final use of the ethylene byproduct, the recovery section costs may be reduced via use of an absorption process to produce dilute ethylene product rather than polymer grade. The technology produces

50 wt%-60 wt% propylene plus ethylene, with a propylene yield about twice that of ethylene, from typical C_4 and C_5 raffinate streams [186-190]. Some typical yields are. Table 6 shows Product Distribution for different feedstocks in Kellogg Process and Figure 11 shows PFD of Propylene Production Unit licensed by Kellog Brown & Root LLC.

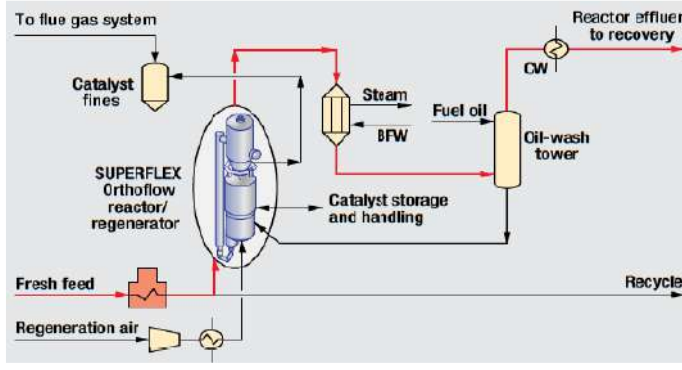

Figure 11. PFD of Propylene Production Unit licensed by Kellog Brown & Root LLC.

Table 6. Product Distribution for different feedstocks in Kellogg Process

Feedstock	Olefin rich C_4s	Olefin-rich C_5s	FCC LCN	Coker LN
Fuel gas	7.2	12	13.6	11.6
Ethylene	22.5	22.1	20.0	19.8
Propylene	48.2	43.8	40.1	38.7
Propane	5.3	6.5	6.6	7.0
C6+ gasoline	16.8	15.6	19.7	22.9

3.5. The Lummus Technology

Technology for dehydrogenation of propane to make high-purity propylene. The CATOFIN process uses specially formulated proprietary catalyst from Sud-Chemie. The CATOFIN reaction system consists of parallel fixed-bed reactors and a regeneration air system. The reactors are

cycled through a sequence consisting of reaction, regeneration and evacuation/purge steps. Multiple reactors are used so that the reactor feed/product systern and regeneration air system operate in a continuous manner [191-194]. Fresh propane feed is combined with recycle feed from the bottom of the product splitter (6). The total propane feed is then vaporized and raised to reaction temperature in a charge heater (1) and fed to the reactors (2). Reaction takes place at vacuum conditions to maximize feed conversion and olefin selectivity. A purge stream, taken from the total propane feed, is passed through a deoiler (8) to remove C_4 and heavier components. After cooling, the reactor effluent gas is compressed (3) and sent to the recovery section (4), where inert gases, hydrogen, and light hydrocarbons are separated from the compressed reactor effluent. The ethane, propane and propylene components are then sent to the product purification section deethanizer (5) and product splitter (6), where propylene product is separated from unreacted propane. The propane is recycled to the reactors. After a suitable period of onstream operation, feed to an individual reactor is discontinued and the reactor is reheated/regenerated. Reheat/regeneration air heated in the regeneration air heater (7) is passed through the reactors. The regeneration air serves to restore the temperature profile of the bed to its initial onstream condition in addition to burning coke off the catalyst. When reheat/regeneration is completed, the reactor is re-evacuated for the next onstream period. The low operating pressure and temperature of the CATOFIN reactors, along with the robust Sud-Chemie catalyst, allows the CATOFIN technology to process propane feedstock from a variety of sources [195-200]. The simple reactor construction, with its simple internals, results in a very high onstream factor. Yields and product quality: Propylene produced by the CATOFIN process is typically used for the production of polypropylene, where purity demands are the most stringent (>99.5%). The consumption of propane (100%) is 1.17 metric ton (mt) per mt of propylene product. Where a large amount of low value LPG is available, the CATOFIN process is the most economical way to convert it to high value product. The large single-train capacity possible with CATOFIN units (the largest to date is for 650,000 metric tpy propylene) minimizes the investment cost/mt of product. Currently eight CATOFIN

dehydrogenation plants are on stream producing over 1,800,000 metric tpy of isobutylene and 1,160,000 metric tpy of propylene. There are now two CATOFIN propane dehydrogenation units in operation with a design capacity of 455,000 metric tpy propylene. These are the world's largest single-train units [201-204]. Both plants have successfully met their guarantees and continue to operate well above design capacity. Figure 12 shows PFD of Propylene Production Unit licensed by Lummus Technology.

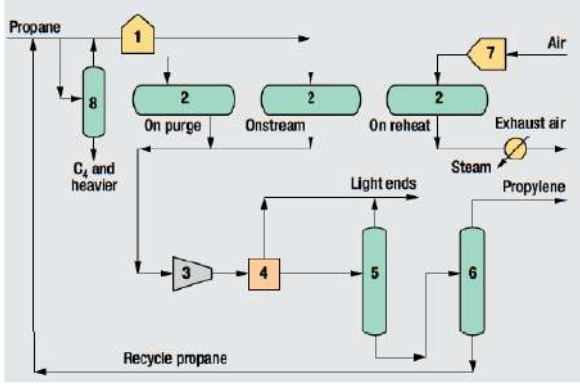

Figure 12. PFD of Propylene Production Unit licensed by Lummus Technology.

3.6. The UOP LLC, Honeywell Technlogy

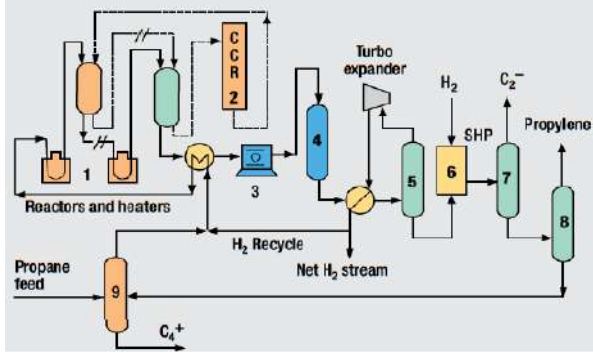

Figure 13. PFD of Propylene Production Unit licensed by UOP LLC, Honeywell Technology (I).

The Oleflex process is used to produce polymer-grade propylene from propane. The complex consists of a reactor section, continuous catalyst regeneration (CCR) section, product separation section and fractionation section [205-210]. Four radial-flow reactors (1) are used to achieve optimum conversion and selectivity for the endothermic reaction. Catalyst activity is maintained by continuously regenerating catalyst (2). Reactor effluent is compressed (3), dried (4) and sent to a cryogenic separation system (5). A net hydrogen stream is recovered at approximately 90 mol°/0 hydrogen purity [211]. The olefin product is sent to a selective hydrogenation process (6) where dienes and acetylenes are removed. The propylene stream goes to a deethanizer (7) where light-ends are removed prior to the propane-propylene splitter (8). Unconverted feedstock is recycled back to the depropanizer (9) where it combines with fresh feed before being sent back to the reactor section. Propylene yield from propane is approximately 85 wt% of fresh feed. Hydrogen yield is about 3.6 wt% of fresh feed. The US Gulf Coast inside battery limits investment for the production of a 450,000 tpy polymer-grade propylene facility is approxi mately $600/tpy. Thirteen Oleflex units are in operation to produce propylene and isobutylene. Eight of these units produce propylene. These units represent 2.1 million metric tpy of propylene production. Three additional Oleflex units for propylene production are in design or under construction [212-215]. Figure 13 shows PFD of Propylene Production Unit licensed by UOP LLC, Honeywell Technology (I).

3.7. The Lummus Technology (II)

The Total Petrochemicals/UOP Olefin Cracking Process (OCP) is used to primarily produce propylene from C_4 to C_8 olefins supplied by steam crackers, refineries and/or methanol-to-olefins (MTO) plants. The Olefin Cracking Process was jointly developed by Total Petrochemicals (formerly ATOFINA) and UOP to convert low-value C_4 to C_8 olefins to propylene and ethylene. The process features fixed-bed reactors operating at temperatures between 500°C and 600°C and pressures between 1 and 5 bars gauge. This

process uses a proprietary zeolitic catalyst and provides high yields of propylene. Usage of this catalyst minimizes reactor size and operating costs by allowing operation at high-space velocities, and high conversions and selectivities without requiring an inert diluent stream [216-218]. A swing-reactor system is used for catalyst regeneration. Separation facilities depend on how the unit is integrated into the processing system. The process is designed to utilize olefin feedstock's from steam crackers, refinery FCC and coker units, and MTO units, with typical C_4 to C_8 olefin and paraffin compositions. The catalyst exhibits little sensitivity to common impurities such as dienes, oxygenates, sulfur compounds and nitrogen compounds. Economics: Capital and operating costs depend on how the process is integrated with steam cracking, refinery or other facilities. Product yields are dependent on feedstock composition [219-221]. The process provides propylene/ethylene production at ratios of nearly 4:1. Case studies of olefin cracking integration with naphtha crackers have shown 30% higher propylene production compared to conventional naphtha-cracker processing. Petrochemicals operate a demonstration unit that was installed in an affiliated refinery in Belgium in 1998. Total installed a second demonstration unit in 2009 that is integrated with a semi-commercial MTO/OCP process demonstration unit [222-225]. Figure 14 shows PFD of Propylene Production Unit licensed by UOP LLC, Honeywell Technology (II).

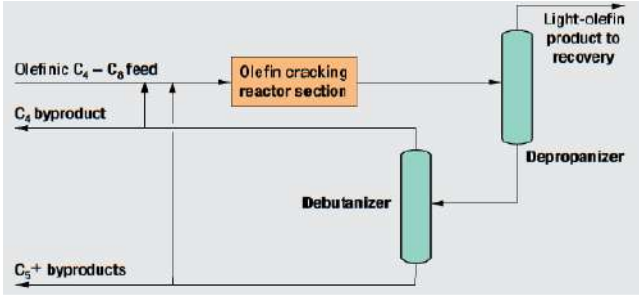

Figure 14. PFD of Propylene Production Unit licensed by UOP LLC, Honeywell Technology (II).

4. FUNDAMENTAL TO ZEOLITS

Microporous materials with regular pore architectures comprise wonderfully complex structures and compositions. Their fascinating properties, such as ion-exchange, separation, catalysis, and their roles as hosts in nanocomposite materials, are essentially determined by their unique structural characters, such as the size of the pore window, the accessible void space, the dimensionality of the channel system, and the numbers and sites of cations, etc. [189, 226, 49-51]. Zeolites constitute the most important family in microporous materials. Traditionally, the term 'zeolite' refers to a crystalline alumina silicate or silica polymorph based on corner-sharing TO4 (T¼Si and Al) tetrahedral forming a three-dimensional four connected framework with uniformly sized pores of molecular dimensions. Nowadays, the term 'zeolite framework' generally refers to a corner sharing network of tetrahedral coordinated atoms. The 5th Edition of the Atlas of Zeolite Framework Types published by Baerlocher, Meier, and Olson on behalf of the Structure Commission of the International Zeolite Association in 2001 comprised 133 zeolite structure types. Up to October 2006, the number of entries had risen to 167[189, 52-54]. Each framework type is assigned a three-capital-letter code in alphabetical order. The codes are generally derived from the names of the type materials. They only describe and define the network of corner sharing tetrahedral coordinated framework atoms. Framework types do not depend on composition, distribution of the T-atoms (Si, Al, P, Ga, Ge, B, Be, etc.), cell dimensions, or symmetry [189, 227-228, 55].

4.1. Zeolite Materials: A Definition

Today the Structure Commission of the International Zeolite Association (IZA) has accepted 176 different framework types of different zeolite structures or topologies [190, 186-187] with discrete acronyms [191, 56-60]. They will be given in brackets when referring to zeolite samples. Each of the different framework topologies with distinct pore size

and architecture can vary in chemical composition, as each framework type can be viewed as a tridimensional silicate in which $Si–O_4$ tetrahedral have common apices, several elements may be fully or partly substituted for Si and give rise to discrete materials encompassing a range of different hydrophilicity/hydrophobicity ratios, framework charge densities and framework compositions yielding different strengths of Brønsted/Lewis acid sites and redox properties[192, 61-64]. The definition for catalytic purposes of a "zeolite" reads as follows: a crystalline material with microspores and cation-exchange capacity that is insoluble in water and common organic solvents and has sufficient thermal stability that allows removal of all pore-filling agents present in the as- synthesized materials. This definition is narrower than that of the IZA Constitution, which includes mesoporous solids, metal organic frameworks (MOFs), cationic and anionic clays [192, 65-67]. An inspection of the industrial use of zeolites as catalysts shows, however, that only a rather limited number of zeolite topologies are currently used in major industrial processes. Among the more important ones are ultra-stable Y (USY) (FAU), rare-earth-exchanged faujasite-type (X, Y) (FAU) and ZSM-5-type (MFI) zeolites in fluid catalytic cracking (FCC) of oil fractions; noble-metal loaded USY for hydro isomerization and hydrocracking of naphtha feedstock's; mordent (MOR) and zeolite Omega (MAZ) -based catalysts for C_4-C_6 alkane isomerization; zeolites ZSM-23 (MTT), ZSM-35 (FER), ZSM-5 for selective oil dewaxing; ZSM-5, silica lite (MFI), MCM-22 (MWW), Betatype (BEA) zeolites for aromatics alkylation to yield ethylbenzene, p-xylene, cumin, p-ethyl toluene; zeolites ZSM-5, SAPO-34 (CHA) for methanol to olefins and/or larger hydrocarbons; transition-metal-exchanged faujasite for catalytic combustion of volatile organic chemicals (VOCs); Fe, Cu, Cr, V, Ce-containing mordent, ZSM-5, and faujasite-type zeolites for NO*x* reduction with ammonia; Beta-type zeolites in Frieda–Crafts catalysis, viz. acetylation of anisole; ZSM-5-type zeolites for synthesis of pyridines from acetaldehyde, formaldehyde, and ammonia; TS-1 (MFI) for liquid-phase oxygenation, viz. of phenol, propene, and oximes; Fe-ZSM-5 for benzene oxygenation conversion to phenol with nitrous oxide [193, 229-230, 67-70].; Zeolite

RHO for dimethylamine from methanol and ammonia; and ZSM-22 (TON) and ZSM-23 for propene trimerization [194, 71].

4.2. Brønsted Acidity in Metallo Silicate Zeolites

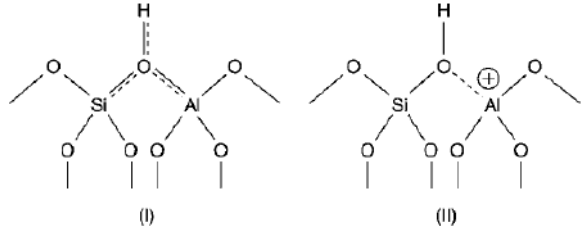

Figure 15. Brønsted acid sites in zeolites represented as a resonance hybrid between two extreme structures I and II.

Whereas in zeolites Si4+ is substituted for M3+ elements, viz. Al, Ga, B, or Fe, the majority of the work on isomorphic substitution refers to aluminosilicates. The substitution is governed by Loewenstein's rule, stating that only Si–O–Si and Si–O–Al bonds are stable, excluding formation of Al–O–Al bonds [195, 72-73, 243-250]. The resulting negative framework charges, if compensated by H+, are at the basis of formation of a solid Brønsted acid, with zeolite-specific bridging hydroxyl groups. Such bridged silanol groups used for catalyst-activity-type relationships and catalytic-activity rationalizations, are viewed as resonance hybrids between two extreme structures (Figure 15), viz. "a fully bridged oxygen with a weakly bound proton," and "a silanol group with a weak Lewis acid interaction of the hydroxyl oxygen with Al" [195, 74-75]. The latter structure would represent the site in amorphous silica-alumina in which no stabilization by long-range symmetry exists. Parameters affecting the zeolite acidity spectrum are shown in Figure 15. Acid zeolites compared to their amorphous compositional counterparts often show several orders of magnitude enhanced intrinsic activity. Parameters invoked to rationalize this behavior are the higher concentration of AlIV in the respective matrices, the higher intrinsic turnovers of each of such sites, as well as the enhanced reactant

concentration in the intracrystalline voids, favoring intermolecular hydrogen transfer [195-196, 76]. The latter effect is more pronounced in monodimensional tubular channels compared to cages, viz. in mordenite or mazzite compared to faujasite, suggesting that enhanced activity due to enhancement of bimolecular reaction rates contains a geometric component [195-196, 77-79].

4.3. Brønsted Acidity in Aluminophosphates

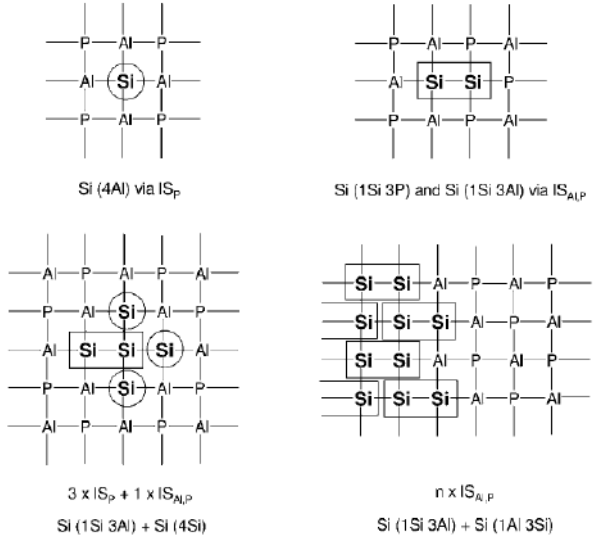

Figure 16. 2-Dimensional grid representation of possible T-atom configurations in an SiAlPO4-n framework obtained by substitution of P (ISP, circles; top left), of both one P and one Al atom(ISAl,P, rectangles, top right), via recurrent replacement of Al, P couples (n ISAl,P,bottom right), and via a combination of both pathways (bottom left). Si–P represent unstable chemical bonds.

Isomorphic substitution in microporous aluminophosphates (AlPO4-n) is more complex than in traditional M3+-containing metallosilicate zeolites. Crystalline microporous aluminophosphates, showing alternation between P4+ and Al3+ T-atoms in tetrahedrally arranged frameworks, do not show residual negative framework charges and do not contain Brønsted acidity.

Al-OHgroups present in AlPO4-hydrates, AlPO4-hydroxides, and AlPO4-fluorides [197, 80-81]. show insufficient acid strength and/or stability for vapor-phase catalysis. No attempts are reported for use of such materials in liquid-phase low-temperature catalysis. The framework charges generated by substitution in a M, Al, P-containing synthesis gel, are neutralized by a template to allow crystallization of a four-coordinated MAlPO4-n framework. The size of and charge density on a template molecule, often protonated amines or tetraalkylammonium ions, will determine the degree of substitution. The concept of template/framework stoichiometry, that is, the maximum framework charge that can be balanced by a template molecule, dictates the substitution limit. When this ratio is exceeded, viz. with low-valent ions, the substituting ions are accommodated in charge-compensating cation positions. With Co2+, Fe2+, and Mn2+, charge compensation occurs already at low substitution degrees [198, 82-85]. Si substitution in AlPO4-n is complex and even for a given topology can yield a whole family of SiAlPO4 (SAPOs) with a variety of acid properties (Figure 16). Via pathway ISP a neutral framework is obtained with Si(4Al) environments. The ISAl,P path yields thermodynamically unstable Si–O–P bonds and is only hypothetical. The recurrent application of substitution mechanism ISAl,P starting from the crystal rim circumvents this problem, yielding a neutral AlPO4-n framework with a topotactic siliceous overlayer. At the boundary between the two domains electroneutral environments, viz. Si(3Si,1Al) and Si(1Al, 3Si), appear[199, 86-87]. When Si substitution occurs via a combination of both pathways, the formation of Si-O-P bonds is avoided, resulting in the formation of silicon patches with AlPO4-n topology. In the majority of SAPO4-n materials, isolated Si is first accommodated in P sites, often significantly before the stoichiometric ratio is obtained. Further on, simultaneous substitution by the two mechanisms results in extensive silica patch formation. Zeolitic acidity is then generated via Al incorporation in the silica islands. It is clear that correlations between Brønsted acidity and degree of overall substitution will be complex. All synthesis parameters such as degree of substitution, nature of the organic template, crystallization temperature, and time, which may affect the relative importance of the substitution mechanisms, influence the Brønsted acid

spectrum of the resulting materials [200, 88-90]. Discrimination among rival substitution mechanisms has been attempted for several SAPO4-n topologies. In SAPO-5 up to 25% of the T atoms was replaced by large siliceous patches, concentrating at the crystals surface. During SAPO-11 crystallization, the ISP mechanism dominates with dipropylamine as template, while with diisopropylamine both ISp mechanisms occur [201, 90]. SAPO-34 synthesized with fluoride containing triethylamine also showed evidence for substitution via both mechanisms. Unfortunately, the relative importance of formation of patches versus silica overlayers and Brønsted acid sites formation in each of them is not known.

4.4. Zeolite Selection for Processes

Catalytic sites associated with a zeolite often affect reaction selectivity. A number of classical concepts are useful to the catalyst designer for their rationalizing and even predicting power. Molecules can be excluded from chemical activation at intracrystalline active sites, depending on the size, shape of the pores, and the reactant. To all such phenomena the concept of reactant shape selectivity (RSS) was coined. From a mixture of product molecules desorbing from the intracrystalline active sites the faster-diffusing "slimmer" molecules will be abundantly present, generating a pseudothermodynamic equilibrium in the bulk. The phenomena are described as product diffusion shape selectivity (PDSS). Geometric restrictions near the active site can inhibit formation of some transition states and affect product selectivity. The phenomena are known as *transition-state shape selectivity* (TSSS). Whereas for RSS and PDSS crystallite encapsulated sites are needed, TSSS may occur in half-open cages at crystal terminating locations as well. Although such effects were mainly reported for hydrocarbons and alkylaromatics in medium-pore zeolites with 10-membered rings (10-MRs) of lattice atoms, viz. MFI, MEL, TON, the concepts are applicable to functionalized organics and other topologies as well. The nature of the sites is also not limited to Brønsted acid sites, but also applies to metal and redox sites. The area has been reviewed thoroughly

[201, 91-93]. The use of the concepts implies compositional homogeneity across the crystals and the existence of only intracrystalline sites that all show identical selectivity. Initially, it was proposed that pore size and tortuosity, as well as pore architecture determined by the zeolite topology, were influencing intrazeolitic fields and field gradients, thus affecting differently the relative rates of primary and secondary reactions and overall selectivity. Recently, effects of confinement on various kinetic and even thermodynamic effects were shown that provide an understanding of the confinement effect on adsorption and diffusion [202, 94-96]. Configurational-bias Monte Carlo techniques allowed simulation of slowly diffusing molecules, trapped in cages or at adsorption sites in zeolite topologies. This approach consisting of mapping the free-energy landscape in the intracrystalline space, ignores effects of local differences in site architecture, or concentration on reaction selectivity. To a number of unexpected shape-selectivity phenomena with long alkane hydroconversion the term *inverse* shape selectivity was coined. In zeolite pore widths of 0.65–0.74 nm, the opposite was encountered, as expected from mere geometric effects, that is, preferential formation of branched over linear hydrocarbons, viz. the formation of high yields of dibranched from n-alkanes over 10-MR zeolites like AFI (SAPO-5), the phenomenon being confirmed by adsorption experiments [203, 97]. The molecular basis of such effects has been attributed to a purely entropic effect in monodimensional pores at high pressures expelling larger molecules by smaller ones [203, 98]. Several shape-selective phenomena were attributed to topology-dependent structural sites. Such nest effects were the result of tuning of the curved catalyst surface to the configuration of adsorbed species, entropic effects governing the fitting. A distinction between two types of extra-framework catalysis mainly in ZSM-22 (TON), was made using the terms of *pore mouth* and keylock selective catalysis (Figure 16). Apparently, it is possible for alkanes via hydro conversion to be transformed in a selective way into products that are unable to be formed in or desorb from the zeolite. The abundant formation of some molecules, viz. 2-methylbranched alkanes from n-alkanes, was assigned to transformation in a single pore mouth. Others, viz. 2,4-dimethyloctane from n-decane, happened to be formed at neighboring pore

mouths, as their selectivity was chain length as well as topology dependent [203, 99].

4.5. Structures of Commercially Significant Zeolites

Commercially signifi cant zeolites include the synthetic zeolites type A (LTA), X (FAU), Y (FAU), L (LTL), mordenite (MOR), ZSM-5 (MFI), beta (BEA/BEC), MCM - 22 (MTW), zeolites F (EDI) and W (MER) and the natural zeolites mordenite (MOR), chabazite (CHA), erionite (ERI) and clinoptilolite (HEU). Details of the structures of some of these are given in this section. Tables in each section lists the type material (the common name for the material for which the three letter code was established), the chemical formula representative of the unit cell contents for the type material, the space group and lattice parameters, the pore structure and known mineral and synthetic forms[204-205, 100-101].

4.6. ZSM - 5 (MFI)

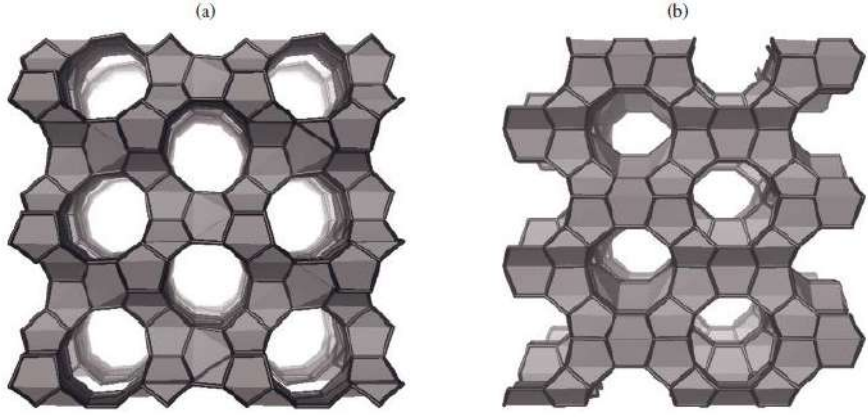

Figure 17. MFI framework views: (a) down the straight ten - ring channel system, (b) down the zig-zag ten-ring channel system.

Table 7. MFI structure type

Type material	ZSM-5
Chemical formula	$\lvert Na_n^+(H_2O)_{16}\rvert[Al_nSi_{96-n}O_{192}] - MFI, n < 27$
Space group	Orthorhombic, Pnma, a = 20.07 Å, b = 19.92 Å, c = 13.42 Å
Pore structure	Three - dimensional ten - ring
Mineral forms	Encilite, mutinaite
Synthetic forms	AMS-1B, AZ-1, Bor-C, Boralite C, FZ-1, LZ-105, NU-4, NU-5, Silicalite, TS-1, TSZ, TSZ-III, TZ-01, USC-4, USI-108, ZBH, ZKQ-1B, ZMQ-TB, ZSM-5

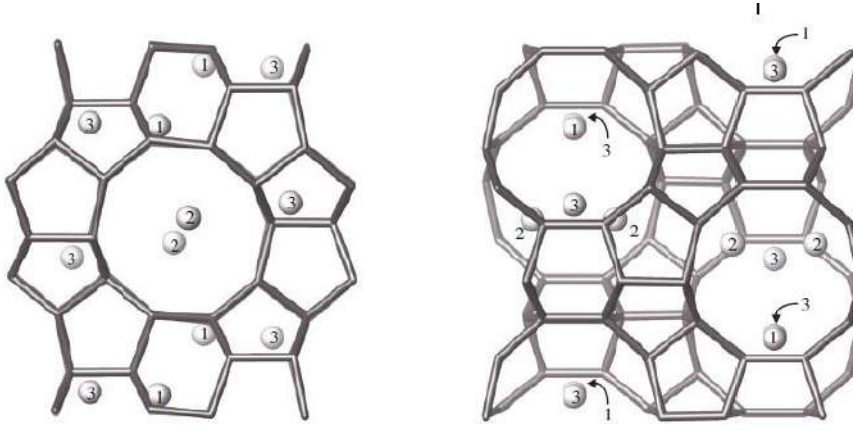

Figure 18. Cation sites in MFI. Site 1 is in near the intersection of the two ten - ring channel systems. Site 2 is in the straight ten - ring channel. Site 3 is in the zigzag ten - ring channel

The MFI framework (Table 7, Figure 17) can be built from five - rings and contains cavities interconnected by a straight ten - ring channel systems and a zigzag ten - ring channel system. Primary cation sites (Figure 18). Are site 1 near the intersection of the two ten - ring channel systems, site 2 in the straight ten - ring channel, and site 3 in the zigzag ten - ring channel [218, 109]. MFI-type zeolites are highly siliceous with Si/Al ratios from about 10 to infinity; generally, the higher the Si/Al ratio the easier the synthesis. MFI zeolites are reported to be hydrophobic and organophilic and for that reason useful for removing organics from water streams and stable for separations and catalysis in the presence of water. Since MFI zeolites are highly

siliceous the number of cations is small. However, since all the cation sites are in the MFI channels, all changes to cation number and type can affect the adsorption properties. The adsorption capacity of alkanes in MFI has been shown to increase with decreasing non-framework cation density (increasing Si/Al ratio) [219, 110-111]. and the linear/branched separation selectivity increases with increasing non-framework cation density.

CONCLUSION

In catalytic cracking processes, several catalysts have been investigated so that the studies mostly have been conducted due to the suitable performance of the zeolites in hydrocarbons cracking reactions on the zeolite catalysts. In mentioned studies, such diverse zeolites as SAPO-11, HZSM-5 have been used. Also, in order to enhance catalytic performance and increase the stability of the catalyst, such metal types as soil alkaline metals, transition metals, rare soil metal, etc. have been used. The catalytic cracking process is still in the research phase and faces some problems to be industrialized. Production of diverse hydrocarbons and coke during the process is one of the most important disadvantages of this process. Given the importance of light olefins and such issues as high energy consumption, greenhouse gases emission and environmental problems in the conventional thermal cracking process, it makes sense to conduct more studies on the catalytic cracking process and its catalyst performance improvement.

REFERENCES

[1] Wade, L.E., Gengelbach, R.B. Trumbley, J.L. (1981). *Methanol, Encyclopedia of Chemical Technology*, vol. 15, John Wiley, 398-415. https://books.google.com/books?isbn=0824792238.

[2] Froment, G.F. Dehertog, W.J.H. (1992). J. Zeolite Catalysis in The Conversion of Methanol into Olefins. *Catalysis*, 9, 1-64. http://dx.doi.org/10.1039/9781847553218-00001.

[3] Chang C.D., and A.J. Silvestri (1987). MTG Origin, Evolution Operation, *CHEMTECH* 10, 624–631. https://books.google.com/books?isbn=0824792238.

[4] Chen, N.Y., Reagan, W.J. (1979). Evidence of autocatalysis in methanol to hydrocarbon reactions over zeolite catalysts, *Journal of Catalysis*, vol. 59, Issue 1, August, 123-129. https://doi.org/10.1016/S0021-9517(79)80050-0.

[5] Dessau R.M., LaPierre R.B. (1982)On the mechanism of methanol conversion to hydrocarbonsover HZSM-5, *Journal of Catalysis*, vol 78(1), November,136-141. doi: 10.1039/F19817702209.

[6] *CMAI World Propylene Supply Study*. CMAI Report 2001, www.cmaiglobal.com.

[7] Chenier, P.J. (2002). *Survey of Industrial Chemistry*, 3rd Edition, Kluwer Academic Publishers Inc. New York. doi: 10.1007/978-1-4615-0603-4.

[8] Venner, R., Kantorowicz, S. (2001). *Metathesis: Refinery and Ethylene PlantApplication, in Proceedings of the European Petrochemical Technology Conference(EPTC),* Vienna, Austria. https://epca.eu/.

[9] Chen, T.J., Ruziska, P.A., Stuntz, G.F., Ladwig, P.K. (2002). *Multiple Feed Processfor the Production of Propylene*, U.S. Patent No. 6,339,181, January 15.

[10] Fu, A. (1998). Deep Catalytic Cracking Plant Produces Propylene in Thailand. *Oil &Gas J*. 96, 49.

[11] Alwahabi S.M. (2003). *Conversion of methanol to light olefins on SAPO-34: Kinetic modeling and reactor design*, Ph.D Dissertation, King Saud University. http://hdl.handle.net/1969.1/1579.

[12] Farrauto, R., Bartholomew, C. (1997). *Fundamentals of Industrial Catalytic Processes;* Blackie Academic and Professional: London, 411. ISBN-13978-0-471-45713-8.

[13] Kianfar E., Salimi M., Pirouzfar V., Koohestani B. *Synthesis and modification of Zeolite ZSM-5 catalyst with solutions of calcium carbonate (CaCO3) and sodium carbonate (Na2CO3) for Methanol to Gasoline Conversion*, 16(7):1-7 https://doi.org/10.1515/ijcre-2017-0229.

[14] Cavani, F. Trifiro, F. (1995). The Oxidative Dehydrogenation of Ethane and Propane as an Alternative Way for the Production of Light Olefins. *Catal. Today* 24, 307-313. https://doi.org/10.1016/0920-5861(95)00051-G.

[15] Weyten, H. Luyten, J. Keizer, K. Willems, L. Leysen, R. (2000). Membrane Performance: The Key Issues for Dehydrogenation Reactions in a Catalytic Membrane Reactor. *Catal. Today* 56, 3-11. https://doi.org/10.1016/S0920-5861(99)00257-6.

[16] Keller, G.E. Bhasin, M.M. (1982). Synthesis of Ethylene via Oxidative Coupling of Methane. *J. Catal.* 73, 9. https://doi.org/ 10.1016/0021-9517(82)90075-6.

[17] Hinsen, W. Bytyn, W. Baerns, M. (1984) Oxidative Dehydroge-nation and Coupling of Methane, In *Proceedings of the 8th International Congress on Catalysis*, Berlin 3, 581. ISBN: 0895733722 (U.S.).

[18] Ito, T., Wang, J.X., Lin, C.H. Lunsford, J.H. (1985). Oxidative Dimerization ofMethane over a Lithium-Promoted Magnesium Oxide Catalyst. *J. Am. Chem. Soc*. 107, 5062. doi: 10.1021/ja00304a008.

[19] Burch, R. Squire, G.D. Tsang, S.C. (1989). Role of Chlorine in ImprovingcSelectivity in the Oxidative Coupling of Methane to Ethylene. *Appl. Catal.* 46, 69-87. https://doi.org/10.1016/S0166-9834(00)81395-0.

[20] Lunsford, J.H. (2000). Catalytic Conversion of Methane to more Useful Chemicals and Fuels: a Challenge for the 21st Century. *Catal. Today 63*, 165-174. https://doi.org/10.1016/S0920-5861(00)00456-9.

[21] Keil, F.J. (1999). Methanol-to-hydrocarbons: Process Technology. *Micropor. Mesopor. Mat.* 29, 49-66. https://doi.org/10.1016/S1387-1811(98)00320-5.

[22] Chang, C.D. (1983). *Hydrocarbons from Methanol*, Marcel Dekker: New York. ISBN:0.471—41782-3.

[23] Vora, B.V., Marker, T.L. Barger, P.T. Nilsen, H.R. Kvisle, S., Fuglerud, T. (1997). Economic Route for Natural Gas Conversion to Ethylene and Propylene. *Stud Surf Sci Catal,* 107, 87-98. https://doi.org/10.1016/S0167-2991(97)80321-7.

[24] Li, Zhibin, Joaquín Martínez-Triguero, Jihong Yu, Avelino Corma. (2015). Conversion of methanol to olefins: Stabilization of nanosized SAPO-34 by hydrothermal treatment, *Journal of Catalysis* 329, 379–388. https://doi.org/10.1016/j.jcat.2015.05.025.

[25] Sherwin, M.B. (1981). Chemicals from Methanol, *Hydrocarobon Pro.* vol. March. 79-84.

[26] Alpine, P.W. (1986). The New Zealand Gas-to-Gasoline Project, *Chem. Eng. In Australlia,* vol 11(4),7-13.

[27] Yaripour,F, Zahra Shariatinia, Saeed Sahebdelfar, Akbar Irandoukht. (2015). Conventional hydrothermal synthesis of nanostructured H-ZSM-5 catalysts using various templates for light ole fi ns production from methanol, *Journal of Natural Gas Science and Engineering*, 22, 260-269. https://doi.org/10.1016/j.jngse.2014.12.001.

[28] Jianqing Li, Zhuo Li, Dezhi Han, Jinhu Wu. (2014). Facile synthesis of SAPO-34 with small crystal size for conversion of methanol to olefins, *Powder Technology*, 262, 177–182. https://doi.org/10.1016/j.powtec.2014.04.082.

[29] Usman, A.N. (1990). *Methanol Conversion to LightOlefins over Commercial Zeolites.* MSC Thesis, King Fahad Universit of Petroleum & Minerals.

[30] Mei, C., P. Wen, Z. Liu, H. Liu, Y. Wang, W. Yang, Z. Xie, W. Hua, Z. Gao, Selective production of propylene from methanol: Mesoporosity development in high silica HZSM-5, *Journal of Catalysis*, 258 (2008) 243-249. ps://doi.org/10.1016/j.jcat.2008.06.019.

[31] Yang, Q., H. Zhang, M. Kong, X. Bao, J. Fei, X. Zheng, Hierarchical mesoporous ZSM-5 for the dehydration of methanol to dimethyl ether, *Chinese Journal of Catalysis*, 34 (2013) 1576-1582. https://doi.org/10.1016/S1872-2067(12)60621-4.

[32] Wei, R., C. Li, C. Yang, H. Shan, Effects of ammonium exchange and Si/Al ratio on the conversion of methanol to propylene over a novel and large partical size ZSM-5, *Journal of Natural Gas Chemistry*, 20 (2011) 261-265. https://doi.org/10.1016/S1003-9953(10)60198-3.

[33] Liu, J., C. Zhang, Z. Shen, W. Hua, Y. Tang, W. Shen, Y. Yue, H. Xu, Methanol to propylene: Effect of phosphorus on a high silica HZSM-5 catalyst, *Catalysis Communications*, 10 (2009) 1506-1509. https://doi.org/10.1016/j.catcom.2009.04.004.

[34] Papari, S., A. Mohammadrezaei, M. Asadi, R. Golhosseini, A. Naderifar, Comparison of two methods of iridium impregnation into HZSM-5 in the methanol to propylene reaction, *Catalysis Communications*, 16 (2011) 150-154. https://doi.org/10.1016/j.catcom.2011.09.024.

[35] Hu, S., J. Shan, Q. Zhang, Y. Wang, Y. Liu, Y. Gong, Z. Wu, T. Dou, Selective formation of propylene from methanol over high-silica nanosheets of MFI zeolite, *Applied Catalysis A: General*, 445–446 (2012) 215-220. https://doi.org/10.1016/j.apcata.2012.08.032.

[36] Prinz, D., L. Riekert, Formation of ethene and propene from methanol on zeolite ZSM-5: I. Investigation of Rate and Selectivity in a Batch Reactor, *Applied Catalysis*, 37 (1988) 139-154. https://doi.org/10.1016/S0166-9834(00)80757-5.

[37] Patcas, F.C., The methanol-to-olefins conversion over zeolite-coated ceramic foams, *Journal of Catalysis*, 231 (2005) 194-200. https://doi.org/10.1016/j.jcat.2005.01.016.

[38] Firoozi, M., M. Baghalha, M. Asadi, The effect of micro and nano particle sizes of H-ZSM-5 on the selectivity of MTP reaction, *Catalysis Communications*, 10 (2009) 1582-1585. https://doi.org/10.1016/j.catcom.2009.04.021.

[39] Jiao, Y., C. Jiang, Z. Yang, J. Zhang, Controllable synthesis of ZSM-5 coatings on SiC foam support for MTP application, *Microporous and Mesoporous Materials*, 162 (2012) 152-158. https://doi.org/10.1016/j.micromeso.2012.05.034.

[40] Kumita, Y., J. Gascon, E. Stavitski, J.A. Moulijn, F. Kapteijn, Shape selective methanol to olefins over highly thermostable DDR catalysts,

Applied Catalysis A: General, 391 (2011) 234-243. https://doi.org/10.1016/j.apcata.2010.07.023.

[41] Hu, S., Y. Gong, Q. Xu, X. Liu, Q. Zhang, L. Zhang, T. Dou, Highly selective formation of propylene from methanol over high-silica EU-1 zeolite catalyst, *Catalysis Communications*, 28 (2012) 95-99. https://doi.org/10.1016/j.catcom.2012.08.011.

[42] Abu-Dahrieh, J., D. Rooney, A. Goguet, Y. Saih, Activity and deactivation studies for direct dimethyl ether synthesis using CuO–ZnO–Al2O3 with NH4ZSM-5, HZSM-5 or γ-Al2O3, *Chemical Engineering Journal*, 203 (2012) 201-211. https://doi.org/10.1016/j.cej.2012.07.011.

[43] Khandan, N., M. Kazemeini, M. Aghaziarati. (2009). Dehydration of Methanol to Dimethyl Ether Employing Modified H-ZSM-5 Catalysts, *Iranian Journal of Chemical Engineering*, Vol. 6, No. 1, 3-11.

[44] Tang, Q., H. Xu, Y. Zheng, J. Wang, H. Li, J. Zhang, Catalytic dehydration of methanol to dimethyl ether over micro–mesoporous ZSM-5/MCM-41 composite molecular sieves, *Applied Catalysis A: General*, 413–414 (2012) 36-42. https://doi.org/10.1016/j.apcata.2011.10.039.

[45] Rownaghi, A.A., F. Rezaei, M. Stante, J. Hedlund, Selective dehydration of methanol to dimethyl ether on ZSM-5 nanocrystals, *Applied Catalysis B: Environmental*, 119–120 (2012) 56-61. https://doi.org/10.1016/j.apcatb.2012.02.017.

[46] Hosseini, S., M. Taghizadeh, A. Eliassi, Optimization of hydrothermal synthesis of H-ZSM-5 zeolite for dehydration of methanol to dimethyl ether using full factorial design, *Journal of Natural Gas Chemistry*, 21 (2012) 344-351. https://doi.org/10.1016/S1003-9953(11)60375-7.

[47] Hassanpour, S., F. Yaripour, M. Taghizadeh, Performance of modified H-ZSM-5 zeolite for dehydration of methanol to dimethyl ether, *Fuel Processing Technology*, 91 (2010) 1212-1221. https://doi.org/10.1016/j.fuproc.2010.03.035.

[48] Wolf, D., Dropka, N. Smejkal, Q. Buyevskaya, O. (2001). Oxidative Dehydrogenation of Propane for Propylene Production – Comparison

of Catalytic Processes. *Chem. Eng. Sci*. 56, 713-719. https://doi.org/10.1016/S0009-2509(00)00280-3.

[49] Hemelsoet, K., J.V. Mynsbrugge, K.D. Wispelaere, M. Waroquier, and V.V. Speybroeck, Unraveling the Reaction Mechanisms governing methanol to olefins catalysis by theory and experiment, *Chem Phys Chem* 2013, 14, 1526 – 1545. https://doi.org/10.1002/cphc.201201023.

[50] Wakui, K., K. Satoh, G. Sawada, K. Shiozawa, K. Matano, K. Suzuki, T. Hayakawa, Y. Yoshimura, K. Murata, F. Mizukami (2012), "Dehydrogenative Cracking of n-Butane over Modified HZSM-5 Catalysts", *Catalysis Letters*, 81, 83–88. https://doi.org/10.1023.

[51] Al-Shammari, A., S. Ali, N. Yassir, A. Aitani, K. Ogunronbi (2014), "Catalytic cracking of heavy naphtha-range hydrocarbons over different zeolites structures", *Fuel ProNissing Technology* 122, 12–22. https://doi.org/10.1016/j.fuproc.2014.01.021.

[52] Xu, R., J.Liu, C. Liang, Wen-hao (2011), "Understanding the enhanNiment of catalytic performanNi for olefin cracking: Hydrothermally stable acids in P/HZSM-5". *J. Fuel Chemistry and Technology* 39, 449-454. https://doi.org/10.1016/j.jcat.2007.02.022.

[53] Lee, J., U. Hong, S. Hwang, M. Youn, I. Song (2013), "Catalytic cracking of C5 raffinate to light olefins over lanthanum-containing phosphorous-modified porous ZSM-5: Effect of lanthanum content", *Fuel ProNissing Technology*, 109, 189-195. https://doi.org/10.1016/j.fuproc.2012.10.017.

[54] Bleken, F.L., Janssens, T.V.W., Svelle, S. et al. *Microporous Mesoporous Mater*. 2012, 164, 190-198.

[55] Jang, H., H. Min, S. Hong, G. Seo (2013), "Tetramethylbenzenium radical cations as major active intermediates of methanol-to-olefin conversions over phosphorous-modified HZSM-5 zeolites", *Journal of Catalysis*, 299, 240-248. https://doi.org/10.1016/j.jcat.2012.12.014.

[56] Han, S.Y., C.W. f, J.R. Kim, N.S. Han, W.C. Choi, C.H. Shin, Y.K. Park (2014), "Selective formation of light olefins by the cracking of heavy naphtha over acid catalysts", *Fuel*, 153, 157,160. doi: 10.1016/S0167-2991(04)80237-4.

[57] Xue, N., L. Nie, D. Fang, X. Guo, J. Shen, W. Ding (2013), "Synergistic effects of tungsten and phosphorus on catalytic cracking of butene to propene over HZSM-5", *Applied Catalysis A: General*, 352, 87–94. https://doi.org/10.1016/j.apcata.2008.09.029.

[58] Themba, E., E.M. Tshabalala, S. Scurrell (2015), Aromatization of n-hexane over Ga, Mo and Zn modified H-zsm5 zeolite catalysts, *Catalysis communication*, 72, 49-52. https://doi.org/10.1016/j.catcom.2015.06.022.

[59] Zheng, A., Z. Zhao, S. Chang, Z. Huang (2014), "Effect of crystal size of ZSM-5 on the aromatic yield and selectivity from catalytic fast pyrolysis of biomass", *Journal of Molecular Catalysis A: Chemical*, 383, 23-30. https://doi.org/10.1016/j.molcata.2013.11.005.

[60] Majhi, S., K.K. Pant (2014), "Direct conversion of methane with methanol toward higher hydrocarbon over Ga modified Mo/H-ZSM-5 catalyst", *Journal of Industrial and Engineering Chemistry* 20, 2364–2369. https://doi.org/10.1016/j.jiec.2013.10.014.

[61] Jang, H., K. Ha, J. Kim, Y. Sugi, G. Seo (2014) "Ceria and Lanthana as Blocking Modifiers for the External Surface of MFI Zeolite", *Applied Catalysis A: General* 476 175–185. https://doi.org/10.1016/j.apcata.2014.02.028.

[62] Wei, R., Ch. Li, Ch. Yang, H. Shan (2011). "Effects of ammonium exchange and Si/Al ratio on the conversion of methanol to propylene over a novel and large partical size ZSM-5", *Journal of Natural Gas Chemistry* 20, 261–265. https://doi.org/10.1016/S1003-9953(10)60198-3.

[63] Fayyazbakhsh, Ahmad, Vahid Pirouzfar, Comprehensive overview on diesel additives to reduce emissions, enhance fuel properties and improve engine performance, *Renewable & Sustainable Energy Reviews*. 2017, 74,891-901. https://doi.org/10.1016/j.rser.2017.03.046.

[64] Wang, S., Fang, C., Wang, Y. Spatiotemporal variations of energy-related CO_2 emissions in China and its in fl uencing factors: an empirical analysis based on provincial panel data. *Renew Sustain*

Energy Rev. 2016;55:505–15. https://doi.org/10.1371/journal.pone.0138666.

[65] Bogarra, M., Herreros J.M., Tsolakis A., York A.P.E., Millington P.J. Study of particulate matter and gaseous emissions in gasoline direct injection engine using on-board exhaust gas fuel reforming. *Appl Energy*. 2016; 180:245–55. https://doi.org/10.1016/j.apenergy.2016.07.100.

[66] Maikawa, C.L., Zimmerman N., Rais K., Shah M., Hawley B., Pant P., et al. Murine precision-cut lung slices exhibit acute responses following exposure to gasoline direct injection engine emissions. *Sci Total Environ.* 2016;568: 1102–9. doi: 10.1016/j.scitotenv.2016.06.173.

[67] Kianfar, E. et al., Synthesis of modified catalyst and stabilization of CuO/NH4-ZSM-5 for conversion of methanol to gasoline. *Int J Appl Ceram Technol.* 15(2018) 734-741. https://doi.org/10.1111/ijac.12830.

[68] Wang, Yeqing, Qinming Wu, Xiangju Meng, Feng-Shou Xiao, Insights into the Organotemplate-Free Synthesis of Zeolite Catalysts. *Engineering* 3 (2017) 567–574. https://doi.org/10.1016/J.ENG.2017.03.029.

[69] Fathi, Sohrab, Morteza Sohrabi, Cavus Falamaki, Improvement of HZSM-5 performance by alkaline treatments: Comparative catalytic study in the MTG reactions. *Fuel* 116 (2014) 529–537. https://doi.org/10.1016/j.fuel.2013.08.036.

[70] Yang, Lingzhi, Zhiyuan Liu, Zhi Liu, Wenyong Peng, Yunqi Liu, Chenguang Liu Correlation between H-ZSM-5 crystal size and catalytic performance in the methanol-to aromatics reaction. *Chinese Journal of Catalysis* 38 (2017) 683–690. doi: 10.1016/S1872-2067(17)62791-8.

[71] Yang, Lingzhi, Zhiyuan Liu, Zhi Liu, Wenyong Peng, Yunqi Liu & Chenguang Liu, Product distribution and catalytic performance of nano-sized H-ZSM-5 zeolites in the methanol-toaromatics (MTA) reaction. *Journal Petroleum Science and Technology*, Volume 35,

2017 - Issue 10, 955-962. https://doi.org/10.1080/10916466.2017.1292293.

[72] Pan, Meng, Peng Li, Jiajun Zheng, Yujian Liu, Qinglan Kong, Huiping Tian, Ruifeng Li, Zeolite-zeolite composite composed of Y zeolite and single-crystallike ZSM-5 zeolite: Fabricated by a process like big fish swallowing little one. *Materials Chemistry and Physics* 194 (2017) 49-54. https://doi.org/10.1016/j.matchemphys.2017.03.022.

[73] Ghorbanpour, A., A. Gumidyala, L.C. Grabow, S.P. Crossley, J.D. Rimer, Epitaxial growth of ZSM-5@Silicalite-1:a core-shell zeolite designed with passivated surface acidity, *Acs Nano* 9 (2015) 4006-4016. doi: 10.1021/acsnano.5b01308.

[74] Zhao, Q., B. Qin, J. Zheng, Y. Du, W. Sun, F. Ling, X. Zhang, R. Li, Coreeshell structured zeoliteezeolite composites comprising Y zeolite cores and nano-b zeolite shells: synthesis and application in hydrocracking of VGO oil, *Chem. Eng. J.* 257 (2014) 262-272. doi: 10.1016/j.cej.2014.07.056.

[75] Pirngruber, G.D., C. Laroche, M. Maricar-Pichon, L. Rouleau, Y. Bouizi, V. *Zeolite–zeolite composite fabricated by polycrystalline Y zeolite crystals parasitizing ZSM-5 zeolite.* Volume 30, Issue 16 28 August 2015, pp. 2434-2446 . https://doi.org/10.1557/jmr.2015.225.

[76] Zheng, J., Q. Zeng, Y. Zhang, Y. Wang, J. Ma, X. Zhang, W. Sun, R. Li, Hierarchical porous zeolite composite with a core-shell structure fabricated using b-zeolite crystals as nutrients as well as cores, *Chem. Mater*. 22 (2010) 6065-6074. doi: 10.1021/cm101418z.

[77] Greer, H., P.S. Wheatley, S.E. Ashbrook, R.E. Morris, W. Zhou, Early stage reversed crystal growth of zeolite A and its phase transformation to sodalite, *J. Am. Chem. Soc.* 131 (2009) 17986-17992. doi: 10.1021/ja907475z.

[78] Wang, Z., W. Wan, J. Sun, W. Carrillo-Cabrera, D. Grüner, X. Yin, S. Qiu, G. Zhu,X. Zou, Epitaxial growth of core-shell zeolite X-A composites, *Cryst Eng Comm* 14 (2012) 2204-2212. doi: 10.1039/C2CE06432D.

[79] Mante, O.D., F.A. Agblevor, S.T. Oyama, R. Mcclung, Catalytic pyrolysis with ZSM-5 based additive as co-catalyst to Y-zeolite in two reactor configurations, *Fuel* 117 (2014) 649-659. doi: 10.1016/j.fuel. 2013.09.034.

[80] Zhang, H., Y. Ma, K. Song, Y. Zhang, Y. Tang, Nano-crystallite oriented selfassembled ZSM-5 zeolite and its LDPE cracking properties: effects of accessibility and strength of acid sites, *J. Catal.* 302 (2013) 115-125. https://doi.org/10.1016/j.jcat.2013.03.019.

[81] Huang, S., P. Chen, B. Yan, S. Wang, Y. Shen, X. Ma, Modification of Y zeolitewith alkaline treatment: textural properties and catalytic activity for diethyl carbonate synthesis, *Ind. Eng. Chem. Res*. 52 (2013) 6349-6356. doi: 10.1021/ie3032235.

[82] Zahra,G, Sourinejad Hossein, Kazemian and Sohrab Rohani, Application of zeolites in aquaculture industry: a review. *Reviews in Aquaculture* (2016) 0, 1–21. https://doi.org/10.1111/raq.12148.

[83] Li, L, Xiaojing Cui, Junfen Li,and Jianguo Wang, Synthesis of SAPO-34/ZSM-5 Composite and Its Catalytic Performance in the Conversion of Methanol to Hydrocarbons. *J. Braz. Chem. Soc.*, Vol. 26, No. 2, 290-296, 2015. http://dx.doi.org/10.5935/0103-5053.20140279.

[84] Yu, Q, Xiaolong Tang, Honghong Yi, Fabrication of ZSM-11(5) particles with nanorods oriented-stacking morphology by an *in-situ* feeding method. *Chemical Engineering Journal*, Volume 314, 15 April 2017, Pages 212-222. https://doi.org/10.1016/j.cej.2016.12.116.

[85] Song, C. and Kirby S. 'Shape-selective alkylation of naphthalene with isopropanol over mordenite catalysts', *Microporous Materials.* 1994, 2(5), pp. 467-476. https://doi.org/10.1016/0927-6513(94)00024-7.

[86] Barthomeuf, D. 'Zeolite acidity dependence on structure and chemical environment. Correlations with catalysis', *Materials Chemistry and Physics.* 1987, 17(1-2), pp. 49-71. https://doi.org/10.1016/0254-0584(87)90048-4.

[87] Smith, K. and Roberts, S.D. 'Regioselective dialkylation of naphthalene', *Catalysis Today,* 2000, 60(3-4), pp. 227-233. https://doi.org/10.1016/S0920-5861(00)00339-4.

[88] Smith, M.B. March's Advanced Organic Chemistry: Reactions, Mechanisms, and Structure. *Wiley*, 2013. doi: 10.1021/ed046p537.1.

[89] Song, C. and Kirby, S.'Shape-selective alkylation of naphthalene with isopropanol over mordenite catalysts', *Microporous Materials.*1994, 2(5), pp. 467-476. https://doi.org/10.1016/0927-6513(94)00024-7.

[90] Mingjin, Z., Anmin, Z., Feng, D., Yong, Y. and Chaohui, Y. 'Surface chemical modification of zeolites and their catalytic performance for naphthalene alkylation', *Science in China Series B: Chemistry*, 2003, 46(2), pp. 216-223. https://doi.org/10.1360/03yb9030.

[91] Wang, J., Park, J.-N., Park, Y.-K. and Lee, C.W. 'Isopropylation of naphthalene by isopropyl alcohol over USY catalyst: an investigation in the high-pressure fixed-bed flow reactor', *Journal of Catalysis*, 2003,220(2), pp. 265-272. https://doi.org/10.1016/S0021-9517(03) 00212-4.

[92] Marathe, R.P., Mayadevi, S., Pardhy, S.A., Sabne, S.M. and Sivasanker, S. 'Alkylation of naphthalene with t-butanol: use of carbon dioxide as solvent', *Journal of Molecular Catalysis A: Chemical*, 2002, 181(1-2), pp. 201-206. https://doi.org/10.1016/ S1381-1169(01)00364-8.

[93] Liu, Z., Moreau, P. and Fajula, F. 'Liquid phase selective alkylation of naphthalene with t-butanol over large pore zeolites', *Applied Catalysis A: General.* 1997, 159(1-2), pp. 305-316. https://doi.org/ 10.1016/S0926-860X(97)00060-4.

[94] Gläser, R. and Weitkamp, J., 'Supercritical Carbon Dioxide as a Reaction Medium for the ZeoliteCatalyzed Alkylation of Naphthalene', *Industrial & Engineering Chemistry Research*, 2003, 42(25), pp. 6294-6302. doi: 10.1021/ie000153v.

[95] Krithiga, T., Vinu, A., Ariga, K., Arabindoo, B., Palanichamy, M. and Murugesan, V.,'Selective formation 2,6-diisopropyl naphthalene over mesoporous Al-MCM-48 catalysts', *Journal of Molecular Catalysis A: Chemical*, 2005,237(1-2), pp. 238-245. https://doi.org/10.1016/ j.molcata.2005.05.008.

[96] Anand, R., Maheswari, R., Gore, K.U., Khaire, S.S. and Chumbhale, V.R., 'Isopropylation of naphthalene over modified faujasites: effect

of steaming temperature on activity and selectivity', *Applied Catalysis A: General*, 2003, 249(2), pp. 265-272. https://doi.org/10.1016/S0926-860X(03)00204-7.

[97] Abdel-Wahhab, M.A., Nada S.A., Khalil F.A. Physiological and toxicological responses in rats fed aflatoxin-contaminated diet with or without sorbent materials. *Animal Feed Science and Technology.* 2002, 97: 209–219. https://doi.org/10.1016/S0377-8401(01)00342-X.

[98] Al-Nasser, A, Al-Zenki S, Al-Saffar A, Abdullah F, Al-Bahouh M, Mashaly M ., Zeolite as a feed additive to reduce salmonella and improve production performance in broilers. *International Journal of Poultry Science.* 2011, 10: 448–454. doi: 10.3923/ijps.2011.448.454.

[99] Amend, D.F., Croy T.R., Goven B.A., Johnson K.A., McCarthy D.H., *Transportation of fish in closed systems: methods to control ammonia, carbon dioxide, ph, and bacterial growth*, 1982. https://doi.org/10.1577/1548-8659(1982)111<603:TOFICS>2.0.CO;2.

[100] Saxena, S.K., Viswanadham N., Al-Muhtaseb A.H. Enhanced production of high octane gasoline blending stock from methanol with improved catalyst life on nano-crystalline ZSM-5 catalyst. *J Ind Eng Chem* 2014;20:2876–82. https://doi.org/10.1016/j.jiec.2013.11.021.

[101] Ariful, Islam M., Nahid Hasan M., Mahmud Y., Reza M.S., Mahmud M.S., Kamal M. et al., Obtainable drugs for fish hatchery operation and grow-out ponds in Bangladesh. *Annual Research & Review in Biology 2014*, 4: 1036–1044. doi: 10.9734/ARRB/2014/7287.

[102] Hensen, E.J.M., Zhu Q., Janssen R.A.J., Magusin P.C.M.M., Kooyman P.J., Van santen RA. Selective oxidation of benzene to phenol with nitrous oxide over MFI zeolites.1. On the role of iron and aluminum. *J Catal* 2005; 233:123–35. https://doi.org/10.1016/j.jcat.2005.04.009.

[103] Phu, N.H., Hoa T.T.K., Tan N.V., Thang H.V., Ha P.L. Characterization and activity of Fe–ZSM-5 catalysts for the total oxidation of phenol in aqueous solutions. *Appl Catal B* 2001;34:267–75. https://doi.org/10.1016/S0926-3373(01)00220-X.

[104] Ashraful, Alam M., Mamnur Rashid M. Use of aquamedicines and chemicals in aquaculture in Shatkhira district, Bangladesh. *IOSR*

Journal of Pharmacy and Biological Sciences. 2014, 9: 5–9. doi: 10.3923/ajava.2013.401.408.

[105] Dyballa, M., P. Becker, D. Trefz, E. Klemm, A. Fischer, H. Jakob, M. Hunger, Parameters Influencing the Selectivity to Propene in the MTO Conversion on 10-Ring Zeolites: Directly Synthesized Zeolites ZSM-5, ZSM-11, and ZSM-22, *Appl. Catal. A: Gen.*, 510 (2015) 233-243. https://doi.org/10.1016/j.apcata.2015.11.017.

[106] Usman, A.N. (1990). Methanol Conversion to Light Olefins over Commercial Zeolites. MSC Thesis, *King Fahad Universit of Petroleum & Minerals.* https://eprints.kfupm.edu.sa/10223/1/10223.pdf.

[107] Wu, G., Hei F., Guan N., Li L. Oxidative dehydrogenation of propane with nitrous oxide over Fe–MFI prepared by ion-exchange: effect of acid post-treatments. *Catal Sci Technol* 2013;3:1333–42. doi: 10.1039/C3CY20782J.

[108] Chen, N.Y., Reagan, W.J. (1979).Evidence of autocatalysis in methanol to hydrocarbon reactions over zeolite catalysts, *Journal of Catalysis*, vol. 59, Issue 1, August, 123-129. https://doi.org/10.1016/S0021-9517(79)80050-0.

[109] Dessau, R.M., LaPierre R.B. (1982)On the mechanism of methanol conversion to hydrocarbonsover HZSM-5, *Journal of Catalysis*, vol 78(1), November,136-141. doi: 10.1039/F19817702209.

[110] CMAI World Propylene Supply Study. *CMAI Report 2001*, www.cmaiglobal.com.

[111] Ren, Y., Liu G., Mi Z. An introduction on spectroscopy identification of framework hetero-atom in molecular sieves. *Chem* 2004;6:433–8. https://www.scopus.com/record/display.uri?eid=73549123030&origin=inward&txGid=046754024d742b3da77e77766680ebe9.

[112] Benito P.L., Agayubo A.G., Aguayo A.T., Castilla M., Bilbao J. Concentrationdependent kinetic model for catalyst deactivation in the MTG process. *Ind Eng Chem Res* 1996; 35:81–9. doi: 10.1021/ie950124y.

[113] Chen, T.J., Ruziska, P.A., Stuntz, G.F., Ladwig, P.K. (2002). *Multiple Feed Process for the Production of Propylene*, U.S. Patent No. 6,339,181, January 15.

[114] Fu, A. (1998). Deep Catalytic Cracking Plant Produces Propylene in Thailand. *Oil &Gas J.* 96, 49.

[115] Alwahabi, S.M. (2003), *Conversion of methanol to light olefins on SAPO-34: Kinetic modeling and reactor design*, Ph.D Dissertation, King Saud University.

[116] Teketel, Shewangizaw, Wegard Skistad, Sandrine Benard, Unni Olsbye, Karl Petter Lillerud, Pablo Beato, and Stian Svelle, Shape Selectivity in the Conversion of Methanol to Hydrocarbons: The Catalytic Performance of One-Dimensional 10-Ring Zeolites: ZSM-22, ZSM-23, ZSM-48, and EU-1. *ACS Catal.*, 2012, 2 (1), pp 26–37. doi: 10.1021/cs200517u.

[118] Losch, Pit, Thomas C. Hoff, Joy F. Kolb, Claire Bernardon, Jean-Philippe Tessonnier, and Benoît Louis, Mesoporous ZSM-5 Zeolites in Acid Catalysis: Top-Down vs. Bottom-Up Approach. *Catalysts* 2017, *7*, 225; doi: 10.3390/catal7080225.

[119] Bjørgen, Morten, Finn Joensen, Martin Spangsberg Holm, Unni Olsbye, Karl-Petter Lillerud, Stian Svelle, Methanol to gasoline over zeolite H-ZSM-5: Improved catalyst performance by treatment with NaOH. *Applied Catalysis A: General* 345 (2008) 43–50. https://doi.org/10.1016/j.apcata.2008.04.020.

[120] Zuoxing Di, Cheng Yang, Xuejing Jiao, Jianqing Li, Jinhu Wu, Dongke Zhang, A ZSM-5/MCM-48 based catalyst for methanol to gasoline conversion. *Fuel* 104 (2013) 878–881. https://doi.org/10.1016/j.fuel.2012.09.079.

[121] Bjørgen, M., Svelle, S., Joensen, F., Nerlov, J., Kolboe, S., Bonino, F., Palumbo, L., Bordiga, S., Olsbye, U., 2007. Conversion of methanol to hydrocarbons over zeolite H-ZSM-5: on the origin of the olefinic species. *J. Catal.* 249, 195-207. https://doi.org/10.1016/j.jcat.2007.04.006.

[122] Shareh, F.B., Kazemeini, M., Asadi, M., Fattahi, M., 2014. Metal promoted mordenite catalyst for methanol conversion into light

olefins. *Pet. Sci. Technol.* 32, 1349-1356. https://doi.org/10.1080/10916466.2012.656871.

[123] Zhijian, W, Wei Wu, Wan Chen, Hong Yang, and Dongke Zhang, Direct Synthesis of Hierarchical ZSM-5 Zeolite and Its Performance in Catalyzing Methanol to Gasoline Conversion. *Ind. Eng. Chem. Res.*, 2014, *53* (50), pp 19471–19478. doi: 10.1021/ie5036308.

[124] Zhang, J., Zhang, H., Yang, X., Huang, Z., Cao, W., 2011. Study on the deactivation and regeneration of the ZSM-5 catalyst used in methanol to olefins. *J. Nat. Gas Chem.* 20, 266-270. https://doi.org/10.1016/S1003-9953(10)60183-1.

[125] Keil, F.J., 1999. Methanol-to-hydrocarbons: process technology. *Microporous Mesoporous Mater.* 29, 49-66. https://doi.org/10.1016/S1387-1811(98)00320-5.

[126] He, Y., Liu, M., Dai, C., Xu, S., Wei, Y., Liu, Z., Guo, X., 2013. Modification of nanocrystalline HZSM-5 zeolite with tetrapropylammonium hydroxide and its catalytic performance in methanol to gasoline reaction. *Chin. J. Catal.* 34, 1148-1158. https://doi.org/10.1016/S1872-2067(12)60579-8.

[127] Dagle, R.A., Lizarazo-Adarme, J.A., Lebarbier Dagle, V., Gray, M.J., White, J.F., King, D.L., Palo, D.R., 2014. Syngas conversion to gasoline-range hydrocarbons over Pd/ZnO/Al2O3 and ZSM-5 composite catalyst system. *Fuel Process. Technol.* 123, 65-74. https://doi.org/10.1016/j.fuproc.2014.01.041.

[128] Bjørgen, M., Joensen, F., Lillerud, K.-P., Olsbye, U., Svelle, S., 2009. The mechanisms of ethene and propene formation from methanol over high silica H-ZSM-5 and H-beta. *Catal. Today* 142, 90-97. https://doi.org/10.1016/j.cattod.2009.01.015.

[129] Wu, L., Degirmenci, V., Magusin, P.C.M.M., Lousberg, N.J.H.G.M., Hensen, E.J.M., 2013. Mesoporous SSZ-13 zeolite prepared by a dual-template method with improved performance in the methanol-to-olefins reaction. *J. Catal.* 298, 27-40. https://doi.org/10.1016/j.jcat.2012.10.029.

[130] Lee, J.H., Park, M.B., Lee, J.K., Min, H.-K., Song, M.K., Hong, S.B., 2010. Synthesis and characterization of ERI-type UZM-12 zeolites

and their methanol-to-olefin performance. *J. Am. Chem. Soc.* 132, 12971-12982. doi: 10.1021/ja105185r.

[131] Kumar, V.A., K.K. Pant, D. Kunzru (1997), "Potassium-Containing Calcium Aluminate Catalysts for Pyrolysis of N-heptane". *Applied Catalysis A:*, 162, 193-200. https://doi.org/10.1016/S0926-860X(97)00097-5.

[132] Zimmermann, H., R. Karimzadeh, M. Akbarnejad (2002), "Steam Cracking of Naphtha in Packed Bed Reactors", *Ind. Eng. Chem. Res*, 41, 1419-1424. doi: 10.1021/ie010636e.

[133] Bellussi, G., P. Pollesel (2005), "Industrial Applications of Zeolite catalysts: Production and Uses of Light Olefins", *Studies in SurfaNi ScienNi and Catalysis*, 158, 1201–1212. https://doi.org/10.1016/S0167-2991(05)80466-5.

[134] Meng, Pan, Peng Li, Jiajun Zheng, Yujian Liu, Qinglan Kong, Huiping Tian, Ruifeng Li, Zeolite-zeolite composite composed of Y zeolite and single-crystallike ZSM-5 zeolite: Fabricated by a process like "big fish swallowing little one", *Materials Chemistry and Physics*. 2017 194, 49-54. https://doi.org/10.1016/j.matchemphys.2017.03.022.

[135] Johari, S., Kalbassi M., Soltani M., Yu I. Application of nanosilver-coated zeolite as water filter media for fungal disinfection of rainbow trout (Oncorhynchus mykiss) eggs. *Aquaculture International*. 2015, 24: 23–38. https://doi.org/10.1007/s10499-015-9906-7.

[136] Ogura, M., S. Shinomiya, J. Tateno, Y. Nara, M. Nomura (2001), "Alkali-treatment technique — new method for modification of structural and acid-catalytic properties of ZSM-5 zeolites", *Applied Catalysis A: General*, 219, 33-43. https://doi.org/10.1016/S0926-860X(01)00645-7.

[137] Wakui, K., K. Satoh, G. Sawada, K. Shiozawa, K. Matano, K. Suzuki, T. Hayakawa, Y. Yoshimura, K. Murata, F. Mizukami (2012), "Dehydrogenative Cracking of n-Butane over Modified HZSM-5 Catalysts", *Catalysis Letters*, 81, 83–88. https://doi.org/10.1023/A:1016064123823.

[138] Al-Shammari, A., S. Ali, N. Yassir, A. Aitani, K. Ogunronbi (2014), "Catalytic cracking of heavy naphtha-range hydrocarbons over different zeolites structures", *Fuel ProNissing Technology* 122, 12–22. https://doi.org/10.1016/j.fuproc.2014.01.021.

[139] Xu, R., J. Liu, C. Liang, Wen-hao (2011), "Understanding the enhanNiment of catalytic performanNi for olefin cracking: Hydrothermally stable acids in P/HZSM-5". *J. Fuel Chemistry and Technology* 39, 449-454. https://doi.org/10.1016/j.jcat.2007.02.022.

[140] Kumara, V.A., K.K. Pant, D. Kunzru (1997), "Potassium-Containing Calcium Aluminate Catalysts for Pyrolysis of N-heptane". *Applied Catalysis A:*, 162, 193-200. https://doi.org/10.1016/S0926-860X(97)00097-5.

[141] Pant, K.K., D. Kunzru (2002), "Catalytic Pyrolysis of N-Heptane on Unpromoted and Potassium Promoted Calcium Aluminates", *Chemical Engineering Journal*, 87, 219-225. https://doi.org/10.1016/S1385-8947(01)00231-5.

[142] Maia, A.J., B.G. Oliveira, P.M. Esteves, B. Louis, Y.L. Lam, M.M. Pereira (2011), "Isobutane and n-butane cracking on Ni-ZSM-5 catalyst: Effect on light olefin formation", *Applied Catalysis A: General*, 403, 58-64. https://doi.org/10.1016/j.apcata.2011.06.014.

[143] Lee, J., U. Hong, S. Hwang, M. Youn, I. Song (2013), "Catalytic cracking of C5 raffinate to light olefins over lanthanum-containing phosphorous-modified porous ZSM-5: Effect of lanthanum content", *Fuel ProNissing Technology*, 109, 189-195. https://www.ncbi.nlm.nih.gov/pubmed/24245282.

[144] Wang, X., Z. Zhao, C. Xu, A. Duan, L. Zhang, G. Jiang (2007), "Effects of Light Rare Earth on Acidity and Catalytic PerformanNi of HZSM-5 Zeolite for Catalytic Cracking of Butane to Light Olefins", *Journal of Rare Earths*, 25, 321–328. doi: 10.1021/ie1006245.

[145] Kenichi, W., S. Ko-ichi, S. Goro, S. Koji, M. Koichi (1999), "1-Butene cracking to propene over HZSM-5". *Stud. Surf. Sci. Catal.* 125, 449–456. https://doi.org/10.1016/j.molcata.2010.05.004.

[146] Wakui, K., K. Sato, G. Sawada, K. Matano, T. Hayakawa, Y. Yoshimura, K. Murata, F. Mizukami (2002), "Cracking of n-Butane

Over Alkaline Earth-Containing HZSM-5 Catalysts", *Catalysis Letters*, 84, 259–264. doi: 10.1023/A:1021448508130.

[147] Lu, J., Z. Zhao, C. Xu, A. Duan, P. Zhang (2006), "CrHZSM-5 zeolites - Highly efficient catalysts for catalytic cracking of isobutane to produNi light olefins", *Catalysis Letters*, 109, 65-70.

[148] Xu, R., J. Liu, C. Liang, Wen-hao (2011), "Understanding the enhanNiment of catalytic performanNi for olefin cracking: Hydrothermally stable acids in P/HZSM-5", *J. Fuel Chemistry and Technology* 39, 449-454.

[149] Hassanpour, S., F. Yaripour, M. Taghizadeh, Performance of modified H-ZSM-5 zeolite for dehydration of methanol to dimethyl ether, *Fuel Processing Technology*, 91 (2010) 1212-1221.

[150] Hosseini, S., M. Taghizadeh, A. Eliassi, Optimization of hydrothermal synthesis of H-ZSM-5 zeolite for dehydration of methanol to dimethyl ether using full factorial design, *Journal of Natural Gas Chemistry*, 21 (2012) 344-351. https://doi.org/10.1016/S1003-9953(11)60375-7.

[151] Abu-Dahrieh, J., D. Rooney, A. Goguet, Y. Saih, Activity and deactivation studies for direct dimethyl ether synthesis using CuO–ZnO–Al2O3 with NH4ZSM-5, HZSM-5 or γ-Al2O3, *Chemical Engineering Journal*, 203 (2012) 201-211. https://doi.org/10.1016/j.cej.2012.07.011.

[152] Khandan, N., M. Kazemeini, M. Aghaziarati. (2009). Dehydration of Methanol to Dimethyl Ether Employing Modified H-ZSM-5 Catalysts, *Iranian Journal of Chemical Engineering*, Vol. 6, No. 1, 3-11. http://www.sid.ir/en/journal/ViewPaper.aspx?ID=170105.

[153] Tang, Q., H. Xu, Y. Zheng, J. Wang, H. Li, J. Zhang, Catalytic dehydration of methanol to dimethyl ether over micro–mesoporous ZSM-5/MCM-41 composite molecular sieves, *Applied Catalysis A: General*, 413–414 (2012) 36-42. https://doi.org/10.1016/j.apcata.2011.10.039.

[154] Prinz, D., L. Riekert, Formation of ethene and propene from methanol on zeolite ZSM-5: I. Investigation of Rate and Selectivity in a Batch Reactor, *Applied Catalysis*, 37 (1988) 139-154. https://doi.org/10.1016/S0166-9834(00)80757-5.

[155] Hu, S., Y. Gong, Q. Xu, X. Liu, Q. Zhang, L. Zhang, T. Dou, Highly selective formation of propylene from methanol over high-silica EU-1 zeolite catalyst, *Catalysis Communications*, 28 (2012) 95-99. https://doi.org/10.1016/j.catcom.2012.08.011.

[156] Lee, J., U. Hong, S. Hwang, M. Youn, I. Song (2013), "Catalytic cracking of C5 raffinate to light olefins over lanthanum-containing phosphorous-modified porous ZSM-5: Effect of lanthanum content", *Fuel ProNissing Technology*, 109, 189-195. https://doi.org/10.1016/j.fuproc.2012.10.017.

[157] Jang, H., H. Min, S. Hong, G. Seo (2013), "Tetramethylbenzenium radical cations as major active intermediates of methanol-to-olefin conversions over phosphorous-modified HZSM-5 zeolites", *Journal of Catalysis*, 299, 240-248. https://doi.org/10.1016/j.jcat.2012.12.014.

[158] Lu, J., Z. Zhao, C. Xu, A. Duan, X. Wang, P. Zhang (2009), "Catalytic cracking of isobutane over HZSM-5, FeHZSM-5 and CrHZSM-5 catalysts with different Si/Al ratios", *Journal of Porous Materials*, 15, 213-220. doi:10.1016/j.catcom.2005.10.011.

[159] Han, S.Y., C.W. f, J.R. Kim, N.S. Han, W.C. Choi, C.H. Shin, Y.K. Park (2014), "Selective formation of light olefins by the cracking of heavy naphtha over acid catalysts", *Fuel*, 153, 157,160. doi: 10.1016/S0167-2991(04)80237-4.

[160] Xue,T., Q. Zhang, H. Song (2012), "Fluoride-treated H-ZSM5 as a highly selective and stable catalyst for the production of propylene from methyl halides", *Journal of catalysis"*, 295, 232-241. https://doi.org/10.1016/j.jcat.2012.08.014.

[161] G. Zhao, J. Teng, Z. Xie, W. Jin, W. Yang, Q. Chen, Y. Tang (2008), "Effect of phosphorus on HZSM-5 catalyst for C4-olefin cracking reactions to produNi propylene", *Journal of Catalysis* 248, 29–37. doi: 10.1016/j.jcat.2007.02.027.

[162] Xue, N., L. Nie, D. Fang, X. Guo, J. Shen, W. Ding (2013), "Synergistic effects of tungsten and phosphorus on catalytic cracking of butene to propene over HZSM-5", *Applied Catalysis A: General*, 352, 87–94. https://doi.org/10.1016/j.apcata.2008.09.029.

[163] Han, Dongmin, Nannan Sun, Jianwei Liu, Chunyi Li, Honghong Shan, Chaohe Yang, Synergistic effect of W and P on ZSM-5 and its catalytic performance in the cracking of heavy oil, *Journal of Energy Chemistry* 23(2014)519–526. https://doi.org/10.1016/S2095-4956(14)60180-7.

[164] Themba, E., E.M. Tshabalala, S. Scurrell (2015), Aromatization of n-hexane over Ga, Mo and Zn modified H-zsm5 zeolite catalysts, *Catalysis communication,* 72,49-52. https://doi.org/10.1016/j.catcom. 2015.06.022.

[165] Rownaghi, A., F. Rezaei, J. Hedlund (2012), "Selective formation of light olefin by n-hexane cracking over HZSM-5: InfluenNi of crystal size and acid sites of nano- and micrometer-sized crystals", *Chemical Engineering Journal,* 191, 528-533. https://doi.org/10.1016/j.cej. 2012.03.023.

[166]Olah, G.A. Beyond oil and gas: the methanol economy. *Angew Chem Int Ed* 2005;44:2636–9.https://doi.org/10.1002/anie.200462121.

[167] Bjorgen, M., Joensen F., Holm M.S., Olsbye U., Lillerud K.P., Svelle S. Methanol to gasoline over zeolite H-ZSM-5: improved catalyst performance by treatment with NaOH. *Appl Catal A* 2008;345:43–50. https://doi.org/10.1016/j.apcata.2008.04.020.

[168] Van de Loosdrecht, J, Datt M, Visagie JL. Carbon coated supports for cobalt based Fischer–Tropsch catalysts. *Top Catal* 2014;57:430–6. https://doi.org/10.1007/s11244-013-0198-8.

[169] Salkuyeh, Y.K., Adams T.A. Combining coal gasification, natural gas reforming, and external carbonless heat for efficient production of gasoline and diesel with CO2 capture and sequestration. *Energy Convers Manage* 2013;74:492–504. https://doi.org/10.1016/j. enconman.2013.07.023.

[170] Ni, Y., Sun A., Wu X., Hai G., Hu J., Li T., et al. The preparation of nano-sized H[Zn, Al]ZSM-5 zeolite and its application in the aromatization of methanol. *Microporous Mesoporous Mater* 2011;143:435–42. https://doi.org/10.1016/j.micromeso.2011.03.029.

[171] Ghassemi, H., Shahsavan-Markadeh R. Effects of various operational parameters on biomass gasification process; a modified equilibrium

model. *Energy Convers Manage* 2014; 79:18–24. https://doi.org/10.1016/j.enconman.2013.12.007.

[172] Lefevere, Jasper, Steven Mullens, Vera Meynen, Jasper Van Noyen, Structured catalysts for methanol-to-olefins conversion: a review., *Chemical Papers*, September 2014, Volume 68, Issue 9, pp 1143–1153. https://doi.org/10.2478/s11696-014-0568-0.

[173] Jiao, Y.L., Jiang, C.H., Yang, Z.M., & Zhang, J.S. (2012). Controllable synthesis of ZSM-5 coatings on SiC foam support for MTP application. *Microporous and Mesoporous Materials*, 162, 152–158. doi: 10.1016/j.micromeso.2012.05.034.

[174] Bleken, F.L., Chavan, S., Olsbye, U., Boltz, M., Ocampo, F.,& Louis, B. (2012). Conversion of methanol into light olefins over ZSM-5 zeolite: Strategy to enhance propene selectivity. *Applied Catalysis A: General*, 447–448, 178–185. doi: 10.1016/j.apcata.2012.09.025.

[175] Lee, Y.J., Kim, Y.W., Viswanadham, N., Jun, K.W., & Bae, J.W. (2010). Novel aluminophosphate (AlPO) bound ZSM-5 extrudates with improved catalytic properties for methanol to propylene (MTP) reaction. *Applied Catalysis A: General*, 374, 18–25. doi: 10.1016/j.apcata.2009.11.019.

[176] Jiao, Y.L., Jiang, C.H., Yang, Z.M., Liu, J., & Zhang, J.S. (2013). Synthesis of highly accessible ZSM-5 coatings on SiC foam support for MTP reaction. *Microporous and Mesoporous Materials*, 181, 201–207. doi: 10.1016/j.micromeso.2013.07.013.

[177] Zaidi, H.A., and K.K. Pant, Catalytic Activity of Copper Oxide ImpregnatedHZSM-5 in Methanol Conversion to Liquid Hydrocarbons, *The Canadian Journal of chemical engineering*, volume 83, (2005). https://doi.org/10.1002/cjce.5450830606.

[178] Bjørgen, Morten, Finn Joensen, Martin Spangsberg Holm, Unni Olsbye, Karl-Petter Lillerud, Stian Svelle, Methanol to gasoline over zeolite H-ZSM-5: Improved catalyst performance by treatment with NaOH, *Applied Catalysis A: General* 345 (2008) 43–50. https://doi.org/10.1016/j.apcata.2008.04.020.

[179] Li, Liping, Xiaojing Cui, Junfen Lia and Jianguo Wang, Synthesis of SAPO-34/ZSM-5 Composite and Its Catalytic Performance in the

Conversion of Methanol to Hydrocarbons, *J. Braz. Chem. Soc.*, Vol. 26, No. 2, 290-296, 2015. http://dx.doi.org/10.5935/0103-5053.20140279.

[180] Lønstad Bleken, Francesca, Sachin Chavan, Unni Olsbye, Marilyne Boltz, Fabien Ocampo, Benoit Louis, Conversion of methanol into light olefins over ZSM-5 zeolite: Strategy to enhance propene selectivity, *Applied Catalysis A: General* 447–448 (2012) 178–185. https://doi.org/10.1016/j.apcata.2012.09.025.

[181] Samaneh Hosseini, Majid Taghizadeh, Ali Eliassi, Optimization of hydrothermal synthesis of H-ZSM-5 zeolite for dehydration of methanol to dimethyl ether using full factorial design, *Journal of Natural Gas Chemistry* 21(2012)344–351. https://doi.org/10.1016/S1003-9953(11)60375-7.

[182] Hassanpour, Samaneh, Fereydoon Yaripour, Majid Taghizadeh, Performance of modified H-ZSM-5 zeolite for dehydration of methanol to dimethyl ether, *Fuel Processing Technology* 91 (2010) 1212–1221. https://doi.org/10.1016/j.fuproc.2010.03.035.

[183] Sabour, Behrouz, Mohammad Hassan Peyrovi, Touba Hamoule, Mehdi Rashidzadeh, Catalytic dehydration of methanol to dimethyl ether (DME) over Al-HMS catalysts, *Journal of Industrial and Engineering Chemistry*,20(2014),222-227. https://doi.org/10.1016/j.jiec.2013.03.044.

[184] Rownaghi, Ali A., Fateme Rezaei, Matteo Stante, Jonas Hedlund, Selective dehydration of methanol to dimethyl ether on ZSM-5 nanocrystals, *Applied Catalysis B: Environmental* 119–120 (2012) 56–61. https://doi.org/10.1016/j.apcatb.2012.02.017.

[185] Abu-Dahrieh, ehad, David Rooney, Alexandre Goguet, Youssef Saih, Activity and deactivation studies for direct dimethyl ether synthesis using CuO–ZnO–Al2O3 with NH4ZSM-5, HZSM-5 or γ -Al2O3, *Chemical Engineering Journal* 203 (2012) 201–211. https://doi.org/10.1016/j.cej.2012.07.011.

[186] Nuria, Martín, Zhibin Li, Joaquín Martínez-Triguero, Jihong Yu, Manuel Moliner and Avelino Corma. Nanocrystalline SSZ-39 zeolite

as an efficient catalyst for the methanol-to-olefin (MTO) process, *Chem. Commun.*, 2016, 52, 6072-6075.

[187] Kianfar, Ehsan. Recent advances in synthesis, properties, and applications of vanadium oxide nanotube, *Microchemical Journal*, 145:966-978, 2019.

[188] Kianfar, E., M. Salimi, S. Hajimirzaee, B. Koohestani, Methanol to gasolin econversion over CuO/ZSM 5 catalyst synthesized using sonochemistry method, *Int. J. Chem. React. Eng.* 17(2)(1-10)(2019).

[189] Kianfara, E., Synthesis and characterization of AlPO4/ZSM-5 catalystformethanol conversion to dimethylether, *Russ. J. Appl. Chem.* 91(10)(2018)1710–1720.

[189] Keil, F.J. "Methanol-to-hydrocarbons: Process Technology", *Micropor. Mesopor. Mat.*, 29 (1999) 49-66.

[190] *http://izasc.ethz.ch/fmi/xsl/IZA-SC/ft.xsl* (last consulted: January 29th 2008).

[191] *http://www.iza-online.org*.

[192] *http://www.iza-online.org/IZA const IZA.pdf* (last consulted January 30th 2008).

[193] Uriarte, A.K., Rodkin, M.A., Gross, M.J., Kharithonov, A.S. and Panov, G.I. "Direct hydroxylation of benzene to phenol by nitrous oxide", *Stud. Surf. Sci. Catal.*, 110 (1997) 857.

[194] Martens, J.A., Verrelst, W.H., Mathys, G.M., Brown, S.H. and Jacobs, P.A. *Angew. Chem. Int. Ed.*, 44 (2005) 5687.

[195] Corma, Avelino. "State of the art and future challenges of zeolites as catalysts", *Journal of Catalysis* 216.1 (2003) 298-312.

[196] Paal, Zoltan, and P.G. Menon. "*Hydrogen effects in catalysis*", Marcel Dekker, New York, (1988) 449.

[197] Martens, J.A. and Jacobs, P.A. Stud. Surf., "Crystalline Microporous Phosphates: a Family of Versatile Catalysts and Adsorbents", *Sci. Catal.*, 85 (1994) 653.

[198] Ernst, S., Puppe, L. and Weitkamp, "Synthesis and Characterization of CoAPO and CoAPSO Molecular Sieves", *J. Stud. Surf. Sci. Catal.*, 49A (1988) 231.

[199] Martens, J.A., Grobet, P.J. and Jacobs, "Catalytic activity and Si, Al, P ordering in microporous silicoaluminophosphates of the SAPO-5, SAPO-11, and SAPO-37 type", *P.A. J. Catal.*, 126 (1990) 299.

[200] Weisz, P.B. and Frilette, "Catalysis by crystalline aluminosilicates: III. Dehydration of isopropyl alcohol catalyzed by sodium faujasite in the presence of CO2", *V.J. J. Phys. Chem.*, 64 (1964) 382.

[201] Froment, G.F., Dehertog, W.J.H., Marchi, A.J. "Zeolite Catalysis in The Conversion of Methanol into Olefins". *Catalysis*, 9 (1992) 1-64.

[202] Denayer, J.F., Ocakoglu, A.R., Martens, J.A. and Baron, "Investigation of inverse shape selectivity in alkane adsorption on SAPO-5 zeolite using the tracer chromatography technique", *G.V. J. Catal.*, 226 (2004) 240.

[203] Derouane, E.G., Andr´e, J.M. and Lucas, "Surface curvature effects in physisorption and catalysis by microporous solids and molecular sieves", *A.A. J. Catal.*, 58 (1988) 110.

[204] Martens, J.A., Parton, R., Uytterhoeven, L., Jacobs, P.A. and Froment, "Selective conversion of decane into branched isomers: A comparison of platinum/ZSM-22, platinum/ZSM-5 and platinum/USY zeolite catalysts", *G.F. Appl. Catal.*, 76 (1991) 95.

[205] Barrer, R.M., Baynham, J.M., and McCallum, N. "Hydrothermal Chemistry of Silicates", Compounds structurally elated to Analcite. *J. Chem. Soc.*, Part V (1953) 4035–4041.

[206] Barrer \, R.M. and White, E.A.D. "The hydrothermal chemistry of silicates- Synthetic crystalline sodium aluminosilicates", *J. Chem. Soc.*, Part II(1952) 1561–1571.

[207] Barrer, R.M. and White, E.A.D. The hydrothermul chemistry of silicates. "Synthetic lithium aluminusilicates", *J. Chem. Soc.*, Part I (1951) 1267–1278.

[208] Garcia-Sanchez, A., Garcia-Perez, E., Dubbeldam, D., Krishna, R., and Calero, S. "A simulation study of alkanes in Linde type A zeolites", *Adsorp. Sci. Technol.*, 25 (2007) 417–427.

[209] Breck, D.W., Eversole, W.G., Milton, R.M., Reed, T.B., and Thomas, T.L. "Crystalline zeolites. I. Properties of a new synthetic zeolite, type A", *J. Am. Chem. Soc.*, 78 (1956) 5963–5971.

[210] Frising, T. and Leflaive, P. "Extraframework cation distributions in X and Y faujasite zeolites: a review", *Micropor. Mesopor. Mat*., 114 (2008), 27–63.

[211] Mortier, W.J., Pluth, J.J., and Smith, J.V. "Positions of cations and molecules in zeolites with the mordenite-type framework", I. Dehydrated calcium- exchanged ptilolite. *Mat. Res. Bull.,* 10 (1975) 1037–1045.

[212] Raatz, F., Marcilly, C., and Freund, E., "Comparison between small port and large port mordenites", *Zeolites,* 5 (1985), 329–333.

[213] Tillmanns, E., Fischer, R.X., and Baur, W.H. "Chabazite-type framework in the new zeolite willhendersonite", $CaAl_3Si_3O_{125}H_2O$., *Neues Jahrb. Mineral. Monats.,* 12 (1984) 547–558.

[214] Diaz-Cabanas, M.J., Barrett, P.A., and Camblor, M.A. "Synthesis and structure of pure Si O2 chabazite: the SiO2 polymorph with the lowest framework density", *Chem. Commun*., (1998) 1881–1882.

[215] Smith, J.V. and Bennett, J.M., "Enumeration of 4-connected 3-dimensional nets and classification of framework silicates: the infinite set of ABC-6 nets; the Archimedean and. sigma. - related nets". *Am. Mineral.,* 66 (1981), 777–788.

[216] Mentzen, B.F., "Crystallographic determination of the positions of the monovalent H, Li, Na, K, Rb, and Tl cations in fully dehydrated MFI Type Zeolites", *J. Phys. Chem.* C, 111 (2007), 18932–18941.

[217] Calleja, G., Pau, J., and Calles, J.A., "Pure and multicomponent adsorption equilibrium of carbon dioxide, ethylene, and ropane on ZSM-5 zeolites with different Si/Al ratios", *J. Chem. Eng. Data,* 43 (1998), 994–1003.

[218] Kaarsholm, M., Rafii B, Joensen F, Cenni R, Chaouki J, Patience GS. "Kinetic modeling of methanol-to-olefin reaction over ZSM-5 in fluid bed", *Ind Eng Chem Res*, 49 (2010) 29-38.

[219] "Effect of SAPO-34's composition on its physico-chemical properties and deactivation in MTO process", *Applied Catalysis A: General*, 364 (2009) 48–56.

[220] United States Patent, "*Synthesis of SAPO-34 with essentially pure CHA framework*", US7691354.

[221] Mokharab, S., W.A. Poe, J.G. Speight, *Handbook of natural gas transmission and processing,* Elsevier Inc. Burlington, 2006.
[222] Methanex Co., *Methanol Annual Report,* 2012.
[223] Shana.ir, *Iran Produces 12% of World Methanol*, Dec 22, 2012.
[224] *IHS Chemical World Analysis,* Propylene Annual Production, 2013.
[225] ICIS Co., *Annual Report, Propylene Prices: markets & analysis,* 2013.
[226] Venner, R., Kantorowicz, S. Metathesis; "Refinery and Ethylene Plant Application", in *Proceedings of the European Petrochemical Technology Conference* (EPTC), Vienna, Austria, 2001.
[227] Mokrani, Touhami, and Mike Scurrell. "Gas Conversion to Liquid Fuels and Chemicals: The Methanol Route-Catalysis and Processes Development", *Catalysis Reviews,* 51 (2009) 1-145.
[228] Fu, A., "Deep Catalytic Cracking Plant Produces Propylene in Thailand", *Oil & Gas J*. 96 (1998) 49-52.
[229] Kirk-othmer, "*Encyclopedia of Chemical Technology*", 4th edition, John Wiley & Sons publishers, New York 1993.
[230] Cavani, F., Trifiro, F., "The Oxidative Dehydrogenation of Ethane and Propane as an Alternative Way for the Production of Light Olefins", *Catal. Today,* 24 (1995) 307-a313.
[231] Hinsen, W., Bytyn, W., Baerns, M., "Oxidative Dehydrogenation and Coupling of Methane", In *Proceedings of the 8th International Congress on Catalysis,* Berlin, 3 (1984) 581.
[232] Burch, R., Squire, G.D., Tsang, S.C., "Role of Chlorine in Improving Selectivity in the Oxidative Coupling of Methane to Ethylene", *Appl. Catal.* 46 (1989) 69-87.
[233] Hydrocarbon processing, KBR, "*Petrochemical Processes 2010 Index*", Gulf Publishing Co.
[234] Keil, F.J. "Methanol-to-hydrocarbons: Process Technology", *Micropor. Mesopor. Mat.*, 29 (1999) 49-66.
[235] *http://izasc.ethz.ch/fmi/xsl/IZA-SC/ft.xsl* (last consulted: January 29th 2008).
[236] *http://www.iza-online.org.*

[237] *http://www.iza-online.org/IZA const IZA.pdf* (last consulted January 30th 2008).

[238] Uriarte, A.K., Rodkin, M.A., Gross, M.J., Kharithonov, A.S. and Panov, G.I. "Direct hydroxylation of benzene to phenol by nitrous oxide", *Stud. Surf. Sci. Catal.*, 110 (1997) 857.

[239] Martens, J.A., Verrelst, W.H., Mathys, G.M., Brown, S.H. and Jacobs, P.A. *Angew. Chem. Int. Ed.*, 44 (2005) 5687.

[240] Corma, Avelino. "State of the art and future challenges of zeolites as catalysts", *Journal of Catalysis* 216.1 (2003) 298-312.

[241] Paal, Zoltan, and P.G. Menon. *"Hydrogen effects in catalysis*", Marcel Dekker, New York, (1988) 449.

[242] Martens, J.A. and Jacobs, P.A. Stud. Surf., "Crystalline Microporous Phosphates: a Family of Versatile Catalysts and Adsorbents", *Sci. Catal.*, 85 (1994) 653.

[243] Seyed Mohammad Faghih, Ehsan Kianfar, Modeling of fluid bed Reactor of Ethylene Di Chloride production in Abadan Petrochemical based on three-phase hydrodynamic model, *International Journal of Chemical Reactor Engineering*, 16(9):1-14(2018).

[244] Kianfar, Ehsan, Mahmoud Salimi, Farshid Kianfar, Mehran Kianfar, Seyyed Ali Hasan Razavikia, CO2 /N2 separation using polyvinyl chloride iso-phthalic acid/aluminium nitrate nanocomposite membrane, *Macromolecular Research*, 27(1):83–89,2019.

[245] kianfar, Ehsan, Maryam Shirshahi, Farangis Kianfar, farshid kianfar, Simultaneous prediction of the density, viscosity and electrical conductivity of pyridinium-based hydrophobic ionic liquids using artificial neural network, *Silicon*, 10(6):2617–2625,2018.

[246] Salami, Mahmoud, Vahid Pirouzfar Ehsan Kianfar, Enhanced Gas Transport Properties in Silica Nanoparticles Filler-Polystyrene Nanocomposite Membranes, *Colloid and Polymer Science.* January 2017, Volume 295, Issue 1, pp 215–226.

[247] Kianfar, Ehsan, Vahid Pirouzfar, Hossein Sakhaeinia, An experimental study on absorption/stripping CO2 using Mono-ethanol amine hollow fiber membrane contactor, *Journal of the Taiwan*

Institute of Chemical Engineers, Volume 80, November 2017, Pages 954-962.

[248] Salami, Mahmoud, Vahid Pirouzfar, Ehsan Kianfar, Novel nanocomposite membranes prepared with PVC/ABS and silica nanoparticles for CH4/C2H6 separation, *Polymer Science,* Series A, 2017, Vol. 59, No. 4, pp. 566–574.

[249] Kianfar, Ehsan, Mehdi Baghernejad and Yasaman Rahimdashti, Study Synthesis of Vanadium Oxide Nanotubes with two template hexadecylamin and hexylamine(2015), *Biological Forum – An International Journal* 7(1): 16711685(2015).

[250] Kianfar, Ehsan, Production and Identification of Vanadium Oxide Nanotubes(2015), *Indian Journal of Science and Technology*, Vol 8(S9), 455-464, May 2015.

In: Advances in Chemistry Research ISBN: 978-1-53617-112-9
Editor: James C. Taylor

Chapter 2

PHENYLALANINE AMMONIA-LYASE IN HIGHER PLANTS: A KEY ENZYME FOR PLANT DEVELOPMENT

Ana Hortência Fonseca Castro*, Mairon César Coimbra, Sara Thamires Dias da Fonseca and Alessandra Aparecida de Melo Souza
Federal University of São João del-Rei, *Campus* Centro-Oeste, Divinópolis, Minas Gerais, Brazil

ABSTRACT

Phenylalanine ammonia-lyase (PAL) (E.C. 4.3.1.5) is a key and regulatory enzyme of the biosynthesis pathway of the phenylpropanoids and their derivatives. PAL catalyzes the transformation by the non-oxidative deamination of the amino acid *L*-phenylalanine in *trans*-cinnamic acid, without the requirement of cofactors; this is the first step for the biosynthesis of phenylpropanoid-derived compounds. The produced cinnamic acid is the direct precursor of several phenolic

* Corresponding Author's Email: acastro@ufsj.edu.br.

compounds, such as tannins, flavonoids, lignans, coumarins and lignins, which play an important role in plant growth and development. Studies with transgenic plants have shown that the activity of this enzyme is one of the main control points in the regulation of the phenylpropanoid route. Phenylalanine ammonia-lyase may be isolated from various sources, and its presence may be observed in a wide variety of higher plants and in some yeasts, fungi and bacteria. Immunocytochemical methods have shown that in plants, the synthesis of this enzyme can occur in the cytoplasm and chloroplasts. In many plants, a small multi-gene family encodes PAL and the expression of the *PAL* gene is regulated by several factors, such as mechanical injury, infections and plant development. The PAL levels may fluctuate significantly at relatively short intervals in response to a wide variety of stimuli, and the concomitant increase in the phenylalanine ammonia-lyase and phenolic compounds levels has been demonstrated in plant tissues. PAL activity may be regulated by abiotic and biotic factors, such as light, wounding, temperature, UV irradiation, nutrient deficiency, herbivory, growth regulators, mechanical injuries, metal ions, insect attack, fungal and viral infections, as well as the stage of plant development and the degree of cell and tissue differentiation. In some species, elicitors induce PAL transcriptionally and enzymatically. This chapter will present a description of phenylalanine ammonia-lyase, in relation to structure, localization, expression, regulation, assay methods and the factors influencing PAL activity, as well as its importance to the phenylpropanoid pathway for plant growth and development.

Keywords: PAL, phenylpropanoid pathway, plant development

1. INTRODUCTION

The discovery of phenylalanine ammonia-lyase (PAL) started in 1955, when the Canadian plant physiologists Brown and Neish attempted to understand the chemical basis of lignin, a structural component of the plant cell wall. Lignin is an aromatic biopolymer constructed via the oxidative coupling of a number of simple phenylpropanoid alcohols to form a sturdy polymer (Renault, Werck-Reichhart and Weng 2019). Lignin is involved in maintaining the rigidity of plants since it confers essential mechanical properties to the cells required for water transport and structural support (Tobimatsu and Schuetz 2019). Brown and Neish (1955a, 1955b) identified *L*-phenylalanine, cinnamic acid and shikimic acid (C_6, C_3 monomers) as

precursors in lignin biosynthesis in higher plants, and they suggested that the presence of a specific enzyme system may promote lignin formation from these elements (Brown and Neish 1956). Later, McCalla and Neish (1959) and Levy and Zucker (1960) found additional evidence that the key element in the synthesis of lignin was an enzyme that converts *L*-phenylalanine into *trans*-cinnamic acid and ammonia (posteriorly known as phenylalanine ammonia-lyase or PAL). Koukol and Conn (1961) described the isolation, partial purification, and characterization of PAL from barley seedlings (*Hordeum vulgare* L. var. Sravat).

Phenylalanine ammonia-lyase (PAL, E.C. 4.3.1.5) is a member of the lyase family and the first key enzyme of the phenylpropanoid pathway, a secondary metabolism pathway (Jones 1984). According to Cui et al. (2014), recently, this class has been designated as EC 4.3.1.24 (phenylalanine ammonia lyases), EC 4.3.1.25 (tyrosine ammonia lyases) and EC 4.3.1.26 (phenylalanine/tyrosine ammonia lyases). Rösler et al. (1997) reported that PAL from monocotyledonous plants can use tyrosine as a substrate and it also has tyrosine ammonia-lyase (TAL); PAL from dicotyledonous plants only utilizes phenylalanine efficiently (Kyndt et al. 2002). PAL acts as a linkage between primary and secondary metabolism, because this enzyme supplies precursors for different kinds of secondary metabolites through the phenylpropanoid pathway, by controlling the carbon flux (Vogt 2010; Hsieh et al. 2011; Rahmatabadi et al. 2019). PAL catalyzes the transformation by the non-oxidative deamination of the amino acid *L*-phenylalanine in *trans*-cinnamic acid and a free ammonium ion, without the requirement of cofactors; this is the first step for the biosynthesis of phenylpropanoid-derived compounds (Santiago, Louro and Oliveira 2000; Assis et al. 2001; Cui et al. 2014). The produced cinnamic acid is the direct precursor of physiologically important phenolic compounds such as tannins, flavonoids, lignans, coumarins, stilbenes and lignin (Khakdan, Alizadeh and Ranjbar 2018; Rahmatabadi et al. 2019; Tobimatsu and Schuetz 2019). Phenylpropanoid-derived compounds play an important role in plant growth and development, including establishing mechanical support, signaling molecules mediating plant-microbe interactions, antioxidant systems or UV-absorbing compounds, pigments attracting pollinators and disease resistance

(Dixon and Paiva 1995; Dixon et al. 2002; Lau et al. 2007; Zhang and Liu 2015).

A small multi-gene family with two to four copies in the haploid genome encodes the PAL genes, so it presents as multiple isoforms with various expression patterns in different tissues (Liu et al. 2006; Zhang and Liu 2015; Khakdan, Alizadeh and Ranjbar 2018). PAL may be isolated from various sources; its presence may be observed in a wide variety of higher or not plants and in a few yeasts, fungi and bacteria, but not in animals (Camm and Towers 1973; Fritz, Hodgins and Abell 1976; Xiang and Moore 2005; Cui et al. 2014; Zhang and Liu 2015).

PAL activity varies greatly depending on the stage of development, plant species and environmental conditions (Kováčik and Klejdus 2012). The levels of PAL may fluctuate significantly in response to the photoperiod, pathogenic attacks, wounding, UV irradiation, heavy metals, low levels of nitrogen and phosphate, low temperatures and signaling molecules, including jasmonic acid (JA), salicylic acid (SA), and abscisic acid (ABA) (Dixon and Paiva 1995; Weisshaar and Jenkins 1998; Janas et al. 2010; Shang, Li and Dong 2012; Zhang and Liu 2015). Nagai et al. (1988) reported that kinetin induces PAL in tobacco. PAL is highly controlled at the transcription level, reflecting a complex and sophisticated regulatory control mechanism during plant development (Zhang and Liu 2015; Khakdan, Alizadeh and Ranjbar 2018).

This chapter will present a description of phenylalanine ammonia-lyase related to its structure, localization, expression, regulation, assay methods and the biotic and abiotic factors influencing PAL activity, as well as its importance for the phenylpropanoid pathway and plant growth and development.

2. Structure, Localization and Kinetics

Depending on the species, PAL has a variable molecular mass, with the most reported PAL range in size being between 300 and 340 kDa (Hyun et al. 2011); some exceptions have been observed, such as sizes of 280 kDa in

Pinus taeda (Whetten and Sederoff 1992) and 152 kDa in *Ocimum basilicum* (Hao et al. 1996), for example. The dimensions of PAL are 95.72x145.09Å based in its X-ray structure (Calabrese et al. 2004; Macdonald and D'Cunha 2007). PAL can be purified by several sources; however, Hyun et al. (2011) reported difficulties in its purification, due to the low abundance of PAL in cells and changes in its size and properties during purification. PAL developed from histidine ammonia-lyase (HAL), when fungi and plants diverged from other kingdoms, so their structure is similar to HAL folding (Ritter and Schulz 2004; Macdonald and D'Cunha 2007).

PAL is normally a tetrameric protein with four identical subunits, a characteristic that can be found in homotetrameric protein (Hsieh et al. 2010; Hyun et al. 2011; Cui et al. 2014). Pairs of monomers form a protomer with a single active site (Camm and Towers 1973). In parsley (*Petroselinum crispum*), the molecular architecture of PAL is a predominantly helical protein, with 52% of residues in 23 α-helices and only 5% of residues in 8 β-chains (Ritter and Schulz 2004). According to Macdonald and D'Cunha (2007), PAL also has a central core of parallel helices of different lengths. Besides that, there is only one section of β sheet with more than three residues, 231–237 and 240–246, residing in the funnel region leading to the active site.

PAL and their isoforms are soluble proteins; therefore, they do not have any membrane anchor or membrane-spanning domains (Achnine et al. 2004). PAL is localized mainly in the cytosol, but some isoforms have a differential subcellular localization and are located partially in the endoplasmic reticulum and microsomes, as is shown in tobacco (*Nicotiana tabacum*) plants (Rasmussen and Dixon 1999; Santiago, Louro and Oliveira 2000; Achnine et al. 2004).

The proposed mechanism of PAL catalysis involves a post-translational modification that occurs autocatalytically by the cyclization and dehydration of three amino acid residues, alanine, serine and glycine, leading to the formation of a prosthetic electrophile in the active site of PAL, named 4-methylideneimidazole-5-one (MIO) (Schwede, Retey and Schulz 1999; Calabrese et al. 2004; Macdonald and D'Cunha 2007; Turner 2011). Currently, two mechanisms have been proposed for the MIO-dependent

reactions catalyzed by PAL. The first mechanism involves the stabilization of the intermediate carbanion, causing an electrophilic attack of the MIO group on the amine group of the substrate. The second mechanism, named Friedel–Crafts, leads to the activation and hence abstraction of the β-proton followed by the elimination of ammonia and the regeneration of the MIO group (Macdonald and D'Cunha 2007; Cooke, Christianson and Bruner 2009; Turner 2011). Macdonald and D'Cunha (2007) and Turner (2011) verified details about PAL reaction catalysis.

The kinetics of PAL are complex, controversial, highly source dependent and not completely understood (Macdonald and D'Cunha 2007). Whetten and Sederoff (1992) reported the enzymatic kinetics of PAL in loblolly pine (*Pinus taeda*); the isoelectric point was estimated to be 5.8 and the purified enzyme follows Michaelis–Menten kinetics, with a Km of 27 μM for L-phenylalanine. According to Jones (1984), the enzyme is commonly described as showing negative cooperativity. Williams and Hiroms (1967) described the basic catalysis reaction of PAL, in which trans-cinnamic acid was released before ammonia.

3. PAL GENES AND DIFFERENTIAL REGULATION

Usually, a small multi-gene family with two to four copies in the haploid genome encodes PAL genes (Cramer et al. 1989; Khakdan, Alizadeh and Ranjbar 2018), which have multiple isoforms, as demonstrated for the first time by Bolwell et al. (1985) in *Phaseolus vulgaris*. Zhang and Liu (2015) suggested that PAL isoforms might have distinct, but redundant functions in plant growth, development, and plant-environment interactions, since PAL isogenes often exhibit a unique but overlapping spatial and temporal expression pattern. PAL genes have been identified and cloned in many different types of plants, such as *Salvia miltiorrhiza* (Song and Wang 2008), *Dendrobium candidum* (Jin et al. 2013), *Ginkgo biloba* (Zhang, Gou and Liu 2014), *Carthamus tinctorius* (Dehghan et al. 2014) and *Ocimum basilicum* (Khakdan, Alizadeh and Ranjbar 2018). Song and Wang (2008) described a PAL gene designated as *SmPAL1* whose transcription pattern analysis

indicated expression in all examined tissues, but more highly in the leaf. *SmPAL1* was found to be induced by various treatments, including ABA, wounding, and dehydration.

PAL activity is modulated in plants during development in different tissues, and in response to environmental signals (Wanner et al. 1995). Zhang and Liu (2015) provide a good review of PAL regulation. According to these authors, PAL activity regulation can occur through several mechanisms, such as product inhibition, transcriptional and translational regulation, post-translational inactivation and proteolysis, enzyme organization/subcellular compartmentation, and metabolite feedback regulation (Zhang and Liu 2015). Olsen et al. (2008) reported an example of the transcriptional regulation of PAL. Nitrogen depletion particularly induces the expression of *PAL1* and *PAL2* and the downstream phenylpropanoid–flavonoid biosynthetic genes; it increases the accumulation of flavonoids (kaempferol and quercetin), anthocyanins, and sinapic acid. Therefore, studies have revealed that environmental factors might temporarily increase the cellular level of PAL (Jones, 1984). Thus, after the initial increase, PAL often decreases rapidly to near basal levels, considered a post-translational event (Jones 1984; Zhang, Gou and Liu 2014).

4. PAL ASSAY

PAL activity is determined by the observation and measurement of the amount of the *L*-phenylalanine that reacts or the trans-cinnamic acid that is formed at the end of the reaction (Macdonald and D'Cunha 2007). PAL activity has been assayed by spectrophotometry in a wide variety of samples, such as shoots (Kováčik and Klejdus 2012), hypocotyls and cotyledons (Sreelakshmi and Sharma 2008), oil flesh (Machado et al. 2013), leaves (Astaneh et al. 2018), fruits (Assis et al. 2001), roots (Marchand et al. 2010) and leaf rosettes (Olsen et al., 2008). Fresh samples or acetone powder may be used for PAL extraction using sodium borate buffer (pH 8.8), phosphate buffer (pH 7.0) or Tris-HCl buffer (pH 8.0), containing ß-mercaptoethanol,

EDTA and/or polyvinylpolypyrrolidine (Cheng and Breen 1991; Assis et al. 2001; Sreelakshmi and Sharma 2008; Kováčik and Klejdus 2012; Astaneh et al. 2018). The reaction mixture normally contains buffer, *L*-phenylalanine, and crude extract (Cheng and Breen 1991; Assis et al. 2001). The reaction is carried out for 60 to 90 min at 30 to 40°C and the absorbance change is recorded at 290 nm (Zucker 1965). The rate of the formation of *trans*-cinnamic acid is taken as a measure of enzyme activity, using an increase in 0.01 A at 290 nm as the formation of 3.09 nmol of *trans*-cinnamic acid (Saunders and McClure 1975).

Spectrophotometry is the most commonly used method to assay PAL activity due to its low cost and time-saving characteristics (Kováčik and Klejdus 2012). However, in some cases, due to the low activity of this enzyme, spectrophotometric methods used for the detection of *t*-cinnamate are not satisfactory and results differ (Ferrarese, Rodrigues and Ferrarese-Filho 2000). In addition, the presence of numerous UV-absorbing compounds in the plant tissue may interfere in this assay, as well as the composition of blank (with or without phenylalanine) (Kováčik and Klejdus 2012).

High performance liquid chromatography (HPLC) analysis is an additional tool for PAL activity assays. This method requires relatively expensive equipment, but allows for the analysis of numerous samples, low activities of PAL and the unambiguous detection of cinnamic acid due to separation through an HPLC column (Scott et al. 1992; Kováčik and Klejdus 2012). According to Ferrarese, Rodrigues and Ferrarese-Filho (2000), HPLC reduces the analysis time and eliminates the purification steps.

5. PHENYLPROPANOIDS

The pheylpropanoids constitute a group of secondary metabolites that contain a phenyl group attached to a side chain of three carbons in their chemical structure, named phenylpropane (C_6, C_3) (Le Roy et al. 2016). This basic structure forms several compounds with different biological activities.

Phenylpropanoid biosynthesis starts through the shikimate pathway (Vogt 2010), a metabolic route for the biosynthesis of aromatic amino acids, such as phenylalanine, tyrosine, and tryptophan (Zabalza et al. 2017). After this, PAL catalyzes the transformation by the non-oxidative deamination of *L*-phenylalanine in *trans*-cinnamic acid and a free ammonium ion, without the requirement of cofactors (Vanholme, El Houari and Boerjan 2019). *Trans*-cinnamic acid is converted into *p*-coumaroyl CoA (Figure 1), a central metabolite that is the direct precursor for flavonoid or lignin biosynthesis and an indirect precursor for coumarins, lignans and condensed tannins (Vogt 2010).

Phenylpropanoids act as mediators of various processes related to the growth and development of plants, such as reproduction, resistance against pathogens and herbivory, UV radiation protection, indicators of stressful situations (such as light and nutrient variation) and cell wall components (Vogt 2010; Liu, Osbourn and Ma 2015). Therapeutically, phenylpropanoids have antioxidant, anticancer, antihypertensive, antimicrobial and anti-inflammatory activities (Vogt 2010; Liu, Osbourn and Ma 2015; Salehi et al., 2019; Vanholme, El Houari and Boerjan 2019).

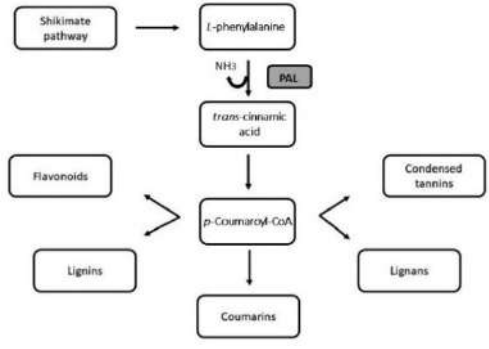

Figure 1. General biosynthetic phenylpropanoids pathway.

5.1. Flavonoids

Known as substances that are responsible for plant color, the chemical structure of flavonoids was identified at the end of the 19th century. The

initial studies focused on the production of pigmentation, and their medical potential was only explored in the 1930s (Perez-Vizcaino and Fraga 2018).

Flavonoids constitute the larger and more diverse group of phenolic compounds (Nabavi et al. 2018), derived from the condensation of two or more phenyl propane units that have a basic skeleton of diphenylpropanes (C_6-C_3-C_6) (Alu'datt et al. 2017). The different types of substitutions in their chemical structure, the degree of oxidation and the pattern of carbon ring hydroxylation form some subclasses: flavones, isoflavones, flavonones, flavonols, flavanols and anthocyanins (Figure 2) (Bakoyiannis et al. 2019; Nagula and Wairkar 2019).

Flavonoids biosynthesis occurs by two routes: the shikimate and the acetate pathways. In the shikimate pathway, *L*-phenylalanine form the *p*-coumaroyl CoA and this binds to three malonyl-CoA molecules derived from the acetate pathway (Raffa et al. 2017; Nabavi et al. 2018). About 7,000 flavonoids are already known and all have the same biosynthesis route. Flavonoids have several biological activities, such as antioxidant, antiallergic, anti-inflammatory, antiplatelet agent, chemoprotective, anticancer, chelator, antimicrobial, antimutagenic and vasodilator activities (Raffa et al. 2017; Nabavi et al. 2018; Nagula and Wairkar 2019). In plants, they are responsible for pigmentation and act as visual attractors, photoreceptors, antioxidants and antimicrobials (Nabavi et al. 2018).

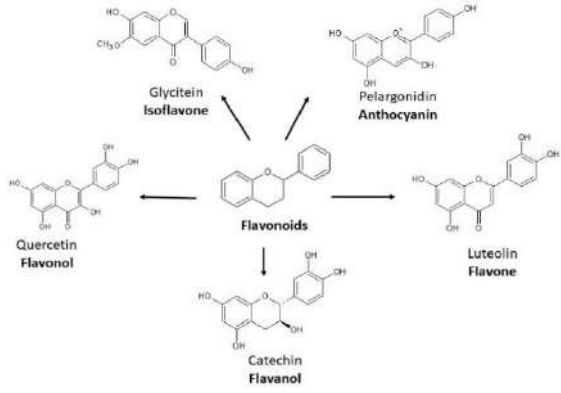

Figure 2. The most common subclasses of flavonoids.

5.2. Lignin

Lignin is a structural component of the plant cell wall and the most abundant aromatic polymer in nature (Xu et al. 2018; Chio, Sain and Qin 2019). Lignin is an aromatic biopolymer constructed via the oxidative coupling of a number of simple phenylpropanoid alcohols to form a sturdy polymer (Renault, Werck-Reichhart and Weng 2019). It is involved in maintaining the rigidity of plants since lignin confers the essential mechanical properties to the cells required for water transport and structural support (Tobimatsu and Schuetz 2019). The chemical structure of lignin is complex and diverse (Chio, Sain and Qin 2019; Vanholme et al. 2019) and it varies according to origin (Xu et al., 2018), plant species, tissue, cell and wall layers, being influenced by internal and external factors (Vanholme et al. 2019).

The main precursors for lignin polymerization are three hydroxycinnamyl alcohols, *p*-coumaryl alcohol, coniferyl alcohol and sinapyl alcohol (Figure 3), through radical coupling, to origin p-hydroxyphenyl (H), guaiacyl (G), and syringyl (S) lignin units, respectively (Chio, Sain and Qin 2019; Renault, Werck-Reichhart and Weng 2019). However, other diverse monomers have already been discovered (Renault, Werck-Reichhart and Weng 2019). Lignin can bind to hemicellulose and cellulose, forming the lignocellulose polymer. The lignocellulose compositions on xylem varying by 40 – 55% of cellulose, 24 – 40% of hemicellulose and 18 – 35% of lignin, depending on the wood type (Chio, Sain and Qin 2019).

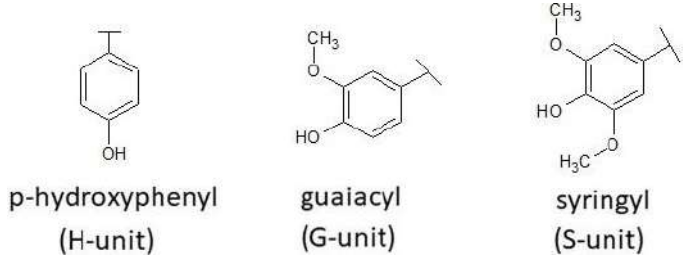

Figure 3. Basic monomers in lignin molecule.

According to the variation of its composition, lignin has several physical-chemical characteristics and biological activities (Renault, Werck-Reichhart and Weng 2019). Lignin is part of the plant cell wall (Guo et al. 2018) and provides hardness to the plant fibers and xylem cells. In addition, lignification confers resistance against animals and microorganisms, being considered a chemical and physical barrier (Renault, Werck-Reichhart and Weng 2019).

5.3. Coumarins

Coumarins are phenolic compounds of the molecular formula $C_9H_6O_2$ and 2H-1-benzopyran-2-one core structure (Matern, Lüer and Kreusch 1999; Garrard 2014; Sui et al. 2019). Currently, there are more than 1,300 known coumarins widely distributed in the Apiaceae, Fabaceae, Rosaceae, Rubiaceae, Rutaceae, Saxifragaceae and Solanaceae families (Sui et al. 2019). Derived from the phenylpropanoid pathway, coumarins resulting from *trans*-cinnamic acids cyclization can be divided into four main categories: furanocoumarins (e.g., psoralen), simple coumarins (e.g., aesculetin, umbelliferone and scopoletin), pyranocoumarins (e.g., seselin) and pyrone-substituted coumarins (e.g., warfarin) (Figure 4) (Matern, Lüer and Kreusch 1999; Lin et al. 2013).

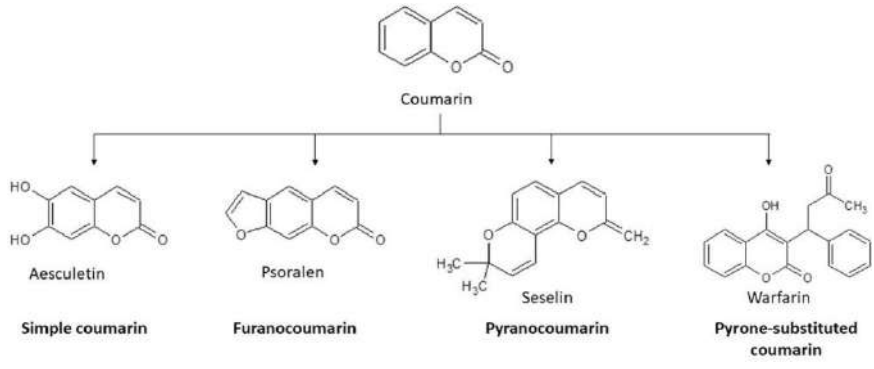

Figure 4. Different categories of coumarins and examples.

Coumarins have many biological activities and industrial uses. Whereas the cosmetics industry uses it in perfumes, coumarins are important for producing anticoagulants in the pharmaceutical industry, such as synthetic warfarin (Lin et al. 2013; Revankar et al. 2017). Coumarins have many known biological activities, such as antifungal (Xu et al. 2019), antiviral (Hwu et al. 2019), antitumor (Dai et al. 2019), anti-inflammatory (Chen et al. 2017) and antithrombotic effects (Kasperkiewicz, Ponczek and Budzisz 2018), and can also regulate plant growth (Abenavoli et al. 2006).

5.4. Tannins

Bate-Smith and Swain (1962) defined tannins as "naturally occurring water soluble polyphenolic compounds having a molecular weight between 500 and 3000, capable of precipitating alkaloids as well as gelatin and other proteins from aqueous solutions". Tannins are compounds that are widely distributed in nature, and found in plants utilized as food (grains, fruits, wine and tea) and feed (forage) that exhibit diverse structures (Chung et al. 1998; Huang et al. 2018; Hoyos-Martínez et al. 2019). Its distribution depends of the species and parts of plants being more abundant in barks, seeds, leaves, roots and rhizomes, as well depending on external factors (e.g., temperature, water, light) (Hoyos-Martínez et al. 2019).

Usually, tannins are classified into two major groups: hydrolysable and condensed tannins (also referred to as proanthocyanidin) (Huang et al. 2018). According to Chung et al. (1998), hydrolysable tannins contain a central core of polyhydric alcohol (mainly glucose), and hydroxyl groups esterified by gallic acid or hexahydroxydiphenic acid, yielding gallotannins and ellagitannins, respectively. After hydrolysis, gallotannins produce gallic acids and ellagitannins produce hexahydroxydiphenic acid that, by lactonization, yield ellagic acid. Condensed tannins are formed by the polymerization of flavonoids molecules, mainly flavan-3-ols and flavan-3,4-diols, or a mixture of the two (Figure 5) (Chung et al. 1998; Huang et al. 2018; Hoyos-Martínez et al. 2019).

In plants, the role of tannins includes protection against UV light and chemical defense against animals, insects, fungi and bacteria (Tondi et al. 2013). Tannins are widely used in the pharmaceutical and food industry (Hoyos-Martínez et al. 2019). They are responsible for the astringency of fruits, juices and wines (Chung et al. 1998). Several biological activities are reported for these compounds, including antioxidant (Arina and Harisun 2019), anti-inflammatory (Maryam et al. 2019), wounding health (Su et al. 2017), and antimicrobial properties (Santos et al. 2017), as well as effects against some vascular complications of diabetes (Laddha and Kulkarni 2019).

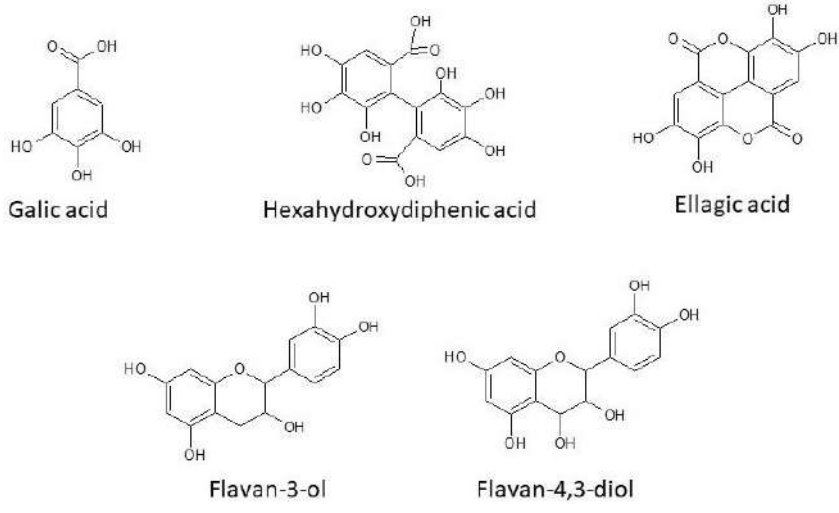

Figure 5. Basic units of hydrolysable and condensed tannins.

5.5. Lignans

Lignans are phenolic compounds that consist of phenylpropanoids dimers formed by monomers, with the basic structure composed of C_6-C_3 units (Landete 2012; Dar and Arumugam 2013; Kiyama 2016; Markulin et al. 2019). Its basic units are linked by the C8 central carbon of their propyl side chains (Umezawa 2003; Dar and Arumugam 2013). These dimers are

divided into three different groups: lignans, neolignans and hybrid lignans (Kumar, Silakari and Kaur 2012). Further, according to the carbon skeleton, oxygen presence and cyclization pattern, these groups are also subdivided into other subgroups: furofuran, furan, dibenzylbutane, dibenzylbutyrolactone, aryltetralin, arylnaphthalene, dibenzocyclooctadiene and dibenzylbutyrolactol (Umezawa 2003; Suzuki and Umezawa 2007). Like other compounds derived from phenylpropanoids, lignans are biosynthesized from *L*-phenylalanine by the phenylpropanoids pathway (Dar and Arumugam 2013; Kiyama 2016).

Lignans can be found in a wide variety of foods and medicinal sources; sesame seeds and flax seeds contain high amounts of lignans (Satake, Ono and Murata 2013; Kiyama 2016). The availability of plant lignans is frequently limited because of the high cost of production and extraction, poor cultivation systems, a long growth phase, and low lignan content (Satake, Ono and Murata 2013). Podophyllotoxin and sesamin are two examples of important lignans that have been extensively investigated (Figure 6) (Chaurasia et al. 2012; Satake, Ono and Murata 2013). Several biological activities have been attributed to lignans, such as antioxidant (Landete 2012; Dar and Arumugam 2013), anticancer (Rauf et al. 2018), anti-estrogenic and estrogenic (Landete 2012; Kiyama 2016), analgesic (Borsato et al. 2000), liver protector (Fukumitsu et al. 2010) and anti-inflammatory activities (During et al. 2012).

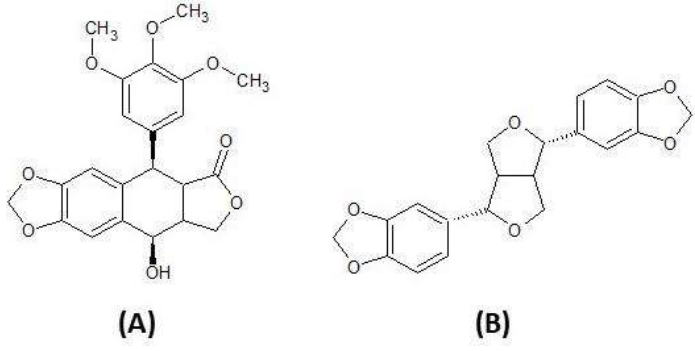

Figure 6. Podophyllotoxin (A) and sesamin (B).

6. Factors Influencing PAL Activity

PAL is considered a key enzyme in the regulation of the biosynthetic phenylpropanoids pathway, which are precursors of an extensive number of phenolic compounds with many functions in plants (MacDonald and D'Cunha 2007; Huang et al. 2010). These compounds play important roles in a number of different pathways and can act as a defense against pathogens, protection against abiotic stresses, signal transduction and communication with other organisms, and also act as regulatory molecules (Wanner et al. 1995; Kim and Hwang 2014). Thus, the evolutionary emergence of the phenylpropanoids pathway in plants is an important adaptation that allows for its defense against abiotic and biotic stresses (Kim and Hwang 2014), and causes PAL to be recognized as a marker of environmental stress in different plant species (MacDonald and D'Cunha 2007).

In any given tissue, PAL levels may fluctuate significantly at relatively short intervals of time and in response to a wide variety of stimuli. These variations do not depend exclusively on their genotype, but also on the age, development, organ and even plant tissue (Camm and Towers 1973). Mechanisms that regulate PAL activity include allosteric effects, inactivation by specific proteases and the inhibition of the final product (Tena, López-Valbuena and Jorrin 1984). There is evidence that *trans*-cinnamic acid also plays an important role in the down regulation of the phenylpropanoid pathway by the inhibition of PAL mRNA transcription (Edwards, Mavanad and Dixon 1990). Numerous reports of variations in levels of PAL activity in plants have already been recorded; some are described below.

6.1. Intrinsic Factors

The levels of PAL activity vary according to the stage of development, differentiation, cell type or tissue, as well as exposure to different stimuli (Jones 1984; Lois et al. 1989; Shufflebottom et al. 1993). PAL levels can be affected during the germination process. Generally, at the beginning of the

germination, the levels of this enzyme are very low or absent, then increase vertiginously, and then decline (Camm and Towers 1973). However, the pattern of these events can vary considerably, as described for brown rice, where PAL activity increased during the first two days of germination, but decreased thereafter (Cho and Lim 2018). Stages of intense cell division may also interfere with PAL levels, as described for *Brassica oleracea* anthers, in which immature anthers about 2 mm in length exhibited higher PAL activity compared to mature anthers or those less than 2 mm long (Kishitani et al. 1993).

6.2. Infections Caused by Pathogens and Insect Attack

Metabolic disorders and the impairment of PAL activity were verified in *Capsicum annuum* plants that had the gene responsible for the expression of the silenced PAL during infection by *Xanthomonas campestris*. In contrast, overexpression of this gene conferred an increase in PAL activity in healthy leaves infected with *Pseudomonas syringae*, compared to wild-type *Arabidopsis* (Kim and Hwang 2014).

The defensive reaction of an apple cultivar (*Malus domestica* Borkh.) was studied after inoculation with three different pathogens (*Penicillium expansum*, *Monilinia fructigena* and *Gloeosporium* spp.). PAL activity varied at the site of the fungal attack, in the tissues around the rotten zone and in the healthy part. The response to infection was different in the fruit peel and pulp. There was also a good correlation between PAL activity and total phenolic content (Schovánková and Opatová 2011).

The activity of PAL in yellow grapefruit peel was inhibited by inoculating the fruit with *Penicillium digitatum*, not only in a place close to the infection, but also in areas further away from it. The degree of inhibition was related to the distance of the fungus from the analyzed region. Other tested fungi, such as *P. digitatum*, *P. italicum* and *Geotrichum candidum*, had a similar effect (Lisker et al. 1983).

Hu et al. (2009) reported a defensive response in poplar plants after the herbivory of insects (*Clostera anachoreta*). The results showed that the

increased PAL activities were found not only in leaves damaged by *C. anachoreta* larvae, but also in their systemic upper leaves, indicating that the phenylpropanoids pathway was activated and the defense response was systemically stimulated.

6.3. Wounding

One of the main causes of the loss of quality in products of a vegetal origin is the darkening caused by the oxidation of phenolic compounds (Lopez-Galvez, Saltveit and Cantwell 1996). Wounds in the tissues of the midrib of lettuce may increase up to three-times the PAL activity when these are stored at 15°C, reducing the size of the central vein from 2.5 × 15 to 0.5 × 1 cm. The wound generally induced maximum levels of enzyme activity within three days at 5°C and 1 day at 15°C (Lopez-Galvez, Saltveit and Cantwell 1996). Martínez-Téllez and Lafuente (1997) also associated the increase in damage caused by *Citrus* peel to an increase in PAL activity.

The significance of glycosylation and the immunolocalization of enzymatic subunits of PAL-induced wounds on potato discs were studied by Shaw, Bolwell and Smith (1990). The results of this study indicate that tunicamycin inhibits the glycosylation of PAL, which, in turn, results in an imperfect folding of the enzymatic protein. The orientation of the active site is altered such that the affinity of the enzyme for its substrate is not affected, while the catalytic activity of the enzyme is reduced.

6.4. Light

It is known that light intensity plays an important role in the production and accumulation of phenolic compounds; therefore, it directly interferes with PAL activity (Rosa et al. 2019). A study conducted on lettuce leaves showed that a mixed blue and red radiation from LEDs increased the activity of PAL by 200%, compared to the control and other light treatments. This significant increase in PAL activity is strongly associated with anthocyanin production in the studied species (Heo et al. 2012). In contrast, the constant

absence of light does not stimulate the production and accumulation of PAL, but rather its inactivation system in apples (Tan 1980). Similar results were observed by Roubelakis-Angelakis and Kliewer (1986), who verified the maximum PAL activity in grapes was related to the presence of light, whereas in the fruits kept in the dark, the activity decreased during the experimental period.

6.5. Ethylene

Ethylene can induce PAL activity (Lisker et al. 1983). It has been shown that ethylene participates in plant defensive responses against stress (Yang and Hoffman 1984), but it is also involved in the induction of areas of necrotic tissue in commercialized plants (Hyodo, Kuroda and Yang 1978). In a citrus cultivar (*Citrus clementina* Hort. Ex Tanaka x *Citrus reticulata* Blanco) kept under refrigeration, PAL activity increased in response to stress caused by cold, and was also higher in fruits kept under the action of ethylene, compared to those maintained only under cold air for the entire storage period (Lafuente, Sala and Zacharias 2004).

It has been shown that the treatment of swede and parsnip roots with low levels of ethylene leads to increased respiration and a large increase in PAL activity. The increase in PAL activity is very sensitive to the level of ethylene; 1 ppm of ethylene is sufficient to induce half of the maximum response. The use of indole-3-acetic acid at 10^{-4} M also stimulates an increase in the endogenous production of ethylene in the studied plants and an increase in PAL activity, but this increase is small in relation to that induced by the saturation of the ethylene levels (Rhodes and Wooltorton 1971).

6.6. Carbohydrates

The association of carbohydrates with PAL activity has been reported for maize and potato enzymes (Havir 1979; Shaw, Bolwell and Smith,

1990). The amount of carbohydrates associated with corn PAL was appreciable. However, removal of the polysaccharide (composed of arabinose and galactose) is accompanied by large decreases of PAL activity. It appears that the *in vivo* localization of the enzyme may depend on its ability to bind to specific polysaccharides (Havir 1979). In potato disks, as in maize, PAL activity is closely related to the presence of sugars. When in the presence of a protein glycosylation inhibitor, potato disks incubated with sucrose, the activity of PAL is reduced (Shaw, Bolwell and Smith, 1990). This behavior is not different in grapefruit, in which the presence of sucrose is a determinant for the increase in PAL activity (Roubelakis-Angelakis and Kliewer 1986).

6.7. Methyl Jasmonate

Methyl jasmonate (MeJA) is a compound that naturally occurs in plants and plays important roles in growth and development, fruit ripening and responses to environmental stresses (Creelman and Mullet 1997). MeJA treatment significantly reduces post-harvest peach diseases by increasing PAL activity (in addition to other enzymes), culminating in the high synthesis of phenolic compounds (Jin et al. 2009).

The effect of MeJA on *in vitro* cultured cells was also studied. The addition of MeJA to the culture medium induced PAL activity in tobacco cell cultures. Complementary experiments showed that the increase in PAL activity was preceded by the accumulation of PAL mRNA. However, PAL was transcriptionally and enzymatically induced faster in cultures treated with *Fusarium solani* extract, compared to the cells treated with MeJA (Sharan et al. 1998). Similar behavior was observed by Gutiérrez-Carbajal et al. (2010), with the addition of 500 μM of MeJA to the cell cultures of *Capsicum chinense*.

6.8. Salinity

The response of plants to salinity is different between the different plant species; this variation can classify these plants as tolerant or sensitive species (Ayers and Westcot 1994). Studies carried out by Astaneh et al. (2018) showed that PAL activity was significantly affected by the application of NaCl and selenium. With increasing selenium concentration in non-saline conditions, the activity of PAL decreases significantly. Under salinity levels (30, 60 and 90 mM NaCl) without the application of selenium, PAL activity increases significantly in garlic leaves. In this study, increased PAL activity may be related to a response to cellular damage caused by higher concentrations of NaCl. A similar result was found for *Salvia* species, in which saline stress can increase PAL activity by 42 – 45% (Valifard et al. 2015).

6.9. Temperature

The literature reports an increase in PAL activity in response to low temperatures in different species (Tan 1980; Graham and Patterson 1982; Leyva et al. 1995; Lafuente, Sala and Zacharias 2004; Jeong et al. 2012). This behavior was also verified by Martinez-Téllez and Lafuente (1995), since the reduction in cold-induced injuries promoted by the packing of citrus fruits at a slightly higher temperature (10°C) may reduce PAL activity.

6.10. Mineral Deficiency

Tan (1980) reports that nitrogen and potassium deficiency increases the accumulation of PAL and decreases the accumulation of the PAL inactivation system in the leaves from apple trees grown in greenhouses. In *Matricaria chamomilla*, PAL activity was significantly higher in nitrogen-deficient foliar rosettes after 4 and 8 days (61% and 23%, respectively), but decreased to the control level at the end of the experiment. Thus, the

mechanism of tolerance to nitrogen deficiency due to the increased activity of PAL is temporally limited (Kováčik et al. 2007). Ibrahim and Jaafar (2011) also showed that as the nitrogen concentration increases, the levels of PAL decrease significantly in *Labisia pumila*.

6.11. UV Radiation

Prolonged exposure to UV-B light can result in decreased biomass, photosynthetic efficiency and plant growth rate (He, Huang and Whitecross 1994). However, plants have a variety of mechanisms to bypass the damage caused by UV light, such as: a) stimulation of the synthesis of compounds that absorb UV-B (Li et al. 1993); b) the increased metabolism of phenylpropanoids and some flavonoids (Kubasek et al. 1992); and c) morphological changes, such as a decrease in plant height and leaf area, and an increase in leaf thickness (Sisson and Caldwell 1976). In the exposure of rice seedlings to UV-B radiation, there was a four-fold increase in PAL activity (Sarma and Sharma 1999). Similar behavior was observed in cucumber plants irradiated with UV-B, 15 days from sowing, for 6 hours per day, in which a 27 – 78% increase in PAL activity was observed (Krizek et al. 1993).

CONCLUSION

PAL is a key enzyme for plant development that connects the carbon flux from primary metabolism with the phenylpropanoids pathway, an economically important metabolic pathway producing secondary metabolites, such as flavonoids, lignans, tannins, coumarins and lignin. Many of these aromatic compounds have high economic value for health human and also for plant growth, development and plant-environment interactions. Advances in studies about the complex regulatory mechanisms of the phenylpropanoid pathway, specially related to PAL, will allow for a deeper understanding of the other roles of these compounds in higher plants.

ACKNOWLEDGMENTS

The authors are grateful to the Universidade Federal de São João del-Rei (UFSJ), Conselho Nacional de Desenvolvimento Científico e Tecnológico (CNPq), Coordenação de Aperfeiçoamento de Pessoal de Nível Superior (CAPES) and Fundação de Amparo à Pesquisa do Estado de Minas Gerais (FAPEMIG) for the financial support to Laboratory of Botany and Medicinal Plants/UFSJ. "This study was financed in part by the Coordenação de Aperfeiçoamento de Pessoal de Nível Superior - Brasil (CAPES) - Finance Code 001."

REFERENCES

Abenavoli, M. R., Cacco, G., Sorgona, A., Marabottini, R., Paolacci, A. R., Ciaffi, M. & Badiani, M. (2006). The inhibitory effects of coumarin on the germination of durum wheat (*Triticum turgidum* ssp. *durum*, cv. simeto) seeds. *Journal of Chemical Ecology, 32*, 489-506.

Achnine, L., Blancaflor, E. B., Rasmussen, S. & Dixon, R. A. (2004). Colocalization of L-phenylalanine ammonia-lyase and cinnamate 4-hydroxylase for metabolic channeling in phenylpropanoid biosynthesis. *The Plant Cell*, *16* (11), 3098–3109.

Alu'datt, M. H., Rababah, T., Alhamad, M. N., Al-Mahasneh, M. A., Almajwal, A., Gammoh, S., Ereifej, K., Johargy, A. & Alli, I. (2017). A review of phenolic compounds in oil-bearing plants: distribution, identification and occurrence of phenolic compounds. *Food Chemistry*, *218*, 99–106.

Arina, M. Z. I. & Harisun, Y. (2019). Effect of extraction temperatures on tannin content and antioxidant activity of *Quercus* infectoria (Manjakani). *Biocatalysis and Agricultural Biotechnology*., *19*, 101-104.

Assis, J. S., Maldonado, R., Munhõz, T., Escribano, M. I. & Merodio, C. (2001). Effect of high carbon dioxide concentration on PAL activity and

phenolic contents in ripening cherimoya fruit. *Postharvest Biology and Technology*, *23* (1), 33-39.

Astaneh, R. K., Bolandnazar, S., Nahandi, F. Z. & Oustan, S. (2018). Effect of selenium application on phenylalanine ammonia-lyase (PAL) activity, phenol leakage and total phenolic content in garlic (*Allium sativum* L.) under NaCl stress. *Information Processing in Agriculture*, *5* (3), 339-344.

Ayers, R. S. & Westcot, D. W. (1994). *Water quality for agriculture*. Food and Agriculture Organization of the United Nations, Rome.

Bakoyiannis, I., Daskalopoulou, A., Pergialiotis, V. & Perrea, D. (2019). Phytochemicals and cognitive health: are flavonoids doing the trick? *Biomedicine and Pharmacotherapy*, *109*, 1488–1497.

Bate-Smith, E. C. & Swain, T. (1962). "Flavonoid compound". In *Comparative Biochemistry*, edited by Mason, H.S., Florkin, 755-809. New York: Academic Press.

Bolwell, G. P., Bell, J. N., Cramer, C. L., Schuch, W., Lamb, C. J. & Dixon, R. A. (1985). L-phenylalanine ammonia-lyase from *Phaseolus vulgaris*: characterization and differential induction of multiple forms from elicitor-treated cell suspension cultures. *Europe Journal Biochemistry*, *149* (2), 41-419.

Borsato, M. L. C., Grael, C. F. F., Souza, G. E. P. & Lopes, N. P. (2000). Analgesic activity of the lignans from *Lychnophora ericoides*. *Phytochemistry*, *55* (7), 809–813.

Brown, S. A. & Neish, A. C. (1955a). Shikimic acid as a precursor in lignin biosynthesis. *Nature*, *175* (4459), 688–689.

Brown, S. A. & Neish, A. C. (1955b). Studies of lignin biosynthesis using isotopic carbon. IV. Formation from some aromatic monomers. *Canadian Journal of Biochemistry and Physiology*, *33* (6), 948–962.

Brown, S. A. & Neish, A. C. (1956). Studies of lignin biosynthesis using isotopig carbon: V. Comparative studies on different plant species. *Canadian Journal of Biochemistry and Physiology*, *34* (4), 769-778.

Calabrese, J. C., Jordan, D. B., Boodhoo, A., Sariaslani, S. & Vannelli, T. (2004). Crystal structure of phenylalanine ammonia lyase: multiple

helix dipoles implicated in catalysis. *Biochemistry*, *43* (16), 11403-11416.

Camm, E. L. & Towers, G. H. N. (1973). Phenylalanine ammonia lyase. *Phytochemistry*, *12* (5), 961-973.

Chaurasia, O. P., Ballabh, B., Tayade, A., Kumar, R., Kumar, G. P. & Singh, S. B. (2012). *Podophyllum* L.: an endangered and anticancerous medicinal plant - an overview. *Indian Journal of Traditional Knowledge*, *11*, 234-241.

Chen, L. Z., Sun, W. W., Bo, L., Wang, J. Q., Xiu, C., Tang, W. J., Shi, J. B., Zhou, H. P. & Liu, X. H. (2017). New arylpyrazoline-coumarins: synthesis and anti-inflammatory activity. *European Journal of Medicinal Chemistry*, *138*, 170–181.

Cheng, G. W. & Breen, P. J. (1991). Activity of phenylalanine ammonia-lyase (PAL) and concentrations of anthocyanins and phenolics in developing strawberry fruit. *Journal of the American Society of Horticultural Science*, *116* (5), 865-869.

Chio, C., Sain, M. & Qin, W. (2019). Lignin utilization: a review of lignin depolymerization from various aspects. *Renewable and Sustainable Energy Reviews*, *107*, 232–49.

Cho, D. H. & Lim, S. T. (2018). Changes in phenolic acid composition and associated enzyme activity in shoot and kernel fractions of brown rice during germination. *Food Chemistry*, *256*, 163-170.

Chung, K. T., Wong, T. Y., Wei, C. I., Huang, Y. W. & Lin, Y. (1998). Tannins and human health: a review. *Critical Reviews in Food Science and Nutrition*, *38* (6), 421-464.

Cooke, H. A., Christianson, C. V. & Bruner, S. D. (2009). Structure and chemistry of 4-methylideneimidazole-5-one containing enzymes. *Current Opinion in Chemical Biology*, *13* (4), 460-468.

Cramer, C. L., Edwards, K., Dron, M., Liang, X., Dildane, S. L., Bolwel, G. P., Dixon, R. A., Lamb, C. J. & Schuch, W. (1989). Phenylalanine ammonia-lyase gene organization and structure. *Plant Molecular Biology*, *12* (4), 367-383.

Creelman, R. A. & Mullet, J. E. (1997). Biosynthesis and action of jasmonate in plants. *Annual Review in Plant Physiology*, *48*, 355-381.

Cui, J. D., Qiu, J. Q., Fan, X. W., Jia, S. R. & Tan, Z. L. (2014). Biotechnological production and applications of microbial phenylalanine ammonia lyase: a recent review. *Journal Critical Reviews in Biotechnology*, *34* (3), 258-268.

Dai, H., Huang, M., Qian, J., Liu, J., Meng, C., Li, Y., Ming, G., Zhang, T., Wang, S., Shi, Y., Yao, Y., Ge, S., Zhang, Y. & Ling, Y. (2019). Excellent antitumor and antimetastatic activities based on novel coumarin/pyrazole oxime hybrids. *European Journal of Medicinal Chemistry*, *166*, 470-479.

Dar, A. A. & Arumugam, N. (2013). Lignans of sesame: purification methods, biological activities and biosynthesis - a review. *Bioorganic Chemistry*, *50*, 1–10.

Dehghan, S., Saeghi, M., Pöppel, A., Fischer, R., Lakesharlan, R., Kavousi, H. R., Vilcinskas, A. & Rahnamaeian, M. (2014). Differential inductions of phenylalanine ammonia-lyase and chalcone synthase during wounding, salicylic acid treatment, and salinity stress in safflower, Carthamus tinctorius. *Bioscience Reports*, *34* (3), 273-282.

Dixon, R. A. & Paiva, N. L. (1995). Stress-induced phenylpropanoid metabolism. *Plant Cell*, *7* (7), 1085-1097.

Dixon, R. A., Achnine, L., Kota, P., Liu, C. J., Srinivasa, M. S. & Wang, L. J. (2002). The phenylpropanoid pathway and plant defence - a genomics perspective. *Molecular Plant Pathology*, *3* (5), 371-390.

During, A., Debouche, C., Raas, T. & Larondelle, Y. (2012) Among plant lignans, pinoresinol has the strongest anti-inflammatory properties in human intestinal CACO-2 cells. *The Journal of Nutrition*, *142* (10), 1798-1805.

Edwards, R., Mavanad, M. & Dixon, R. A. (1990). Metabolic fate of cinnamic acid in elicitor treated cell suspension cultures of *Phaseolus vulgaris*. *Phytochemistry*, *9*, 1867-1873.

Ferrarese, M. L. L., Rodrigues, J. D. & Ferrarese-Filho, O. (2000). Phenylalanine ammonia-lyase activity in soybean roots extract measured by reverse-phase high performance liquid chromatography. *Plant Biology*, *2* (2), 152-153.

Fritz, R. R., Hodgins, D. S. & Abell, C. W. (1976). Phenylalanine ammonia-lyase. Induction and purification from yeast and clearance in mammals. *The Journal of Biological Chemistry*, *251* (15), 4646-4650.

Fukumitsu, S., Aida, K., Shimizu, H. & Toyoda, K. (2010). Flaxseed lignan lowers blood cholesterol and decreases liver disease risk factors in moderately hypercholesterolemic men. *Nutrition Research***,** *30* (7), 441–446.

Garrard, A. (2014). Coumarins. *Encyclopedia of Toxicology*. Third Edition., *1*, 1052–1054.

Graham, D. & Patterson, B. D. (1982). Responses of plants to low, non-freezing temperatures: proteins, metabolism and acclimation. *Annual Review in Plant Physiology*, *33*, 347-372.

Guo, L., Wang, P., Jaini, R., Dudareva, N., Chapple, C. & Morgan, J. A. (2018). Dynamic modeling of subcellular phenylpropanoid metabolism in *Arabidopsis* lignifying cells. *Metabolic Engineering*, *49*, 36–46.

Gutiérrez-Carbajal, M. G., Monforte-González, M., Miranda-Ham, M. de L., Godoy-Hernández, G. & Vázquez-Flota, F. (2010). Induction of capsaicinoid synthesis in *Capsicum chinense* cell cultures by salicylic acid or methyl jasmonate. *Biologia Plantarum*, *54* (3), 430-434.

Hao, Z., Charles, D. J., Yu, L. L. & Simon, J. S. (1996). Purification and characterization of phenylalanine ammonia lyase from *Ocimum basilicum*. *Phytochemistry*, *43* (4), 735-739.

Havir, E. A. (1979). L-phenylalanine ammonia-lyase: binding of polysaccharide by the enzyme from maize. *Plant Science Letters*, *16*, 297-304.

He, J., Huang, L. K. & Whitecross, M. I. (1994). Chloroplast ultrastructure changes in Pisum sativum associated with supplementary ultraviolet (UV-B) radiation. *Plant, Cell and Environment*, *17*, 771-775.

Heo, J. W., Kang, D. H., Bang, H. S., Hong, S. G., Chun, C. & Kang, K. K. (2012). Early growth, pigmentation, protein content, and phenylalanine ammonia-lyase activity of red curled lettuces grown under different lighting conditions. *Korean Journal of Horticultural Science and Technology*, *30* (1), 6-12.

Hoyos-Martínez, P. L., de Merle, J., Labidi, J. & El Bouhtoury, F. C. (2019). Tannins extraction: a key point for their valorization and cleaner production. *Journal of Cleaner Production*, *206*, 1138–1155.

Hsieh, L. S., Hsieh, Y. L., Yeh, C. S., Cheng, C. Y., Yang, C. C. & Lee, P. D. (2011). Molecular characterization of a phenylalanine ammonia-lyase gene (BoPAL1) from *Bambusa oldhamii*. *Molecular Biology Reports*, *38* (1), 283-290.

Hsieh, L. S., Ma, G. J., Yang, C. C. & Lee, P. D. (2010). Cloning, expression, site-directed mutagenesis and immunolocalization of phenylalanine ammonia-lyase in *Bambusa oldhamii*. *Phytochemistry*, *71*, 1999–2009.

Hu, Z. H., Zhang, W., Shen, Y. B., Fu, H. J., Su, X. H. & Zhang, Z. Y. (2009). Activities of lipoxygenase and phenylalanine ammonia lyase in poplar leaves induced by insect herbivory and volatiles. *Journal of Forest Research*, *20* (4), 372-376.

Huang, J., Min, G., Lai, Z., Fan, B., Shi, K., Zhou, Y. H., Yu, J. Q. & Chen, Z. (2010). Functional analysis of the Arabidopsis PAL gene family in plant growth, development, and response to environmental stress. *Plant Physiology*, *153* (4), 1526-1538.

Huang, Q., Liu, X., Zhao, G., Hu, T. & Wang, Y. (2018). Potential and challenges of tannins as an alternative to in-feed antibiotics for farm animal production. *Animal Nutrition*, *4* (2), 137-150.

Hyodo, H., Kuroda, H. & Yang, S. F. (1978). Induction of phenylalanine ammonia-lyase and increase in phenolics in lettuce leaves in relation to the development of russet spotting caused by ethylene. *Plant Physiology*, *62*, 31-35.

Hyun, M. W., Yun, Y. H., Kim, J. Y. and Kim, S. H. (2011). Fungal and plant phenylalanine ammonia-lyase. *Mycobiology*, *39* (4), 257-265.

Hwu, J. R., Huang, W. C., Lin, S. Y., Tan, K. T., Hu, Y. C., Shieh, F. K., Tsay, S. C., Bachurin, S. O., Ustyugov, A. & Tsay, S. H. (2019). Chikungunya virus inhibition by synthetic coumarin–guanosine conjugates. *European Journal of Medicinal Chemistry*, *166*, 136-143.

Ibrahim, M. H. & Jaafar, H. Z. E. (2011). Involvement of carbohydrate, protein and phenylanine ammonia lyase in up-regulation of secondary

metabolites in *Labisia pumila* under various CO_2 and N_2 levels. *Molecules*, *16*, 4172-4190.

Janas, K. M., Zielińska-Tomaszewska, J. Rybaczek, D., Maszewski, J., Posmyk, M. M., Aramowicz, R. & Kosińska, A. (2010). The impact of copper ions on growth, lipid peroxidation, and phenolic compound accumulation and localization in lentil (*Lens culinaris* Medic.) seedlings. *Journal of Plant Physiology*, *167* (4), 270-276.

Jeong, M. J., Cho, B. S., Bae, D. W., Shin, S. C., Park, S. U., Lim, H. S., Kim, J., Kim, J. B., Cho, B. K. & Bae, H. (2012). Differential expression of kenaf phenylalanine ammonia-lyase (PAL) ortholog during developmental stages and in response to abiotic stresses. *Plant Omics Journal*, *5* (4), 392-399.

Jin, P., Zheng, Y., Tang, S., Rui, H. & Wang, C. Y. (2009). Enhancing disease resistance in peach fruit with methyl jasmonate. *Journal of the Science and Food and Agriculture*, *89*, 802-808.

Jin, Q., Yao, Y., Cai, Y. & Lin, Y. (2013). Molecular cloning and sequence analysis of a phenylalanine ammonia-lyase gene from *Dendrobium*. *Plos One*, *8* (4), e62352.

Jones, D. H. (1984). Phenylalanine ammonia-lyase: regulation of its induction, and its role in plant development. *Phytochemistry*, *23* (7), 1349-1359.

Khakdan, F., Alizadeh, H. & Ranjbar, M. (2018). Molecular cloning, functional characterization and expression of a drought inducible phenylalanine ammonia-lyase gene (ObPAL) from *Ocimum basilicum* L. *Plant Physiology and Biochemistry*, *130* (10), 464–472.

Kasperkiewicz, K., Ponczek, M. B. & Budzisz, E. (2018). A biological, fluorescence and computational examination of synthetic coumarin derivatives with antithrombotic potential. *Pharmacological Reports*, *70* (6), 1057-1064.

Kim, D. S. & Hwang, B. K. (2014). An important role of the pepper phenylalanine ammonia-lyase gene (PAL_1) in salicylic acid- dependent signalling of the defence response to microbial pathogens. *Journal of Experimental Botany*, *65* (9), 2295-2306.

Kishitani, S., Yomoda, A., Konno, N. & Tanaka, Y. (1993). Involvement of phenylalanine ammonia-lyase in the development of pollen in broccoli (*Brassica oleracea* L.). *Sexual Plant Reproduction, 6* (4), 244–248.

Koukol, J. & Conn, E. E. (1961). The metabolism of aromatic compounds in higher plants. IV. Purification and properties of the phenylalanine deaminase of *Hordeum vulgare*. *Journal of Biological Chemistry*, *236* (10), 2692-2698.

Kováčik, J. & Klejdus, B. (2012). Tissue and method specificities of phenylalanine ammonia-lyase assay. *Journal of Plant Physiology*, *169* (13), 1317-1320.

Kováčik, J., Klejdus, B., Bačkor, M. & Repčák, M. (2007). Phenylalanine ammonia-lyase activity and phenolic compounds accumulation in nitrogen-deficient *Matricaria chamomilla* leaf rosettes. *Plant Science*, *172* (2), 393-399.

Krizek, D. T., Kramer, G. F., Upadhyaya, A. & Mirecki, R. M. (1993). UV-B response of cucumber seedlings grown under metal halide and high-pressure sodium/deluxe lamps. *Physiologia Plantarum*, *88* (2), 350-358.

Kubasek, W. L., Shirley, B. W., Mckillop, A., Goodman, H. M. & Briggs, W. (1992). Regulation of flavonoid biosynthetic genes in germinating *Arabidopsis* seedlings. *Plant Cell*, *4* (10), 1229-1236.

Kiyama, R. (2016). Biological effects induced by estrogenic activity of lignans. *Trends in Food Science and Technology*, *54*, 186–96.

Kyndt, J. A., Meyer, T. E., Cusanovich, M. A. & Van Beeumen, J. J. (2002). Characterization of a bacterial tyrosine ammonia lyase, a biosynthetic enzyme for the photoactive yellow protein. *FEBS Letters*, *512* (1-3), 240-244.

Laddha, A. P. & Kulkarni, Y. A. (2019). Tannins and vascular complications of diabetes: an update. *Phytomedicine*, *56*, 229–45.

Lafuente, M. T., Sala, J. M. & Zacarias, L. (2004). Active oxygen detoxifying enzymes and phenylalanine ammonia-lyase in the ethylene-induced chilling tolerance in *Citrus* fruit. *Journal of Agricultural and Food Chemistry*, *52*, 3606-361.

Landete, J. M. (2012). Plant and mammalian lignans: a review of source, intake, metabolism, intestinal bacteria and health. *Food Research International*, *46* (1), 410–24.

Lau, C. S., Carrier, D. J., Beitle, R. R., Bransby, D. I., Howard, L. R., Lay Jr. J. J. O., Liyanage, R. & Clausen, E. C. (2007). Identification and quantification of glycoside flavonoids in the energy crop *Albizia julibrissin*. *Bioresource Technology*, *98* (2), 429-435.

Le Roy, J., Huss, B., Creach, A., Hawkins, S. & Neutelings, G. (2016). Glycosylation is a major regulator of phenylpropanoid availability and biological activity in plants. *Frontiers in Plant Science*, *7*, 735.

Levy, C. & Zucker, M. (1960) Cinnamyl and p-coumaryl esters as intermediates in the biosynthesis of chlorogenic acid. *The Journal of Biological Chemistry*, *235* (8), 2418-2425.

Leyva, A., Jarillo, J. A., Salinas, J. & Martinez-Zapater, M. (1995). Low temperature induces the accumulation of phenylalanine ammonia-lyase and chalcone synthase mRNAs of *Arabidopsis thaliana* in a light-dependent manner. *Plant Physiology*, *108*, 39-46.

Li, J. O. L., Raba, R. T. M., Amundson, R. & Last, R. L. (1993). *Arabidopsis* flavonoid mutants are hypersensitive to UV-B irradiation. *Plant Cell*, *5* (2), 171-179.

Lin, Y., Sun, X., Yuan, Q. & Yan, Y. (2013). Combinatorial biosynthesis of plant-specific coumarins in bacteria. *Metabolic Engineering*, *18*, 69-77.

Lisker, N. Cohen, L., Chalutz, E. & Fuchs, Y. (1983). Fungal infections suppress ethylene-induced phenylalanine ammonia-lyase activity in grapefruits. *Physiological and Molecular Plant Pathology*, *22* (3), 331-338.

Liu, J., Osbourn, A. & Ma, P. (2015). MYB transcription factors as regulators of phenylpropanoid metabolism in plants. *Molecular Plant*, *8* (5), 689–708.

Liu, R., Xu, S., Li, J., Hu, Y. & Lin, Z. (2006). Expression profile of a PAL gene from *Astragalus membranaceus* var. Mongholicus and its crucial role in flux into flavonoid biosynthesis. *Plant Cell Reports*, *25* (7), 705-710.

Lois, R., Dietrich, A., Hahlbrock, K. & Schulz, W. (1989). A phenylalanine ammonia-lyase gene from parsley: structure, regulation and identification of elicitor and light responsive cis-acting elements. *EMBO Journal*, *8* (6), 1641-1648.

Lopez-Galvez, G., Saltveit, M. E. & Cantwell, M. I. (1996). Wound induced phenylalanine ammonia-lyase activity: Factors affecting its induction and correlation with the quality of minimally processed lettuce. *Postharvest Biology and Technolology*, *9* (2), 223-233.

MacDonald, M. J. & D'Cunha, G. B. (2007). A modern view of phenylalanine ammonia-lyase. *Biochemistry and Cell Biology*, *85* (3), 273-282.

Machado, M., Felizardo, C., Fernandes-Silva, A. A., Nunes, F. M. & Barros, A. (2013). Polyphenolic compounds, antioxidant activity and L-phenylalanine ammonia-lyase activity during ripening of olive cv. "Cobrançosa" under different irrigation regimes. *Food Research International*, *51* (1), 412-421.

Marchand, C. H., Vanacker, H., Collin, V., Issakidis-Bourguet, E., Le Maréchal, P. & Decottignies, P. (2010). Thioredoxin targets in *Arabidopsis* roots. *Proteomics*, *10* (13): 2418-2428.

Maryam, S., Khan, M. R., Shah, S. A., Zahra, Z., Batool, R. & Zai, J. A. (2019). Evaluation of anti-inflammatory potential of the leaves of *Wendlandia heynei* (Schult.) Santapau & Merchant in sprague dawley rat. *Journal of Ethnopharmacology*, *238*, 111849.

Markulin, L., Drouet, S., Corbin, C., Decourtil, C., Garros, L., Renouard, S., Lopez, T., Mongelard, G., Gutierrez, L., Auguin, D., Lainé, E. & Hano, C. (2019). The control exerted by ABA on lignan biosynthesis in flax *(Linum usitatissimum* L.) is modulated by a Ca^{2+} signal transduction involving the calmodulin-like LuCML15b. *Journal of Plant Physiology*, *236*, 74–87.

Martínez-Téllez, M. A. & Lafuente, M. T. (1997). Effect of high temperature conditioning on ethylene, phenylalanine ammonia-lyase, peroxidase and polyphenol oxidase activities in flavedo of chilled mandarin fruit. *Journal of Plant Physiology*, *150*, 674-678.

Matern, U., Lüer, P. & Kreusch, D. (1999). Biosynthesis of coumarins. *Comprehensive Natural Products Chemistry*, 623-637.

McCalla, D. R. & Neish, A. C. (1959). Metabolism of phenylpropanoid compounds in salvia: II. Biosynthesis of phenolic cinnamic acids. *Canadian Journal of Biochemistry and Physiology*, *37* (4), 537-547.

Nabavi, S. M., Šamec, D., Tomczyk, M., Milella, L., Russo, D., Habtemariam, S., Suntar, I., Rastrelli, L., Daglia, M., Xiao, J., Giampieri, F., Battino, M., Sobarzo-Sanchez, E., Nabavi, S. F., Yousefi, B., Jeandet, P., Xu, S. & Shirooie, S. (2018). Flavonoid biosynthetic pathways in plants: versatile targets for metabolic engineering. *Biotechnology Advances*. https://doi.org/10.1016/j.biotechadv.2018.11.005.

Nagai, N., Kojima, Y., Shimosaka, M. & Okazaki, M. (1988). Effects of kinetin on phenylalanine ammonia-lyase activity in tobacco cell culture. *Agricultural and Biological Chemistry*, *52* (10), 2617-2619.

Nagula, R. L. & Wairkar, S. (2019). Recent advances in topical delivery of flavonoids: a review. *Journal of Controlled Release*, *296*, 190-201.

Olsen, K. M., Lea, U. S., Slimestad, R., Verheul, M. & Lillo, C. (2008). Differential expression of four *Arabidopsis* PAL genes: PAL1 and PAL 2 have functional specialization in abiotic environmental triggered flavonoid synthesis. *Journal Plant Physiology*, *165* (14), 1491–1499.

Perez-Vizcaino, F. & Fraga, C. G. (2018). Research trends in flavonoids and health. *Archives of Biochemistry and Biophysics*., *646*, 107–112.

Raffa, D., Maggio, B., Raimondi, M. V., Plescia, F. & Daidone, G. (2017). Recent discoveries of anticancer flavonoids. *European Journal of Medicinal Chemistry*, *142*, 213–228.

Rahmatabadi, S. S., Sadeghian, I., Ghasemi, Y., Sakhteman, A. & Hemmati, S. (2019). Identification and characterization of a sterically robust phenylalanine ammonia-lyase among 481 natural isoforms through association of *in silico* and *in vitro* studies. *Enzyme and Microbial Technology*, *122*, 36-54.

Rasmussen, S. & Dixon, R. A. (1999). Transgene-mediated and elicitor-induced perturbation of metabolic channeling at the entry point into the phenylpropanoid pathway. *Plant Cell*, *11* (7), 1537–1551.

Rauf, A., Patel, S., Imran, M., Maalik, A., Arshad, M. U., Saeed, F., Mabkhot, Y. N., Al-Showiman, S. S., Ahmad, N. & Elsharkawy, E. (2018). Honokiol: an anticancer lignan. *Biomedicine and Pharmacotherapy*, *107*, 555–562.

Renault, H., Werck-Reichhart, D. & Weng, J. K. (2019). Harnessing lignin evolution for biotechnological applications. *Current Opinion in Biotechnology*, *56***,** 105-111.

Revankar, H. M., Bukhari, S. N. A., Kumar, G. B. & Qin, H. L. (2017). Coumarins scaffolds as COX inhibitors. *Bioorganic Chemistry*, *71*, 146–59.

Rhodes, M. J. C. & Wooltorton, L. S. C. (1971). The effect of ethylene on the respiration and on the activity of phenylalanine ammonia lyase in swede and parsnip root tissue. *Phytochemistry*, *10*(9), 1989-1997.

Ritter, H. & Schulz, G. E. (2004). Structural basis for the entrance into the phenylpropanoid metabolism catalyzed by phenylalanine ammonia-lyase. *Plant Cell*, *16* (1), 3426–3436.

Rosa, L. A. de la, Moreno-Escamilla, J. O., Rodrigo-Garcia, J. & Alvarez-Parrilla, E. (2019). Phenolic compounds. In: *Postharvest Physiology and Biochemistry of Fruits and Vegetables*. Yahia, E.M. and Carrillo-Lopes, A. (eds). Chennai: Woodhead Publishing, pp. 253-271.

Rösler, J., Krekel, F., Amrhein, N. & Schmid, J. (1997). Maize phenylalanine ammonia-lyase has tyrosine ammonia-lyase activity. *Plant Physiology*, *113* (1), 175-179.

Roubelakis-Angelakis, K. A. & Kliewer, W. M. (1986). Effects of exogenous factors on phenylalanine ammonia-lyase activity and accumulation of anthocyanins and total phenolics in grape berries. *American Journal of Enology and Viticulture*, *37*, 275-280.

Salehi, B., Varoni, E. M., Sharifi-Rad, M., Rajabi, S., Zucca, P., Iriti, M. & Sharifi-Rad, J. (2019). Epithelial-mesenchymal transition as a target for botanicals in cancer metastasis. *Phytomedicine*, *55*, 125–36.

Santiago, L. J. M., Louro, R. P. & Oliveira, D. E. (2000). Compartmentation of phenolic compounds and phenylalanine ammonia-lyase in leaves of *Phyllanthus tenellus* Roxb. and their induction by copper sulphate. *Annals of Botany*, *86* (5), 1023- 1032.

Santos, C. dos., Vargas, A., Fronza, N. & Santos, J. H. Z. dos. (2017). Structural, textural and morphological characteristics of tannins from *Acacia mearnsii* encapsulated using sol-gel methods: applications as antimicrobial agents. *Colloids and Surfaces B: Biointerfaces, 151*, 26-33.

Sarma, A. D. & Sharma, R. (1999). Purification and characterization of UV-B induced phenylalanine ammonia-lyase from rice seedlings. *Phytochemistry*, *50* (5), 729-737.

Satake, H., Ono, E. & Murata, J. (2013). Recent advances in the metabolic engineering of lignan biosynthesis pathways for the production of transgenic plant-based foods and supplements. *Journal of Agricultural and Food Chemistry*, *61* (48), 11721-11729.

Saunders, J. A. & McClure, J. W. (1975). Phytochrome controlled phenylalanine ammonia- lyase activity in *Hordeum vulgare* plastids. *Phytochemistry*, *14* (5-6), 1285-1289.

Schovánková, J. & Opatová, H. (2011). Changes in phenols composition and activity of phenylalanine-ammonia lyase in apples after fungal infections. *Horticultural Science (Prague)*, *38*, 1-10.

Schwede, T. F., Retey, J. & Schulz, G. E. (1999). Crystal structure of histidine ammonia-lyase revealing a novel polypeptide modification as the catalytic electrophile. *Biochemistry*, *38* (17), 5355-5361.

Scott, D. A., Hammond, P. M., Brearley, G. M. & Price, C. P. (1992). Identification by high-performance liquid chromatography of tyrosine ammonia-lyase activity in purified fractions of *Phaseolus vulgaris* phenylalanine ammonia-lyase. *Journal of Chromatography*, *573* (2), 309-312.

Shang, Q. M., Li, L. & Dong, C. J. (2012). Multiple tandem duplication of the phenylalanine ammonia-lyase genes in *Cucumis sativus L. Planta*, *236* (4), 1093-1105.

Sharan, M., Taguchi, G., Gonda, K., Jouke, T., Shimosaka, M., Hayashida, N. & Okazak, M. (1998). Effects of methyl jasmonate and elicitor on the activation of phenylalanine ammonia-lyase and the accumulation of scopoletin and scopolin in tobacco cell cultures. *Plant Science, 132*, 13-19.

Shaw, N. M., Bolwell, G. P. & Smith, C. (1990). Wound induced phenylalanine ammonia-lyase in potato (*Solanum tuberosum*) tuber discs. Significance of glycosylation and immunolocalization of enzyme subunits. *Biochemistry Journal*, *267*, 163-170.

Shufflebottom, D., Edwards, K., Schuch, W. & Bevan, M. (1993). Transcription of two members of a gene family encoding phenylalanine ammonia-lyase leads to remarkably different cell specificities and induction patterns. *Plant Journal*, *3*, 835-845.

Sisson, W. B. & Caldwell, M. M. (1976). Photosynthesis, dark respiration, and growth of *Rumex patientia* l. exposed to ultraviolet irradiance (288 to 315 nanometers) simulating a reduced atmospheric ozone column. *Plant Physiology*, *58* (4), 563-568.

Song, J. & Wang, Z. (2008). Molecular cloning, expression and characterization of a phenylalanine ammonia-lyase gene (SmPAL1) from *Salvia miltiorrhiza*. *Molecular Biology Reports*, *36* (5), 939–952.

Sreelakshmi, Y. & Sharma, R. (2008). Differential regulation of phenylalanine ammonia-lyase activity and protein level by light in tomato seedlings. *Plant Physiology and Biochemistry*, *46* (4), 444-451.

Su, X., Liu, X., Wang, S., Li, B., Pan, T., Liu, D., Wang, F., Diao, Y. & Li, K. (2017). Wound-healing promoting effect of total tannins from *Entada phaseoloides* (L.) Merr. in rats. *Burns*, *43* (4), 830-838.

Sui, Z., Luo, J., Yao, R., Huang, C., Zhao, Y. & Kong, L. (2019). Functional characterization and correlation analysis of phenylalanine ammonia-lyase (PAL) in coumarin biosynthesis from *Peucedanum praeruptorum* Dunn. *Phytochemistry*, *158*, 35–45.

Suzuki, S. & Umezawa, T. (2007). Biosynthesis of lignans and norlignans. *Journal of Wood Science*, *53*, 273–284.

Tan, S. C. (1980). Phenylalanine ammonia-lyase and the phenylalanine ammonia-lyase inactivating system: effects of light, temperature and mineral deficiencies. *Australian Journal of Plant Physiology*, *7*, 159-167.

Tena, M., López-Valbuena, R. & Jorrin, J. (1984). Induction of phenylalanine ammonia-lyase in hypocotyls of sunflower seedlings by light, excision and sucrose. *Physiologia Plantarum*, *60*, 159-165.

Tobimatsu, Y. & Schuetz, M. (2019). Lignin polymerization: how do plants manage the chemistry so well? *Current Opinion in Biotechnology*, *56*, 75-81.

Tondi, G., Thévenon, M. F., Mies, B., Standfest, G., Petutschnigg, A. & Wieland, S. (2013). Impregnation of Scots pine and beech with tannin solutions: effect of viscosity and wood anatomy in wood infiltration. *Wood Science Technology*, *47*, 615–626.

Turner, J. N. (2011). Ammonia lyases and aminomutases as biocatalysts for the synthesis of a-amino and b-amino acids. *Current Opinion in Chemical Biology*, *15* (2), 234–240.

Umezawa, T. (2003). Diversity in lignan biosynthesis. *Phytochemistry Reviews*, *2*, 371–390.

Valifard, M., Mohsenzadeh, S., Niazi, A. & Moghadam, A. (2015). Phenylalanine ammonia-lyase isolation and functional analysis of phenylpropanoid pathway under salinity stress in *Salvia* species. *Australian Journal of Crop Science*, *9* (7), 656-665.

Vanholme, B., El Houari, I. & Boerjan, W. (2019). Bioactivity: phenylpropanoids' best kept secret. *Current Opinion in Biotechnology*, *56*, 156–62.

Vanholme, R., Meester, B. de., Ralph, J. & Boerjan, W. (2019). Lignin biosynthesis and its integration into metabolism. *Current Opinion in Biotechnology*, *56*, 230–39.

Vogt, T. (2010). Phenylpropanoid biosynthesis. *Molecular Plant*, *3* (1), 2-20.

Wanner, L. A., Li, G., Ware, D., Somssich, I. E. & Davis, K. R. (1995). The phenylalanine ammonia-lyase gene family in *Arabidopsis thaliana*. *Plant Molecular Biology*, *27* (2), 327-338.

Weisshaar, B. & Jenkins, G. I. (1998). Phenylpropanoid biosynthesis and its regulation. *Current Opinion in Plant Biology*, *1* (3), 251-257.

Whetten, R. W. & Sederoff, R. R. (1992). Phenylalanine ammonia-lyase from loblolly pine: purification of the enzyme and isolation of complementary DNA clones. *Plant Physiology*, *98* (1), 380-386.

Willians, V. R. & Hiroms, J. M. (1967). Reversibility of the "irreversible" histidine ammonia-lyase reaction. *Biochimica et Biophysica Acta*, *139* (1), 214-216.

Xiang, L. & Moore, B. S. (2005). Biochemical characterization of a prokaryotic phenylalanine ammonia lyase. *Journal of Bacteriology*, *187* (12), 4286-4289.

Xu, K., Wang, J. L., Chu, M. P. & Jia, C. (2019). Activity of coumarin against *Candida albicans* biofilms. *Journal de Mycologie Medicale*, *29* (1), 28-34.

Xu, R., Zhang, K., Liu, P., Han, H., Zhao, S., Kakade, A., Khan, A., Du, D. & Li, X. (2018). Lignin depolymerization and utilization by bacteria. *Bioresource Technology*, *269*, 557–66.

Yang, S. F. & Hoffman, N. E. (1984). Ethylene biosynthesis and its regulation in higher plants. *Annual Review of Plant Physiology*, *35*, 155-189.

Zabalza, A., Orcaray, L., Fernández-Escalada, M., Zulet-González, A. & Royuela, M. (2017). The pattern of shikimate pathway and phenylpropanoids after inhibition by glyphosate or quinate feeding in pea roots. *Pesticide Biochemistry and Physiology*, *141*, 96–102.

Zhang, X. & Liu, C. J. (2015). Multifaceted regulations of gateway enzyme phenylalanine ammonia-lyase in the biosynthesis of phenylpropanoids. *Molecular Plant*, *8* (1), 17-27.

Zhang, X., Gou, M. & Liu, C. J. (2014). *Arabidopsis* kelch repeat F-Box proteins regulate phenylpropanoid biosynthesis via controlling the turnover of phenylalanine ammonia-lyase. *Plant Cell*, *25* (1), 4994–5010.

Zucker, M. (1965). Induction of phenylalanine deaminase by light and its relation to chlorogenic acid synthesis in potato tuber tissue. *Plant Physiology*, *40* (5), 779-784.

In: Advances in Chemistry Research ISBN: 978-1-53617-112-9
Editor: James C. Taylor

Chapter 3

CHALCOGENATED LIGANDS/ NANOPARTICLES AND TRANSFER HYDROGENATION

Aayushi Arora[1], Preeti Oswal[1], Gyandshwar Kumar Rao[2], Siddhant Singh[1], Divyanshu Nautiyal[1], Neha Kala[1], Sushil Kumar[1], Arun Kumar[1] and Ajai Kumar Singh[3,*]

[1]Department of Chemistry, School of Physical Sciences,
Doon University, Dehradun, Uttarakhand, India
[2]Department of Chemistry, Amity School of Applied Sciences,
Amity University Haryana (AUH), Manesar, Gurugram, Haryana, India
[3]Department of Chemistry, Indian Institute of Technology,
Delhi, New Delhi, India

[*]Corresponding Author's Email: aksingh@chemistry.iitd.ac.in.

ABSTRACT

Organochalcogen compounds have been used as the building blocks for the development of a variety of catalysts for several chemical transformations including transfer hydrogenation, which has been thoroughly studied during last two decades. Transfer hydrogenation, a reaction in which carbonyl compounds are reduced to the corresponding alcohols, is extremely important as it avoids the requirement and use of inflammable hydrogen gas and equipment associated to handle it. Organochalcogen ligands (with or without co-ligands) in combination with a metal salt have been used as a catalyst for this reaction. Such catalysts include both transition metal complexes as well as nano-catalysts. The catalysts, developed using organochalcogen compounds, have been reported to be less moisture- and air-sensitive. In addition, they are equally efficient as that of phosphorous based catalytic systems and, sometimes more efficient than the phosphorous counterpart. A critical analysis of the the development of molecular as well as nanocatalysts based on organochalcogen ligands and their application in the transfer hydrogenation is presented in this chapter. In addition to covering the synthesis of chalcogen ligands, their metal complexes and nanoparticles (NPs), emphasis has also been laid down on the catalytic potential and mechanisms of catalysis. It also includes the tools used for characterization as well as future scope of this area.

Keywords: Coordination, piano-stool, chalcogen, DFT, transfer hydrogenation

INTRODUCTION

The catalytically important transition metal complexes of organochalcogen ligands were firstly synthesized and structurally characterized in the year 1980 [1, 2]. Such complexes have emerged as a new class of efficient, air-stable and moisture insensitive catalysts during last two decades [1, 2]. Their application in catalysis was reported in year 1998 for the first time when Rutherford and co-workers used a fluorous aliphatic analog of Wilkinson catalyst in catalyzing hydrogenation of alkenes [3]. Subsequently, Yao and co-workers reported a very interesting example of such complexes in year 2004. They used palladium complex of

an organoselenium ligand as a catalyst for the Heck coupling reaction [4]. In this case, the selenium ligated palladium complex was reported to be more efficient than its sulphur and phosphorous counterparts [4]. However, such complexes were not explored as catalysts for transfer hydrogenation reaction at all during the first decade of 20th century. In 2010, Singh and co-workers have designed bidentate and tridentate organochalcogen ligated transition metal complexes, and explored their efficiency for various catalytic reactions such as transfer hydrogenation of ketones and oxidation of alcohols [5]. Transfer hydrogenation holds an important place among all chemical transformations. It involves the reduction of carbonyl compounds (aldehydes and ketones) to yield primary and secondary alcohols [6]. These products have wide applications ranging from pharmaceutical to agrochemical industry. This type of reactions have an edge over other hydrogenation reactions since the carbonyl groups can be conveniently reduced to their respective alcohols without using flammable hydrogen gas and sophisticated experimental setup [7]. The common sources for hydrogen in transfer hydrogenation reactions are solvents like 2-propanol [7], solution of sodium formate, sodium formate-formic acid mixture, glycerol [8], etc. which have easy availability and handling in comparision to the hazardous pressurized hydrogen gas.

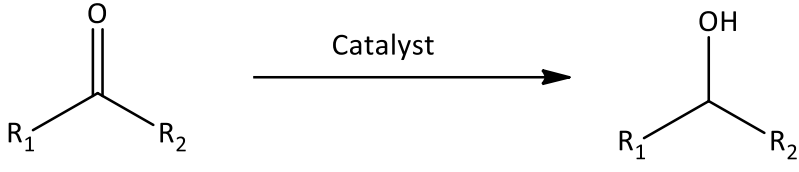

Figure 1. Transfer hydrogenation of aldehydes and ketones.

Over the last two decades, a variety of organochalcogen ligands including (i) pincer type, (ii) chalcogenated Schiff bases and (iii) chalcogenated ethers, have been used for the development of catalysts for transfer hydrogenation as well as other important chemical transformations [5, 7, 9−45]. In addition to stability towards air and moisture, the other advantage associated with the organochalcogen ligands and their metal complexes is the ease in their handling as they do not require inert

atmosphere to carry our air insensitive reaction [44, 46]. The presence of soft donor (S/Se/Te) along with hard donor (N, O^-) in ligands framework allows them to chelate with variety of transition metals like Pd(II), Ru(II), Rh(III), Ir(III), etc. [9−45]. Such metal complexes have also been reported to show an efficient catalytic property. It is due to the easy oxidative addition as chalcogen-metal bond length is longer in comparison to that of phosphorus to metal bond.

CHALCOGEN LIGATED METAL COMPLEXES

Organochalcogen Ligands with Chalcogenoether Functionality

Transition metal complexes of chalcogenoether ligands (ArEAr; E = S/Se/Te) have diverse applications because they serve as scaffolds for biological activity [47], single-source precursors for metal chalcogenide materials [48] and catalysts [13-18]. Their supramolecular chemistry with s, p and d block elements has also received considerable attention [49]. Some interesting reports exist on their exploration as catalysts in chemical transformation such as transfer hydrogenation of aldehydes and ketones. Chalcogen ligated half-sandwich complexes of Ru(II), Rh(III) and Ir(III) have been explored for transfer hydrogenation reactions [5, 9−19]. Ligands L1−L3 with chalcogenoether functionality have been synthesized by reducing their corresponding Schiff base analogs with $NaBH_4$ [5]. Half sandwich Ru(II) complexes 1−3 have been prepared (Scheme 1) by treating these ligands with a suitable Ru(II) precursor [5]. In addition to ^{1}H and ^{13}C NMR spectroscopy, ^{77}Se and ^{125}Te NMR spectroscopic techniques have also been used to characterize the ligands and metal complexes. The signal in ^{77}Se NMR shows a deshielding of 73.3 ppm with respect to the free ligand L2 upon formation of complex 2, indicating the coordination of Se to Ru(II) center. A similar trend has also been observed in ^{125}Te NMR spectrum of L3. The ^{125}Te signal in case of complex 3 showed a deshielding of 258.5 ppm with respect to the free ligand L3. Single crystal diffraction studies indicate a (S, N, E) tri-coordination and benzene occupying an axial position

resulting in the formation of three-legged piano-stool geometry (Scheme 1). These complexes (1−3) have been explored for the transfer hydrogen of ketones at 80ºC with 0.001 mol% of catalyst loading. Acetophenone gave the most efficient conversion with all the three complexes while with aliphatic secondary ketones (such as cyclopentanone, cyclohexanone, 2-penatnone, 2-butanone), around 90% conversion was obtained under optimal reaction conditions. The catalyst efficiency was found to be perturbed by the nature of the chalcogen donor atom. Organotellurium ligated Ru(II) complex 3 was found to be the most efficient followed by selenium analog (2). The organosulphur ligated Ru(II) complex 1 showed least reactivity. This is the same order in which softness of the donor site decreases. The possibility of further increase in the softness of "Te" has been attributed due to the presence of electron releasing methoxy group para to tellurium which in turn resulted in the higher efficiency of the organotellurium ligated Ru(II) complex 3 [5].

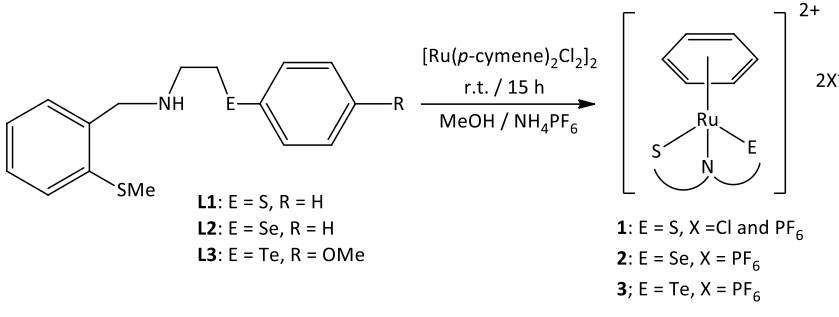

Scheme 1. Preparation of ligands L1−L3 and their Ru(II) complexes 1−3.

Unsymmetric bidentate 1-benzyl-3-phenylchalcogenylmethyl-1,3-dihydrobenzo imidazole-2-chalcogenone ligands (L4−L7) having a unique combination of thione and selone donor sites have been reported (Scheme 2) [9]. The reaction of 1 H-benzoimidazole with benzyl bromide, PhECH2Cl followed by addition of elemental S or Se led to the formation of ligands L4−L7 (Scheme 2). Half sandwich ruthenium complexes 4−7, have been synthesized by reacting appropriate ligand with [(η6-C6H6)RuCl(μ-Cl)]2. The corresponding Ru(II) complexes were precipitated as their PF_6^- salt by

reacting them with NH_4PF_6 at room temperature [9]. ^{77}Se NMR spectroscopic technique has been used to understand the change after complexation. The 77Se signal of selenoether functionality in complexes 4 and 5 appears to be deshielded by 13.4 and 112.0 ppm respectively with respect to that of the corresponding ligands. The peak due to selone group in complex 6 in 77Se NMR showed a shielding of 103.8 ppm. Such a peak was not observed for complex 4 due to broadening of the signal. It has been reported that relaxation time of Se increases when Ru coordinates with selone Se, which in turn results in signal broadening. The crystal structure of complexes exhibited the pseudo-octahedral half sandwich "piano-stool" geometry. Complexes 4−7 have been explored for their catalytic efficiency in transfer hydrogenation of aldehydes and ketones using various sources of hydrogen. Of all the sources screened, 2-propanol and glycerol showed promising results. The higher amount of catalysts was required when glycerol is used as a hydrogen source as compared to 2-propanol. Complex 6 showed maximum efficiency, which has been further corroborated by DFT results as the HOMO−LUMO energy gap was found to be minimum in case of 6 when compared to other complexes. The catalytic pathway involves lengthening or breaking of Ru-Cl bond in order to generate a vacant site for the coordination resulting in the formation of Ru-H intermediate [9]. It is also supported by the appearance of a signal in 77Se NMR for complex 6. The 77Se NMR signal was found to be shifted to higher frequency by 17 ppm.

Two chalcogen containing ligands L8 and L9 have been synthesized (Scheme 3) via the reaction of 1,2-bromomethyl benzene with a suitable sulphur/selenium precursor [10]. The L8 was utilized in the preparation of two half sandwich Rh(III) complexes 8 and 9 (Scheme 3). Ligand L9 was used for the preparation of Ir(III) complexes 10 and 11 (Scheme 3). Multinuclei NMR spectroscopic techniques have been used for the purpose of characterization. ^{77}Se NMR signal was found to be shifted downfield by 9.0 ppm in case of Rh(III) complex 9 with respect to ligand L9, whereas a higher deshielding of 20 ppm was observed in case of complex 11 with respect to corresponding ligand L9. All the four complexes exhibited nearly similar molecular structure.

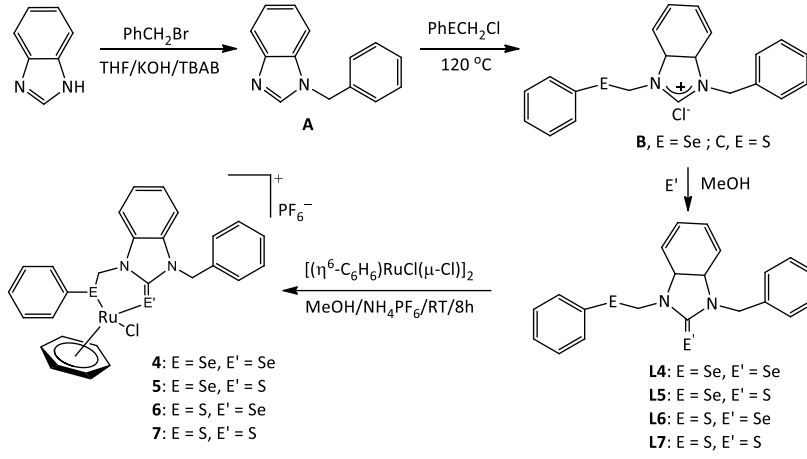

Scheme 2. Synthesis of Ru(II) complexes 4−7.

The cations of these complexes showed pseudo-octahedral half sandwich "piano-stool" geometry around the metal center. CH·F secondary interactions due to involvement of the CH of benzene and F of PF_6^- anion resulted in the formation of chain like structures. All the four complexes have been explored for transfer hydrogenation of carbonyl compounds at 120ºC. It was observed that catalysts 9 and 11 took shorter reaction time when compared with *N*-heterocyclic carbene based Ir(III) complexes [50]. In terms of shorter reaction time, required for the formation of products in significant yields, the complexes 8−11 have been found to be more efficient than some specific Ru(II) precursors such as Ru(*p*-cymene)Cl_2, $RuCl_2(TPPS)_3$ and [Ru(η^6-arene)-(NHC)CO_3] reported by various researchers [51]. These precursors have also been tested for catalyzing the transfer hydrogenation of carbonyl compounds in glycerol [51]. It was also observed that the selenium analogs were superior to their sulfur congeners. It may be attributed to the fact that selenium is a better sigma donor as compared to sulfur in analogous derivatives. Higher sigma donor ability of Se promotes the formation of hydride, which in turn results in higher catalytic efficiencies for selenium ligated metal complexes. The catalytic efficiencies of Rh(III) catalysts 8 and 9 were found to be better than that of Ir(III) catalysts. DFT calculations also corroborated this result as the

HOMO−LUMO energy gap in case of Rh(III) catalysts was found to be lower than Ir(III) catalysts [10].

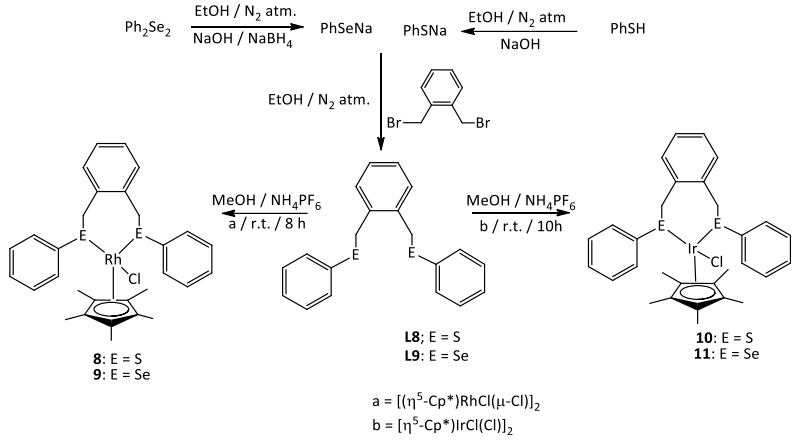

Scheme 3. Synthetic strategy for the preparation of Rh(III) and Ir(III) complexes.

Three bidentate (E,E') chalcogenoether ligands have been reported (Scheme 4) along with their Rh(III) (12−14) and Ir(III) (15−17) complexes by Singh and co-workers [11]. During NMR spectroscopic characterization, a deshielding of ~65 ppm was observed in the ^{77}Se NMR of complexes 13, 14, 16 and 17 with respect to that of corresponding free ligands. Interestingly, the formation of diastereomers occurs in 14 and 17, leading to emergence of two signals in their ^{77}Se NMR spectra. The structure elucidation revealed the "piano stool" arrangement of donor atoms around Rh/Ir in these complexes. The metal complexes were explored for transfer hydrogenation of ketones in iso-propanol at 0.01 mol% of catalyst loading. The most efficient conversion was observed when acetophenone was used as a substrate. The other aliphatic ketones such as cyclopentanone, cyclohexanone, and propiophenone, showed a conversion of >90% in 5 hours of reaction time while in case of 2-octanone and 2-pentanone, a conversion of 85% and 88% have been obtained. In these cases, an average TON of 8000-9000 was observed. A maximum TON of 95000 has been achieved using catalyst 14 for transfer hydrogenation of benzophenone. The nature of chalcogen donor showed a marginal effect on the catalytic potential

of the complex as the compounds containing (Se,Se) donor atom were slightly better in catalyzing the reaction than those containing (Se,S) and (S,S) donor groups. The ^{77}Se NMR spectrum of reaction mixture was also recorded in order to gain insight into the catalytic process. A deshielding of 20-25 ppm was observed which may be attributed to the breaking of M−Cl bond and formation of M−H intermediate [11].

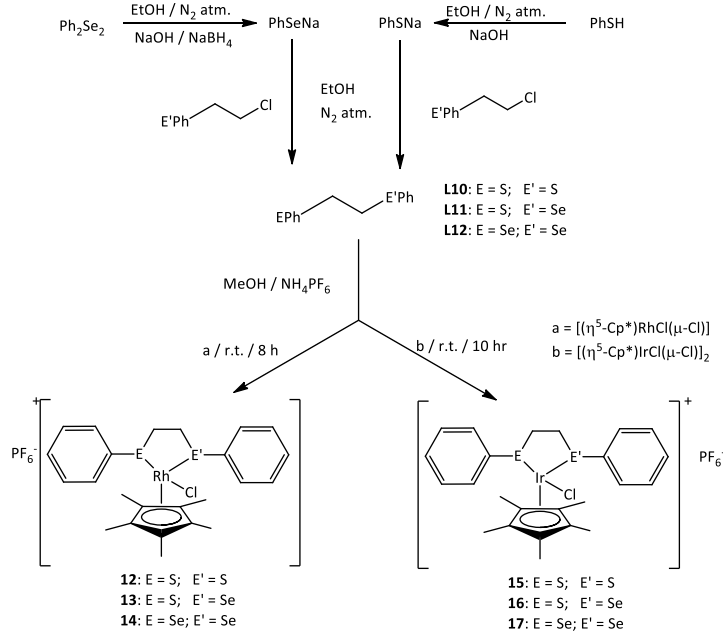

Scheme 4. Synthesis of complexes 12−17.

Organochalcogen Ligands with Triazole Core

Organochalcogen ligands (L13−L16) having a triazole core (Scheme 5) have also emerged as promising building blocks for catalytic systems. Their peculiar feature is the presence of two different types of N donors [N(2) and N(3)] in the framework of the same triazole unit [11]. Click reaction between azidomethyl benzene and phenyl propargyl suphide/selenide have been used to prepare such ligands (Scheme 5). Their half sandwich Ru(II) complexes

18−21 have also been synthesized (Scheme 5) [12]. The interesting fact about click chemistry is the simplicity, easy handling and reliability involved in the synthetic procedure (Scheme 5). The structure elucidation of the Ru(II) complexes revealed that one of the benzene rings occupies one face of the octahedron in all the four complexes. The coordination sphere is completed by the chelation of the nitrogen, sulfur and chlorine atom with the metal center. It was also observed that all four complexes 18−21 exhibit overall three-legged piano stool conformation. All the four complexes have shown good to excellent conversions in the reduction of carbonyl compounds to their respective alcohols in just 3 hours. Complexes 20 and 21 that show involvement of N(2) of triazole in the coordination with the metal were found to be more efficient than the other two complexes (18, 19) where N(3) of triazole ring is involved in coordination with metal center. Theoretical calculations are in line with the experimental results as HOMO−LUMO energy gaps are higher for 18 and 19 in comparison to 20 and 21. When attempts were made to gain insights into the mechanistic aspects, 77Se NMR spectroscopy was used to monitor the reactions under catalysis with complexes 19 and 21. A spectral shift of 17−20 ppm was observed, which indicated the weakening of M−Cl bond in order to create vacant coordination site for M−H bond formation. Thus, it was suggested that reaction proceeded via the formation of the metal hydride intermediate [12].

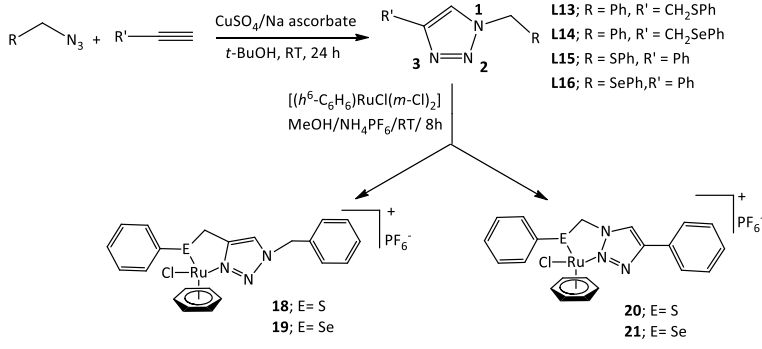

Scheme 5. Synthesis of Ru(II) complexes 18−21 with triazole core.

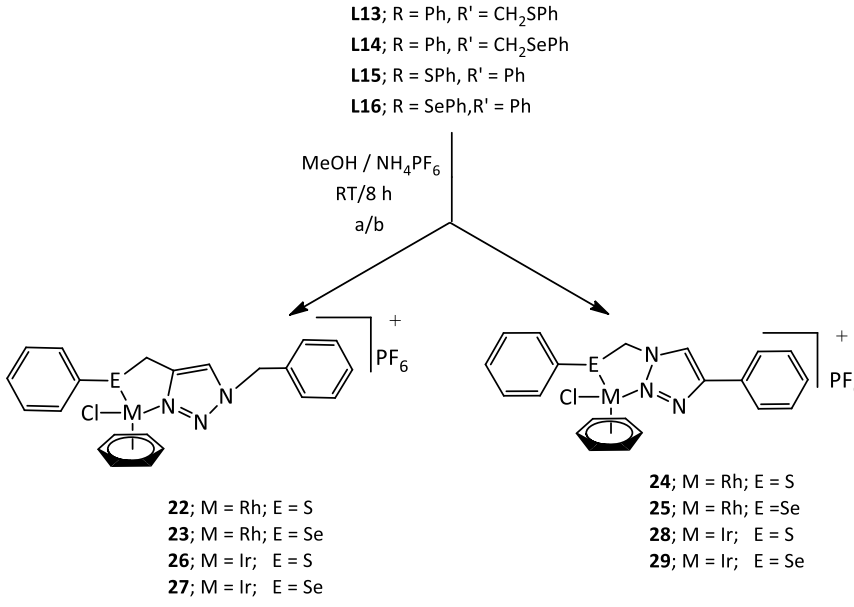

Scheme 6. Preparation of Rh(III) and Ir(III) complexes 22−29.

Triazole based organochalcogen ligands L13−L16 have also been utilized for the synthesis of Rh(III) and Ir(III) complexes (22−29) (Scheme 6) [13]. Such complexes have also been investigated for the reduction of carbonyl compounds. The 77Se NMR signals of the metal complexes 23, 25 and 27 have been found to be deshielded by 65.5, 8.9 and 38.4 ppm respectively in comparision to the corresponding ligands. However, complex 29 showed a shielding of 10.6 ppm with respect to the free ligand in 77Se NMR spectrum. These complexes have been utilized as catalysts for transfer hydrogen reactions using potassium hydroxide as a base at 80 ºC in iso-propanol. The reactions have been carried out at moderate temperature using 0.01-0.001 mol% of catalyst, and good to excellent conversions were observed. The effect of chalcogen donor atom was also evident as selenium ligated complexes were marginally more efficient than their sulfur counterparts. Moreover, Rh(III) analogs were superior in terms of efficiency in comparison to Ir(III) complexes since 0.001 mol % of the former was sufficient to catalyze the reactions in 3h at 80ºC. Transfer hydrogen reactions catalyzed by 23 and 29 have been monitored by 77Se NMR technique to

gather information about the reaction mechanism. A higher shift in the frequency by 20-25 ppm was observed, and also interpreted as an indication of the dissociation of M−Cl bond and the formation of M−H intermediate. A loss of cyclopentadienyl ring occurred in case of both Rh(III) and Ir(III) complexes, which led to the formation of catalytically active species [13].

Another set of triazole based organochalcogen ligands L17 and L18 has been designed (Scheme 7) by Singh and co-workers [14]. The ligands were utilized in the synthesis of Ru(II) complexes 30 and 31 using [Ru(η6-benzene)RuCl(μ-Cl)]2 as a ruthenium source (Scheme 7). In addition to 1H and 13C NMR, the ligands and Ru(II) complexes have also been characterized by the 77Se NMR technique. The 77Se signal shifted downfield by 85.2 ppm in case of 31 with respect to the corresponding free ligand L2. The structures of the metal complexes were also authenticated using single-crystal X-ray crystallography. The metal complexes were explored for the transfer hydrogenation of carbonyl compounds using glycerol as a hydrogen source at 110ºC. Various substrates were explored and it was observed that complex 31 showed better efficiency in catalyzing this reaction in comparison to 30. Conversions >70% have been obtained when complex 31 was used with a maximum conversion of 99%, obtained in the case of acetophenone. The catalytic efficiencies of complexes 30 and 31 were found to be better than those of some Ru(II) precursors. It has been attributed to the strong ligating properties of the chalcogen donor ligands and the steric hindrance on N-arene ring. The nature of catalysis was also investigated using Hg and PPh_3 poisoning tests. As Hg/PPh_3 does not significantly inhibit the yield of the product, the possibility of heterogeneous catalysis may be ruled out [14].

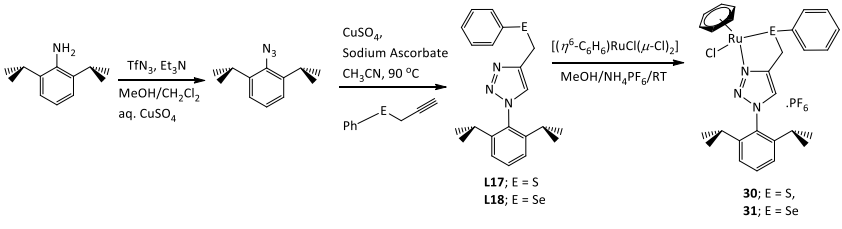

Scheme 7. Synthetic strategy for the synthesis of L17−L18 and 30−31.

Singh and co-workers have also reported the Ru(II) complexes 32−35 of 1,4-bis(phenylthio/selenomethyl)-1,2,3-triazoles L19−L22 synthesized (Scheme 8) via click reaction of sulphated/selenite azide and sulphated/selenated alkyne [15]. The 1H, 13C and 77Se NMR spectra showed a shift in the signal(s) towards higher frequency after the ligation of the metal due the significant change in the distribution of electron density. Single crystal X-ray studies revealed a sheet-like structure for all the four complexes resulted due to the secondary interactions of C−H of arene of cationic complex with the F of PF_6^- anion. These complexes have been explored for transfer hydrogen reaction using 0.01 and 0.5 mol % of Ru(II) catalyst in iso-propanol and glycerol, respectively. The maximum conversion was achieved in 3 hours when either of the hydrogen sources used. In addition, 0.2 mol% and 0.5 mol% of catalyst loading were reported to be optimum in iso-propanol and glycerol respectively. The mechanistic study revealed that reaction proceeded via homogeneous catalytic pathway [15].

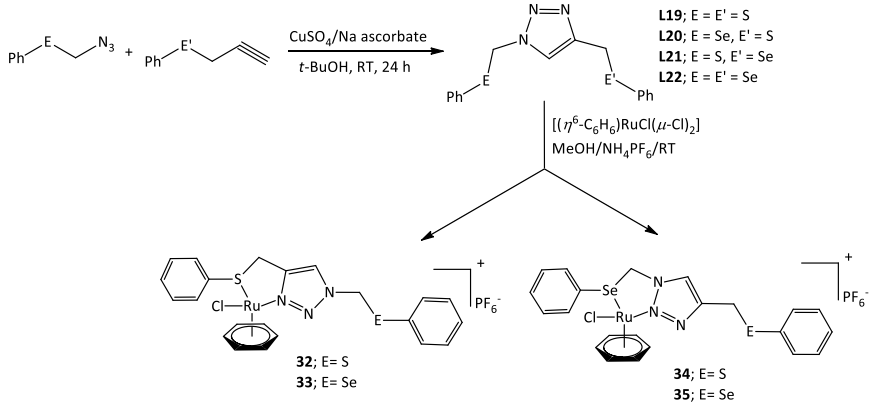

Scheme 8. Ru(II) complexes 32−35.

Organochalcogen Ligands with Pyridine Framework

Substituted pyridine-organochalcogen derivatives have been reported (Scheme 9) to serve as attractive ligands in the designing of catalysts for

transfer hydrogenation reactions [52]. (2-Arylchalcogenomethyl) pyridine [L = L23–L25] and bis(2-pyridylmethyl)chalcogenide [L = L26–L27] (chalcogen = S, Se; Ar = Ph/2-pyridyl for S, Ph for Se) are the examples of such ligands [16]. Though several Ru(II) complexes of pyridine substituted ligands had been reported [53], their utilization as catalysts for transfer hydrogenation is limited. The reactions between (2-arylchalcogenomethyl) pyridine [L23–L25] and [(η6-C6H6)RuCl2]2, followed by anion exchange with NH4PF6 [16], have been used to prepare the half sandwich Ru(II) complexes (36–38) with a general formula [(η6-C6H6)Ru(L)Cl][PF6] (Scheme 9). Similar methodology has been adopted to synthesize Ru(II) complexes (39 and 40) with a general formula [(η6-C6H6)Ru(L)Cl][PF6] (Scheme 9) by reacting bis(2-pyridylmethyl)chalcogenide [L = L26–L27] with [(η6-C6H6)RuCl2]2, followed by anion exchange with NH4PF6 [16]. NMR spectroscopic characterization shows that a deshielding of 25 ppm in the 77Se NMR spectral signal of complex 37 with respect to free ligand L24. However, complex 40 showed a shielding of 32 ppm with respect to corresponding ligand L27 in 77Se NMR spectrum. This may be attributed to the strong binding and shorter bond lengths of Ru−Se in case of 40 in comparison to 37. The crystal structures of Ru(II) complexes showed the coordination of Se with metal center which was also confirmed by 77Se NMR studies. Ru(II) complexes bearing pyridine-based tridentate ligands and 2-(aminomethyl)pyridine showed good conversions as lower reaction time is required at a catalyst loading of 0.1–1.0 mol%. Several other Ru-complexes have been reported for catalysis of transfer hydrogenation but in comparison with 37, either they require higher catalyst loading or longer reaction time. High TON of the order of 10^2−10^3 has been achieved with the highest value of 9.9×10^3. The selenium ligated Ru complexes have shown better catalytic efficiencies than that of Ru–S complexes. Bidentate complexes have been found to show higher activity as compare to tridentate complexes. The results have also been supported by DFT calculations on the basis of HOMO-LUMO energy gaps [16].

A new class of water-soluble half-sandwich complexes 41−43 (Scheme 10) of type [(η^5-C_p*/η^6-benzene)M(L)Cl][PF_6] have also been reported [17]. In such complexes, the ligand (L28) is 2-(pyridine-2-ylmethylsulfanyl)-

benzoic acid. Syntheses 41−43 involve the reaction of L28 with $[(\eta^5\text{-}C_p^*/\eta^6\text{-benzene})MCl(\mu\text{-}Cl)]_2$, (benzene, M = Ru; C_p^*, M = Rh, Ir) followed by anion exchange with NH_4PF_6. These complexes showed water solubility due to the presence of uncoordinated–COOH groups (Scheme 10). Complexes 41−43 have been explored for the transfer hydrogenation of carbonyl compounds in water with glycerol as hydrogen donor and showed good efficiency. Catalytic efficiency for 42 was found to be maximum. The reasons for its high efficiency have also been supported by DFT studies. The HOMO−LUMO energy gap was calculated for complexes 41−43. This energy gap was found to be minimum for rhodium complex 42, indicating its maximum reactivity as observed experimentally [17]**.**

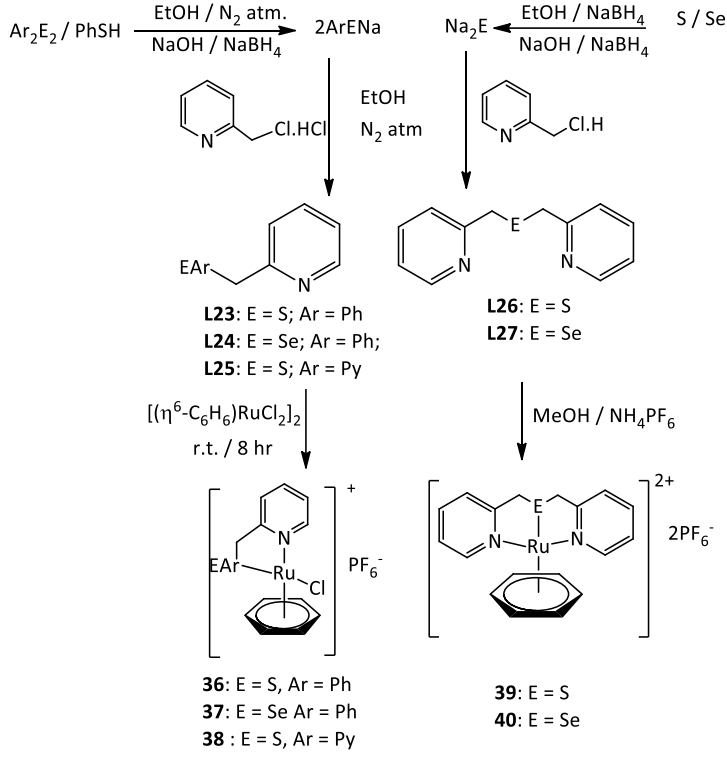

Scheme 9. Ru(II) complexes 36−40 with pyridine scaffold.

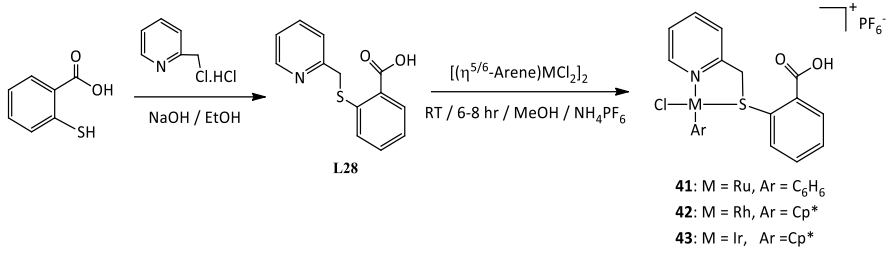

Scheme 10. Synthesis of 41−43.

Organochalcogen Ligands with Imine Functionality

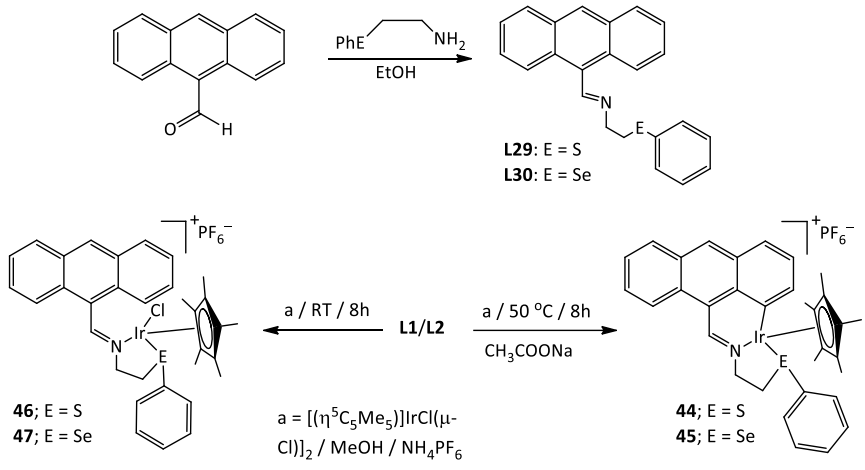

Scheme 11. Synthesis of Ir(III) complexes with anthracene core.

Schiff bases constitute to be an important category of ligands because of their easy preparation and handling. A combination of the soft donor (S/Se/Te) and a hard donor (N_{imine}) can easily be introduced in their frameworks which can further tune their ligation properties [54]. Chalcogenated Schiff base ligands L29 and L30 have been synthesized (Scheme 11) by condensation of anthracene-9-carbaldehyde with 2-(phenylthio/seleno)ethylamine [18]. Further the reaction of ligands L29 and L30 with $[(\eta^5\text{-}C_p^*)IrCl(\mu\text{-}Cl)]_2$ in presence of CH_3COONa resulted in the formation of iridacycles, 44 and 45. When the same reaction was performed

in absence of CH_3COONa, it resulted in the formation of iridium complexes 46 and 47, in which metal center is ligated with L29 and L30 in bidentate manner (Scheme 11). During ligation, the formation of Ir−Se bond is confirmed by a shift of the order of 103-105 ppm in the signal in the ^{77}Se NMR spectra of 45 and 47 with respect to that of ligand. Complexes 44−47 have been used for catalyzing transfer hydrogenation of aldehydes and ketones in 2-propanol at a low catalyst loading of 0.1−0.5 mol%. Out of complexes 44−47, complex 46 displayed maximum efficiency for this reaction. It is attributed to the fact that it can easily give the coordinatively unsaturated species, which led to the formation of final product. There are only few reports available on base free transfer hydrogenation reactions and those required a high catalyst loading of 1.0 mol %. However, complexes 44−47 have been found to be efficient for base free transfer hydrogenation as they catalyze this reaction in the absence of a base at 0.1−0.5 mol % catalyst loading only [18].

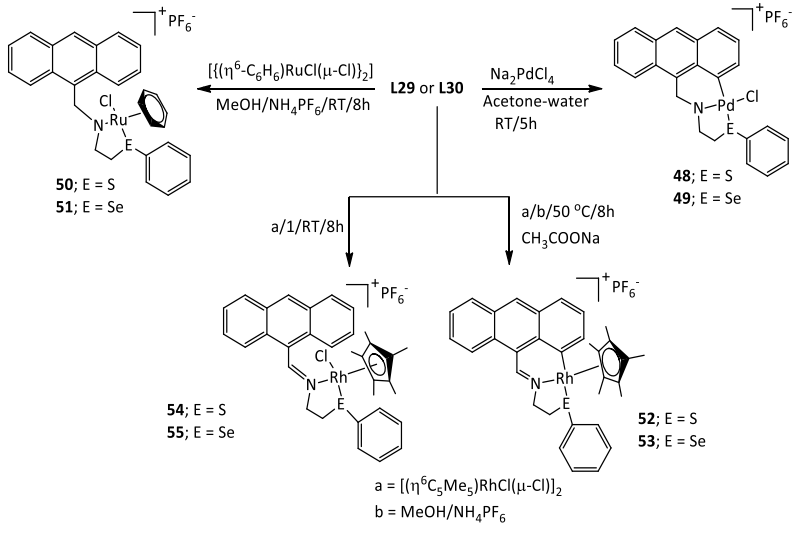

Scheme 12. Preparation of different Pd(II), Ru(II) and Rh(III) complexes.

Palladium (II), ruthenium (II) and rhodium (III) complexes of the ligands L29 and L30 (Scheme 12) have also been reported [19]. The ligands L29 and L30 have been synthesized by known methods in which the

condensation of anthracene-9-carbaldehyde is carried out with 2-(phenylthio/seleno)ethyl amine. For the syntheses of palladium (II) complexes 48 and 49, L29 and L30 have been reacted with Na_2PdCl_4 in the acetone-water mixture. The L29 and L30 behave as (C^-, N, E) donor pincer ligands. The reaction of chloro bridge Ru precursors $[(\eta^5\text{-}C_6H_6)RuCl(\mu\text{-}Cl)]_2$ and $[(\eta^5\text{-}C_6H_6)RhCl(\mu\text{-}Cl)]_2$ with L29 and L30 at room temperature yielded complexes 50,51 and 54, 55, respectively. For the synthesis of rhodium metalacycles, 52 and 53, L29 and L30 have been reacted with $[(\eta^5\text{-}C_6H_6)RhCl(\mu\text{-}Cl)]_2$ in presence of sodium acetate (Scheme 12). A deshielding of 56.4, 159.1 and 114.8 ppm was observed in ^{77}Se NMR spectra of 49, 51 and 53 with respect to corresponding free ligand, indicating the formation of M−Se bond. All complexes 48−55 were air and moisture insensitive and thermally stable. Palladium (48−49) and rhodium (52−55) complexes were explored for the transfer hydrogenation reactions at a catalyst loading of 0.05−0.2 mol % for 48−49 and 0.2-0.5 mol % for 52−55. These complexes showed maximum efficiency in catalyzing these reactions under base free conditions. Complex 54 has displayed maximum efficiency for the catalytic transfer hydrogenation reactions. Mercury poisoning test revealed the homogenous nature of catalysis [19].

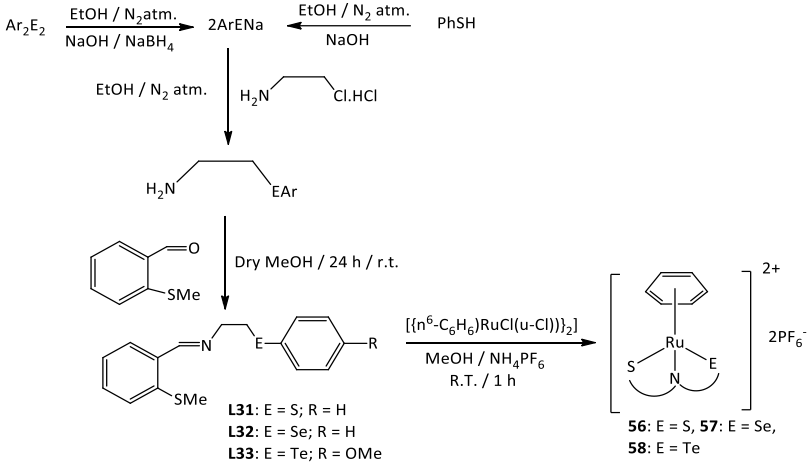

Scheme 13. Ru(II) complexes 56−58.

Singh and co-workers reported three Ru(II) complexes 56-58 (Scheme 13) of type fac-[(η^6-C_6H_6)Ru(L)].2PF_6 [5]. Such complexes have been synthesized by the reaction between 2-Me$SC_6H_4CH{=}NCH_2CH_2E$-C_6H_4-4-R and [{(η^6-C_6H_6)RuCl(μ-Cl)}$_2$] followed by anion exchange with NH_4PF_6 (Scheme 13). During the metalation reaction, similar trend in the change of signal of ^{77}Se and ^{125}Te NMR spectra of ligands was observed. The signal in ^{77}Se and ^{125}Te NMR spectra becomes desheilded by 103.2 and 253.7 ppm upon formation of 57 and 58 respectively from corresponding ligands. The catalysts were investigated for transfer hydrogenation of various ketones in 2-propanol at 0.001 mol % of catalyst loading. The Ru(II) complex containing organotellurium moiety served as the most efficient catalyst among the three. In terms of efficiency, if these Ru(II) complexes containing Schiff bases functionality are compared with the Ru(II) complexes of corresponding secondary amines, it may be observed that there is an insignificant difference among the six complexes. Therefore, it can be concluded that catalytic reaction proceeds through a classical mechanism [5].

COMPARISON AMONG CATALYTIC EFFICIENCY

Among all the complexes, 1−58, investigated for transfer hydrogenation reaction, the best catalytic efficiency has been observed with organotellurium ligated Ru(II) complex 3 (Scheme 1) with a turn over number of 98,000 for the conversion of acetophenone to 1-phenylethanol [5] followed by organotellurium ligated Ru(II) complex 58 [5] bearing an imine functionality (TON = 97,000) [5]. The catalytic efficiency of organoselenium ligated Ru(II) complexes 2 (Scheme 1) and 57 (Scheme 13) is also very high and value of TON (95000) achieved [5] using these complexes is slightly lower than that of the best catalysts i.e., 3 and 58. Among the Rhodium complexes, the highest TON of 78,000 has been shown by Rh(III) complex 25 bearing two selenium atoms in the framework [13]. A high TON value of 9,800 has also been observed with Ir(III) complex 17

[11]. The lowest TON reported for Ru(II), Rh(III) and Ir(III) complexes 41, 8, 10 are 180 [17], 60 [10] and 55 [10] respectively. The least catalytic potential has been reported for Ir(III) complex 10 [10]. It can also be concluded that Ru(II) complexes are more efficient in catalyzing transfer hydrogenation reaction in comparison to Rh(III) and Ir(III) complexes [9-19]. The effect of the ligation properties of chalcogen donor atom was also evident as tellurium ligated metal complexes were most efficient among all [5].

NANOCATALYSTS STABILIZED WITH ORGANOCHALCOGEN LIGANDS

Nanocatalysts have gained significant attention in the recent past. The high surface area to volume ratio of nanoparticles has a great influence on their properties. The high catalytic activity at low concentration makes them significant in catalysis [55]. Recyclability in combination with high selectivity under mild reaction conditions widens their scope [56]. The major drawback associated with them is their tendency to agglomerate in the absence of good stabilizer or in the presence of a poor stabilizing agent. Agglomeration reduces the catalytic activity of nanoparticles (NPs). Thus, NPs have to be stabilized with suitable protecting agents to prevent agglomeration without hampering their catalytic activity [32]. The role of the protecting ligands is to determine the size, dispersion and shape of the nanoparticles. The strong ligation properties of carboxyl, amine and hydroxyl groups stabilize nanoparticles efficiently but inhibit their use as a catalyst [57, 58]. In order to develop the catalytically recyclable nanoparticles, ligands must be strong enough to stabilize them through ligation without comprmising with their catalytic activity [32]. Organochalcogen ligands, in this regard, have proven to be efficient stabilizing ligands. A variety of organochalcogen ligands such as selenoether (didocosyl selenide) [32], thioother (didocosyl sulphide) [59] etc. have been utilized in stabilizing Pd(0) nanoparticles. The nano-catalysts

stabilized with such ligands have shown efficient catalytic potential in C−C coupling reactions [29, 30, 32, 59]. In addition, organochalcogen ligands bearing amine functionality have also been explored in the stabilization of nanocatalysts [29, 30]. It has observed that nanoparticles stabilized with such ligands are recyclable upto five reaction cycles with a conversion rate >90% [29]. For the same reason, anchoring of nanocatalyst on several inert solid supports such as silica, magnetite, graphene, and graphene oxide had been envisaged, and accordingly the work was done. Amongst all the solid support, graphene oxide was chosen in the study reported by Singh and co-workers [20] due to its mechanical strength and chemically inert nature in many reaction media. Graphene oxide was immobilized with (Se, N) donor sites, thereby giving it a character of chelating (Se, N) ligand. It has been synthesized by treating graphene oxide with $ClCH_2COOH$ and $SOCl_2$ [20], which results in increasing −COCl groups on graphene oxide required to bind selenated ethylamine on its surface. The presence of functional groups and defects on graphene oxide helps in the easy immobilization of NPs on the surface. Further, this graphene oxide with −COCl groups was treated with 2-(phenylselenyl) ethylamine resulted in the functionalization of graphene oxide with selenated ethylamine molecules [20]. Subsequent reaction of this (Se, N) grafted graphene oxide with NaOH and Na_2PdCl_4 resulted in the development and immobilization of Pd(0) nanaoparticles on graphene oxide (Scheme 14). The TEM studies revealed the uniform distribution and 1−3 nm size of the nanoparticles. These nanoparticles were investigated for the transfer hydrogenation reactions of carbonyl compounds (aldehydes and ketones)[20]. It has been found that this GO−Se−Pd was more efficient for conversion of aldehydes than ketones. Reusability of GO−Se−Pd has also been explored, and it was found that GO−Se−Pd can give significant yields upto six cycles [20].

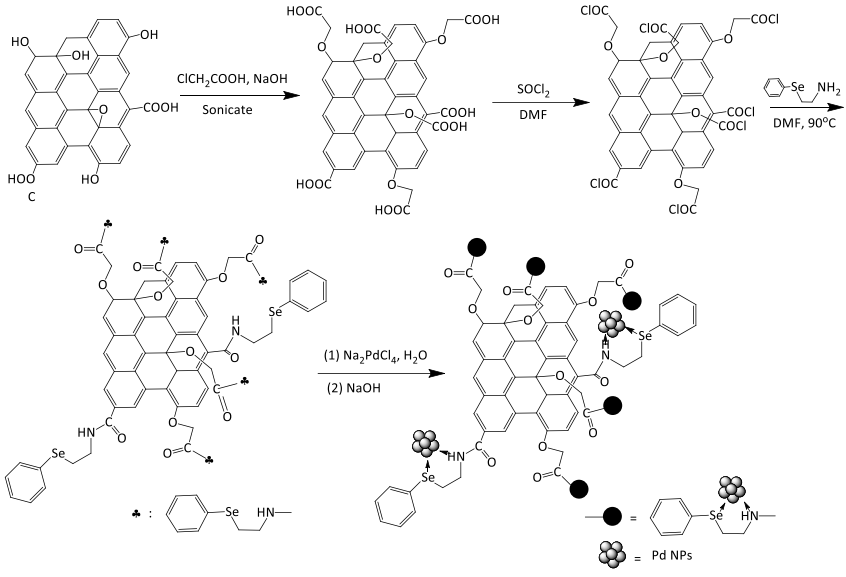

Scheme 14. Immobilization of Pd(0) on functionalized graphene oxide.

SUMMARY OF INSIGHTS OF CATALYTIC PROCESSES OF TRANSFER HYDROGENATION

Catalytic insights of various chemical transformations such as Suzuki Miyaura, Heck coupling are known to proceed via homogeneous as well as heterogenous pathway. The molecular Pd(II) complexes known to catalyze these transformation either act as true catalyst and catalyze the reaction or act as pre-catalyst to dispense Pd(0) during the course of the reaction. Some interesting observations have also been reported in case of catalysis of coupling reactions by some chalcogen ligated Pd(II) complexes [23, 44, 46]. There are several nanosized palladium chalcogenide species that are dispensed *insitu* from Pd(II) complexes such as $Pd_{16}S_7$ [23], Pd_4S, Pd_5S_2 [60], $Pd_{17}Se_{15}$ [25], PdSe [60], Pd_3Te_2 [61] and PdTe [62], etc. However, it has been undisputed so far that regardless of the catalyst being used, Pd(0)-Pd(II) cycle remains intact. Interestingly, similar observations have not been made in the case of catalysis of transfer hydrogen reactions by chalcogen

ligated complexes (1−58). Generation of Ru(0), Rh(0), Ir(0) or chalcogenides of these metals have not been investigated during the course of catalysis. A very limited study has been reported about insights of catalytic process of transfer hydrogenation till the date. Generally, it has been observed that molecular Ru(II), Rh(III) or Ir(III) complexes behave as pre-catalysts. The reaction proceeds mainly via homogeneous pathway in which the cleavage of M−Cl bond occurs and the formation of metal hydride intermediate takes place. Monitoring the catalytic reactions with ^{77}Se and ^{125}Te NMR spectroscopy has corroborated the formation of such an intermediate species. As a result, bidentate ligands have been found to be more efficient than tridentate ligands because the cleavage of M−Cl bond facilitates the catalysis and leads to the formation of M−H intermediate [9−19]. In chalcogenoether ligated metal complexes, the absence of −NH group in the framework suggests that the conventional method involving the development of alkoxide is the most favorable mechanism [63]. In case of triazole functionalized organochalcogen ligated Rh(III) or Ir(III) complexes, it has been further suggested that a loss of cyclopentadienyl ring lead to the formation of catalytically active species $[M(L-H)]^+$ responsible for catalysis. However, it is not the case with iridacycle or rhodacycle. The catalytically active intermediate, generated in situ in this case, is $[Cp^*ML)]^{2+}$. Thus, transfer hydrogenation generally occurs via homogeneous pathway [64].

CONCLUSION AND FUTURE SCOPE

Organosulphur/selenium ligated molecular Ru(II), Pd(II), Rh(III) and Ir(III) complexes have been explored as efficient catalysts for various chemical transformations such as coupling reactions, oxidation of alcohols, cyclotrimerization reaction, silylation reaction, borylation reactions, allylation of aldehydes, polymerization of norbornane, etc. [23]. After the year 2010, significant development has taken place in the exploration of application of such complexes in catalysis of transfer hydrogenation reactions. Maximum reports include the development and use of S or Se

ligated metal complexes. Te ligated metal complexes are rarely explored. Much work is yet to be done on the development and use of such complexes. Ease in syntheses and handling, air stability and moisture insensitivity are the attractive features of the catalysts of such type reported so far. So far, mechanistic insights into the catalytic processes have also not been gained fully. Hence, an extensive investigation about the mechanism of the catalytic pathway is yet to be studied. In addition, nanocatalysts, stabilized with organochalcogen-ligands, have also not been explored to a significant extent. Metal chalcogenide nanoparticles, developed via single source precursor methods, are also not yet explored in transfer hydrogenation reactions. It is further envisaged that such metal chalcogenide nanoparticles may prove to be efficient catalysts and maybe recyclable upto multiple reaction cycles.

REFERENCES

[1] Errington, J., McDonald, W. S. & Shaw, B. L. (1980). "Preparation of the Sixteen-atom Ring Chelates Trans-[$M_2Cl_4\{ButS(CH_2)_5SBut\}_2$], M = Pd or Pt: Crystal Structure of trans-[$Pd_2Cl_4\{ButS(CH_2)_5SBut\}_2$]." *Journal of the Chemical Society, Dalton Transactions*, 2309-2311.

[2] Errington, J., McDonald, W. S. & Shaw, B. L. (1980). "Cyclopalladation of $C_6H_4(CH_2SBut)_2$-1,3 and the Crystal Structure of [$PdCl\{C_6H_3(CH_2SBut)_2$-2,6}]." *Journal of the Chemical Society, Dalton Transactions*, 2312-2314.

[3] Rutherford, D., Juliette, J. J. J., Rocaboy, C., Horváth, I. T. & Gladysz, J. A (1998). "Transition Metal Catalysis in Fluorous Media: Application of a New Immobilization Principle to Rhodium Catalyzed Hydrogenation of Alkenes." *Catalysis Today, 42*, 381-388.

[4] Yao, Q. & Sheets, M. (2004)." A Se−C−Se−Pd(II) Pincer Complex as a Highly Efficient Catalyst for Allylation of Aldehydes with Allyltributyltin." *Journal of Organic Chemistry, 71*, 5384-5387.

[5] Singh, P. & Singh, A. K. (2010). "Transfer Hydrogenation of Ketones and Catalytic Oxidation of Alcohols with Half-Sandwich Complexes

of Ruthenium(II) Designed Using Benzene and Tridentate (S, N, E) Type Ligands (E = S, Se, Te).” *Organo-metallics, 29,* 6433-6442.

[6] Wang, C., Wu, X. & Xiao, J. (2008). “Broader, Greener, and More Efficient: Recent Advances in Asymmetric Transfer Hydrogena-tion.” *Chemistry-An Asian Journal, 3, 10,* 1750-1770.

[7] Ikariya, T., Murata, K. & Noyori, R. (2006). “Bifunctional transition metal-based molecular catalysts for asymmetric syntheses.” *Organic & Bimolecular Chemistry, 4,* 393-406.

[8] Ikariya, T. & Blacker, A. J. (2007). “Asymmetric Transfer Hydrogenation of Ketones with Bifunctional Transition Metal-Based Molecular Catalysts.” *Accounts of Chemical Research, 40, 12,* 1300-1308.

[9] Sharma, A. K., Joshi, H., Sharma, K. N., Gupta, P. L. & Singh, A. K. (2014). “2-Propanol vs Glycerol as Hydrogen Source in Catalytic Activation of Transfer Hydrogenation with (η^6-Benzene) Ruthenium(II) Complexes of Unsymmetrical Bidentate Chalcogen Ligands.” *Organometallics, 33, 13,* 3629-3639.

[10] Prakash, O., Joshi, H., Sharma, K. N., Gupta, P. L. & Singh, A. K. (2014). “Half-Sandwich Rhodium/Iridium(III) Complexes Designed with Cp* and 1,2-Bis(phenylchalcogenomethyl)benzene as Catalysts for Transfer Hydrogenation in Glycerol.” *Organometallics, 33, 10,* 2535-2543.

[11] Prakash, O., Sharma, K. N., Joshi, H., Gupta, P. L. & Singh, A. K. (2014). “(η5-Cp*)Rh(III)/Ir(III) Complexes with Bis(chalcogenoe-thers) (E, E′ Ligands: E = S/Se; E′ = S/Se): Synthesis, Structure, and Applications in Catalytic Oppenauer-Type Oxidation and Transfer Hydrogenation.” *Organometallics, 33, 4,* 983-993.

[12] Saleem, F., Rao, G. K., Kumar, A., Mukherjee, G. & Singh, A. K. (2013). “Half-Sandwich Ruthenium(II) Complexes of Click Generated 1,2,3- Triazole Based Organosulfur/-selenium Ligands: Structural and Donor Site Dependent Catalytic Oxidation and Transfer Hydrogenation Aspects.” *Organometallics, 32, 13,* 3595-3603.

[13] Saleem, F., Rao, G. K., Kumar, A., Mukherjee, G. & Singh, A. K. (2014). “Catalyst Activation with Cp*Rh^{III}/Ir^{III}–1,2,3-Triazole-Based

Organochalcogen Ligand Complexes: Transfer Hydrogenation via Loss of Cp* and *N*-Methylmorpholine *N*-Oxide Based vs Oppenauer-Type Oxidation." *Organometallics*, *33*, *9*, 2341-2351.

[14] Kumar, S., Saleem, F. & Singh, A. K. (2016). "'Click' Generated 1,2,3-Triazole Based Organosulphur/Selenium Ligands and Their Pd(II) and Ru(II) Complexes: Their Synthesis, Structure and Catalytic Applications." *Dalton Transactions*, *45*, 11445-11458.

[15] Saleem, F., Rao, G. K., Kumar, S., Singh, M. P. & Singh, A. K. (2015). "Complexes of (η^6-benzene)ruthenium(II) with 1,4-Bis(phenylthio/seleno-methyl)-1,2,3-triazoles: Synthesis, Structure and Applications in Catalytic Activation of Oxidation and Transfer Hydrogenation." *Dalton Transactions*, *44*, 19141-19152

[16] Prakash, O., Sharma, K. N., Joshi, H., Gupta, P. L. & Singh, A. K. (2013). "Half Sandwich Complexes of Chalcogenated Pyridine Based Bi-(N, S/Se) and Terdentate (N, S/Se, N) Ligands with (η^6-benzene)ruthenium(II): Synthesis, Structure and Catalysis of Transfer Hydrogenation of Ketones and Oxidation of Alcohols." *Dalton Transactions*, *42*, 8736.

[17] Prakash, O., Joshi, H., Sharma, K. N., Gupta, P. L. & Singh, A. K. (2014). "Transfer Hydrogenation (pH Independent) of Ketones and Aldehydes in Water with Glycerol: Ru, Rh, and Ir Catalysts with a COOH Group near the Metal on a (Phenylthio)methyl-2-pyridine Scaffold." *Organometallics*, *33*, *14*, 3804-3812.

[18] Dubey, P., Gupta S. & Singh, A. K. (2018). "Base Free N-alkylation of Anilines with $ArCH_2OH$ and Transfer Hydrogenation of Aldehydes/Ketones Catalyzed by the Complexes of η^5 -Cp*Ir(III) with Chalcogenated Schiff Bases of Anthracene-9-carbaldehyde." *Dalton Transactions*, *47*, 3764.

[19] Dubey, P., Gupta S. & Singh, A. K. (2019). "Complexes of Pd(II), η^6-C_6H_6Ru(II), and η^5-Cp*Rh(III) with Chalcogenated Schiff Bases of Anthracene-9-carbaldehyde and Base-Free Catalytic Transfer Hydrogenation of Aldehydes/Ketones and *N*-Alkylation of Amines." *Organometallics*, *38*, *4*, 944-961.

[20] Bhaskar, R., Joshi, H. & Singh, A. K. (2017). "Reusable Catalyst for Transfer Hydrogenation of Aldehydes and Ketones Designed by Anchoring Palladium as Nanoparticles on Graphene Oxide Functionalized with Selenated Amine." *ACS Applied Materials & Interfaces, 9*, 3, 2223-2231.

[21] Sharma, A. K., Joshi, H., Bhaskar, R. & Singh, A. K. (2019). "Solvent-Tailored $Pd_3P_{0.95}$ Nano−catalyst for Amide–Nitrile Inter-conversion, the Hydration of Nitriles and Transfer Hydrogenation of the C = O bond." *Dalton Transactions, 48*, 10962.

[22] Singh, P. & Singh, A. K. (2010). "Transfer Hydrogenation of Ketones and Catalytic Oxidation of Alcohols with Half-Sandwich Complexes of Ruthenium(II) Designed Using Benzene and Tridentate (S, N, E) Type Ligands (E = S, Se, Te)." *Organometallics, 29*, 6433-6442.

[23] Rao, G. K., Kumar, A., Kumar, S., Dupare, U. B. & Singh, A. K. (2013). "Palladacycles of Thioethers Catalyzing Suzuki–Miyaura C–C Coupling: Generation and Catalytic Activity of Nanoparticles." *Organometallics, 32*, 2452−2458.

[24] Rao, G. K., Kumar, A., Kumar, B., Kumar, D. & Singh, A. K. (2012). "Palladium(II)-Selenated Schiff Base Complex Catalyzed Suzuki–Miyaura Coupling: Dependence of Efficiency on Alkyl Chain Length of Ligand." *Dalton Transactions, 41*, 1931−1937.

[25] Rao, G. K., Kumar, A., Ahmed, J., & Singh, A. K. (2010). "Palladacycle Containing Nitrogen and Selenium: Highly Active Pre-Catalyst for the Suzuki–Miyaura Coupling Reaction and Unprecedented Conversion into Nano-sized $Pd_{17}Se_{15}$." *Chemical Communications, 46*, 5954–5956.

[26] Singh, M. P., Saleem, F., Rao, G. K., Kumar, S., Joshi, H. & Singh, A. K. (2016). "Palladacycles of Unsymmetrical (N,C−,E) (E = S/Se) Pincers Based on Indole: Their Synthesis, Structure and Application in the Catalysis of Heck Coupling and Allylation of Aldehydes." *Dalton Transactions, 45*, 6718−6725.

[27] Kumar, A., Agarwal, M. & Singh, A. K. (2008). "Schiff Bases of 1′-Hydroxy-2′-acetonaphthone Containing Chalcogen Functionalities and Their Complexes with and (*p*-cymene)Ru(II), Pd(II), Pt(II) and

Hg(II): Synthesis, Structures and Applications in C–C Coupling Reactions." *Journal of Organometallic Chemistry*, *693*, 3533–3545.

[28] Joshi, H., Sharma, K. N., Sharma, A. K., Prakash, O. & Singh, A. K. (2013). "Graphene Oxide Grafted with $Pd_{17}Se_{15}$ Nano-particles Generated from a Single Source Precursor as a Recyclable and Efficient Catalyst for C–O Coupling in O-Arylation at Room Temperature." *Chemical Communications*, *49*, 7483-7485.

[29] Oswal, P., Arora, A., Kaushal, J., Rao, G. K., Kumar, S., Singh, A. K. & Kumar, A. (2019). "Ultra-small Palladium Nano-particles Synthesized Using Bulky S/Se and N Donor Ligands as a Stabilizer: Application as Catalysts for Suzuki–Miyaura Coupling." *RSC Advances*, *9*, 22313-22319.

[30] Sharma, P., Arora, A., Oswal, P., Rao, G. K., Kaushal, J., Kumar, S., Kumar, S., Singh, M. P., Singh, A. K. & Kumar, A. (2019). "Bidentate Organochalcogen Ligands (N, E; E = S/Se) As Stabilizers for Recyclable Palladium Nanoparticles and Their Application in Suzuki–Miyaura Coupling Reactions." *Polyhedron*, *171*, 120-127.

[31] Arora, A., Oswal, P., Rao, G. K., Kaushal, J., Kumar, S., Singh, A. K. & Kumar, A. (2019). "Chalcogen (S/Se) Ligated Palladium(II) Complexes of Bulky Ligands: Application in *O*-Arylation of Phenol." *Chemistry Select*, *4*, *36*, 10765-10769.

[32] Rao, G. K., Kumar, A., Kumar, B. & Singh, A. K. (2012). "Didocosyl Selenide Stabilized Recyclable Pd(0) Nanoparticles and Coordinated Palladium(II) as Efficient Catalysts for Suzuki–Miyaura Coupling." *Dalton Transactions*, *41*, 4306-4309.

[33] Kumar, A., Rao, G. K., Kumar, S. & Singh, A. K. (2014). "Formation and Role of Palladium Chalcogenide and Other Species in Suzuki–Miyaura and Heck C–C Coupling Reactions Catalyzed with Palladium(II) Complexes of Organochalcogen Ligands: Realities and Speculations." *Organometallics*, *33*, *12*, 2921-2943.

[34] Das, D., Rao, G. K. & Singh, A. K. (2009). "Palladium(II) Complexes of the First Pincer (Se,N,Se) Ligand, 2,6-Bis((phenylseleno)methyl)pyridine (L): Solvent-Dependent Formation of

[PdCl(L)]Cl and Na[PdCl(L)][$PdCl_4$] and High Catalytic Activity for the Heck Reaction." *Organometallics*, *28*, *20*, 6054-6058.

[35] Kumar, A., Rao, G. K. & Singh, A. K. (2012). "Organochalcogen Ligands and Their Palladium(II) Complexes: Synthesis to Catalytic Activity for Heck Coupling." *RSC Advances*, *2*, 12552-12574.

[36] Kumar, S., Rao, G. K., Kumar, A., Singh, M. P. &Singh A. K. (2013). "Palladium(II)-(E,N,E) Pincer Ligand (E = S/Se/Te) Complex Catalyzed Suzuki Coupling Reactions in Water via Insitu Generated Palladium Quantum Dots." *Dalton Transactions*, *42*, 16939-16948.

[37] Rao, G.K., Kumar, A., Bhunia, M., Singh, M. P. & Singh, A. K. (2014). "Complex of 2-(Methylthio)aniline with Palladium(II) as an Efficient Catalyst for Suzuki–Miyaura C−C Coupling in Eco-friendly Water." *Journal of Hazardous Materials*, *269*, 18-23.

[38] Rao, G. K., Kumar, A., Saleem, F., Singh, M. P., Kumar, S., Kumar, B., Mukherjee, G. & Singh, A. K. (2015). "Palladium(II)-1-phenylthio-2-arylchalcogenoethane Complexes: Palladium Phosphide Nano-peanut and Ribbon Formation Controlled by Chalcogen and Suzuki Coupling Activation ." *Dalton Transactions*, *44*, 6600-6612.

[39] Saleem, F., Rao, G. K., Singh, P. & Singh, A. K. (2013). "Chalcogen-Dependent Palladation at the Benzyl Carbon of 2,3-Bis[(phenylchalcogeno)methyl]quinoxaline: Palladium Complexes Catalyzing Suzuki–Miyaura Coupling via Palladium–Chalcogen Nanoparticles." *Organometallics*, *32*, *2*, 387-395.

[40] Saleem, F., Rao, G. K., Kumar, A., Kumar, S., Singh, M. P. & Singh, A. K. (2014). "Palladium(II) Complexes Bearing the 1,2,3-Triazole Based Organosulphur/Selenium Ligand: Synthesis, Structure and Applications in Heck and Suzuki–Miyaura Coupling as a Catalyst via Palladium Nanoparticles." *RSC Advances*, *4*, 56102-56111.

[41] Singh, V. V., Rao, G. K., Kumar, A. & Singh, A. K. (2012). "Palladium(II)–Selenoether Complexes as New Single Source Precursors: First Synthesis of Pd_4Se and Pd_7Se_4 Nanoparticles." *Dalton transactions*, *41*, 1142-1145.

[42] Sharma, A. K., Joshi, H., Bhaskar, R., Kumar, S. & Singh, A. K. (2017). "Palladacycles of Sulphated and Selenated Schiff Bases of

Ferrocene-Carboxaldehyde as Catalysts for O-Arylation and Suzuki–Miyaura Coupling." *Dalton Transactions*, *46*, 2485−2496.

[43] Sharma, A. K., Joshi, H., Ojha, K. & Singh, A. K. (2019). "Graphene Oxide Supported Cobalt Phosphide Nanorods Designed from a Molecular Complex for Efficient Hydrogen Evolution at Low Overpotential." *Chemical Communications, 55*, 2186-2189.

[44] Kumar, A., Rao, G. K., Saleem, Singh & A. K. (2012). "Organoselenium Ligands in Catalysis." *Dalton Transactions, 41*, 11949−11977.

[45] Kumar, A., Rao, G. K., Saleem, F., Kumar, R. & Singh, A. K. (2014). "Efficient Catalysis of Suzuki–Miyaura C−C Coupling Reactions with Palladium(II) Complexes of Partially Hydrolyzed Bisimine Ligands: A Process Important in Environment Context." *Journal of Hazardous Materials*, *269*, 9-17.

[46] Kumar, A., Rao, G. K., Kumar, S. & Singh, A. K. (2013). "Organosulphur and Related Ligands in Suzuki–Miyaura C–C Coupling." *Dalton Transactions, 42*, 5200−5223.

[47] Cremlyn, R. J. (1996). "An Introduction to Organosulphur Chemistry." *Wiley*: *Chichester, U.K.*

[48] Murray, S. G. & Hartley, F. (1981). "Coordination Chemistry of Thioethers, Selenoethers, and Telluroethers in Transition-Metal Complexes." *Chemical Reviews*, *81*, *4*, 365-414.

[49] Devillanova, F. A. (2007). "Handbook of Chalcogen Chemistry: New Perspectives in Sulfur, Selenium and Tellurium." *Royal Society of Chemistry*, *London*.

[50] Azua, A., Mata, J. A., Peris, E., Lamaty, F., Martinez, J. & Colacino, E. (2012). "Alternative Energy Input for Transfer Hydrogenation using Iridium NHC Based Catalysts in Glycerol as Hydrogen Donor and Solvent." *Organometallics*, *31*, 3911-3919.

[51] (a) Tavor, D., Sheviev, O., Dlugy, C. & Wolfson, A. (2010). "Transfer Hydrogenation of Benzaldehyde Using Glycerol As Solvent and Hydrogen Source." *Canadian Journal of Chemistry*, *88*, 305-308, (b) Farnetti, E., Kaˇspara, J. & Crotti, C. (2009). "A Novel Glycerol Valorization Route: Chemoselective Dehydrogenation Catalyzed by

Iridium Derivatives." *Green Chemistry, 11,* 704-709, (c) Wolfson, A., Dlugy, C., Shotland, Y. & Tavor, D. (2009). "Glycerol As Solvent and Hydrogen Donor in Transfer Hydrogenation–Dehydrogenation Reactions." *Tetrahedron Letters, 50,* 5951–5953, (d) Tavor, D., Popov, S., Dlugy, C. & Wolfson, A. (2010). "Catalytic Transfer-Hydrogenations of Olefins in Glycerol." *Organic Communications, 3,* 70-75, (e) Cravotto, G., Orio, L., Gaudino, E. C., Martina, K., Tavor, D. & Wolfson, A. (2011). "Efficient Synthetic Protocols in Glycerol under Heterogeneous Catalysis." *ChemSusChem, 4,* 1130-1134.

[52] Nareddy, P., Mantilli, L., Guénée, L., & Mazet, C. (2012). "Atropoisomeric (P,N) Ligands for the Highly Enantioselective Pd-Catalyzed Intramolecular Asymmetric α-Arylation of α-Branched Aldehydes." *Angewandte Chemie International Edition, 51,* 3826.

[53] Anna, V. R., Prasad, K. T., Wang, P. & Rao, K. M. (2012). "Study of Half-Sandwich Mono and Dinuclear Complexes of Platinum Group Metals Containing Pyrazolyl Pyridine Analogues: Synthesis and Spectral Characterization." *Journal of Chemical Sciences, 124, 3,* 565-575.

[54] Dubey, P., Gupta, S. & Singh, A. K. (2017) "Trinuclear Complexes of Palladium(II) with Chalcogenated *N*-Heterocyclic Carbenes: Catalysis of Selective Nitrile–Primary Amide Interconversion and Sonogashira Coupling." *Dalton Transactions, 46,* 13065-13076.

[55] Wu, B., Kuang, Y., Zhang, X. & Chen, J. (2011). "Noble Metal Nanoparticles/Carbon Nanotubes Nanohybrids: Synthesis and Applications." *Nano Today, 6,* 75-90.

[56] Astruc, D. (2008). "Nanoparticles and Catalysis." *Wiley-VCH*: *Weinheim, Germany*.

[57] Cuenya, B. R. (2010). "Synthesis and Catalytic Properties of Metal Nanoparticles: Size, Shape, Support, Composition and Oxidation State Effects." *Thin Solid Films, 518,* 3127-3150.

[58] Gniewek, A., Ziółkowski, J. J., Trzeciak, A. M., Zawadzki, M., Grabowska, H. & Wrzyszcz, J. (2008). "Palladium Nanoparticles Supported on Alumina-Based Oxides as Heterogeneous Catalysts of the Suzuki–Miyaura Reaction." *Journal of Catalysis, 254,* 121-130.

[59] Kumar, S., Rao, G. K., Kumar, A., Singh, M. P., Saleem, F. & Singh, A. K. (2015). "Efficient Catalytic Activation of Suzuki–Miyaura C–C Coupling Reactions with Recyclable Palladium Nanoparticles Tailored with Sterically Demanding Di-n-alkyl Sulphides." *RSC Advances, 5,* 20081-20089.

[60] Sharma, K. N., Joshi, H., Singh, V. V., Singh, P. & Singh, A. K. (2013). "Palladium(II) Complexes of Pyrazolated Thio/Selenoethers: Syntheses, Structures, Single Source Precursors of Pd_4Se and PdSe Nano-particles and Potential for Catalyzing Suzuki–Miyaura Coupling." *Dalton Transactions, 42,* 3908-3918.

[61] Rao, G. K., Kumar, A., Singh, M. P. & Singh, A. K. (2014). "Palladium(II) Complex of an Organotellurium Ligand as a Catalyst for Suzuki Miyaura Coupling: Generation and Role of Nano-Sized Pd_3Te_2." *Journal of Organometallic Chemistry, 749,* 1-6.

[62] Singh, P., Das, D., Kumar, A. & Singh, A. K. (2012). "Palladium(II) Complexes of *N*-{2-(Aryltelluro)ethyl}morpholine/piperidine: Synthesis, Structure, Application in Heck Coupling and Unprecedented Conversion into Nano-Sized PdTe." *Inorganic Chemistry Communications, 15,* 163-166.

[63] Noyori, R., Yamakawa, M. & Hashiguchi, S. (2001). "Metal−Ligand Bifunctional Catalysis: A Non−Classical Mechanism for Asymmetric Hydrogen Transfer between Alcohols and Carbonyl Compounds." *Journal of Organic Chemistry, 66,* 7931.

[64] Pandrala, M., Resendez, A. & Malhotra, S. V. (2019). "Polypyridyl Iridium(III) Based Catalysts for Highly Chemoselective Hydrogenation of Aldehydes." *Journal of Catalysis, 378,* 283-288.

In: Advances in Chemistry Research ISBN: 978-1-53617-112-9
Editor: James C. Taylor

Chapter 4

DIMENSIONAL ANALYSIS AND SIMILARITY THEORY IN ELECTROCHEMISTRY

Vyacheslav Protsenko*

Ukrainian State University of Chemical Technology, Dnipro, Ukraine

ABSTRACT

The progress in the application of dimensional analysis and similarity theory in electrochemical kinetics and electrochemical engineering is discussed. The use of dimensionless groups in problems of current density distribution and electrochemical mass transfer is described and the similarity criteria involved are considered. It is shown that dimensional analysis and similarity theory can be successfully used for studying the kinetics of different electrode processes, including the consideration of electrochemical charge transfer. The proper dimensionless quantities (i.e., similarity criteria) are generalized and the approximating relationships between them are analyzed. The results of numerical simulation of the kinetics of a two-stage electrochemical reaction with a partial transfer of intermediates between the electrode surface and the bulk solution are considered in the light of the concept of dimensional analysis and similarity theory. The main advantages of the application of dimensional analysis and

* Corresponding Author's Email: Vprotsenko7@gmail.com.

similarity theory in pure and applied electrochemistry are summarized in this chapter.

Keywords: dimensional analysis, similarity theory, similarity criteria, electrochemical process, charge transfer, electrolysis

INTRODUCTION

Electrochemical processes commonly involve a great number of different physicochemical stages, which are described by complex mathematical expressions containing numerous variables and parameters. For instance, the kinetic equations of consecutive charge transfer processes include various parameters characterizing the kinetic features of both individual electrochemical stages and transport processes in the solution and the near-electrode layer [1–7]. Thus, the analysis of the kinetics of these electrochemical processes causes difficulties, and, as a rule, one has either to use numerical simulation or to consider some simplified particular cases. Owing to these causes, the clarity of the data presentation may be lost and the universality of the conclusions disappears.

In this context, it seems that the application of dimensional analysis and similarity theory is a promising and effective way to examine the behavior of complex and multifactorial electrochemical processes. To emphasize the generalized character of the analysis, these two theories (dimensional analysis and similarity theory) are sometimes considered under the name “the theory of generalized variables” [8]. It is known that the use of dimensionless quantities, derived by means of approaches developed in dimensional analysis and similarity theory, allows decreasing the number of the analyzed variables and simplifying the structure of the equations and relationships that reflect the essence of the mathematical models involved [9].

Dimensional analysis and similarity theory are commonly used in such scientific and technical fields as heat exchange, mass transfer, continuum mechanics, designing of various machines and aggregates, etc. As far as the

use of dimensional analysis for studying physicochemical processes is concerned, the first attempt in that direction was made by D'yakonov [10]. In order to investigate the thermodynamic and kinetic characteristics of chemical processes, D'yakonov not only utilized "common" similarity criteria (such as Péclet number, Grashof number, Reynolds number, etc.) but also introduced some new similarity criteria associated with the specific features of chemical reactions (i.e., the criteria of chemical transformation and chemical similarity).

An electrochemical process can be considered as a particular case of a chemical transformation involving the electric charge transfer through the interface "electrode/electrolyte." Thus, the behavior of complex electrochemical systems is usually described by a great number of diverse parameters and variables. Evidently, the application of the techniques developed in dimensional analysis and similarity theory may be very fruitful and productive to achieve a deeper understanding of the performance of electrochemical systems and generate new ideas both in pure and in applied electrochemistry [11]. This chapter is devoted to a brief review of the literature data on the use of dimensional analysis and similarity theory in electrochemical kinetics and electrochemical engineering.

ELECTROCHEMICAL SIMILARITY CRITERION CHARACTERIZING THE UNIFORMITY OF CURRENT DISTRIBUTION

It is known that the local current density in a real electrochemical cell changes from point to point on the surface of an electrode. A non-uniform current distribution is caused by a number of different factors. These factors are as follows: (i) non-regular geometry of the systems (including complex shape and size of the electrodes and their relative position in an electrolyzer); (ii) low electrical conductivities of the electrolyte and the electrodes; (iii) the appearance of overpotential of electrochemical processes; and (iv) non-uniform hydrodynamic conditions in an electrochemical cell [12, 13].

An actual current distribution strongly affects the performance of an electrochemical system. For instance, the variation of current density over the electrode surface results in the changes of the thickness, morphology and properties of the electrodeposited metal layers, which is highly undesirable. Hence, it is very important to develop a simple mathematical tool that could provide reliable information about the current distribution in real electrochemical systems of various sizes, especially for the design of large-scale electrolytic or galvanic cells.

A scale-up criterion of electrochemical similarity, the so-called Wagner number, is often used to this end [12, 14]. This criterion may be given as follows:

$$W_a = \frac{\partial E}{\partial i} \cdot \frac{\chi}{L_0} \quad (1)$$

where χ is the conductivity of the electrolyte; $\frac{\partial E}{\partial i}$ is the polarizability of the electrode; and L_0 is the characteristic size of the system (for instance, the length of the electrode).

The polarizability of the electrode, $\frac{\partial E}{\partial i}$, corresponds to the local slope of the polarization curve. The polarizability reflects the specific polarization resistance caused by the electrochemical reaction. This value is determined by the kinetics and mechanism of a given electrode process.

It is obvious that the Wagner number is dimensionless; it gives the ratio of the surface polarization resistance to the ohmic resistance of an electrolyte (reciprocal conductivity). Thus, this criterion summarizes the influence of the main geometrical and electrochemical parameters on the uniformity of current distribution in a given electrochemical bath. The higher the Wagner number, the more even is the current density distribution. Equation (1) shows that a decrease in the characteristic size of an electrochemical system and an increase in both the conductivity and the polarization resistance promote better current density distribution.

Further, we will give several examples of the use of Wagner number in electrochemistry. This similarity criterion was numerically simulated and quantified with regard to the process of copper electrodeposition in a rotating cylinder Hull cell [15]. Stricker et al. [16] developed an analytical model that allows calculating the distribution of current density and the values of Wagner number for the electrochemical cell with a small height and with coplanar thin electrodes. The Wagner numbers were used to estimate the current distributions in electrochemical systems that involve gradual changes in electrodes shape and size (electroplating or electrochemical machining) [17]. The calculation of Wagner numbers was successfully used to design redox flow batteries and predict their operational performance [18]. The application of some dimensionless numbers, including Wagner number, was considered to characterize the behavior of scalable reactor systems for different bioelectrochemical processes [19].

DIMENSIONAL ANALYSIS OF ELECTROCHEMICAL MASS TRANSFER PROBLEMS

It was Ibl [20] who first suggested the application of dimensional analysis and similarity theory to solve electrochemical mass transfer problems. It is known that the transport of the reagents between the bulk electrolyte and the surface of the electrodes is a key factor determining the concentrations at the interface and hence influencing the rate of an electrochemical reaction. The limiting current density at which the concentration of an initial product at the electrode surface approaches zero and which corresponds to the maximum achievable rate of an electrochemical process is also depends on the characteristics of mass transfer.

Let us consider some basic assumptions and conclusions given in the work by Ibl [20]. It should be observed that the mass transfer of the reagents during the electrolysis is provided by diffusion, charge migration and

convection. In a first approximation, the flux (N_i) of the *i*th electroactive ionic species can be expressed by the following equation:

$$N_i = -D_i\, grad C_i - \frac{z_i F D_i C_i}{RT} grad\phi + C_i V \qquad (2)$$

where D_i is the diffusion coefficient of the species involved; C_i is its concentration; z_i is the valency of the ionic species; V is the velocity vector of a hydrodynamic flow; ϕ is the electric potential; F, R and T are the Faraday's constant, the universal gas constant and the thermodynamic temperature, respectively.

It was evident that the first, second and third terms on the right hand side of Eq. (2) are associated with the mass transfer by diffusion, migration and convection, respectively. After transforming Eq. (2), the following formula can be obtained that expresses the conservation of mass for the *i*th species:

$$\frac{dC_i}{d\tau} = -div\, N_i = -D_i div\, grad C_i + \frac{z_i F D_i C_i}{RT} div\left(C_i\, grad\phi\right) - V\, grad C_i \qquad (3)$$

Close examination of Eq. (3) reveals that it reflects the time change of concentration in an elementary electrolyte volume of an incompressible liquid. Thus, Eq. (3), the Navier-Stokes equation and the hydrodynamic continuity equation constitute three basic differential equations describing convective mass transfer in a given electrochemical system [20]. To calculate the limiting current density and (or) the concentrations of the reagents on the electrode surface, one has to integrate simultaneously these three equations.

However, the number of variables that are used to characterize convective mass transfer is commonly large enough, which causes serious mathematical difficulties. At the same time, data analysis can be appreciably simplified by the grouping of the variables to form some new dimensionless variables (i.e., similarity criteria), the number of them being less than that of the original dimensional variables [8, 9, 11, 20].

A well-known Buckingham's π theorem [21], which is a key theorem in dimensional analysis, opens the door to the establishment of the sets of dimensionless parameters from given variables, even if the exact form of the equations that couple these variables is still unknown. It should be noted that the similarity criteria could be used for the analysis even under very intricate flow conditions (when the integration of the fundamental differential equations is difficult or impossible).

Ibl considered the application of dimensionless groups (similarity criteria) to electrochemical mass transfer problems giving some concrete examples [20]. A first example was associated with the steady-state mass transfer rate in the course of the electrochemical deposition of a metal coating on a flat electrode along which the electrolyte is flowing. In this case, the following expression can be written for the value of limiting current density:

$$j = f(D, \Delta C, V, \nu, l) \quad (4)$$

where j is the steady-state rate of mass transfer during metal electrodeposition; ΔC is the difference between the concentrations of metal ions on the electrode surface and in the bulk (this difference should be considered as a driving force of diffusion transfer); V is the flow velocity of the solution; ν is the kinematic viscosity; and l is the length of the electrode in the direction of the liquid flow.

The transformation of Eq. (4) by using the Buckingham's π theorem yields the following expression:

$$Nu = F(Sc, Re) \quad (5)$$

where $Nu = \frac{jl}{D\Delta C}$ is the Nusselt number; $Sc = \frac{\nu}{D}$ is the Schmidt number; and $Re = \frac{Vl}{\nu}$ is the Reynolds number.

It is clear that *six* initial dimensional variables have been converted into *three* dimensionless variables: *Nu*, *Sc*, and *Re*. In addition, the initial

differential equation system has been replaced by an algebraic equation. Evidently, this simplifies the problem analysis even for highly complicated special cases. Seemingly, there is no need to go into details on the physical interpretations of the derived similarity criteria, since they are widely used in the fields of hydrodynamics, heat exchange, mass transfer, continuum mechanics, and so on.

Another example considered by Ibl [20] was connected with the steady-state rate of mass transfer during the electrodeposition of a metal on a plane vertical cathode in an electrolyte without any forced agitation. In such a case, buoyancy force acts on the fluid and causes a hydrodynamic flow along the electrode. Then, we get the following equation:

$$j = f\left(D, \Delta C, \nu, g\frac{\Delta\rho}{\rho}, l\right) \quad (6)$$

where g is the acceleration of gravity; ρ is the density of the bulk solution; $\Delta\rho$ is the density difference between interface and bulk; and other variables are explained above.

It was found that only three similarity criteria exhaustively reflected the problem under discussion. Two of these criteria, *Nu* and *Sc*, are characterized above. The third criterion, that is usually introduced to describe natural convection, is the Grashof number $Gr = \frac{g\Delta\rho l_3}{\rho\nu^2} = \frac{g\alpha\Delta Cl^3}{\nu^2}$ (here α is the densification coefficient).

Ibl showed [20] that *Sc* and *Gr* should not be considered separately under the conditions of high Schmidt numbers, which is typical of "common" electrolysis. Then, we can obtain:

$$Nu = F(Sc \times Gr) = F(Ra) \qquad (7)$$

Here, the product $Sc \times Gr$ is the so-called Rayleigh number (*Ra*). The results reported in literature were analyzed by means of dimensionless forms using Eq. (7) [20]. Evidently, such a presentation of experimental data seems

to be simple, intuitive and intelligible, whereas a representation of experimental findings through the initial (i.e., dimensional) parameters is appreciably more intricate.

A number of publications reported the application of dimensional analysis and similarity theory to study the generation of electrostatic streaming currents that appeared during the flow of a liquid [22–24]. The initial dimensional parameters characterizing the process concerned were transformed into non-dimensional similarity criteria and the physical significance of them was examined in those works. The main equation was used in the following form [22]:

$$\frac{\partial \sigma_{\pm}}{\partial \tau} = D_{\pm}\nabla^2\sigma_{\pm} - \nabla\cdot\left(\lambda_{\pm}E\right) + \alpha C_m - \beta C_{+}C_{-} \quad (8)$$

where $\sigma_{\pm}$ is the charge density; E is the electric field; ε is the dielectric constant; $\lambda_{\pm}$ is the electrical conductivity; C_{m} is the concentration of molecular species; α is the dissociation coefficient; and β is the recombination coefficient. The signs (±) refer to the cations and anions, respectively.

In addition, the Poisson equation (9) and the summation of charge density (10) should be taken into account.

$$\sigma = \nabla\cdot\left(\varepsilon E\right) \quad (9)$$

$$\sigma = \sigma_{+} + \sigma_{-} \quad (10)$$

Two equations (8) (for cations and anions, respectively) together with Eqs. (9) and (10) constitute a set of differential equations reflecting the processes under consideration. The five following dimensionless similarity criteria were derived [22]:

$$\frac{i_s^2}{\rho U^4 \varepsilon l^2},\ \frac{\varepsilon U}{\lambda_0 l},\ \frac{D\varepsilon}{\lambda_0 l^2},\ \frac{\rho U l}{\mu},\ \frac{D_{+}}{D_{-}} \quad (11)$$

where i_s is the streaming current; ρ is the density of a liquid; U is the velocity of a reference liquid; l is the characteristic length; λ_0 is the electrical conductivity at $\sigma = 0$; μ is the viscosity of a liquid; and $2D = D_+ + D_-$.

It was stated that the behavior of the electrochemical system under study could be definitely described by the relationships between the similarity criteria (11). It is interesting to characterize the physical meaning of them. The first non-dimensional criterion, $\frac{i_s^2}{\rho U^4 \varepsilon l^2}$, shows the ratio between the field force of a fluid and the fluid inertia force. The second criterion, $\frac{\varepsilon U}{\lambda_0 l}$, characterizes the ratio between the convection current and the conduction current. The third criterion, $\frac{D\varepsilon}{\lambda_0 l^2}$, displays the ratio between the diffusion current and the conduction current. The fourth criterion, $\frac{\rho U l}{\mu}$, is the Reynolds number. Finally, the fifth criterion, $\frac{D_+}{D_-}$, is the so-called Knudsen number.

DIMENSIONAL ANALYSIS OF CHARGE TRANSFER PROCESSES

Charge transfer at the interface “electrode/electrolyte” is known to be a specific step of any electrochemical reaction. A number of papers [25–27] reported the application of dimensional analysis and similarity theory to the interpretation of kinetic equations concerning the processes of electrochemical charge transfer.

Thus, a one-stage electrochemical reaction was considered that obeys the following equation of the slow discharge theory [25]:

$$i = i_0 \left\{ \exp\left[\frac{\alpha F \eta}{RT} \right] - \exp\left[-\frac{(1-\alpha) F \eta}{RT} \right] \right\} \exp\left[\frac{(\alpha - z_0) F \psi_1}{RT} \right] \quad (12)$$

where i is the cathode current density of a reaction O + e^- ↔ R; $i_0 = F k_s C_O^{1-\alpha} C_R^{\alpha}$ is the exchange current density; $\eta = (E^0 - E)$ is the value of cathode polarization; α is the transfer coefficient; k_s is the heterogeneous rate constant; C_O and C_R are the concentrations of oxidized and reduced species, respectively; z_O is the electric charge of species O; and ψ_1 is the electric potential at the point where the reacting particles are situated prior to the charge transfer (according to the Frumkin's theory of the influence of the electric double layer on the electrochemical kinetics).

It was shown [25] that four dimensionless complexes can be derived if Eq. (12) is valid. These complexes are presented as follows:

$$\pi_1 = \frac{i}{i_0},\ \pi_2 = \frac{F\eta}{RT},\ \pi_3 = \frac{z_O F \psi_1}{RT},\ \pi_4 = \frac{F\psi_1}{RT} \quad (13)$$

The complex π_1 reflects the ratio of the current density to the exchange current density; hence it gives a relative (i.e., dimensionless) rate of the electrochemical reaction. The second complex π_2 shows the relationship between the electric work consumed in charge transfer due to polarization ($F\eta$) and the thermal motion energy (RT). In such a case, the complex π_2 expresses the dimensionless form of electrode polarization and is a measure of the driving force of an electrochemical process.

The mathematical structures of the complexes π_3 and π_4 are similar. Obviously, these complexes allow one to compare the thermal motion energy with the works of an electric field relating to the transfer of particles O (π_3) and the electron (π_4) to the plane in an electric double layer where an activated complex is situated. These two similarity criteria characterize a relative intensity of two effects that are associated with the influence of the electric double layer upon the discharge rate.

It is interesting that the transfer coefficient (α) turned out to be a specific electrochemical similarity criterion [25]. Indeed, any simple electrochemical reaction obeys the Brønsted relation in the following form:

$$\Delta G^{\neq} = \Delta G_0^{\neq} + \alpha F \eta \quad (14)$$

where $\Delta G_0^{\neq}$ and $\Delta G^{\neq}$ are the free energies of activation at an equilibrium potential and at a specified value of polarization (η), respectively.

After a simple transformation of Eq. (14), we can obtain:

$$\alpha = \frac{\Delta G^{\neq} - \Delta G_0^{\neq}}{F\eta} \quad (15)$$

Equation (15) explicitly shows that the transfer coefficient is the ratio between the free activation energy due to the electrode polarization and the electric work of the electron transfer induced by polarization.

At the same time, it is well known that each similarity criterion quantitatively characterizes a balance between the intensities of the action of two physical effects that are crucial to the process under study [8]. Hence, the transfer coefficient is a peculiar similarity criterion; it should be considered as the fifth similarity criterion together with those expressed by Eq. (13).

The transformation of Eq. (12) by means of the methods of dimensional analysis and similarity concept yields the following universal expression of the slow discharge theory in terms of dimensionless similarity criteria [25]:

$$\pi_1 = \{\exp[\pi_2\pi_5] - \exp[\pi_2(\pi_5 - 1)]\}\exp[-\pi_3]\exp[\pi_4\pi_5] \quad (16)$$

Analysis of Eq. (16) showed [25] that this expression can be somewhat simplified for some important individual cases. Thus, the presence of an excess of a supporting electrolyte ensures that $\psi_1 = 0$. In other words, the electric double layer will not influence on the electrochemical kinetics. Then we obtain $\pi_3 = \pi_4 = 0$ and Eq. (16) is transformed into the following form:

$$\pi_1 = \{\exp[\pi_2\pi_5] - \exp[\pi_2(\pi_5 - 1)]\} \quad (17)$$

Figure 1 shows the dependence plotted according to Eq. (17) for a wide range of π_2. One can see that the dependence ln π_1 *vs.* ln π_2 is changed into a straight-line function if $\pi_2 < 1$ (i.e., at small deviations from an equilibrium state). It is important that the slope of this linear section is equal to unity, irrespective of the value of π_5.

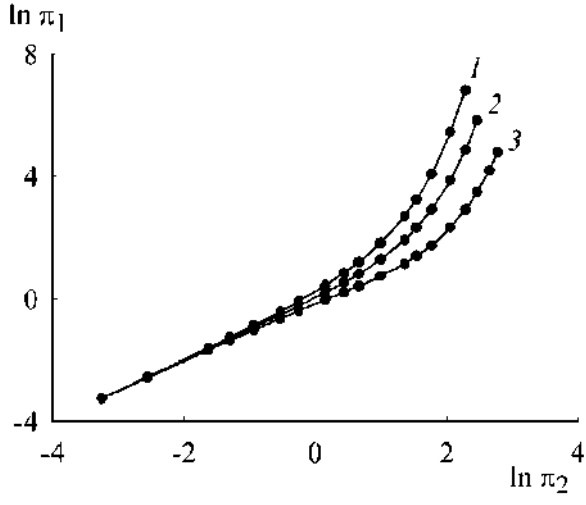

Figure 1. Dependences ln π1 vs. ln π2 at different values of π5: (1) 0.7, (2) 0.5, and (3) 0.3. (Reprinted from [25] by permission of Springer Nature, Copyright 2005).

When $\pi_2 > 1$ (at larger deviations from an equilibrium state), the dependence under consideration is curved and its location depends on the value of π_5. The higher the value of π_5, the greater is the value of π_1.

The presentation of the calculation data in terms of dimensionless complexes allows expressing the main idea of the slow discharge theory in a very clear and explicit form. Indeed, let us consider the case when the electric double layer has no effect on the rate of an electrochemical process (i.e., $\pi_3 = \pi_4 = 0$). Then the relative rate of the charge transfer (π_1) is equal to the dimensionless form of the electrode polarization (π_2) if $\pi_2 < 1$.

However, the value of π_1 increases proportionally to the exponent of the product $\pi_2 \cdot \pi_5$, provided that $\pi_2 > 1$.

It should be observed that the theory of slow discharge involves the concept developed by Butler and Volmer [28]. This model is considered empirical, and it cannot explain the effects of the features of molecular structures of the reagents and the medium as well as the nature of the electrode on the rate of the charge transfer. Meanwhile, the theory developed by Marcus [29] allows for all these effects. The Marcus theory is based on the idea of the energy of reorganization. The reorganization energy is an energy that is required to change the atomic configurations of the reacting molecules and their solvation shells into those typical of the equilibrium state of the products, provided the electron transfer had not happened [28, 29].

Chidsey further improved the Marcus theory and derived the following expression for the rate constant of an electrochemical reaction [28, 30]:

$$k_{red}^{MH} = k_0 e^{-(1/2)\theta} \frac{I(\theta,\Lambda)}{I(0,\Lambda)} \quad (18)$$

where $\theta = \frac{F(E-E^0)}{RT}$; E^0 is the standard electrode potential; k_0 is the standard rate constant (at $E = E^0$), $\Lambda = \frac{\lambda}{RT}$; λ is the reorganization energy; $I(\theta,\Lambda) = \int_{-\infty}^{\infty} \frac{\exp\left[-\frac{(\varepsilon-\theta)^2}{4\Lambda}\right]}{2\cosh\left[\frac{\varepsilon}{2}\right]} d\varepsilon$ is an improper integral which can be calculated only by means of numerical techniques.

Based on the concept developed by Chidsey, Protsenko and Danilov [27] obtained three following dimensionless complexes:

$$\pi_6 = \frac{F(E-E^0)}{RT} = \theta,\ \pi_7 = \Lambda = \frac{\lambda}{RT},\ \pi_8 = \frac{k_{red}^{MH}}{k_0} \quad (19)$$

The value π_6 characterizes the ratio between the electric work of the electron transfer and the thermal motion energy. This means that the similarity criterion π_6 is a dimensionless form of the electrode polarization (i.e., the driving force of an electrochemical process).

The value of π_7 reflects the ratio of the reorganization energy to the thermal motion energy. Evidently, this value is a reduced form of the reorganization energy.

Finally, the value π_8 shows the ratio between the rate constant at a given electrode potential and the rate constant at the standard electrode potential. Hence, this criterion exhibits the relative normalized rate of the charge transfer.

In terms of dimensional analysis, the electron transfer process, which is described by Eq. (18), should obey the following criterion equation [27]:

$$\pi_8 = f(\pi_6, \pi_7) \qquad (20)$$

The calculated data plotted as a 3D surface are shown in Figure 2. The following equation of correlation between dimensionless complexes π_6, π_7 and π_6 was reported [27]:

$$\ln \frac{k_{red}^{MH}}{k_0} = (1.33 + 0.2726\Lambda)\left(1 - e^{\left(\frac{2.0827}{3.989+\Lambda}\right)\theta}\right) \qquad (21)$$

The use of mathematical tools developed in dimensional analysis and similarity theory opens some new possibilities for the rational and simple interpretation of both experimental and theoretical results. Indeed, these methods allow decreasing the number of parameters and variables, which is very important when examining the performance of complex and multifactorial electrochemical systems.

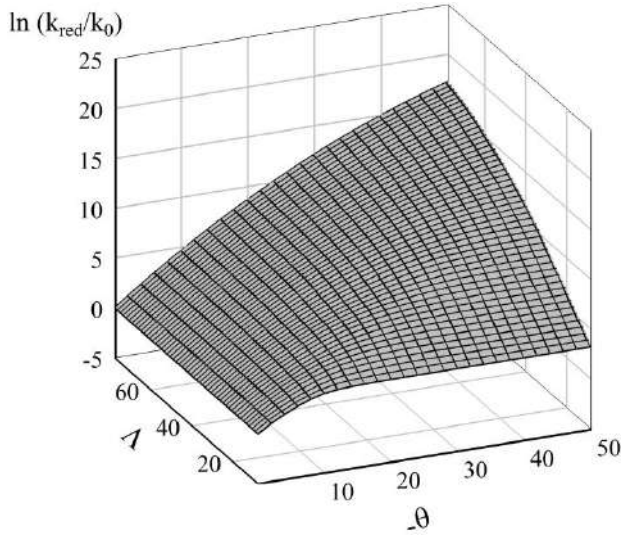

Figure 2. Plot in coordinates $\pi 8 = f(\pi 6, \pi 7)$. (Reprinted from [27], Copyright 2012, with permission from Elsevier).

In addition, the influence of various physical and physicochemical factors on the behavior of a system is reflected via dimensionless quantities in their combined interactions. As a result, internal relationships in the system appear clearer and more definite. This means that the mathematical formalism of dimensional analysis allows not only diminishing the number of values under consideration but also systematizing them rationally. For instance, the results reported in work [27] revealed that the effects of the reorganization energy and the thermal motion energy upon the rate of an electrochemical reaction should not be examined separately and independently but only in their mutual combination, which is reflected via the similarity criterion π_6.

It must be noted that any point in the 3D surface shown in Figure 2 corresponds to the infinity of different combinations of the parameters characterizing the charge transfer process (electrode overpotential, temperature, reorganization energy and the rate of the process). This indicates that the application of dimensional analysis and similarity theory enables considering generalized cases rather than the infinite number of individual special cases. Therefore, the mathematical treatment performed

by means of dimensional analysis imparts a generalized character to the interpretation of experimental and theoretical data.

DIMENSIONAL ANALYSIS OF ELECTROCHEMICAL PROCESSES INVOLVING CONSECUTIVE CHARGE TRANSFER

The advantages of dimensional analysis and similarity theory become especially apparent in the investigation of the performance of multistage electrochemical processes [7, 26].

Further, we will consider a consecutive electrochemical reaction of the following type [7]:

$$A \xrightarrow{+e^-} P \xrightarrow{+e^-} B \quad (22)$$

where *A*, *P* and *B* are the initial reactant, the intermediate and the target product, respectively.

Fick's law is valid for non-steady-state linear diffusion with respect to the species *A* and *P*:

$$\frac{\partial C_A}{\partial \tau} = D_A \frac{\partial^2 C_A}{\partial x^2}, \quad \frac{\partial C_P}{\partial \tau} = D_P \frac{\partial^2 C_P}{\partial x^2} \quad (23)$$

The initial and boundary conditions can be expressed in the following way:

$$\begin{aligned} &C_{A,\tau=0} = C_{A0}, \; C_{P,\tau=0} = C_{P0} \\ &D_A\left(\frac{\partial C_A}{\partial x}\right)_{x=0} = \frac{i_1}{F}, \; D_P\left(\frac{\partial C_P}{\partial x}\right)_{x=0} = \frac{i_2}{F} - \frac{i_1}{F} \\ &C_{A,x\to\infty} = C_{A0}, \; C_{P,x\to\infty} = C_{P0} \end{aligned} \quad (24)$$

where i_1 and i_2 are the current densities of the first and second stages in the reaction scheme (22), respectively.

The set of differential equations (23) can be solved together with the above initial and boundary conditions using common tabular integration [7]. However, the analysis of the obtained data involves difficulties since these formulae contain *fourteen* variables and parameters. The problem can be sufficiently simplified if the methods of dimensional analysis and similarity concept are used [7]. In this case, the number of the analyzed values is reduced and only *eight* following dimensionless complexes completely reflect the behavior of the electrochemical process under consideration:

$$X_1 = \frac{\tau\left(k_1^0\right)^2}{D_A},\ P_1 = \frac{D_P}{D_A},\ P_2 = \frac{k_2^0}{k_1^0},\ P_3 = \frac{C_{P0}}{C_{A0}}$$
$$\pi_9 = \frac{\alpha_1 F\left(E_1^0 - E\right)}{RT},\ \pi_{10} = \frac{\alpha_2 F\left(E_2^0 - E\right)}{RT} \quad (25)$$
$$Y_1 = \frac{i_1}{F k_1^0 C_{A0}},\ Y_2 = \frac{i_2}{i_1}$$

The dimensionless value X_1 involves current time (τ), thus being a dimensionless characteristic of time. The complex Y_1 is a dimensionless representation of the rate of an electrochemical reaction (i.e., the current density of the first stage in the consecutive process (22)). The dimensionless parameter Y_2 shows the ratio of the current density in the second stage of the reaction (22) to the current density in the first stage of the process involved, thus expressing the relationship between the rates of these stages.

As follows from the Buckingham's π theorem, the investigation of the consecutive electrochemical reaction (22) in terms of dimensional analysis and similarity theory implies the examination of *only two* criterion equations [7]:

$$Y_1 = f_1\left(X_1; P_1, P_2, P_3; \pi_9; \pi_{10}\right) \quad (26)$$
$$Y_2 = f_2\left(X_1; P_1, P_2, P_3; \pi_9; \pi_{10}\right) \quad (27)$$

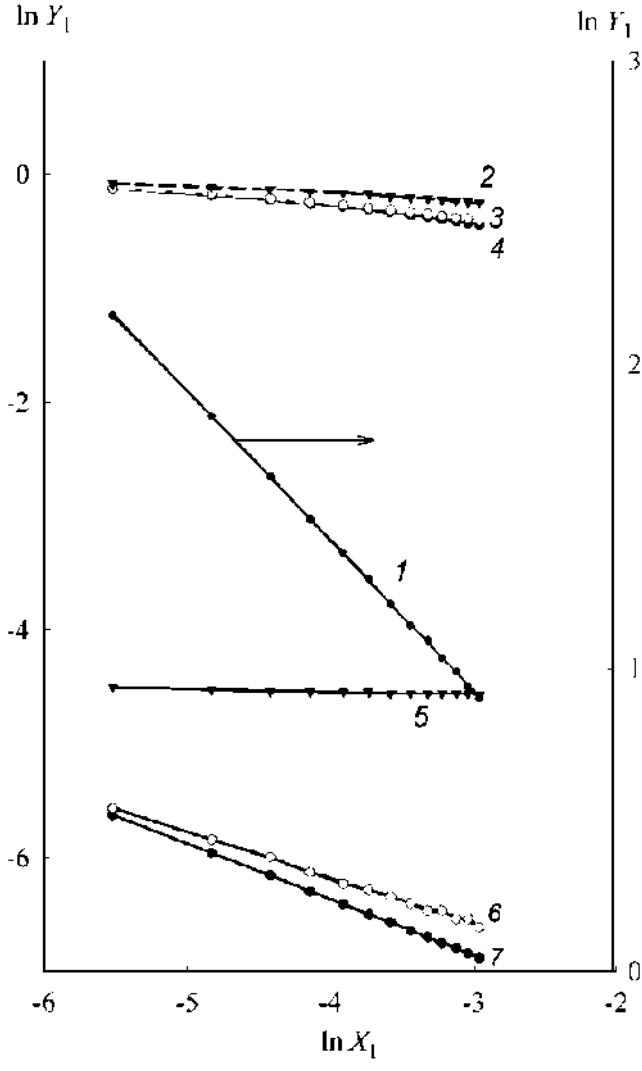

Figure 3. Plots of ln Y1 vs. ln X1. (P1 = 1, P2 = 1, P3 = 0). (1) π9 = 3.89, π10 = –3.89; 0; and 3.89; (2) π9 = 0, π10 = 3.89; (3) π9 = 0, π10 = 0; (4) π9 = 0, π10 = –3.89; (5) π9 = –3.89, π10 = 3.89; (6) π9 = –3.89, π10 = 0; (7) π9 = –3.89, π10 = –3.89. (Reprinted from [7] by permission of Springer Nature, Copyright 2005).

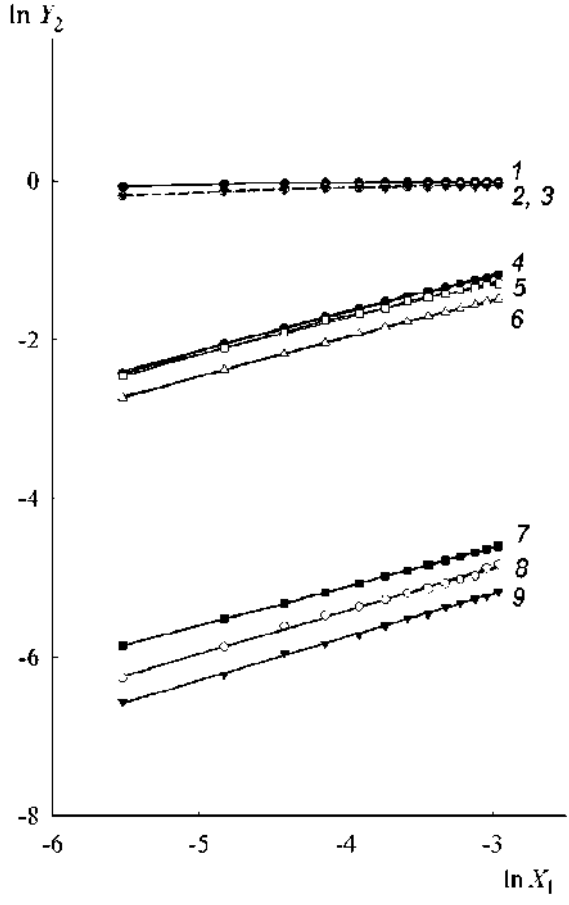

Figure 4. Plots of ln Y2 vs. ln X1. (P1 = 1, P2 = 1, P3 = 0). (1) π9 = 3.89, π10 = 3.89; (2) π9 = –3.89, π10 = 3.89; (3) π9 = 0, π10 = 3.89; (4) π9 = 3.89, π10 = 0; (5) π9 = –3.89, π10 = 0; (6) π9 = 0, π10 = 0; (7) π9 = –3.89, π10 = –3.89; (8) π9 = 3.89, π10 = –3.89; (9) π9 = 0, π10 = –3.89. (Reprinted from [7] by permission of Springer Nature, Copyright 2005).

A thorough investigation of the criterion functions (26) and (27) reveals a number of characteristic features of the electrochemical process (22) [7]. For instance, the obtained results suggest that an increase in the dimensionless polarization π_9 in the first stage of the reaction (22) leads to an increase in the value of Y_1. The value of Y_1 is affected by the changes in the dimensionless polarization π_{10} (i.e., in the driving force of the second

stage of the electrode process under study) only if the complex π_9 is negative (Figure 3). It is important that a quasi-steady-state diffusion mass transfer can be observed only if two following conditions are satisfied: $\pi_9 \leq 0$ and $\pi_{10} > 0$.

The plots Y_2 *vs.* X_1 in in the logarithmic coordinates show linear dependences (Figure 4). It is clear that the value of Y_2 gradually increases with time (i.e., with an increase in X_1) and tends to a limit $\lim_{X_1 \to \infty} Y_2 = 1$. The location and slope of the $\ln Y_2$ *vs.* $\ln X_1$ dependences are determined by the value of π_{10}; however, they are practically independent of the complex π_9.

In general, the examination of the criterion dependences reveals both the influence of different factors on the rate of individual stages in the consecutive electrochemical process (22) and the conditions that are required for the realization of a quasi-steady-state regime [7].

Protsenko et al. [31] reported the application of similarity theory and dimensional analysis to obtain a universal system of similarity criteria that characterize the kinetics of a metal electrodeposition process occurring on a rotating disc electrode. The developed model considers possible participation of some relatively stable intermediates in the course of an electrochemical reaction. Fourteen dimensionless complexes were derived and their physical meanings were discussed.

It was shown that a modified Reynolds number could be written in the following way:

$$Re = \frac{r^2 \omega}{\nu} \qquad (28)$$

where r is the radius of a disc electrode; $\omega = 2\pi f$ is the rotation electrode angular velocity (here $\pi = 3.14$ and f is the disc rotation velocity); and ν is the kinematic viscosity of an electrolyte.

In addition, a modified Stanton diffusion criterion was introduced to estimate the ratio between the flux of the initial reagent transferred by convection and the total mass transfer in the heterogeneous reaction:

$$St = \frac{C_1\sqrt{vf}}{i\varepsilon} \quad (29)$$

where C_1 is the concentration of the depositing metal ions; i is the current density on a rotating disc electrode; and ε is the electrochemical equivalent of the electrodeposited metal in an electrochemical reaction under consideration.

Evidently, any electrochemical reaction can be considered as a non-linear resistive element of an electrical circuit. To evaluate the behavior of such a resistive element, the following dimensionless complex was suggested:

$$\pi_{11} = \frac{\frac{\partial i}{\partial \eta}\cdot\eta}{i} = \frac{\partial \ln i}{\partial \ln \eta} = m \quad (30)$$

Here $\frac{\partial \eta}{\partial i}$ is the polarization resistance at the electrode/electrolyte interface. The value of $\frac{\partial \eta}{\partial i}$ varies with the electrode polarization (in other words, with the applied current density). If we conditionally accept that the relationship between the current density (i) and the electrode polarization (η) obeys the following simplified non-linear equation: $i = \text{const}\cdot\eta^m$ (where m is some dimensionless value that may depend on η), then we can conclude that the complex $\pi_{11} = m$ characterizes the degree of non-linearity of a given electrochemical reaction [31]. If $m = 1$, then the current density *vs.* polarization dependence is linear (for instance, when a deviation from the equilibrium is slight). It is clear that the value $m = 0$ corresponds to the limiting current density.

The developed mathematical model was successfully used for the interpretation of experimental data on the multistage process of chromium electroplating from oxalate and formate Cr(III) electrolytes on a rotating disc cathode [31]. It was stressed that the mathematical tools of dimensional analysis opens the way for an effective and theoretically grounded approach

to the planning of an electrochemical experiment and careful consideration of the obtained results.

DIMENSIONAL ANALYSIS IN APPLIED ELECTROCHEMISTRY

The dimensional analysis and similarity theory are fruitfully used in electrochemical engineering. Thus, Kreysa [32] reported the similarity criteria (the so-called “performance criteria” or “figures of merit”) which characterize the behavior of different electrochemical cells and processes with regard to technical and economic aspects. By way of illustration, only several criteria from those described in work [32] will be further considered.

1. *Current efficiency*. This value can be served as a "yield of charge" of any electrochemical reaction. The current efficiency is a dimensionless parameter that is written as follows:

$$CE = \frac{Q_i}{Q_\Sigma} \qquad (31)$$

where CE is the current efficiency; Q_i is the electric charge consumed in a given electrochemical reaction; and Q_Σ is the total electric charge passed through the electrode.

Obviously, current efficiency as an implicit similarity factor is very often used in pure and applied electrochemistry.

2. *Fractional conversion*. This value is determined by the following equation:

$$X = 1 - \frac{n}{n^0} \qquad (32)$$

where X is the fractional conversion; n^0 is the initial molar amount of a reagent; and n is the final molar amount of a reagent.

3. *Energy yield*. It characterizes the efficiency of energy consumption in an electrochemical reaction and is defined as:

$$\gamma = \frac{U_0 \cdot CE}{U_c} \quad (33)$$

where γ is the energy yield; U_0 is the reversible cell voltage; and U_C is the current cell voltage.

There are a number of some other studies that report the application of dimensional analysis to simulate different electrochemical systems, thereby effectively analyzing and optimizing their performance. Some examples include redox flow batteries [18], bioelectrochemical processes [19], metal electrodeposition processes [31], polymer electrolyte membranes for fuel cells [33], electromembrane reactors for recycling and resource recovery of flue gas desulfurization residuals [34], electrochemical pitting corrosion [35], transport-limited electrolysis in the electric-field-enhanced smelting and refining process (Fe/FeO system) [36], microelectrodes or microscale resistors for the use in microtechnique processes [37], and proton exchange membranes in fuel cells [38].

CONCLUSION

The data given in literature testify that dimensional analysis and similarity theory is a powerful tool for the simulation and characterization of various electrochemical processes and systems. Thus, the use of dimensional analysis in pure and applied electrochemistry offers the following main advantages:

1) There is a possibility to reduce the number of quantitative characteristics and parameters that are involved in analysis. This can appreciably simplify solving the problems.
2) The effects of various factors on the performance of the system under consideration are reflected in their close interactions. Therefore, the quantitative relationships become more definite and informative.
3) The methods of dimensional analysis and similarity theory can be used to assess the performance of new electrochemical systems and processes based on the features of the existing similar ones.
4) The use of dimensional analysis and similarity theory imparts a generalized character to the investigation and designing, because analysis is carried out not for some individual cases but for an infinite number of the combinations of various numerical characteristics of an electrochemical system.

REFERENCES

[1] Bachmann, K. J. and Bertocci, U. (1970). Metal/metal-ion electrodes with two charge-transfer steps: Me/Me^{z+} and $Me^{z+}/Me^{(z+1)+}$. Potentiostatic transients under charge-transfer and diffusion control. *Electrochimica Acta*, 15 (12): 1877-1886.

[2] Harrington, D. A. (1998). Electrochemical impedance of multistep mechanisms: a general theory. *Journal of Electroanalytical Chemistry*, 449: 9-28.

[3] Batchelor-McAuley, C. and Compton, R. G. (2012). Voltammetry of multi-electron electrode processes of organic species. *Journal of Electroanalytical Chemistry*, 669: 73-81.

[4] Klymenko, O., Svir, I. and Amatore, C. (2010). Theoretical study of the EE reaction mechanism with comproportionation and different diffusivities of reactants. *Electrochemistry Communications*, 12: 1378-1382.

[5] Danilov, F. I. and Protsenko, V. S. (2004). Multistage electrochemical reactions with the transfer of intermediates between near-electrode layer and bulk solution: Analysis of a kinetic model and computer-aided modeling. *Russian Journal of Electrochemistry*, 40 (1): 1-8.

[6] Danilov, F. I. and Protsenko, V. S. (2004). Multistage electrochemical reactions with the transfer of intermediates between the near-electrode layer and the bulk solution: The accumulation of the intermediates and the current redistribution between the stages during electrolysis. *Russian Journal of Electrochemistry*, 40 (4): 456-459.

[7] Protsenko, V. S. and Danilov, F. I. (2005). Multistep electrochemical reactions involving transport of intermediates between the near-electrode layer and the bulk solution: The kinetics of two-step processes in conditions of non-steady-state diffusion. *Russian Journal of Electrochemistry*, 41 (12): 1274-1281.

[8] Gukhman, A. A. (1973). *Vvedenie v teoriyu podobiya* [Theory of similarity: an introduction]. Vysshaya Shkola, Moscow.

[9] Lira, I. (2013). Dimensional analysis made simple. *European Journal of Physics*, 34: 1391-1401.

[10] D'yakonov, G. K. (1956). *Voprosy teorii podobiya v oblasti phiziko-khimicheskikh protsessov* [Issues of similarity theory in the field of physico-chemical processes]. AN USSR, Moscow.

[11] Protsenko, V. S. (2014). Application of dimensional analysis and similarity theory in electrochemistry: a review. *Voprosy Khimii i Khimicheskoi Tekhnologii*, (3): 5-15.

[12] Popov, K. I., Djokić, S. S., and Grgur, B. N. *Fundamental Aspects of Electrometallurgy*. Boston: Springer, 2002.

[13] Wagner, C. (1951). Theoretical analysis of the current density distribution in electrolytic cells. *Journal of the Electrochemical Society*, 98 (3): 116-128.

[14] Stanković, V. (2012). Electrochemical engineering – its appearance, evolution and present status. Approaching an anniversary. *Journal of Electrochemical Science and Engineering*, 2 (2): 53-66.

[15] Kim, K. R., Kim, S. K., Kim, J. G., and Nam, H. O. (2018). CFD approach to Wagner number estimation for a current distribution

uniformity in a rotating cylinder Hull cell. *International Journal of Electrochemical Science*, 13: 8686-8693.

[16] Stricker, E. A., Ke, X., Wainright, J. S., Unocic, R. R. and Savinell, R. F. (2019). Current density distribution in electrochemical cells with small cell heights and coplanar thin electrodes as used in ec-S/TEM cell geometries. *Journal of the Electrochemical Society*, 166 (4): H126-H134.

[17] Deconinck, J., Maggetto, G. and Vereecken, J. (1985). Calculation of current distribution and electrode shape change by the boundary element method. *Journal of the Electrochemical Society*, 132 (12): 2960-2965.

[18] Kapoor, M., Gautam, R. K., Ramani, V. K. and Verma, A. (2020). Predicting operational capacity of redox flow battery using a generalized empirical correlation derived from dimensional analysis. *Chemical Engineering Journal*, 379: 122300.

[19] Enzmann, F., Mayer, F., Stöckl, M., Mangold, K. M., Hommel, R. and Holtmann, D. (2019). Transferring bioelectrochemical processes from H-cells to a scalable bubble column reactor. *Chemical Engineering Science*, 193: 133-143.

[20] Ibl, N. (1959). The use of dimensionless groups in electrochemistry. *Electrochimica Acta*, 1 (2-3): 117-129.

[21] Buckingham, E. (1915). The principle of similitude [1]. *Nature*, 96 (2406): 396-397.

[22] Gibbings, J. C. and Hignett, E. T. (1966). Dimensional analysis of electrostatic streaming current. *Electrochimica Acta*, 11 (7): 815-826.

[23] Gibbings, J. C. (1967). Non-dimensional groups describing electrostatic charging in moving fluids. *Electrochimica Acta*, 12 (1): 106-110.

[24] Klinkenberg, A. (1967). On the electric streaming current. *Electrochimica Acta*, 12 (1): 104-105.

[25] Protsenko, V. S. and Danilov, F. I. (2005). Theory of generalized variables in electrochemical kinetics: Simulation of the slow discharge theory equations. *Russian Journal of Electrochemistry*, 41 (1): 104-107.

[26] Protsenko, V. S. and Danilov, F. I. (2005). Multistep electrochemical reactions involving transport of intermediates between the near-electrode layer and the bulk solution: A kinetics analysis based on theory of generalized variables (theory of similarity). *Russian Journal of Electrochemistry*, 41 (1):108-112.

[27] Protsenko, V. S. and Danilov, F. I. (2012). Application of dimensional analysis and similarity theory for simulation of electrode kinetics described by the Marcus-Hush-Chidsey formalism. *Journal of Electroanalytical Chemistry*, 669: 50-54.

[28] Henstridge, M. C., Laborda, E., Rees, N. V. and Compton, R. G. (2011). Marcus-Hush-Chidsey theory of electron transfer applied to voltammetry: A review. *Electrochimica Acta*, 84: 12-20.

[29] Marcus, R. A. (1956). On the theory of oxidation-reduction reactions involving electron transfer. I. *Journal of Chemical Physics*, 24 (5): 966-979.

[30] Chidsey, C. E. D. (1991). Free energy and temperature dependence of electron transfer at the metal–electrolyte interface. *Science*, 215: 919-922.

[31] Protsenko, V. S., Butyrina, T. E. and Danilov, F. I. (2007). Applying a theory of generalized variables to electrochemical kinetics: Interpreting the results of studying chromium deposition from Cr(III) baths. *Protection of Metals*, 43 (4): 398-406.

[32] Kreysa, G. (1985). Performance criteria and nomenclature in electrochemical engineering. *Journal of Applied Electrochemistry*, 15: 175-179.

[33] Chevalier, S., Josset, C. and Auvity, B. (2018). Analytical solutions and dimensional analysis of pseudo 2D current density distribution model in PEM fuel cells. *Renewable Energy*, 125: 738-746.

[34] Yang, C., Cao, L. and Yang, J. (2018). Dimensional analysis of an electromembrane reactor for recycling and resource recovery of flue gas desulfurization residuals. *Environmental Engineering Science*, 35 (2): 76-87.

[35] Shi, Y. Y., Zhang, Z., Cao, F. H. and Zhang, J. Q. (2008). Dimensional analysis applied to pitting corrosion measurements. *Electrochimica Acta*, 53 (6): 2688-2698.

[36] Pongsaksawad, W., Powell, A. C. and Dussault, D. (2007). Phase-field modeling of transport-limited electrolysis in solid and liquid states. *Journal of the Electrochemical Society*, 154 (6): F122-F133.

[37] Duchanoy, C. and Lapicque, F. (2000). Similarity approach for the measurement of local current density on micropatterned electrodes. *Journal of the Electrochemical Society*, 147 (9): 3401-3405.

[38] Russo, L., Sorrentino, M., Polverino, P. and Pianese, C. (2017). Application of Buckingham π theorem for scaling-up oriented fast modelling of proton exchange membrane fuel cell impedance. *Journal of Power Sources*, 353: 277-286.

BIOGRAPHICAL SKETCH

Vyacheslav Protsenko

Affiliation: Ukrainian State University of Chemical Technology

Education:

- Nov 1994 – Oct 1997 – Ukrainian State University of Chemical Technology
- Postgraduate course, electrochemistry (Dnipropetrovsk, Ukraine)
- Sep 1989 – Jun 1994 – Ukrainian State University of Chemical Technology
- Specialist (equivalent to Master's degree), electrochemistry (Dnipropetrovsk, Ukraine)

Business Address: Ukrainian State University of Chemical Technology, Gagarin Ave., 8, Dnipro, 49005 Ukraine

Research and Professional Experience:

Research activity is focused on the following main topic:

I. electrodeposition and characterization of various metals, alloys and composites (trivalent chromium electroplating, iron, nickel, tin, lead electrodeposition, electrodeposited composites containing dispersed particles of titania, zirconia etc.);
II. electrodeposition of coatings using deep eutectic solvents (DES, a new type of ionic liquids);
III. electrodeposition and characterization of electrocatalytic (hydrogen evolution reaction, HER, and oxygen evolution reaction, OER, for hydrogen energy) and photocatalytic coatings (organic pollutants degradation for wastewater treatment);
IV. kinetics and mechanism of stepwise electrochemical reactions with the participation of intermediates (theory, mathematical models, and simulation)

Professional Appointments:

- Feb 2014 – present – Professor (Full), Ukrainian State University of Chemical Technology, Department of Physical Chemistry (Dnipro, Ukraine)
- Nov 1997 – Jan 2014 – Associate Professor, Ukrainian State University of Chemical Technology, Department of Physical Chemistry (Dnipropetrovsk, Ukraine)

Honors:

State Prize of Ukraine in the field of science and technology.

It is the highest state Ukrainian award in the field of science and technology that is awarded according to the decree of the President of Ukraine.

Publications from the Last 3 Years:

1) Protsenko, V. S., Vasil'eva, E. A., Tsurkan, A. V., Kityk, A. A., Korniy, S. A. and Danilov, F. I. (2017). Fe/TiO_2 composite coatings modified by ceria layer: Electrochemical synthesis using environmentally friendly methanesulfonate electrolytes and application as photocatalysts for organic dyes degradation. *Journal of Environmental Chemical Engineering*. 5: 136-146.
2) Protsenko, V. S., Bobrova, L. S. and Danilov, F. I. (2017). Physicochemical properties of ionic liquid mixtures containing choline chloride, chromium (III) chloride and water: effects of temperature and water content. *Ionics*. 23 (3): 637-643.
3) Kityk, A. A., Shaiderov, D. A., Vasil'eva, E. A., Protsenko, V. S. and Danilov, F. I. (2017). Choline chloride based ionic liquids containing nickel chloride: Physicochemical properties and kinetics of Ni(II) electroreduction. *Electrochimica Acta*. 245: 133-145.
4) Protsenko, V. S., Vasil'eva, E. A., Tsurkan, A. V. and Danilov F.I. Electrodeposition of electrocatalytic and photocatalytic Fe/TiO_2 composite coatings using methanesulfonate electrolytes. In: *Electrospinning and electroplating: Fundamentals, methods and applications*. Edited by Toby Jacobs. Chapter 6. 177-226. New York: Nova Science Publishers, Inc. 2017.
5) Protsenko, V. S., Kityk, A. A., Bobrova, L. S., Shaiderov, D. A. and Danilov, F.I. Physicochemical and electrochemical properties of deep eutectic solvents containing dissolved Ni(II) and Cr(III) salts: The effects of water content. In: *Ionic liquids: Electrochemistry, uses and challenges*. – Edired by Bình Xuân. Chapter 1. 1-34. New York: Nova Science Publishers, Inc. 2017.
6) Danilov, F. I., Protsenko, V. S., Kityk, A. A., Shaiderov, D. A., Vasil'eva, E. A., Pramod Kumar, U., Joseph Kennady, C. (2017). Electrodeposition of nanocrystalline nickel coatings from a deep eutectic solvent with water addition. *Protection of Metals and Physical Chemistry of Surfaces*. 53 (6): 1131-1138.

7) Protsenko, V. S., Tsurkan, A. V., Vasil'eva, E. A., Baskevich, A. S., Korniy, S. A., Cheipesh, T. O. and Danilov, F. I. (2018). Fabrication and characterization of multifunctional Fe/TiO_2 composite coatings. *Materials Research Bulletin*. 100: 32-41.
8) Protsenko, V. S., Bobrova, L. S., Baskevich, A. S., Korniy, S. A. and Danilov, F. I. (2018). Electrodeposition of chromium coatings from a choline chloride based ionic liquid with the addition of water. *Journal of Chemical Technology and Metallurgy*. 53: 906-915.
9) Protsenko, V., Bobrova, L. and Danilov, F. (2018). Trivalent chromium electrodeposition using a deep eutectic solvent. *Anti-Corrosion Methods and Materials*. 65 (5): 499-505.
10) Protsenko, V. S., Bobrova, L. S., Korniy, S. A., Kityk, A. A. and Danilov, F. I. (2018). Corrosion resistance and protective properties of chromium coatings electrodeposited from an electrolyte based on deep eutectic solvent. *Functional Materials*. 25 (3): 539-545.
11) Protsenko, V. S., Bobrova, L. S., Golubtsov, D. E., Korniy, S. A. and Danilov, F. I. (2018). Electrolytic deposition of hard chromium coatings from electrolyte based on deep eutectic solvent. *Russian Journal of Applied Chemistry*. 91 (7): 1106-1111.
12) Protsenko, V. S., Bobrova, L. S., Butyrina, T. E. and Danilov, F. I. (2019). Hydrogen evolution reaction on Cr–C electrocatalysts electrodeposited from a choline chloride based trivalent chromium plating bath. *Vorposy Khimii i Khimicheskoi Tekhnologii*. (1): 61-66.
13) Rublova, Y. D., Kityk, A. A., Bannyk, N. G., Protsenko, V. S. and Danilov, F. I. (2019). The influence of various factors on corrosion of mild steel in deep eutectic solvents. *Materials Today: Proceedings*. 6: 232-236.
14) Protsenko, V. S., Kityk, A. A., Vasil'eva, E. A., Tsurkan, A. V. and Danilov, F. I. Electrodeposition of composite coatings as a method for immobilizing TiO_2 photocatalyst. In: *Nanophotocatalysis and environmental applications. Environmental chemistry for a sustainable world*. Edited by Inamuddin, Sharma, G., Kumar, A., Lichtfouse, E. and Asiri A. 29: 263-301. Springer Nature Switzerland AG. 2019.

15) Danilov, F. I., Kityk, A. A., Shaiderov, D. A., Bogdanov, D. A., Korniy, S. A. and Protsenko, V. S. (2019). Electrodeposition of Ni–TiO_2 composite coatings using electrolyte based on a deep eutectic solvent. *Surface Engineering and Applied Electrochemistry*. 55 (2): 138-149.
16) Kityk, A. A., Protsenko, V. S., Danilov, F. I., Kun, O. V. and Korniy, S. A. (2019). Electropolishing of aluminium in a deep eutectic solvent. *Surface and Coatings Technology*. 375: 143-149.
17) Protsenko, V. S., Bogdanov, D. A., Korniy, S. A., Kityk, A. A., Baskevich, A. S. and Danilov, F. I. (2019). Application of a deep eutectic solvent to prepare nanocrystalline Ni and Ni/TiO_2 coatings as electrocatalysts for the hydrogen evolution reaction. *International Journal of Hydrogen Energy*. 44 (45): 24604-24616.

In: Advances in Chemistry Research ISBN: 978-1-53617-112-9
Editor: James C. Taylor

Chapter 5

MICRO EXTRACTION: AN ECOCOMPATIBLE EXTRACTION TECHNIQUE

Pratik Kumar Jagtap, PhD
Department of Chemistry, Kalinga University,
Nawa Raipur, Chhattisgarh, India

ABSTRACT

Sample pretreatment involving extraction, pre-concentration and clean-up has become a bottleneck in the method development and sample analysis. Thus in this chapter we focus on various solvent-minimized sample pre-treatment procedure which are inexpensive and since a very little solvent is used in these techniques, there is minimal exposure to toxic organic solvents during sample analysis. A comparative discussion on the various advantages and limitations of each technique has also been discussed. Emphasis has been towards the selection of a method which can be used for routine analysis of drugs or environmental pollutants based on recent analytical techniques such as HPLC and GC. The effects of several variables on the method performance has been also detailed the technique of Microextraction has several advantages over traditional methods such as simple operation, miniaturization of technique and minimization of organic solvents used in sample preparation. These techniques are rapid,

sensitive and virtually solvent free. Motive is towards selection of a green sample preparation techniques over traditional extraction methods in routine laboratory.

INTRODUCTION

Sample pretreatment involving extraction, pre-concentration and clean-up has become a bottleneck in the method development and sample analysis because most of the analytical instruments cannot directly handle the sample matrix [1-4] (S.Pedersen et al. 2000), (A. Khraiwesh et al. 2011), (B. N. Patel et al. 2011) and (C. Frahnert et al. 2003) also, sample preparation prior to instrumental analysis of biological samples is required to improve the sensitivity and specificity of the assay by removing majority of interference while concentrating analytes. Thus, sample preparation aims at reducing and eliminating the interferences originally present in the sample to facilitate their determination even at low concentrations. Clinical monitoring of therapeutic drugs is achieved using immunoassay methods but this method can be sometimes problematic such as for antidepressant drugs because of their cross-reactivity and thus creating complications when monitoring patients treated with more than one such drugs at a time and also during transition between medication periods [5, 6] (A. S. Yasdi and A. Amiri 2010), (Y. He and H. K. Lee 1997). Current analytical sample pretreatment methods are dependent on procedures which are fast, simple, inexpensive, requires little solvent and produces little waste thus leading to minimization of organic solvents and simplification of the technique. Various sample pretreatment methods or, extraction methods available today are Head space solid phase micro-extraction (HS-SDME), liquid phase micro-extraction (LPME), single drop micro-extraction (SDME) and liquid-liquid micro-extraction (LLME) etc.

TYPES OF SAMPLE PREPARATION TECHNIQUES

Liquid-Liquid Extraction (LLE)/Liquid Phase Micro-Extraction (LPME)

It is one of the oldest sample preparation method and has the advantages of simplicity, acceptable extraction efficiency and extensive sample clean-up for human plasma samples but this technique is at the same time tedious and time consuming and leads to cross-talks with compounds which produces fragments with similar masses in Liquid chromatography-mass spectroscopy (LC-MS). Recent research trends involve miniaturization of the traditional liquid-liquid extraction (LLE) principle by greatly reducing the acceptor-to-donor phase ratio as in the case of LPME which reduces the analyte enrichment problems of LLE from small biological samples and also eliminates the compatibility problems with different analytical instruments like capillary electrophoresis (CE) [7, 8] (J. Zhang et al. 2005) and (J. F. Liu et al. 2003), gas chromatography (GC) and high performance liquid chromatography (HPLC). Here a few micro-litre (µL) of solvents are used, has minimal exposure to toxic organic solvents and produces minimal wastes, also this method combines extraction, enrichment, clean-up and sample introduction into a single step prior to chromatographic process, however there is no information currently available on LPME of highly hydrophobic drugs. Various LPME techniques can be effectively utilized for extraction of target analytes from various sample solutions. In LPME target analytes are separated and pre-concentrated into micro-amount of organic solvents from sample solution, the principle involves the distribution of analyte between extracting solvent (acceptor-phase) and aqueous phase (donar phase). The main advantage of miniaturized techniques are their high efficiency and environment friendly operation because of use of minimal solvents.

CLASSIFICATION OF LPME

- Single drop micro-extraction (SDME):

It was developed as a solvent-minimized sample pre-treatment procedure which is inexpensive and since a very little solvent is used there is minimal exposure to toxic organic solvents, also no preconditioning is required unlike SPME. They are of basically two types:

  - Headspace SDME
  - Direct immersion SDME

- Hollow fiber liquid phase micro-extraction (HF-LPME):
- Dispersive liquid –liquid micro-extraction (DLLME):

Single Drop Micro-Extraction (SDME)

Head Space Hanging-Drop Micro-Extraction (HS-HDME)

Here a micro-drop of a water immiscible organic solvent with a fixed amount of internal standard is left suspended at the end of a Teflon rod as suggested by Jeannot and Cantwell or, directly in a micro-syringe. Dasgupta and liu [9-11] (Y. He at al. 2007), (A. Sarafraz et al. 2007) and (M. A. Jeannot et al. 2010) were the first to introduce this technique where the micro-syringe is pre-rinsed more than 10 times with the same solvent and is immersed in a stirred aqueous solution containing solvent to extract volatile analytes. Here the analytes are distributed among three phases (water sample, head space and the organic drop). After extraction the organic phase is retracted back into the syringe and is injected into a detector system for further analysis.

HS-SDME has the advantage of being suitable for a wider varities of solvents to choose from [12] (H. Chen et al. 2007) which also enhances the

range of extractable analytes. There are two modes of LPME procedures known a). Static LPME b). Dynamic LPME

In case of Dynamic LPME as suggested by He and Lee extraction occurs in the thin organic film formed in the micro-syringe needle and barrel, by withdrawing aqueous sample into a micro-syringe already containing solvent [13] (D. A. Lambrropoulou 2004). The aqueous phase is then pushed out of the syringe and process is repeated several times for better extraction, finally the remaining solvent is injected into the detector for further analysis. Dynamic LPME provides higher enrichment within a short interval of time.

Zhang et al. introduced a modified environmental friendly techniques of head space water based LPME which used water instead of high boiling organic solvents for the extraction of analytes, and is thus totally free from the use of organic solvents [14] (L. Xu et al. 2007).

Liu et al. used ionic liquids (ILs) as extraction solvents due to their low vapor pressure, high boiling point, high viscosity, good thermal stability and miscibility with water and organic solvents but suffers the disadvantage of blocking the GC columns because of its high viscosity. This process basically uses water immiscible solvents for the analysis of the extracts [15] (M.A. Jeannot et al. 2010).

Also SDME is more suited for the volatile and semi-volatile analytes which are of more hydrophobic nature thus necessitating the use of immiscible extracting solvents and thus disqualifying the use of HPLC from being considered for analysis. Moreover HPLC required an additional step of solvent exchange and also limits the choice of solvents.

HS-SDME is similar to traditional headspace sampling in which volatiles are sampled from the vapors above the sample thus, avoiding interferences from the sample matrix. An alternative technique HS- SPME, has the further advantage of improved directivity, which results from the use of a coated fiber chosen for its selectivity for the analyte. In HS-SDME, the fiber used in SPME is replaced by a liquid micro-drop that can also be chosen for its selectivity as shown in Figure 1. (http://www.chromacademy.com/lms/sco61/images/P1-figure-1.jpg).

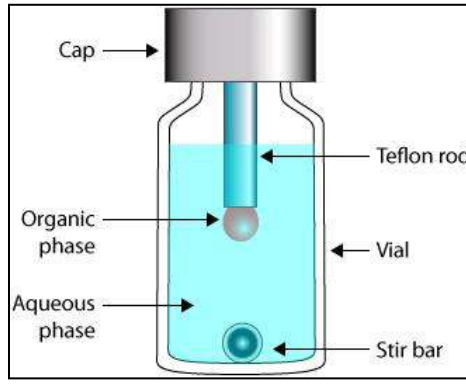

Figure 1. A µL droplet of extracting solvent on the tip of a microsyringe.

The International Conference on Harmonization (ICH), formed in 1997 to create worldwide uniformity of policy in the pharmaceutical industry, identified fourclasses of residual solvents that must be monitored in pharmaceutical formulations.Class 1 solvents have unacceptable toxicity and are to be avoided during Pharmaceutical manufacture. They are not routinely analysed, although confirmation of their absence could be part of the development process. Class 2 solvents are less toxic, Class 3 are of lower risk to human health, and Class 4 solvents are those for which no adequate toxicological data were found. These last three classes of solvents are the ones most commonly analysed. Parameters that have been considered for SDME include the following: size of drop; shape of needle tip; temperature of sampling; equilibration time; sampling (extraction) time; effect of stirring and ratio of headspace volume to sample volume Figure 2 (http://www.chromacademy.com/lms/sco61/images/P2-figure-2.jpg).

The parameters influencing the HSME procedure, including the nature of solvent used as extractant, stirring speed, volume of the micro-drop, temperature of bulk analyte solution and micro-drop, volume of analyte solution, extraction time, and the ionic strength and pH of analyte solution. There is no need for a delicate and expensive apparatus for the proposed method. Water based solvents can also be used for amphetamines and methamphetamines [16] (K. Shrivas and H. F. Wu 2007).

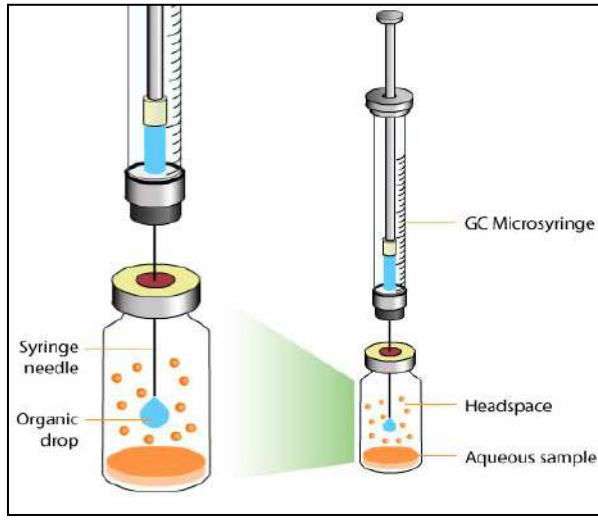

Figure 2. Schematic diagram of the HSME apparatus.

Although the precision and accuracy are still not ideal, the extreme simplicity and cost effectiveness of HSME make it quite attractive when compared with the SPME and other labor intensive methods such as LLE or, solid-phase extraction (SPE). Two basic TCAs amitryptyline and nortryptyline were extracted from 2.5 ml of aqueous sample, adjusted to pH 12 into 10 µL of toluene and delivered to the vortex of the stirred sample solution, finally after certain time a portion of the extract was withdrawn and injected into GC-FID (gas chromatography-flame ionization detection) [17] (J. M. Kokosa et al. 2009).

Direct Immersion SDME

In DI-SDME, a drop of a water-immiscible solvent is suspended directly from the tip of a micro syringe needle immersed in the aqueous sample, here, the needle of a 10µL syringe containing 1-5 µL of water immiscible organic solvent is penetrated through the septum of the vial until the tip reaches the level below the surface of the sample solution as shown in Figure 3 (http://pubs.rsc.org/services/images/RSCpubs.ePlatform.Service.FreeContent.ImageService.svc/ImageService/Articleimage/2013/AY/c2ay26560e/c2ay26560e-f1.gif).

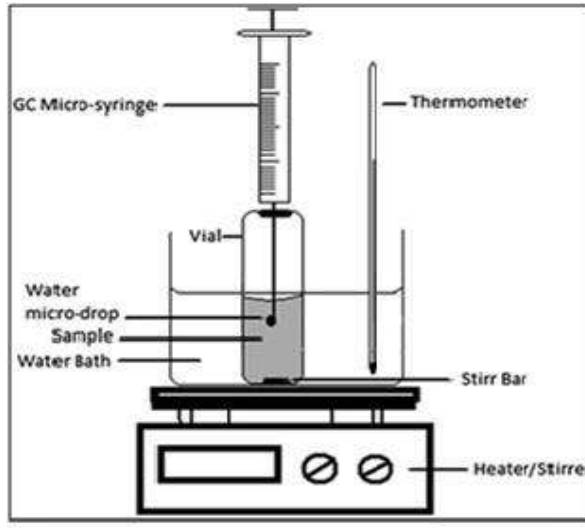

Figure 3. Diagram for DI-SDME.

The plunger of the syringe is pushed to cause the solvent to form a drop inside the sample solution, once the equilibrium is reached the drop is retracted back into the syringe and subjected to further instrumental analysis. Agitation of the sample reduces the time required to attain the equilibrium and hence better extraction can be achieved [18] (C. Yao et al. 2009) however stirring at higher speed causes formation of air bubbles and solvent drop dislodgement and is generally not recommended in this method, [19, 20] (L. Vidal et al. 2010) and (C. D. Stalikas and Y. C. Fiamegos 2008). Extraction increases with drop volume but usually 1-3 µL solvent drop is used because larger drops are more prone to fall and also it increases the time required to attain equilibrium, although diffusion coefficient increases with temperature and equilibrium is attained faster but sometimes leads to drop dissolution and hence the time of extraction must be properly optimized, this method is applicable to only liquid samples containing non-polar or, moderately polar analytes and makes use of water immiscible organic solvents thus GC is the accepted method for final analysis [21, 22] (L. Xu et al. 2009) and (A. A. Nuhu et al. 2011). Use of methyl tri-Octyl ammonium chloride and SDME in the analysis of amitryptyline, nortryptyline, quinine, imipramine and trimerazine salts in human urine has

also been reported [23] (R. Sekar and H. F. Wu 2006). Derivatization using DI-SDME has been used to enhance extraction, chromatographic separation and detection of analytes providing higher extraction recoveries and excellent sample clean up in short possible time. DI-SDME along with GC-FID has been used to detect amitryptyline and nortriptyline in urine and plasma samples using 1μL of iso-octane as extracting solvent. For DI-SDME ionic liquids have been proposed as alternative to organic solution due to low vapor pressure and high viscosity and final analysis by HPLC [24, 25] (T.G. Halvorsen et al. 2001) and (S. Pedersen et al. 1999). Here we conclude that the agitation of sample enhances mass transfer and hence its extraction efficiency. Derivatization along with DI-SDME has been used to improve extraction, chromatographic separation and detection of analytes [26-28] (K. E. Rasmussen et al. 2004), (K. Tapadia et al. 2011) and (A. Jain and K. K. Verma 2011) also direct combination of DI-SDME with MS without using chromatographic separation is suitable with AP-MALDI-MS for drugs [29] (Y. C. Fiamgos and C. D. Stalikas 2007).

Hollow Fiber Liquid Phase Micro-Extraction (HF-LPME)

Pedersen-Bjergaard and Rasmussen introduced HF-LPME [30] (H. Kataoka 2010) technique which uses a supported liquid membrane such as polypropylene hollow fiber membrane. It is used as a sample preparation technique with the objective to isolate and concentrate the analytes of interest such as drugs and their metabolites from biological samples such as urine, blood and hair for their analytical quantitation. Before its first use, all SPME fibers were re-conditioned in order to remove contaminants by warming in the heated injection port of a gas chromatograph at a particular temperature for specific time interval. All extractions were performed in 10 ml glass vials sealed with PTFE (poly tetrafluroethylene) faced septum caps. Prior to extraction, the analysed sample (0.5 g) was transferred into the sampling vial and preheated at the extraction temperature for some 10-20 min. The appropriate SPME fiber 50/30 μm DVB (di-vinyl benzene) /CAR (carboxene) /PDMS (poly di-methyl siloxane) was exposed to the headspace

above the dried sample. After preliminary optimization experiments, the exposure time and temperature were selected as the suitable extraction conditions. After extraction, the SPME fiber was removed from the sample vial and immediately inserted into the GC injection port where the thermal desorption was carried out.

HF-LPME is performed directly on a PDMS/DVB coated fiber with appropriate stirring rate, pH and temperature adjustments, then the drug desorption is carried out by exposing the fiber to mobile phase using lab-made SPME-LC interface and for chromatographic analysis RP-18 columns can be used.

RESULTS AND DISCUSSION

The major extraction parameters that significantly control the extraction of analyte from the sample solution into the acceptor phase include the selection of organic solvent, extraction time, exposure volume of solvent, pH and salt concentration. Therefore these parameters were optimized. Extraction efficiency of the antidepressants from sample solution was evaluated from average peak area of three successive GC injections.

The disposable nature of hollow fiber eliminates the possibility of sample carry over and ensures high reproducibility and the small pore size prevents the large molecules present in the donar phase and particles from entering into the acceptor phase leading to very clean extracts. HF-LPME has been found to be very useful for extracting drugs and analytes from biological matrices with simultaneous clean up of the extracts. HF-LPME of citalopram and its metabolite N-desmethylcitalopram has been reported [31] (K. Shrivas and H. F. Wu 2007) and has the advantage of high sample clean up because salts, proteins and majority of endogenic substances were unable to penetrate the hexyl ether layer and the aqueous extracts can be directly injected to CE instrument and this has also shown the possibility of LPME of hydrophobic drugs prior to CE.

Hollow Fiber Drop to Drop Microextraction: (HF-DDME)

It is a simple, effective and virtually solvent free sample preparation technique and indicated to be a good alternative for traditional LLE, it makes use of a micro-syringe (usually 10 micrometer volume) with blunt tip and porous polypropylene hollow fiber containing extracting solvent for extraction and pre-concentration of ADs from sample solution [32, 33] (K. Shrivas and D. K. Patel 2011) and (K. Agrawal and H. F. Wu 2007).

Here a segment of hollow fiber usually of 1.0 cm is cut and one end of it is heat sealed using hot nipper to prevent the flow of solvent from it, the fiber is sonicated using acetone to remove contaminants from fiber and solvent is finally allowed to evaporate completely. Then the micro-syringe is filled with appropriate amount of organic acceptor phase and was inserted into the hollow fiber followed by introduction of acceptor phase into the hollow fiber for separation and pre-concentration of analyte from the samples Figure 4 (http://pubs.rsc.org/services/images/RSCpubs.ePlatform.Service.FreeContent.ImageService.svc/ImageService/Articleimage/2013/AY/c2ay26560e/c2ay26560e-f1.gif).

Finally the enriched acceptor phase with analytes was withdrawn from hollow fiber and it was discarded, this drug enriched acceptor phase was then used for further analytical procedure of AD.

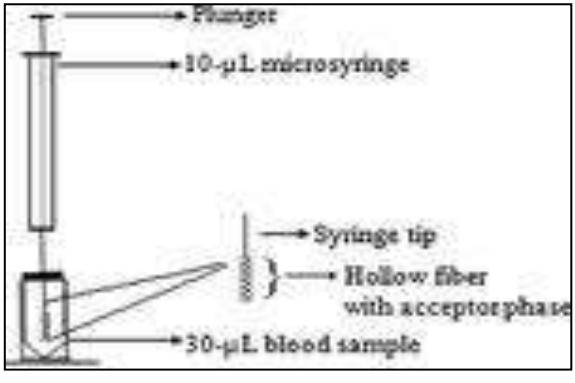

Figure 4. Schematic diagram for HF-DDSME.

Various parameters that significantly affects the extraction of AD from sample solution into acceptor phase includes [34] (M. Rezaee et al. 2006):

- *Selection of organic solvent*: it is one of the critical step for efficient extraction of drugs, various solvents used are toluene, o-xylene and n-hexane. The solvents should have properties of low solubility in aqueous medium, high distribution coefficient for analyte and low vapor pressure, and good chromatographic behavior, most commonly toluene is used because of having higher extraction efficiency.
- *Extraction time*: extraction efficiency increases with extraction time up-to certain limit beyond which there was a gradual decline which may be due to loss of solvent and formation of air bubbles occurring on the surface of hollow fiber which causes poor extraction of analytes from samples, longer periods causes depletion of solvent and decreased extraction efficiency [35] (H. Xu et al. 2009).
- *Exposure volume of organic phase*: in order to study the effect of exposure volume of organic phase different volumes of it for fixed time and a particular pH was checked and it was found that extraction efficiency increases with increase in exposure volume of acceptor phase upto only certain extent however further increase of exposure volume of acceptor phase into hollow fiber doesn't increase the extraction of analyte possibly due to attainment of equilibrium of analyte between the two phases.
- *Effect of salt*: addition of salt like NaCl to sample solution increases extraction efficiency of target analytes from sample through salting out effect also sometimes it may have an adverse effect when there is decrease in extraction efficiency of analyte from sample solution into the organic solvent which may be due to addition of salt which leads to changes in the physical properties of extraction film thus reducing diffusion rates of analytes into organic phase.
- *Effect of pH*: the effect of pH is studied by the addition of HCl and NaOH using fixed amount of exposure volume of organic phase at room temperature. But it is important here that the pH of the solution

should be higher than the pKa value of the analytes because at this condition the analytes were easily transferred from donar to acceptor phase. Also it has been found that the extraction efficiency increases with the increase in the pH and beyond a certain pH there was no significant increase in the extraction efficiency.

This technique has been extensively used for the determination of ADs in very small amounts of human blood, serum,saliva and plasma samples of psychiatric patients here the calibration curve obtained from the analysis is used to calculate concentration of a particular drug thus acting as a separating and pre-concentrating probe and excludes problems of interferences from biological samples because each time new piece of fiber is used, thus it has got unique value in situations where the sample volume available is very small such as in determination of drug concentration [36] (C. Alves et al. 2007).

It has been applied in the pharmacokinetic studies of trimeprazine involving extraction in 0.6 μL of toluene from 8 μL of urine and blood samples of rats and analysis of extract by GC-MS. Extraction of caffeine in beverages and food samples using chloroform as solvent and its further analysis by GC-MS [37] (C.G. Zambonin 2003) and also in determination of nicotine in nightshades vegetables and commercial food products using appropriate mixture of aqueous solution and toluene as extraction solvents. DDSME along with MALDI-MS is used for the determination of β-blockers agents in human serum [38] (G. Vas and K. Vekey 2004) and nicotinic acid in urine samples. Along with GC-MS it has been used in the detection of concentration of trimeprazine in urine and blood samples using 0.6 μL of toluene as extracting solvent [39] (J. Pawliszyn 1997).

Dispersive Liquid-Liquid Micro-Extraction (DLLME)

This technique was introduced by Assadi and coworkers [40] (H. Lord and J. Pawliszyn 2000). It makes use of microliter volumes of extraction solvent along with a few ml of dispersive solvents (in appropriate concentration)

such as acetone, methanol, ethanol, acetonitrile and Tetrahydrofuran which when injected into an aqueous sample containing the analytes of interest forms a cloudy solution. In this method the hydrophobic solvent is dispersed into the bulk aqueous phase followed by its centrifugation and the analytes in the settled phase can be determined by various analytical techniques like GC-MS, LC-MS and HPLC. This method leads to a better mass transfer of analytes from the aqueous phase to organic phase which enhances the extraction efficiency and reduces the time taken for extraction of analytes.

DLLME has the advantage of being simple, rapid, and low cost. The method has high recovery, high enrichment factor and short extraction time and is thus used in ultra trace analysis. Later Feng et al. demonstrated a new DLLME method based on solidifying floating organic droplet method (DLLME-SFO) which has twice the enrichment factor as that of traditional LPME method [41] (G.A. Mills and V. Walker 2000). The main disadvantage of DLLME is that it is not a selective extraction technique however interferences from matrix co-extractives are often present and moreover it requires the use of third component (disperser solvent) for extraction process.

Also DLLME can also be combined with SPE and LLE to improve the selectivity of sample preparation process and/or to reduce the LOQs (Limit of quantitation) achieved for complex matrices. DLLME can also be combined with EME (electro membrane extraction) followed by GC-FID for the trace analysis of drugs in untreated biological samples such as human plasma and urine samples. This technique not only provides high sample clean up and sensitivities but also improves incompatibility problems of EME with GC-FID. This technique has the advantage of short analysis time, low cost, extraction clean up in urine and plasma samples [42] (S. Ulrich 2000). Various steps of DLLME has been shown in Figure 5 (http://www.chrom-china.com/fileup/PIC/20131031195159.jpg).

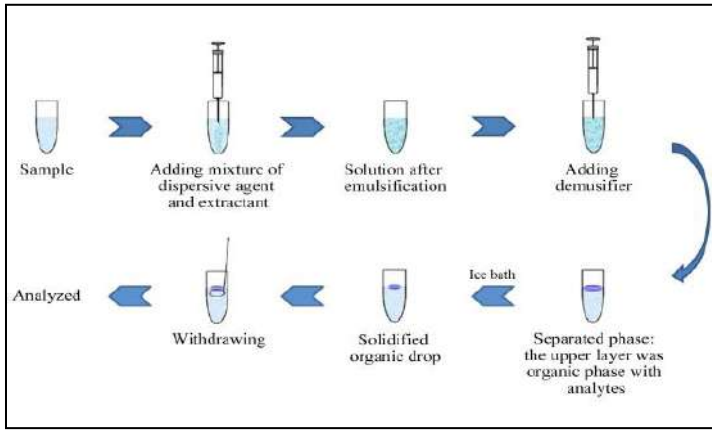

Figure 5. Different steps of DLLME.

Solid Phase Microextraction(SPME)

It is basically solid phase miniaturized extraction technique introduced by Pawliszyn and group in the year 1990 [43] (T. Kumazawa 2003) which doesn't uses any solvent for extraction so solvent disposal problem is eliminated. SPME integrates sampling, extraction, pre-concentration and sample introduction into a single step. SPME applications uses either sorption via exposure of the sample to a thin layer of sorbent coated on the outer surface of fiber or, on the internal surface of the capillary tube as shown in Figure 6 (http://www.chrom-china.com/fileup/PIC/201203 02102325.jpg). The various fibers used are PDMS/DVB which is a multiple component bipolar sorbent coating commercially available in film thickness of 65 micrometer, here DVB is suspended in the PDMS phase or, PDMS a single component, non polar liquid adsorbent phase coated on fused silica commercially available in film thickness of 30 and 100 micrometers and can be used in combination with GC and HPLC or, DVB/CAR/PDMS multiple component bipolar phase that contains a combination of DVB-PDMS layered over CAR-PDMS thus expanding the analyte molecular weight range. In this method the polarity of the sorbent coating should match the polarity of the analyte of interest and the coating should be pH and

temperature resistant also they should lack the affinity for interfering compounds, SPME is different from SPE in that here exhaustive extraction of the analyte from the sample matrix is not achieved, samples are analyzed after equilibrium is reached or, at specific time prior to achieving equilibrium.

The distribution constant K_{fs} between the coated fiber SPME sorbent and aqueous sample matrix is given by:

$$K_{fs} = C_f / C_s$$

Where C_f = concentration of analyte in the fiber sorbent and

C_s = concentration of analyte in the aqueous sample.

Thus higher the K_{fs} higher the sensitivity of the analytical procedure.

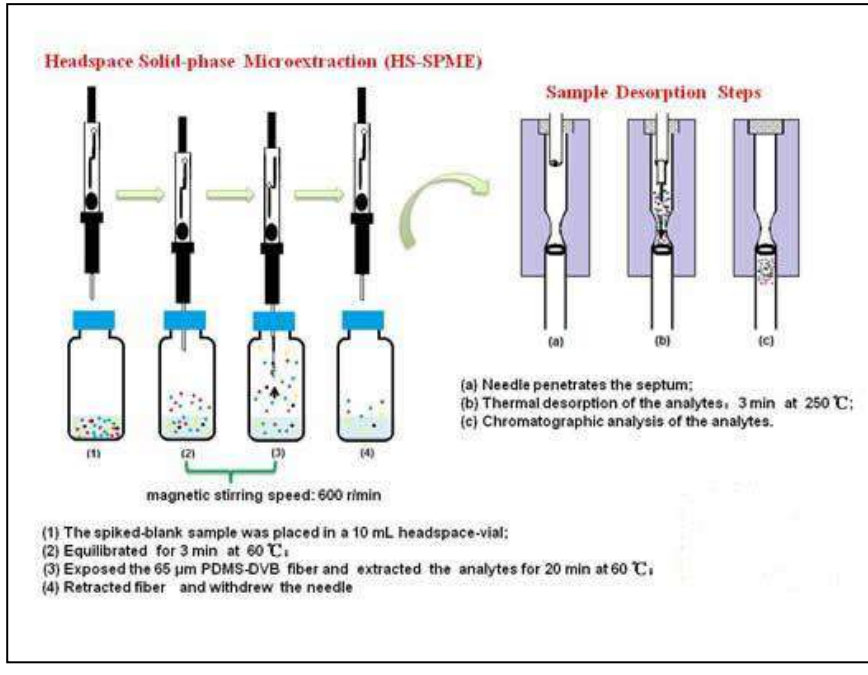

Figure 6. Steps of the SPME technique.

The two primary approaches for carrying out SPME procedures are either with sorbents coated fibers or, with the sorbent coated on the internal surface of capillary tube. In the fiber design, a fused silica core fiber is coated with a thin film (7-100 micrometer) of liquid polymer or, a solid sorbent in combination with a liquid polymer, fiber length is generally 1 cm.

The in–tube designs for the SPME uses 0.25 micrometer ID-capillary tube with about 0.1µL of coating of sorbent on the internal surface of the tube. Here basically thin polymeric layer coated on fused fiber is exposed into the sample or, its head space. During exposure the analyte present in the sample matrix and with chemical affinity for SPME fiber coating are sorbed and retained on fiber [44-49] (N.H. Snow 2000), (Q. Costa 2004), (C. Alves et al. 2007), (L.F. Gram 1984), (P.J. Goodnick 1994) and (B.B. Rasmussen and K. Brosen 2000). The dimensions of the fused silica fiber are accurately known so that the volume of the fused silica core can be subtracted from the total volume of the fiber to yield the phase volume of the sorbent.

The general SPME process consists of two steps:

1. The sorbent either an externally coated fiber or, an internally coated tube is exposed to the sample for a specified period of time.
2. The sorbent is transferred to a device that interfaces with an analytical instrument for thermal decomposition using GC or, for solvent desorption using HPLC.

In the fiber mode the sorbent coated fiber is housed in a micro-syringe like protective holder, the needle is used to pierce the septum of the sample vial then the plunger is depressed to expose the sorbent coated fiber to the sample as shown in Figure 7 (http://www.chem.sc.edu/analytical/chem 621/lab/images/RGFig1.JPG) and after the specified time the fiber is retracted into the micro-syringe and the needle is withdrawn from the sample finally, the sorbent is interfaced with different analytical instruments.

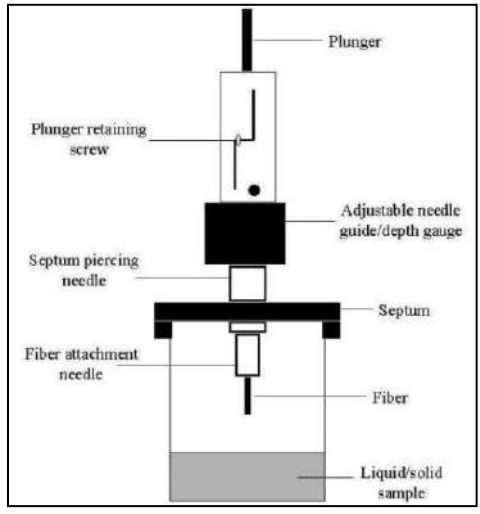

Figure 7. SPME Apparatus.

Whereas in the in-tube mode a sample aliquot is repeatedly aspirated and depressed into an internally coated capillary and finally an organic solvent desorbs into the analyte and sweeps it into the injection. SPME has the advantage of being the most attractive sample pretreatment technique in forensic, clinical and pharmaceutical analysis of complex matrices system prior to chromatographic and CE process, other advantages includes low operating costs, ease of operation, speed, also it pose no environmental harm as it is solvent-less sample preparation procedure and can be easily automated it also facilitates unique investigations such as investigations from very small samples.

Despite of various advantages short fiber life, high cost and matrix effect can be major disadvantage of SPME process also SPME can be used to extract analytes from only clean samples as the extraction from dirtier matrices is more difficult.

Analysis of antidepressants (Tricyclic) in plasma samples using SPME along with LC-MS has been reported where factorial design approach was used to optimize MS parameters and lab-made SPME interface combines SPME to LC-MS [50] (P. Baumann 1996).

CONCLUSION

This chapter focuses on various micro-extraction techniques over other classical sample pretreatment procedures because of its several advantages viz. miniaturization, minimization, automation, time efficiency and onsite analysis. LPME is basically a solvent minimized sample pretreatment process over LLE, it is simple, rapid, sensitive and virtually solvent free green procedure and is also compatible with various analytical instruments like GC, HPLC and CE. SDME has got excellent application range from trace organic to inorganic analysis, here the nature of analyte basically determines the separation and detection technique to be used for analysis and this finally dictates the choice of sample preparation method. SDME produces better LODs than SPME also derivatization process is critical to obtain sufficiently good chromatographic separations with increasing volatility, detector sensitivity and selectivity. SPME uses an appropriate stationary phase (sorbent) coated either on fibers or, on the inner surface of the capillary tube and is attractive over other techniques as is used even for sample pretreatment of complex sample matrices and hence finds extensive application in forensic, clinical and pharmaceutical analysis. Thus, micro-extraction exhibits many advantages such as its simplicity, low cost, short extraction time and minimum requirement of solution and solvent for separation and pre-concentration processes.

REFERENCES

[1] Pedersen, S., Bjergaard, and. Rasmussen K.E. 2000. Liquid phase microextraction and capillary electrophoresis of acidic drugs. *Electrophoresis*. 21 (3): 579-85.

[2] Khraiwesh, A., I. Papoutsis, Nikolaou P., Pistos C., Spiliopoulou C., and Athanaselis S. 2011. Development and validation of an EI-GC/MS method for the determination of sertraline and its major metabolite desmethyl-sertraline in blood. *J. Chromatography.B*. 879. 2576–2582.

[3] Patel, B.N., Sharma N., Sanyal M., and P.S. Shrivastav. 2008. Liquid chromatography tandem mass spectrometry assay for the simultaneous determination of venlafaxine and O- desmethylvenlafaxine in human plasma and its application to a bioequivalence study, *J. Pharmaceutical and Biomedical Analysis*. 47. 603–611.

[4] Frahnert, C., M.L. Rao, and Grasmader K., (2003) Analysis of eighteen antidepressants, four atypical antipsychotics and active metabolites in serum by liquid chromatography:a simple tool for therapeutic drug monitoring, *J. Chromatography*. *B.*794. 35–47.

[5] Yazdi, A.S. and Amiri A. 2010. Liquid phase microextraction, Trends in Analytical. *Chemistry*. 29. 1.

[6] He, Y., and. Lee H.K. 1997. Liquid phase microextraction in a single drop of organic solvent by using a conventional microsyringe, *Analytical Chemistry*. 69. 4634.

[7] Zhang,J., T. Su, and Lee H.K. 2005. Headspace water based liquid phase microextraction, *Analytical Chemistry*. 77. 1988.

[8] Liu, J.F., Jiang G.B., Chi Y. G., Cai Y. Q., Zhou Q.-X, and Hu. J.T. 2003. Use of ionic liquids for liquid phase microextraction of polycyclic aromatic hydrocarbon, *Analytical Chemistry*. 75. 5870.

[9] He, Y., Vargas A., and. Kang Y.J. 2007. Direct screening of water samples for benzene hydrocarbon compounds by head-space liquid phase microextraction-gas chromatography, *Analytica Chimica Acta*. 589.225–230.

[10] Sarafraz, A., Yazdi, Raouf-Yazdinejad S., and Es'haghi Z. 2007. Directly suspended droplet microextraction and analysis of amitryptyline and nortryptyline by GC, *Chromatographia*. 66. 613–617.

[11] Jeannot, M.A., Przyjazny A, and Kokosa J.M. 2010. Residual solvents determination in pharmaceuticals by static headspace gas-chromatography and headspace liquid phase microextraction and gas – chromatography, *J.Chromatography A.*1217. 2326-2336.

[12] Chen, H., Chen R., Feng R., and S. Li. 2009. Environmental chemistry for the a sustainable world, volume 2 remediation of air and water pollution, *Chromatographia*. 70. 165–172.

[13] Lambrropoulou, D.A., E.Psillakis,N.Kaogerakis, 2004 Persistant organic pollutants analytical techniques environmental fate and biological effects, *Analytica Chimica Acta*. 516. 205-211.

[14] Xu,L., Basheer C., and Lee H.K. 2007. Developments in single drop microextraction (review article) *J. Chromatography*. A. 1152. 184–192.

[15] Jeannot, M.A., Przyjazny A., and. Kokosa J.M. 2010. Residual solvents determination in pharmaceuticals by static headspace gas-chromatography and headspace liquid phase microextraction and gas – chromatography, *J.Chromatography A*. 1217. 2326-2336.

[16] Shrivas, K., and H.F. Wu, 2007 Single drop microextraction as a concentrating probe for rapid screening of low molecular weight drugs from human urine, *Rapid Communication in. mass Spectrometry*. 21. 3103–3108.

[17] Kokosa, J.M.,Przyjazny, A., and. Jeannot M.A., *Solvent Microextraction – Theory and Practice*, John Wiley & Sons, Inc., Hoboken, NJ.

[18] Yao, Y., Pitner W.R., and Anderson J.L., 2009 Ionic liquids containing the tris, (pentafluoroethyl) trifluorophosphate anion: a new class of highly selective and ultra hydrophobic solvents for the extraction of polycyclic aromatic hydrocarbons using single drop microextraction *Analytical Chemistry*. 81. 5054–5063.

[19] Vidal, L., Chisvert A., Canals A., and Salvador A., 2010. *Ionic liquid based single drop microextraction liquid chromatography ultraviolet spectrometry detection to determine typical ultraviolet filters in surface water samples*, Talanta. 81. 549.

[20] Stalikas, C.D., and Fiamegos Y.C. 2008. Speciation studies in soil, sediment and environmental samples, *Trends in Analytical Chemistry*. 27. 533–542.

[21] Xu, L., Basheer, C., and. Lee H.K., 2009 Chemical reactions in liquid phase microextraction, *J. Chromatography. A*. 1216. 701–707.

[22] Nuhu. A.A., Basheer C., Saad B. 2011. Derivatization of carbohydrate for GC and GC-MS analysis, *J. Chromatography B.* 879. 1180–1188.

[23] Sekar, R. and Wu H.F. 2006. Quantitative method for the analysis of monensin in soil, water and urine by direct combination of single-drop microextraction with atmospheric pressure matrix assisted laser desorption ionization mass spectrometry. *Anal. Chem*. 2006 78 (18). 6306-13.

[24] Halvorsen, T.G., Bjergaard S.P., and Rasmussen K.E. 2001. Liquid phase microextraction and capillary electrophoresis of citalopram- an antidepressant, *Journal of chromatography A.* 90. 87-93.

[25] Pedersen, S., Bjergaard and. Rasmussen K.E. 1999. Liquid phase micrextraction for sample preparation of biological fluids prior to capillary electrophoresis, *Analytical Chemistry*. 71. 2650–2656.

[26] Rasmussen, K.E., and S. Pedersen-Bjergaard. 2004. Extraction and determination of three chlorophenols by hollow fibreliquid phase microextraction-spectrophotometric analysis, and evaluation procedure using mean centering ratio spectra method, *Trends in Analytical Chemistry*. 23. 1–10.

[27] Tapadia, K., Shrivas K., Upadhyay, L.S.B. 2011. GC-MS coupled with hollow fiber drop to drop solvent micro-extraction for the determination of antidepressants in human blood sample. *Chromatographia*.74. 437-442.

[28] Jain, A., and Verma K.K. 2011. Recent advances in applications of Single drop micro-extraction, *Analytica chemical acta*. 706. 37-65.

[29] Fiamegos, Y.C., and. Stalikas C.D. 2007. In-drop derivatization liquid phase microextraction assisted by ion-pairing transfer for the gas chromatographic determination of phenolic endocrine disruption, *Anal. Chim. Acta*.597. 32–40.

[30] Kataoka, H., 2010. Recent developments and applications of micro-extraction techniques in drug analysis, *Journal of Analytical and Bioanalytical Chemistry*. 396. 339–364.

[31] Shrivas, K., and Wu H.F. 2007. Rapid determination of caffeine in one drop of beverages and foods using drop to drop solvent micro-extraction with GC/MS, *J. Chromatography. A*.1170. 9–14.

[32] Shrivas, K., Patel D.K. 2011. Matrix assisted laser desorption/ionization mass spectrometry for the quantitative

determination of beta blocker drugs in one drop of human serum, *J. Chromatogr. B*. 879. 35–40.

[33] Agrawal, K., and H.-F. Wu. 2007. Drop to drop solvent microextraction coupled with GC/MS for the rapid determination of trimeprazine in urine and blood of rats: application to pharmacokinetic studies, *Rapid Communication in Mass Spectrometry*. 21. 3352–3356.

[34] Rezaee, M., Assadi, Y., Millani M.R., Aghaee E., Ahmadi F., and. Berijani S. 2006. Determination of organic compounds in water using dispersive liquid-liquid micro-extraction. *J. Chromatography. A.*1116. 1.

[35] Xu, H., Ding Z., L. Lv, D. Song, and Y.Q. Feng. 2009.A novel dispersive liquid-liquid microextraction based on floating organic drop method for the determination of polycyclic aromatic hydrocarbon in aqueous samples. *Analytica Chimica Acta*.636.

[36] Alves, C., A.J.S. Neto, Fernandes C., J.C. Rodrigues, and F.M.Lancas. 2007.Analysis of tricyclic antidepressant drugs in plasma by means of solid phase micro-extraction liquid phase micro-extraction, *J. Mass Spectrometry*. 42. 1342-1347.

[37] Zambonin. C. G. 2003. Coupling solid-phase microextraction to liquid chromatography. *Analytical and Bioanalytical Chemistry*; 375:73.

[38] Vas, G. and.Vekey K. 2004. Solid-phase microextraction: a powerful sample preparation tool prior to mass spectrometric analysis. *Journal of Mass Spectrometry*. 39. 233.

[39] Pawliszyn, 1997. *J. Solid Phase Microextraction: Theory and Practice.*Wiley-VCH: Ontario. 247.

[40] Lord, H. and Pawliszyn. 2000. J. Microextraction of drugs. *Journal of Chromatography A*; 902: 17.

[41] Mills, G. A., and Walker V. 2000. Headspace solid-phase microextraction procedures for gas chromatographic analysis of biological fluids and materials. *Journal of Chromatography* A; 902: 267,

[42] Ulrich, S. 2000. Solid-phase microextraction in biomedical analysis. *Journal of Chromatography* A; 902: 167,

[43] Kumazawa, T., Lee X. P., Sato K., and Suzuki O. 2003. Solid-phase microextraction and liquid chromatography/mass spectrometry in drug analysis. *Analytica Chimica Acta*; 492: 49.

[44] Snow.N.H. 2003. Solid-phase micro-extraction of drugs from biological matrices. *Journal of Chromatography A* 2000; 885: 445.

[45] Costa Queiroz ME., and Lancas FM. 2004.*Practical tips on preparing plasma samples for drug analysis using SPME*. LCGC North America; 22: 970.

[46] Alves, C., A.J.S. Neto, Fernandes C., Rodrigues J.C., and Lancas F.M. 2007.Analysis of tricyclic antidepressant drugs in plasma by means of solid phase micro-extraction liquid phase micro-extraction, *J. Mass Spectrometry*. 42. 1342-1347.

[47] Gram, L. F.,Kragh-sorensen P., Kristensen C. B., moller M., Pedersen O. L., and Thayssen. P.1984. Plasma level monitoring of antidepressants in theoretical basis and clinical applications. *Adv. Biochem. Psychopharmacol*. 39.399.

[48] Goodnick, P.J., 1994. Pharmacokinetic optimization of therapy with newer antidepressants. *Clinical Pharmacokinetics*. 27. 307.

[49] Rasmussen, B.B., and Brosen K. 2000. Is therapeutic drug monitoring a case of optimizing clinical outcome and avoiding interactions of selective serotonin reuptake inhibitors? *Drug Monitoring.* 22. 143.

[50] Baumann, P., 1996. Pharmacokinetic-pharmacodynamic relationships of selective serotonin reuptake inhibitors. *Clinical. Pharmacokinetics*. 31. 444.

In: Advances in Chemistry Research ISBN: 978-1-53617-112-9
Editor: James C. Taylor

Chapter 6

BIS-AZIDES

Róbson R. Teixeira[1,*], PhD,
Deborah Campos Tomaz[1], MD,
Sara Maria Ribeiro de Sousa[1], MD,
Ana Paula Martins de Souza[1], MD,
Michelle Peixoto Rodrigues [1], MD,
Alex Ramos de Aguiar[1], PhD,
Adilson Vidal Costa[2], PhD,
Fabiola Suelen dos Santos[3], MD
and Rossimíriam Pereira de Freitas[3], PhD

[1]Chemistry Department, Universidade Federal de Viçosa, Viçosa, Minas Gerais State, Brazil
[2] Physics and Chemistry Department, Universidade Federal do Espírito Santo, Alegre, Espírito Santo State, Brazil
[3]Chemistry Department, Universidade Federal de Minas Gerais, Minas Gerais State, Brazil

[*] Corresponding Author's Email: robsonr.teixeira@ufv.br.

ABSTRACT

Organic azides are an important and versatile class of chemical compounds. They present industrial, academic, and biological applications. In addition, they can be obtained from a variety of synthetic methods. The present book chapter will focus specifically on bis-azides, *i.e.*, organic compounds presenting two azido (-N_3) groups in their structures. The utility of them is going to be covered in synthetic group transformation, polymer chemistry, in the preparation of bioactive compounds, in click chemistry, and in the synthesis of cross-linked DNA.

Keywords: Azides, Organic Azides, Bis-Azides

INTRODUCTION

Organic azides are an important and versatile class of chemical compounds [1]. They present industrial applications [2], are biologically active substances [3], and have great synthetic utility in conjunction with their easy accessibility via several synthetic routes [3-5].

The history of organic azides goes back to 1864 when the German chemist Peter Griss, who first prepared the diazonium salts [6, 7], obtained aryl azides from the reaction of arenediazonium perbromides with ammonia [8]. Later on, Theodor Curtius found that the treatment of benzoyl hydrazine with nitrous acid afforded benzoyl azide. Alkaline hydrolysis of benzoyl azide gave sodium azide which, in turn, by acidification resulted in the formation of hydrazoic acid (HN_3). In Curtius´ laboratory, a procedure was also developed for the preparation of alkyl azides via the treatment of alkyl iodides with AgN_3. He also discovered that the reaction of benzoyl azide with hot ethanol gave rise to *N*-phenylcarbamate [8]. The coversion of acyl azides to the corresponding carbamates is known as The Curtius Rearrangement and it is one step involved in the general method that converts carboxylic acids to amines [9]. Since these initial studies, azides have attracted the attention of several researchers.

The present book chapter will focus specifically on bis-azides, *i.e.*, organic compounds presenting two azido ($-N_3$) groups in their structures. It is going to be covered the utility of them in polymer chemistry, synthetic group transformation, in the preparation of bioactive compounds, in click chemistry, and in the synthesis of cross-linked DNA. It is not our intention to make an exhaustive description of all aspects related to bis-azides.

FUNCTIONAL INTERCONVERSION EMPLOYING BIS-AZIDES

The esterification is an important process in organic chemistry. Esters can be prepared using mineral acids, a variety of activating agents, and several catalysts [10]. Ponnuswam and co-authors found that the combination of bis-azides with trialkyl phosphites or triphenyl phosphine is an alternative method for the preparation of esters [11]. Thus, treatment of carboxylic acids with 1,3-diazidopropane (1) in the presence of triethyl phosphite or trimethyl phosphite afforded methyl or ethyl esters (2-23) in good yields (Scheme 1). Reactions were carried out at room temperature and under solvent free condition.

The proposed mechanism for this reaction is depicted in Scheme 2 [11].

The inconvenience of the aforementioned method is that the phosphites must be prepared before running the esterification. Considering this, it was hypothesized that the trialkyphosphites could be replaced by triphenylphospine. In fact, the reaction of bis-azide (1) with carboxylic acids in the presence of triphenylphospine and an alcohol afforded esters with good yields, as shown in Scheme 3.

The proposed mechanism for the formation of esters (24)-(36) is presented in Scheme 4 [11].

The chemistry of 3,3-diazidoenones (38) has been recently investigated [12]. These compounds can be prepared from the corresponding 3,3-dichlorovinyl ketones (37) which, in turn, can be made from 1,1-dichloroethene and acyl chlorides (Scheme 5).

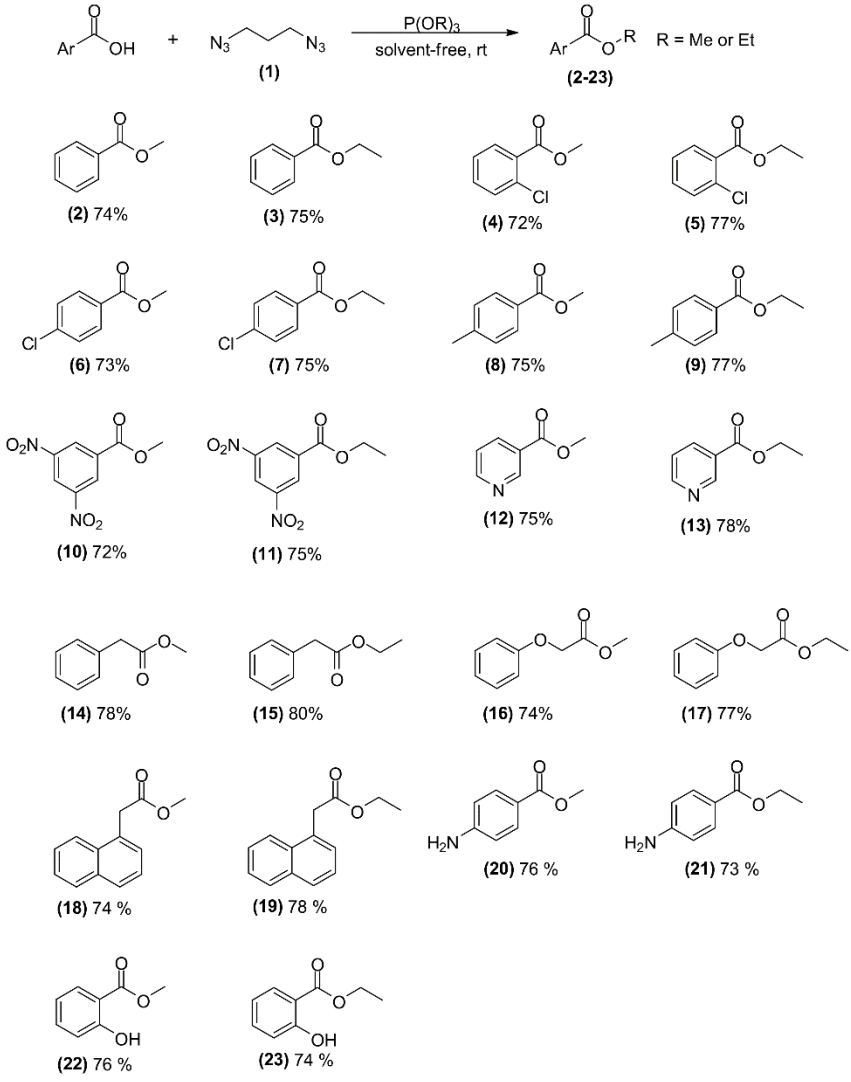

Scheme 1. Preparation of esters from bis-azide (1) and trimethyl or triethyl phosphites. Reaction conditions: 1,3-diazidopropane (1) (0.5 mmol), trimethyl phospite/triethyl phosphite (1.0 mmol) and carboxylic acid (1.0 mmol) were stirred at room temperature for 20 min.

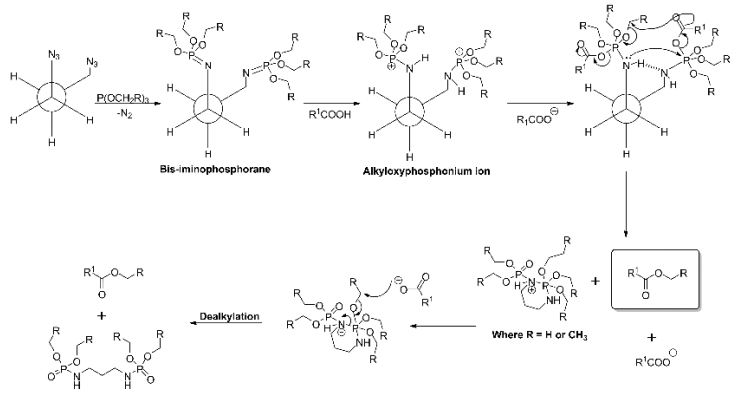

Scheme 2. Proposed mechanism for the esterification using triakylphosphites.

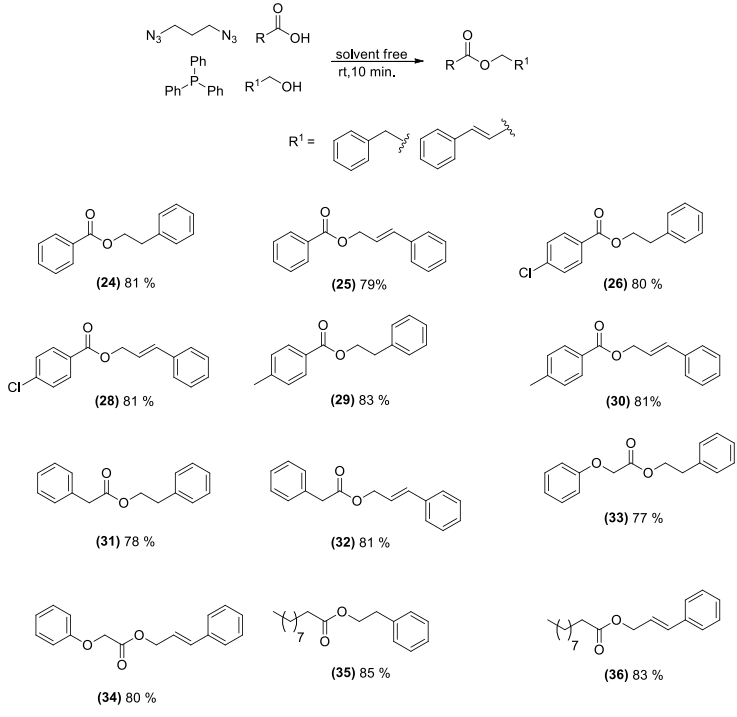

Scheme 3. Preparation of esters (24)-(36). Reaction conditions: To a mixture of triphenylphosphine (1.0 mmol), 2-phenylethanol/cinnamyl alcohol (1.0 mmol) and carboxylic acid (1.0 mmol), 1,3-diazidopropane (1) (0.5 mmol) was added slowly in a drop wise manner (to avoid accumulation of azide) and the mixture was stirred at room temperature for 10 min.

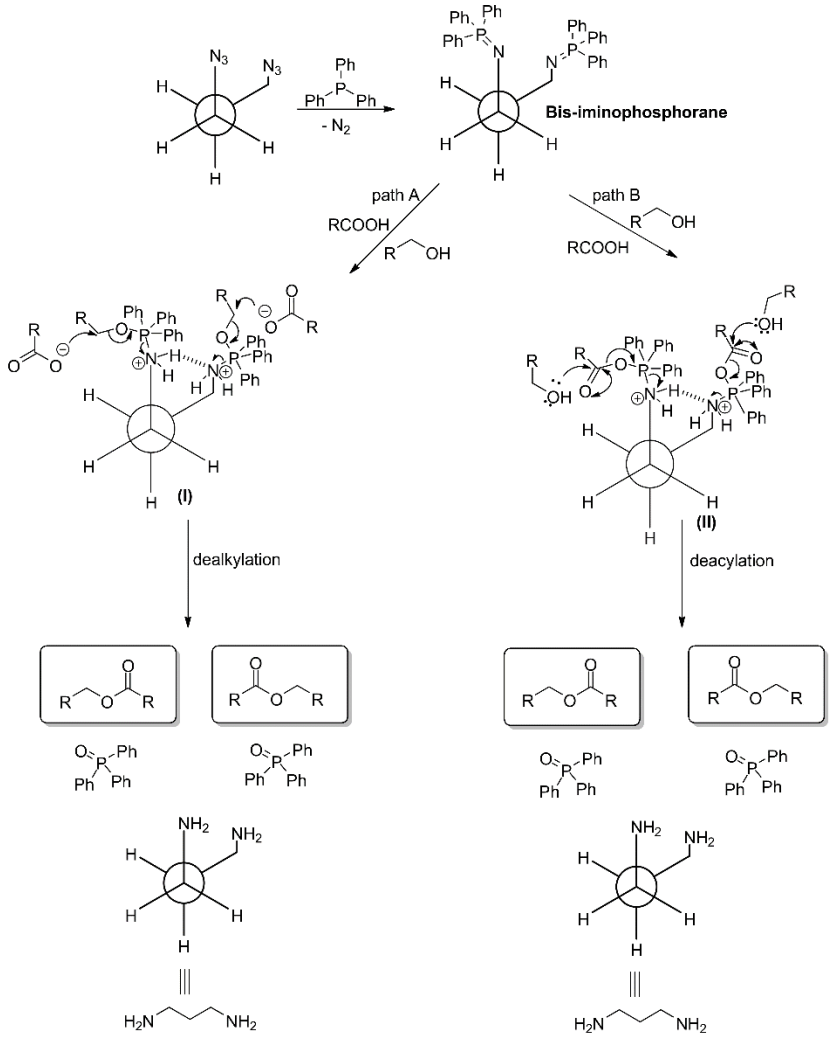

Scheme 4. Proposed mechanism of the formation of esters from azides using triphenylphospine.

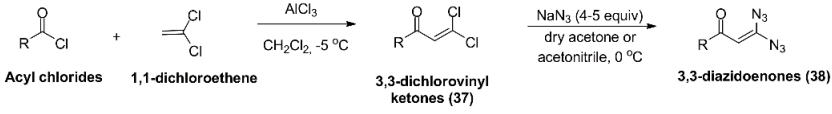

Scheme 5. Preparation of 3,3-diazidoenones (38).

The formation of 3,3-diazidoenones (38) was evidencied by NMR spectroscopy. It was found that these compounds can undergo cyclization to afford azido isoxazoles (39). This process can be understood considering the nucleophilic attack of carbonyl oxygen on the nitrogen atom accompanied by N_2 release. For dichlorovinyl ketones with aromatic portions, the azidoisoxazoles were obtained in yields ranging from 52%-62%. (Table 1). The reactions were carried out at room temperature in acetonitrile. The fastest conversion of (37d) was associated with the presence of the electron withdrawing group (-NO_2) in the aromatic ring [12].

The conversion of 3,3-diazidovinyl ketones in azidoisoxazoles were also performed in ionic liquids. This was done in order to find more environmentally friendly alternatives to the traditional organic solvents. As can be seen in Table 2, the azidoisoxazoles were obtained in good yields and the best ones were prepared running the reactions in $[emin]^+[OTf]^-$.

The formation of azidoixosazoles from dichlorovinyl ketones with aliphatic portions was also investigated and the results are depicted in Table 3.

Table 1. Formation of azidoisoxazoles (39a-d)

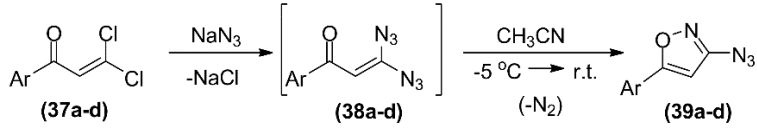

(37a-d) **(38a-d)** **(39a-d)**

Starting ketone	Ar	Time for the conversion of (37a-d) to (38a-d), h	Yield of (39) (%)
37a	4-Br-C_6H_4	2.5 (38a)	62 (39a)
37b	4-Cl-C_6H_4	3.0 (38b)	56 (39b)
37c	Ph	4.0 (38c)	52 (39c)
37d	3-NO_2-C_6H_4	1.5 (38d)	61 (39d)

Table 2. Formation of azidoisoxazoles in ionic liquids

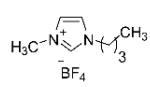 [bmin]$^+$[BF$_4$]$^-$	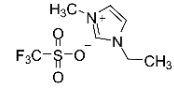 [emin]$^+$[OTf]$^-$	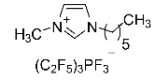 [hmin]$^+$[PF$_3$(C$_2$F$_5$)$_3$]$^-$	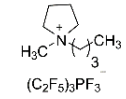 [bmpyrr]$^+$[PF$_3$(C$_2$F$_5$)$_3$]$^-$	
Compound	Yield of compounds (39a-c)			
	[bmin]$^+$[BF4]$^-$	[emin]$^+$[OTf]$^-$	[hmin]$^+$[PF$_3$(C$_2$F$_5$)$_3$]$^-$	[bmpyrr]$^+$[PF$_3$(C$_2$F$_5$)$_3$]$^-$
39a	70	74	62	57
39b	67	74	63	58
39c	65	75	N/A	N/A

Table 3. Preparation of azidoisoxazoles (41e-h)

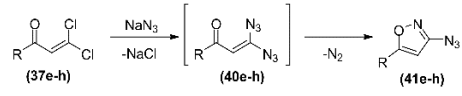

Starting ketone	R	Time for the conversion of (40) to (41), h	Yield of (41) (%)
37e	$CH_3CH_2CH_2$	36.0 (40e)	30 (41e)
37f	$CH_3CH_2CH_2CH_2$	40.0 (40f)	36 (41f)
38g	$(CH_3)_2CBr$	1.5 (40g)	36 (41g)
39h	CF_3	1.0 (40h)	40 (41h)

The yields of the azidoisoxazoles (41e-h) were lower compared to the compounds (39a-d). This fact was ascribed to side reaction to form oligomeric products. It is likely that enolization of the ketones is responsible for this behavior. Another possibility is the high volatily of compounds (41e-h) that have low molecular weight. This fact made the isolation of azidoisoxales (41e-h) in pure form a difficulty task. In fact, it was not possible to isolate compound (41h) with good purity. Its formation was confirmed by trapping the azidoisoxazole, via strain promoted alkyne-azide cicloaddition (SPAAC) [13, 14], with cyclooctyne resulting in the formation of adduct (42) (Scheme 6).

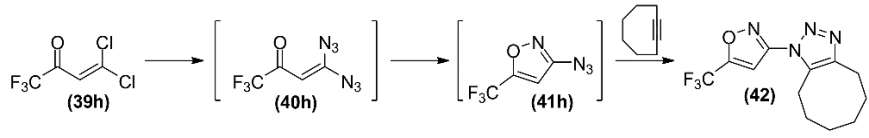

Scheme 6. Trapping reaction of compound (41h) with cyclooctyne.

The 3,3-diazidoenones can also react with cyclooctyne to afford 1,2,3-triazoles as exemplified in Scheme 7 for the reaction of divinyl ketone (38a) resulting in the bis-1,2,3-triazole (43) in 88% yield. When the reaction was warmed to promote the converstion of (38a) in azidoisoxazole (39a), subsequent addition of cyclooctine resulted in the formation of (44) in 93% yield [12].

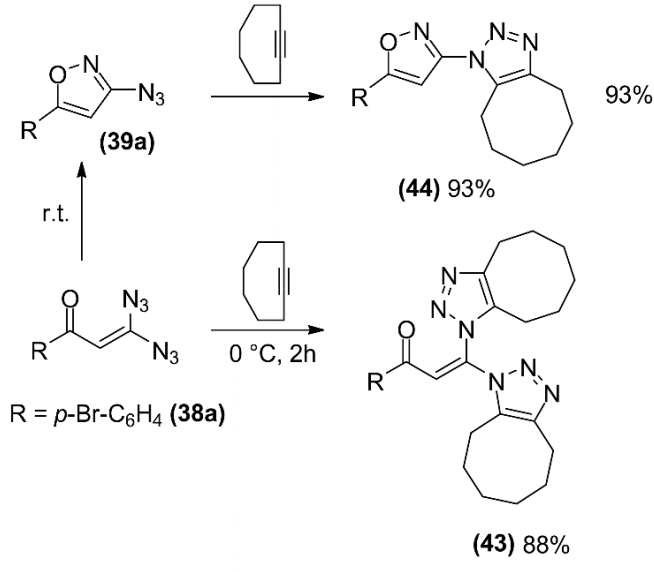

Scheme 7. Preparation of 1,2,3-triazoles from 3,3-diazidoenone (38a).

The azidoisoxazoles are synthetically useful compounds. They can be converted in 1,2,3-triazoles via CuAAC reactions (vide infra for a more detailed discussion regarding this reaction) as exemplified in Scheme 8 for the conversion of (39b) in compound (45). Compound (39b) was also

converted in 1,4,5-tribustituted-1,2,3-triazole (46) by reacting it with malodinitrile and sodium etoxide.

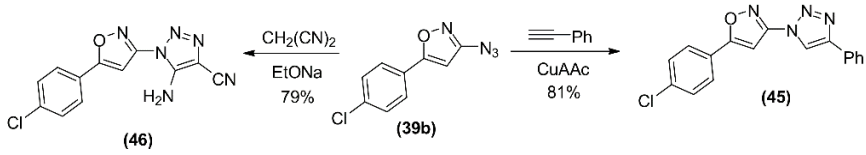

Scheme 8. Conversion of isoxazole (39b) into compounds (45) and (46).

To further demonstrate their synthetic utility, azidoisoxazoles (39a-c) were converted in the phosphorous and nitrogen derivatives shown in Scheme 9.

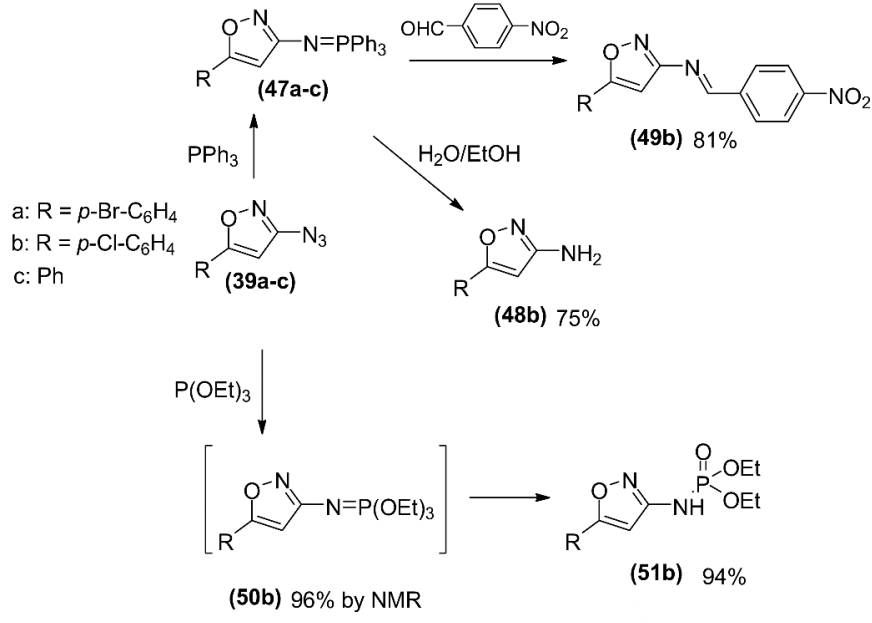

Scheme 9. Conversion of azidoisoxazoles in nitrogen and phosphorus derivatives.

BIS-AZIDES AND CUAAC REACTION

Azides have been widely used in the Copper(I)-catalyzed Alkyne-Azide Cycloaddition (CuAAC), also known as click reaction [15-18]. In this transformation, an alkyne and an azide react to afford 1,4-disubstituted-1,2,3-triazole derivatives. The process is catalyzed by copper(I) species (Scheme 10).

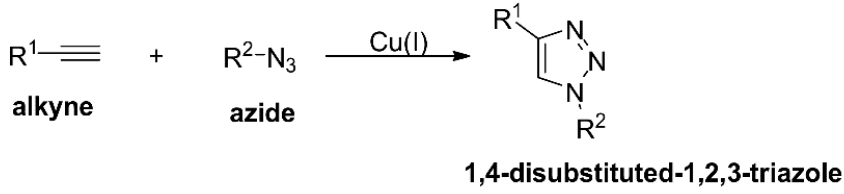

Scheme 10. General scheme of the CuAAC reaction.

This important transformation has found applications in the preparation of pharmaceuticals, agrochemicals, in material science, in carbohydrate chemistry, among others [19-28].

As expected, bis-azides can be engaged in CuAAC chemistry. The review by Abu-Orabi [29] shows several examples of the use of bis-azides in click chemistry.

More recently, Freitas and co-workers [30] synthesized a series of novel symmetric 1,4-disubstituted-1,2,3-triazoles via double CuAAC from aliphatic bis-azides (52a-d) and a tetraethylene glycol bis-azide derivative (52e). The eighteen derivatives (53a-53r) were obtained with good to excellent yields (Scheme 11) and had their cytotoxicity evaluated *in vitro* against human breast adenocarcinoma (MDA-MB 231) and ovarian adenocarcinoma (TOV-21G).

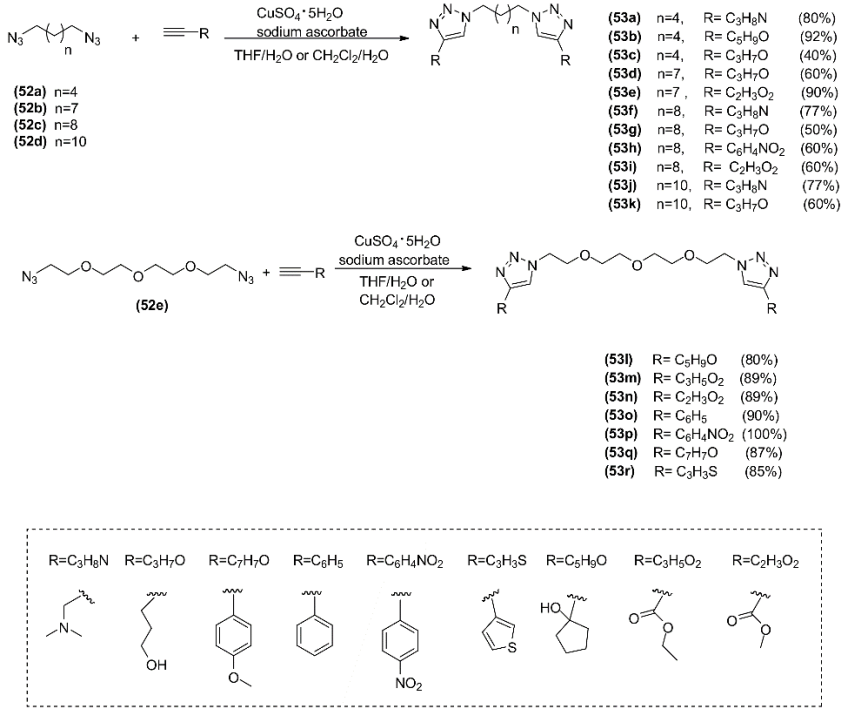

Scheme 11. Synthesis of symmetrical 1,4-dissubstituted-1,2,3-triazoles (53a-53r).

The MTT cytotoxic assay revealed that the most active compounds were (53j) and (53q). The latter was more active against MDA-MB 231 cell line compared to the standard drug doxorubicin (used as positive control). It is important to mention that both compounds exhibited better selectivity index than the positive control (Table 4). The Selectivity Index (SI) of cytotoxicity was calculated based on the IC_{50} values obtained for each compound as follows:

$$SI = IC_{50}\ Y / IC_{50}\ X,$$

where IC_{50} X is the IC_{50} value obtained for the MDA-MB 231 and TOV-21G cell lines and IC_{50} Y is the IC_{50} value obtained for WI-26VA4, the human non-tumor cell line used as a reference.

Table 4. Results of the cytotoxicity evaluation of compounds (53j) and (53q) against MDA-MB231 (human breast adenocarcinoma), TOV-21G (ovarian adenocarcinoma), and WI-26VA (non-tumor human cell line)

	IC_{50} (μmol L^{-1}) ± SD			Selective Index (SI)	
Compound	MDA-MB 231	TOV-21G	WI-26VA	MDA-MB 231	TOV-21G
53j	28.83 ± 14.20	7.29 ± 3.63	69.36 ± 15.76	2.41	9.51
53q	5.07 ± 1.75	31.64 ± 9.40	24.03 ± 6.78	4.74	0.76
Doxorrubicine	7.22 ± 0.77	3.68 ± 2.78	1.67 ± 1.73	0.23	0.45

IC_{50} = the compound concentration that reduced cell viability by 50%.
SD = standard deviation.

These compounds induced apoptosis in both tested cell lines, as assessed by BrdU assay. The findings suggested that these structurally simple compounds may be promising prototypes for antitumoral agents.

The synthetic strategy used for the preparation of compounds (53a-53r) has also been recently utilized by other researchers [31].

The synthesis of unsymmetrical bis-triazoles via organoclick-click sequence was examined by Bressy and co-workers [32]. The organoclick step combined a ketone and an unsymmetrical bis-azide in the presence of proline as the organocatalyst as shown in Scheme 12. This approach afforded the monotriazoles in moderate to good yields. It was noticed the formation of azidoanilines resulting from a selective reduction of the aromatic azide function and the obtained yields for them are shown between parentheses in Scheme 12.

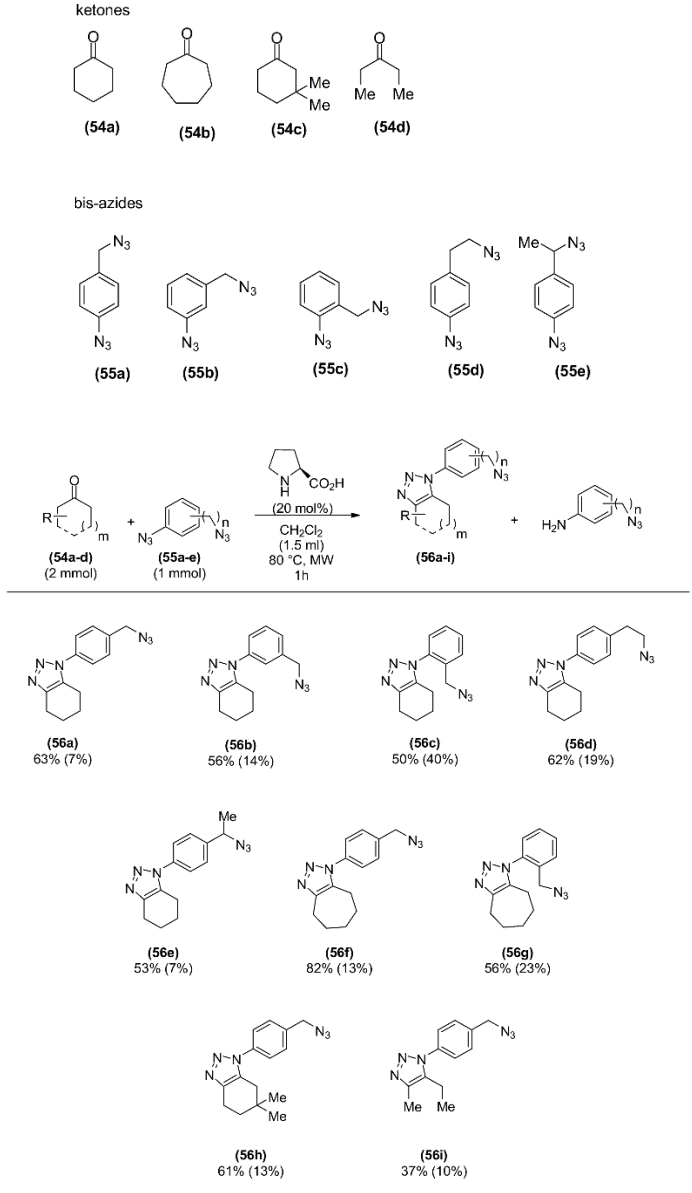

Scheme 12. Organoclick step of the organoclick-click sequence reported by Bressy and co-workers [32].

With the compounds (56a-i) in hands, they were submitted to CuAAC reaction (click chemistry) with different alkynes giving rise to the bis-triazoles (Scheme 13).

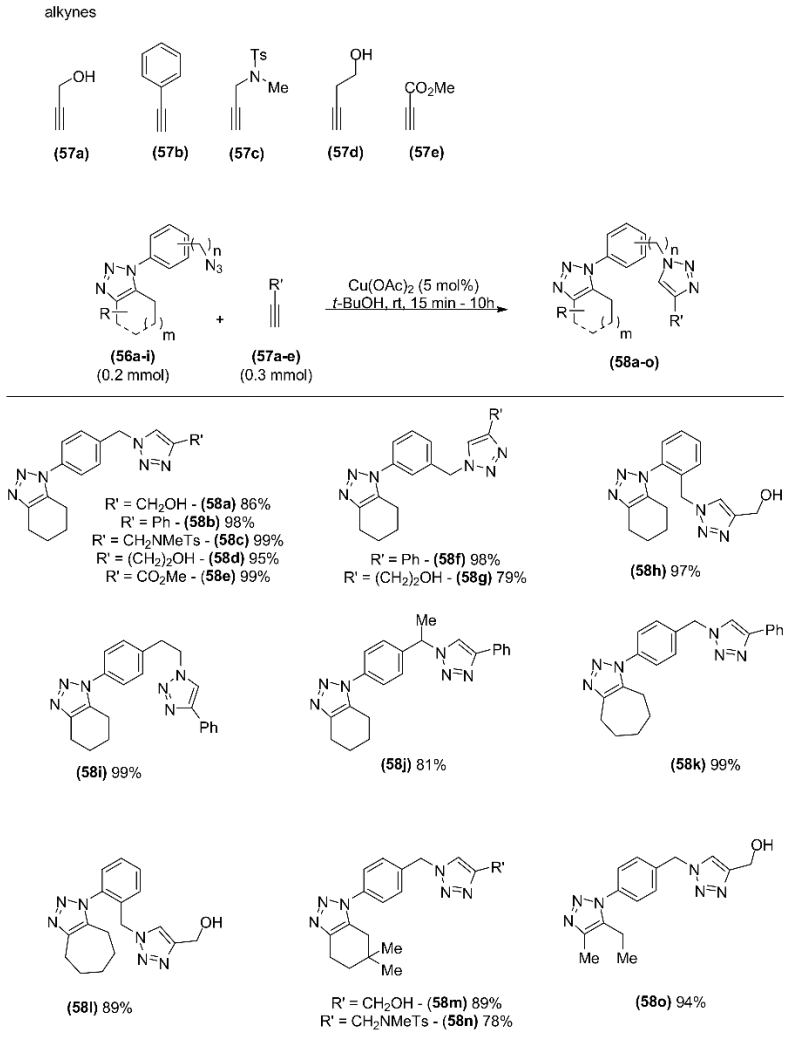

Scheme 13. Click step of the organoclick-click sequence reported by Bressy and co-workers [32].

A one-pot procedure was also developed. In this case, the monoazide intermediate was not isolated (Scheme 14).

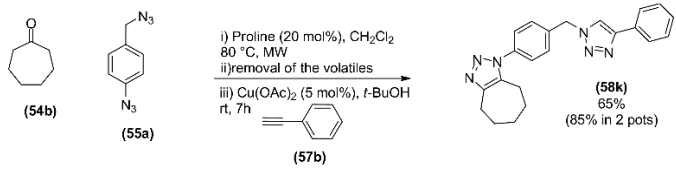

Scheme 14. One pot procedure for the preparation of bis-1,2-3-triazoles.

SYNTHESIS OF FUNCTIONALIZED MACROCYCLES

Macrocycles bis-iminophosphoranes can be efficiently synthesized via Staundinger reaction between bis-azides and bis-phosphines as shown in Scheme 15 [33]. Thus, the bis-azide (59a) was converted in cyclic compound (60a) in 79% yield. The incorporation of heteroatoms in the chain connecting the aromatic rings did not decrease the yield of the cyclic products (preparation of compounds 60b-60d).

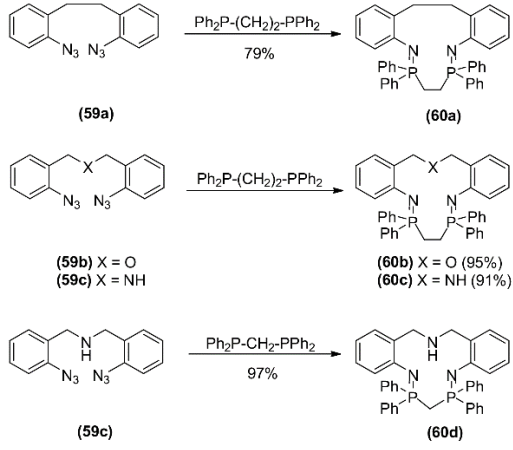

Scheme 15. Synthesis of functionalized macrocyles by means of reaction of bis-azides and bis-phosphines [33].

Variations of this reaction were developed (Scheme 16). Starting from aldehydes (61a-b), the imines (62a-b) were obtained and treated with bisphosphines affording the macrocyles (63a-c) with moderate yields.

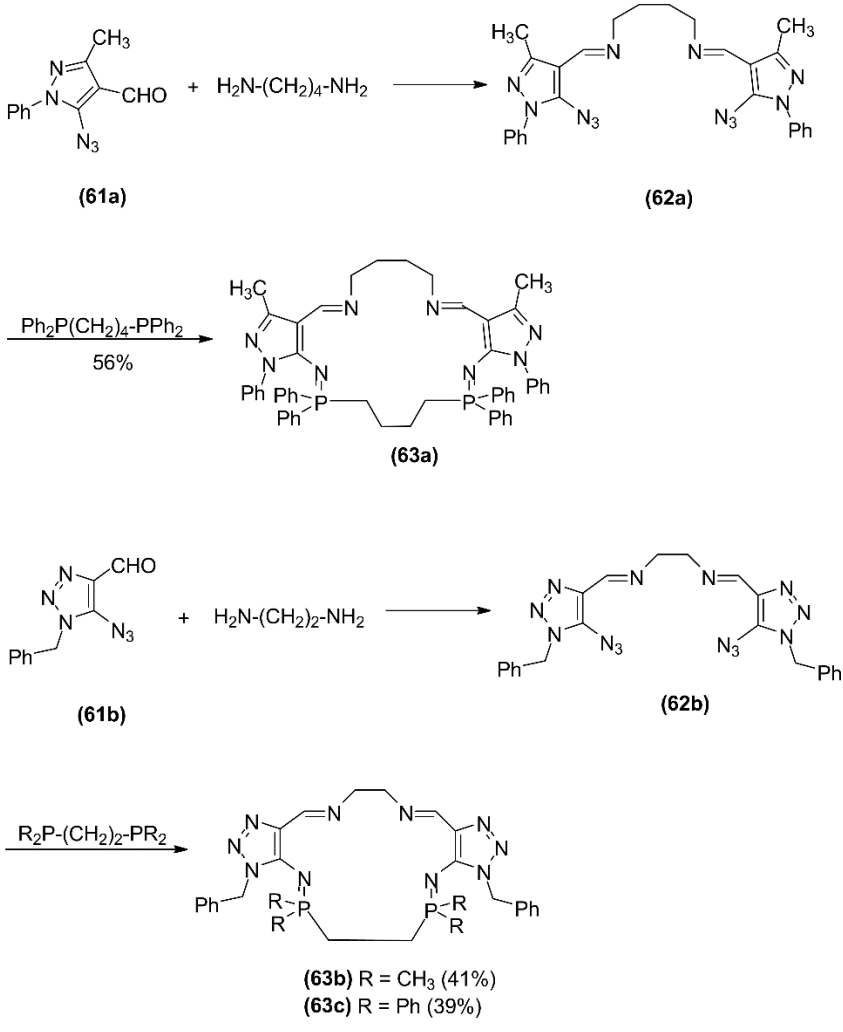

Scheme 16. Synthesis of macrocycles (63a-c) via imine formation followed by Staundinger reaction [33].

USE OF BIS-AZIDES IN POLYMER CHEMISTRY

Poly(1-trimethylsilyl-1-propyne) [PTMSP] is a high free volume glassy polymer and presents extraordinary gas permeability. Cross-linkable films of PTMSP were obtained from toluene solutions composed of PTMSP and either 4,4-diazidobenzophenone (64) or 4,4´-(hexafluoroisopropylidene)diphenyl azide (65). The preparation of these bis-azides was accomplished via diazotization followed by treatment of the diazonium salt with sodium azide as shown in Scheme 17.

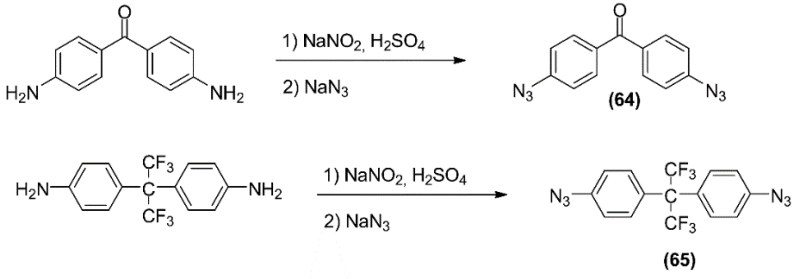

Scheme 17. Synthesis of bis-azides (64) and (65).

The films were cross-linked via UV-irradiation at room temperature or thermal annealing at 180 ºC. The formation of the films can be understood considering that photoirradiation or thermal treatment of azides leads to the loss of nitrogen and the formation of nitrene. This, in turn, can add to double bonds of PTMSP (66) do give aziridines or insert into C-H bonds to give amines (Scheme 18).

The cross-linked films were tested for the N_2 and O_2 gas permeability. It was found that the cross-linked polymers were less permeable than PTMSP (66) [34].

PREPARATION OF CROSS-LINKED DNA

In this last section, it is pointed out that heterodimeric interstrand cross-linked DNA was obtained by Xiong and Seella [35]. Their approache

involved a double-click reaction between preformed oligonucleotide duplexes and the bis azide (67) (Scheme 19).

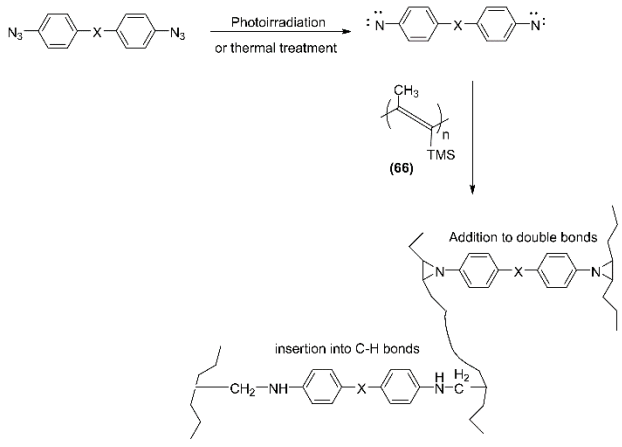

Scheme 18. Formation of the cross-linked PTMSP films.

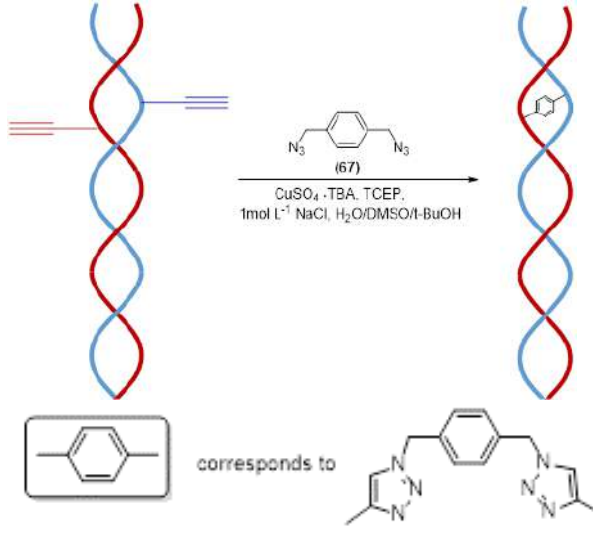

Scheme 19. Construction of heterodimeric interstrand cross-linked DNA via double-click reaction.

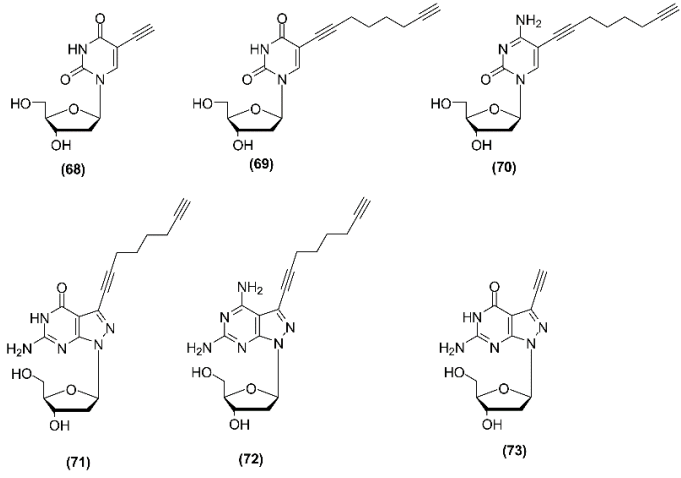

Scheme 20. Alkynylated nucleotides utilized in the preparation of oligonucleotide duplexes.

The structures of alkynylated nucleotides (68-73), used in the preparation of oligonucleotide duplexes, which were utilized in the double click-reaction, are shown in Scheme 20.

It was found that the stability of cross-linked DNA depends on the linker length and the site of modification. It was worth to mention that cross-linked DNA may be helpful in cancer therapy [36].

CONCLUDING REMARKS

This book chapter covered several reports showing the utility of bis-azides. The usefulness of this class of compounds was demonstrated in functional group interconversion, in polymer chemistry, in the preparation of macrocycles, and in the formation of biomolecules. So far, the bis-azides have been mainly applied in the CuAAC reaction (also known as click chemistry). There are other reports in the literature related to the use of bis-azides. However, as previously mentioned, it was not our intention to make an exhaustive discussion concerning bis-azides. Finally, it is possible to

antecipate that many other applications of this class of versatile compounds will be described in the future.

CONFLICT OF INTERESTS

The authors declare that there is no conflict of interests.

ACKNOWLEDGMENT

One of us (RRT) are greatful to Fudação de Amparo à Pesquisa do Estado de Minas Gerais (FAPEMIG) for financial support.

REFERENCES

[1] Bräse, S., Banert, K. (Eds). (2010). *Organiz azides: Synthesis and applications*. John Wiley & Sons Ltd, United Kingdom, 507 pages.

[2] Haase, J. (2010). Large scale and usage of azides. *In: Organiz azides – Synthesis and applications*. John Wiley & Sons Ltd, United Kingdom, 29-52.

[3] Bräse, S., Gil, C., Knepper, K., & Zimmermann. (2005). Organic azides: an exploding diversity of a unique class of compounds. *Angewandte Chemie International Edition, 44*, 5188-5240.

[4] Scriven, E. F. & Turnbull, K. (1988). Azides: Their preparation and synthetic uses. *Chemical Reviews, 88*, 297-368.

[5] Tanimoto, H. & Kakiuchi, K. Recent applications and developments of organic azides in total synthesis of natural products. *Natural Product Communications, 8*, 1021-1034.

[6] Heines, S. V. (1958). Peter Griess – Discoverer of diazo compounds. *Journal of Chemical Education, 35*, 187-191.

[7] Yates, E. & Yates, A. (2016). Johann Peter Griess FRS (1829-88): Victorian brewer and synthetic dye chemist. *Notes and Records, 70*, 65-81.

[8] Huisgen, R. & München. (2010). Foreword. *In: Organiz azides – Synthesis and applications*. John Wiley & Sons Ltd, United Kingdom, xiii-xv.

[9] Kürti, L. & Czakó, B. (2005). *Strategic applications of named reactions in organic synthesis*. Elsevier Academir Prest, Amsterdam, 116-117.

[10] Otera, J. & Nishikido, J. (2010). *Esterification: Methods, reactions, and applications.* Wiley-VCH Verlag GmbH & Co, Second Edition, Germany.

[11] Dinesh, M., Archana, S., Ranganathan, R., Sathishkumar, M. & Ponnuswamy, A. (2015). Bis-azide-triphenylphosphine as a reagent for esterification at room temperature. *Tetrahedron, 56*, 6975-6979.

[12] Lemport, P. S., Smolyar, I. V., Khrustalev, V. N., Roznyatovsky, V. A., Popov, A. V., Kobelevskaya, V. A., Rozentsveig, I. B. & Nenajdenko, V. G. (2019). 3,3-diazidoenones – new types of highly reactive bis-azides. Preparation and synthetic transformations. *Organic Chemistry Frontiers, 6*, 335-341.

[13] Wittig, G. & Krebs, A. (1961). Zur existenz niedergliedriger cycloaline, I [For the existence of lower-link cycloalines, I.]. *Chemische Berichte, 94*, 3260-3275.

[14] Sletten, E. M. & BERTOZZI, C. R. (2013). From mechanism to mouse: A tale of two bioorthogonal reactions. *Accounts of Chemical Research, 44*, 666-676.

[15] Kolb, H. C., Finn, M. G. & Sharpless, K. B. (2001). Click chemistry: Diverse chemical function from a few good reactions. *Angewandte Chemie International Edition, 40*, 2004-2021.

[16] Tornøe, C. W., Christensen, C. & Meldal, M. (2002). Peptidotriazoles on solid phase: [1,2,3] triazoles by regiospecific copper(I)-catalyzed 1,3-dipolar cycloaddition of terminal alkynes to azides. *Journal of Organic Chemistry, 67*, 3057-3064.

[17] Meldal, M. & Tornøe. (2008). Cu-catalyzed azide-alkyne cycloaddition. *Chemical Reviews, 106*, 2952-3015.

[18] de Oliveira Freitas, L. B., Ruela, F. A., Pereira, G. R., Alves, R. B. & Freitas, R. P. (2011). The "click" reaction in the synthesis of 1,2,3-triazoles: Chemical aspects and applications. *Química Nova, 34*, 1791-1804.

[19] Dheer, D., Singh, V. & Shankar, R. (2017). Medicinal attributes of 1,2,3-triazoles: Current developments. *Bioorganic Chemistry, 71*, 30-54.

[20] Tron, G. C., Pirali, T., Billington, R. A., Canonico, P. L., Sorba, G. & Genazzani, A. (2007). Click chemistry reactions in medicinal chemistry: Applications of the 1,3-dipolar cycloaddition between azides and alkynes. *Medicinal Research Reviews, 28*, 278-308.

[21] Meghani, N. M., Amin, H. H. & Lee, B. -J. (2017). Mechanistic applications of click chemistry for pharmaceutical drug discovery and drug delivery. *Drug Discovery Today, 22*, 1604-1619

[22] Borgati, T. F., Alves, R. B., Teixeira, R. R., Freitas, R. P., Perdigão, T. G., da Silva, S. F., dos Santos, A. A. & Bastidas, A. J. O. (2013). Synthesis and phytotoxicity activity of 1,2,3-triazole derivatives. *Journal of the Brazilian Chemical Society, 24*, 953-961.

[23] Xi, W., Scott, T. F., Klaxin, C. J. & Bowman, C. (2017). Click chemistry in materials science. *Advanced Functional Materials, 24*, 2572-2590.

[24] Kushwaha, D., Dwivedi, P., Kuanar, S. K. & Tiwari, V. K. (2013). Click reaction in carbohydrate chemistry: Recent developments and future perspective. *Current Organic Synthesis, 2013*, 90-135.

[25] Liang, L. & Astruc, D. (2011). The copper(I)-catalyzed alkyne-azide cycloaddition (CuAAC) "click" reaction and its applications. An overview. *Coordination Chemistry Reviews, 255*, 2933-2945.

[26] Tăbăcaru, A., Furdui, B., Ghinea, I. O., Cârâc, G. & Dinică, R. M. (2017). Recente advances in click chemistry reactions mediated by transition metal based systems. *Inorganica Chimica Acta, 455*, 329-349.

[27] Moses, J. E. & Moorhouse, A. D. (2007). The growing applications of click chemistry. *Chemistry Society Reviews, 36,* 1249-1262.

[28] Kolb, H. C. & Sharpless, K. B. (2003). The growing impact of click chemistry on drug discovery. *Drug Discovery Today, 8,* 1128-1137.

[29] Abu-Orbai, S. T. (2002). 1,3-dipolar cycloaddition reactions of substituted benzyl azides with acetylenic compounds. *Molecules, 7,* 302-314.

[30] Reis, W. J., Moreira, P. O. L., Alves, R. B., Oliveira, H. H. M., Silva, L. M., Varotti, F. P., Freitas, R. P. (2018). Novel symmetrical 1,4-disubstituted-bis-1,2-3,triazoles: Synthesis by double CuAAC and cytotoxicity evaluation. *Current Topics in Medicinal Chemistry, 18,* 1475-1482.

[31] Düğcdü, E., Ünlüer, D., Çelik, F., Sancak, K., Karaoğlu, S. A. & Özel, A. (2016). 1,2,3-bistriazole derivatives via 'click chemistry' and their biological evaluation. *Molecules, 21*, 659, doi: 10.3390/ molecules21050659].

[32] Belkheira, M., El Abed, D., Pons, J. –M. & Bressy, C. (2018). Chemoselective organoclick-click sequence. *Synthesis, 50,* 4254-4262.

[33] Molina, P., Arques, M. A. A., Sánches-Andrada, P., Vidal A. & Vinader, M. V. (1997). Na eficiente preparation of macrocyles containing two tetra-coordinate phosphorus atoms. *Journal of Organometallic Chemistry, 529,* 121-125.

[34] Jia, J. & Baker, G. L. (1998). Cross-linking of poly[1-(trimethysily)-1-propyne] membranes using bis (aryl azides). *Jounal of Polymer Science: Part B: Polymer Physics, 36,* 959-968.

[35] Xiong, H. & Seela, F. (2012). Croos-linked DNa: Site-selective "click" ligation in duplexes with bis-azides and stability changes caused by internal croos-links. *Bioconjugate Chemistry, 23,* 1230-1243.

[36] Carrette, L. L., Gyssels, E., De Laet, N. & Madder, A. (2016). Furan oxidation based croos-linking: a new approach for the study and targeting nucleic acid and protein interactions. *Chemical Communication, 28,* 1539-1554.

CONTENTS OF EARLIER VOLUMES

Advances in Chemistry Research. Volume 58

Advances in Chemistry Research. Volume 57

Advances in Chemistry Research. Volume 56

Advances in Chemistry Research. Volume 55

Advances in Chemistry Research. Volume 54

INDEX

C

D

E

F

G

H

I

K

L

M

N

O

P

R

S

T

U

V

W

Y

Z